UNCLASSIFIED

ORNL
MASTER COPY

EXTERNAL TRANSMITTAL AUTHORIZED
ORNL
Central Files Number
57-8-5

OAK RIDGE SCHOOL OF REACTOR TECHNOLOGY

REACTOR DESIGN AND FEASIBILITY STUDY

DESIGN STUDY OF AN ADVANCED TEST REACTOR

NOTICE

This document contains information of a preliminary nature and was prepared primarily for internal use at the Oak Ridge National Laboratory. It is subject to revision or correction and therefore does not represent a final report.

OAK RIDGE NATIONAL LABORATORY
OPERATED BY
UNION CARBIDE NUCLEAR COMPANY
Division of Union Carbide Corporation
UCC
POST OFFICE BOX X · OAK RIDGE, TENNESSEE

UNCLASSIFIED

LEGAL NOTICE

This report was prepared as an account of Government sponsored work. Neither the United States, nor the Commission, nor any person acting on behalf of the Commission:

A. Makes any warranty or representation, express or implied, with respect to the accuracy, completeness, or usefulness of the information contained in this report, or that the use of any information, apparatus, method, or process disclosed in this report may not infringe privately owned rights; or

B. Assumes any liabilities with respect to the use of, or for damages resulting from the use of any information, apparatus, method, or process disclosed in this report.

As used in the above, "person acting on behalf of the Commission" includes any employee or contractor of the Commission to the extent that such employee or contractor prepares, handles or distributes, or provides access to, any information pursuant to his employment or contract with the Commission.

O R N L
Central Files Number
57 - 8 - 5

Copy No. 55

OAK RIDGE SCHOOL OF REACTOR TECHNOLOGY

Reactor Design and Feasibility Study

"DESIGN STUDY OF AN ADVANCED TEST REACTOR"

Prepared by:

W. L. Carter, Group Leader
C. D. Cagle
C. W. Garrett
F. E. Hankins
E. L. Humez
W. L. Kirk
C. L. Morrison
D. J. Niehaus
R. E. Woodard

August 1957

Distribution:

1. A. M. Weinberg
2. J. A. Swartout
3. R. A. Charpie
4. W. H. Jordan
5. Lewis Nelson
6. D. C. Hamilton
7. C. O. Smith
8. J. H. Marable
9. P. G. Lafyatis
10. Herbert Pomerance
11. W. A. Lloyd
12. W. Zobel
13. E. D. Arnold
14. J. W. Ullman
15. A. T. Gresky
16. C. S. Walker
17. E. P. Blizard
18. L. B. Holland
19. W. E. Kinney
20. W. R. Gall
21. A. P. Fraas
22. J. A. Lane
23. P. R. Kasten
24. A. F. Rupp
25. C. E. Winters
26. R. B. Briggs
27. A. L. Boch
28. W. T. Furgerson
29. R. V. Meghreblian
30. L. R. Dresner
31-32. W. L. Carter
33-34. C. D. Cagle
35-36. C. W. Garrett
37-38. F. E. Hankins
39-40. E. L. Humez
41-42. W. L. Kirk
43-44. C. L. Morrison
45-46. D. J. Niehaus
47-48. R. E. Woodard
49-50. Martin Skinner
51-52. REED Library
53-54. Central Research Library
55-65. Laboratory Records
66-71. ORSORT Files
72-86. TISE
87. InterNuclear Company, 7 N. Brentwood, Clayton 5, Missouri (Attn: Lawrence Widdoes)

PREFACE

In September, 1956, a group of men experienced in various scientific and engineering fields embarked on the twelve months of study which culminated in this report. For nine of those months, formal classroom and student laboratory work occupied their time. At the end of that period, these nine students were presented with a problem in reactor design. They studied it for ten weeks, the final period of the school term.

This is a summary report of their effort. It must be realized that, in so short a time, a study of this scope can not be guaranteed complete or free of error. This "thesis" is not offered as a polished engineering report, but rather as a record of the work done by the group under the leadership of the group leader. It is issued for use by those persons competent to assess the uncertainties inherent in the results obtained in terms of the preciseness of the technical data and analytical methods employed in the study. In the opinion of the students and faculty of ORSORT, the problem has served the pedagogical purpose for which it was intended.

The faculty joins the authors in an expression of appreciation for the generous assistance which various members of the Oak Ridge National Laboratory gave. In particular, the guidance of the group consultant, C. E. Winters, is gratefully acknowledged.

Lewis Nelson

for

The Faculty of ORSORT

ACKNOWLEDGMENTS

A number of people have contributed to the progress of this study; however, this group would especially like to express its appreciation to Dr. C. E. Winters and Dr. R. A. Charpie for their guidance and many helpful suggestions; to Mr. W. E. Kinney for his assistance with ORACLE calculations; to Dr. A. D. Callihan for suggestions concerning the control system; to Mr. C. W. Nestor, Jr. for assistance in preparing group constants; to Mr. R. D. Cheverton for his many helpful suggestions and the use of information from a previous ORSORT study group; to Dr. M. L. Nelson and the ORSORT faculty for their cheerful assistance with many technical problems; and to the staff of the ORACLE for guidance in making machine calculations.

ABSTRACT

A conceptual design of an advanced engineering test reactor is presented. The reactor is a heavily-loaded, fully-enriched U-235 system containing four 8-inch diameter experiment tubes penetrating the core. The core configuration is two fuel slabs separated by a D_2O moderating region containing the four experiment tubes. A fast neutron reflector of 70 volume percent aluminum and 30 volume percent D_2O comprises the region at the outside of the fuel slabs. Unperturbed thermal neutron fluxes as high as 2.48×10^{15} neutrons/cm^2-sec can be supplied to the experiment region for a core lifetime of greater than 12 days at a total reactor power not exceeding 500 MW.

TABLE OF CONTENTS

	Page
List of Figures	8
List of Tables	12
I. Introduction	14
A. General Comments	14
B. Reactor Design Criteria	14
C. Scope of Study	15
II. Preliminary Considerations	16
III. Description of Double-Slab Reactor	19
A. General Description	19
B. Reactor Test Region	24
C. Reactor Core and Reflector	25
D. Shutdown and Control System	30
E. Reactor Fuel Handling	34
F. Heat Production in the Central D_2O Region	36
G. Heat Production and Heat Transfer in the Aluminum-D_2O Reflector	38
IV. Reactor Core Analysis	41
A. General Considerations	41
B. The Power Equation and its Implications	41
C. Core Geometry	43
D. Heavily-Loaded Slab Geometry Calculations	47
E. Lightly-Loaded Cylindrical Cores	80
F. Validity of the Calculations	85
V. Bibliography	90
VI. Appendices	93
A. Three-Group Constants	93
B. Nuclear Heating in Fast Neutron Reflector	110
1. Heat Production in the Al-D_2O Fast Reflector	110
2. Heat Transfer Calculations for the Aluminum Reflector	119
C. Nuclear Heating in D_2O Reflector	123
1. Calculation of Heat Production in the Central D_2O Region	123
D. Fuel Burnup and Fission Product Effects	124
1. Fuel Burnup	125
2. Xenon-135 Concentration	128
3. Xenon-135 Poisoning	138
4. Samarium Concentration	139

Page

5. Samarium Poisoning 143
6. Total Fission Product Poisoning 143
7. Xenon over-ride 143
8. Xenon Instability 149

E. Fuel Element Design 154
1. Fuel Element Calculations and Design 154
2. Fuel Alloy Composition 158

F. Core Heat Removal 161
1. Heat Production, Transfer and Removal Calculations 161
2. D_2O-Coolant Flow and Temperature Calculations 169
3. Heat Transfer Coefficients 174
4. Fuel Plate Temperatures 175

G. External Coolant Circuit Calculations 184
1. Pressure Drop Calculations for External Circuit 184
2. Heat Exchanger Calculations 185
3. Pressure Drop Across Heat Exchanger 187
4. Total System Pressure Drop 189
5. Pumping Requirements 189
6. Cooling Water (H_2O) Requirements 189

H. Temperature Distribution in Fuel Plates 190

LIST OF FIGURES

Figure No.	Title	Page
1.	Elevation of Reactor Building	20
2.	Sectional View of Reactor	21
3.	Plan View of Reactor	22
4.	Isometric View of Reactor	23
5.	Fuel Element Sketch	27
6.	Safety System Schematic	31
7.	Control System Schematic	33
8.	Effect of Mass of Cadmium on Multiplication Constant	35
9.	Average Heat Production in Central D_2O Region for Total Operating Power Level of 500 MW	37
10.	Average Heat Distribution in Homogenized Side Reflectors	39
11.	Comparison of Cylindrical and Slab Geometries	45
12.	Illustration of Dimensional Notation (Double Slab Geometry)	48
13.	Effect of Various Reflectors on Reactivity and Flux Peaking	50
14.	Multiplication Constant (k_{eff}) vs Fuel Loading for Three Types of Reflectors	51
15.	Core Effectiveness (Pe/RM) vs Fuel Thickness for Various Reflectors	52
16.	Multiplication Constant vs Fuel Concentration for Typical Fuel Zone Thickness for Three Types of Reflectors	53
17.	Core Effectiveness (Pe/RM) vs Fuel Concentration for Three Types of Reflectors for Typical, Constant Fuel Zone Thickness	54
18.	Typical Flux for a D_2O Reflected Core	56
19.	Typical Flux Plot for a 70% Zirconium Reflected Core	57

Figure No.	Title	Page
20.	Typical Flux Plot for a 70% Al Reflected Core	58
21.	Peak and Average Power Densities Required to Deliver Equal Experiment Fluxes for Various Types of Reflectors	59
22.	Multiplication Constant, Flux Peaking and Core Effectiveness vs Fuel Thickness for a 70% Al Reflected Reactor	62
23.	Multiplication Constant and Core Effectiveness vs Fuel Concentration for a 70% Al Reflector	63
24.	Multiplication Constant and Core Effectiveness vs Metal/Water Ratio	64
25.	Multiplication Constant and Core Effectiveness vs R_1 Thickness	66
26.	Relative Core Effectiveness (Pe/RM) vs Experiment (3.5 cm)+ D_2O Thickness	68
27.	Multiplication Constant and Core Effectiveness as a Function of Experiment U-235 Concentration	69
28.	Relative Core Effectiveness (Pe/R) as a Function of Experiment Slab Thickness	70
29.	Results of Temperature Coefficient Calculations for Constant D_2O Reflector Temperature of 50°C (k_{eff} vs Fast Reflector Temperature)	71
30.	Results of Temperature Coefficient Calculations for Constant D_2O Reflector Temperature of 50°C (k_{eff} vs Fuel Region Temperature)	72
31.	Results of Temperature Coefficient Calculations for Constant Fast Reflector Temperature of 100°C (k_{eff} vs Fuel Region Temperature)	73
32.	Results of Temperature Coefficient Calculations for Constant Fast Reflector Temperature of 100°C (k_{eff} vs Temperature of D_2O Moderator)	74
33.	Multiplication Constant vs D_2O Reflector Thickness	76
34.	Multiplication Constant and Core Effectiveness vs Thickness of 70% Aluminum Reflector	77
35.	Thermal Flux in the Fuel Zone--Y Traverse	78

Figure No.	Title	Page
36.	Thermal Flux in the Fuel Zone--Z Traverse	79
37.	Multiplication Constant and Core Effectiveness as a Function of Reflector Savings in the Y and Z Directions	81
38.	Effect of Experiment Absorbers on Thermal Flux for Experiment at 40 cm Radius (Cylindrical Core)	83
38a.	Effect of Experiment Absorbers on Thermal Flux for Experiment at 60 cm Radius (Cylindrical Core)	84
39.	One-Speed Diffusion Theory Results (Cylindrical Core)	87
40.	Dimensional Notation for Capture-Gamma Heating	116
41.	Dimensional Notation for Heat Transfer Calculations	120
42.	U-235 Concentration vs Time	126
43.	Average Thermal Flux vs Time for Constant Power	127
44.	Maximum Xe-135 Concentration vs Average Thermal Flux During Operation	132
45.	Xe-135 Cross Section vs Operating Time	134
46.	Xe-135 Growth and Decay After Shutdown	137
47.	Samarium Cross Section vs Operating Time	142
48.	Increase in Xe-135 Cross Section Following Shutdown	146
49.	Multiplication Constant vs Operating Time	147
50.	Allowable Length of Shutdown to Permit Restart vs Operating Time	148
51.	Change in Σ_a^{Xe} versus Time Following +10%, +20% and -20% Change in Average Flux	151
52.	Thermal Flux vs R_2	164
53.	Fission Rate Density vs R_2 (at avg. $\phi(z)$ and $\phi(y)$)	165
54.	Fission Rate Density vs R_2 (at Center of Reactor)	166
55.	Coolant Flow Schematic	170

Figure No.	Title	Page
56.	Coolant Flow Channel in Fuel Element	176
57.	Temperature Identification for Heat Exchanger	188
58.	Dimensional Notation of Fuel Plate	190
59.	Temperature Notation (Fuel Plate)	193
60.	Dimensional Notation (Fuel andCladding)	194
61.	Temperature Distribution in Fuel Plate	198
62.	Dimensional Notation (Fuel)	201
63.	Fuel Element and Fuel Slab Dimensions	205

Table No.	Title	Page
1.	Effect of Multiplication Factor and Experiment Zone Thermal Flux of Varying Concentrations of Fissionable Material in the Experiment Region	25
2.	Summary of Double-Slab Reactor Calculations	28
3.	One-Speed Diffusion Theory Results	86
4.	Microscopic Cross Sections of Elements	98
5.	Three-Group Constants for Various Uranium Concentrations, Bucklings and Metal-to-Water Ratios	100
6.	Weighting Functions ($\Phi \Delta U$) for Calculating Group Constants	105
7.	Three-Group Constants for Several Materials in Temperature Range 25°C to 150°C	107
8.	Three-Group Constants for Several Metal-to-Water Ratios and Several Uranium Concentrations	109
9.	Gamble's Energy Spectrum for Fission Gammas	112
10.	Gamma Energy Absorption Coefficients	112
11.	Neutron Elastic Scattering Constants	115
12.	Energy Spectrum for Capture Gammas in Aluminum	118
13.	Constants for Calculating Capture-Gamma Heating	118
14.	Gamma Absorption Coefficients for D_2O	123
15.	Maximum Xe Concentrations for Several Fluxes	131
16.	Xe^{135} Concentration as a Function of Reactor Operating Time	133
17.	Xe^{135} Growth and Decay After Shutdown	136
18.	Change of Reactivity and Multiplication Constant Due to Xe^{135} as a Function of Reactor Operating Time	140
19.	Sm Cross Section as a Function of Operating Time	141
20.	Allowable Shutdown Time for Xe^{135} Override as a Function of Reactor Operating Time for Cold Reactor	144

Table No.	Title	Page
21.	Allowable Shutdown Time for Xe^{135} Override as a Function of Reactor Operating Time for Hot Reactor	145
22.	Effect of Step Changes in Average ϕ on Xe^{135} Cross Section	150
23.	Fission Rate Densities in Core	163

I. INTRODUCTION

A. General

Today's nuclear power and nuclear propulsion programs urgently require the results of in-pile tests of fuel elements in high neutron fluxes and with high accumulated neutron dosage (nvt). A testing reactor for this purpose should be capable of irradiating whole or partial test fuel elements at a thermal neutron flux of greater than 1×10^{15} n/cm^2-sec in order to accelerate the testing programs by reducing testing times. With widely diverse reactor programs underway, the testing reactor should provide facilities for irradiating fuel elements with a variety of coolants such as gases, water, organic liquids, fused salts, and liquid metals as well as fuel solutions for liquid-fueled reactors.

Since the need for such a testing reactor is urgent, it is desirable to utilize existing and proven technology in order to assure more rapid implementation of the facility. This requirement was kept in mind throughout this study, and consideration was given only to systems based upon proven technology.

B. Reactor Design Criteria

Certain design criteria and limitations have been imposed as boundaries and goals for this particular study. They are:

a. The reactor is to be used for fuel element tests and fuel element experiments only. Other types of research and electrical power production are not to be considered.

b. Four eight-inch diameter through-pipes are to be provided for testing and experiments.

c. A thermal neutron flux of 1×10^{15} neutrons/cm^2-sec or greater should be delivered to the experiment.

d. The thermal neutron flux available for the experiments should not vary by more than 50% over the experiment region.

e. The reactor power should not be in excess of 500 megawatts.

f. A reasonable core life in excess of seven days is desirable.

g. Use of components requiring extensive development is to be avoided because of the immediate need for the reactor. Only existing technology is to be considered.

C. Scope of Study

This study has been primarily concerned with the core design of a reactor to meet the above requirements. Geometrical considerations have been limited to arrangements that will place experiment tubes in regions of highest thermal flux. This investigation was not extended to a complete design of a reactor facility but has been directed principally toward providing an experiment zone having the desired nuclear properties. A nominal amount of engineering has been considered to recognize some of the problems associated with the construction of such a reactor and to investigate means of heat dissipation.

No attempt has been made to estimate the cost of a complete facility of this type. It is felt that existing or planned reactor facilities, without extensive technical modifications, will serve adequately as a guide to the extension of the reactor design.

II. PRELIMINARY CONSIDERATIONS

None of the design parameters such as core geometry, fuel concentration, metal-to-water ratio, etc., for the advanced engineering test reactor were fixed at the beginning of this study. Therefore a considerable portion of the initial work was directed toward fixing principal parameters in order that a more detailed study of the system could be made.

Providing a high thermal neutron flux in a reactor at a given power level can be accomplished in two ways: (1) by using a lightly-loaded fuel region and taking advantage of the inverse dependence of average thermal flux upon mass, or (2) by using a heavily-loaded fuel region with a high fast flux leakage into a flux trap composed of a moderating material. The work of Cheverton et al[1], calculations performed on the Mighty Mouse reactor[2] and flux plot data on the Argonaut[19] and Thermal Test reactors[20] highlight the use of the flux trap principle for obtaining thermal flux peaking. Whereas a lightly-loaded cylinder of the NRX type exemplifies production of high thermal flux with a lightly-loaded system.

Physical disposition of fissionable material, the location of test facilities, fuel enrichment, moderating and reflecting materials, and core geometry received much early attention. Because of the need of a high, infinite multiplication factor (k_∞) it was decided to consider only fully-enriched U-235 systems. Nevertheless, it should be pointed out that a U-233 system with its high value of η ($\sim$2.29) should make an even more satisfactory fuel. Other values were mutually related and primarily dependent upon core geometry.

A variety of geometries utilizing the flux trap principle for boosting thermal flux in the experiment region were considered for further study:

1. A cylindrical annulus of fuel 75 cm inside radius with the four experiment tubes and moderator in the central region and reflector in the outer region.
2. A cruciform fuel loading with an experiment tube located in each quadrant.
3. A single finite slab that has the experiment tubes adjacent to one face and either a fast or thermal reflector on the other face.
4. A double-slab configuration with the four experiment tubes on the center line between the slabs.
5. A lightly-loaded cylinder of the NRX type with an experiment tube in each quadrant.

Calculations of configurations 1 and 2 appeared to be impossible using the available one-dimensional, three-group, three-region ORACLE code.[5] However, calculations were performed on the single slab geometry for the following conditions:

Fuel slab dimensions	180 cm x 120 cm x 14 cm
U-235 concentration	9.18×10^{19} atoms/cm^3
Metal-to-water ratio	0.73
Reflector savings for Y & Z directions	20 cm
Moderator	D_2O

On one 120-cm x 180-cm face a 200-cm-thick D_2O reflector-moderator was used and on the opposite face a fast reflector 60 cm thick composed of 70% Al and 30% D_2O by volume was used. In this single slab geometry the effective multiplication factor (k_{eff}) was found to be 1.12. However, at this time more promising results from the double slab geometry calculations and its flux trap advantage suggested that this approach would be more profitable; consequently, further study of the single slab was dropped.

Concurrently, calculations were being performed on the lightly-loaded cylindrical reactor; details of these calculations are recorded in Section IV E. For these cases, fuel concentrations of the order 2×10^{18} U-235 atoms per cm^3 and dimensions in the range 6 to 10 ft high by 6 to 12 ft diameter were used. Critical mass calculations and flux plots indicated that the lightly-loaded cylinder was not a "stiff" system, i.e., the presence of highly-absorbing experiments, such as PWR fuel elements, would too greatly reduce the flux at the experiment. In addition, the critical mass of about 7 kilograms would make difficult the control problem incurred by adding the 3-4 kilograms excess mass required for lifetime and fission product poisoning.

The lack of a two-dimensional (r-θ) code hampered the cylindrical reactor calculations since approximations had to be made in forming the mathematical model. This problem, however, was not as serious for the slab calculations. It appeared that the better geometry for the advanced engineering test reactor would be the double slab, and a series of parameter studies was undertaken to optimize the separate regions.

III. DESCRIPTION OF DOUBLE-SLAB REACTOR

A. General

The core configuration adjudged to be optimum for the requirements of the advanced engineering test reactor is the double slab geometry with the experiment tubes located midway between the slabs. A pictorial representation of this reactor is given in Figures 1, 2, 3, and 4. The reactor core including its reflectors is in the general shape of a rectangular parallelepiped. The four 8-inch diameter experiment tubes are arranged on the center line between the slabs and are spaced 40 cm apart center to center. These tubes penetrate the core vertically, parallel to the 180 cm x 120 cm faces of the slabs; the distance from the center of the tubes to the face of the fuel slab is 20 cm.

Beyond the fuel slabs on both sides of the reactor are fast neutron reflectors consisting of aluminum plates cooled by heavy water. The fast reflectors are composed of 70% Al and 30% D_2O by volume. The top, bottom, and ends of the reactor are D_2O reflected. In addition, D_2O serves as the coolant for the MTR type fuel elements that make up the fuel slabs and fills the region around the experiment tubes between the fuel slabs.

The core region will be subjected to relatively high heat fluxes, and pressurization will be necessary to preclude nucleate boiling in the fuel element channels. A hot spot temperature of 464°F will require pressurization of the system to at least 500 psi. The core will be cooled by downflow of D_2O because:

1. Fluid forces tend to maintain the fuel elements in the bottom grid plate and simplifies top grid construction.
2. Downflow aids in the gravity drop of the safety curtains.
3. Downflow carries the gamma-active N^{16} to the bottom of the core permitting the least radio-active coolant to be at the top. Thereby the top shield can be of less complicated construction.

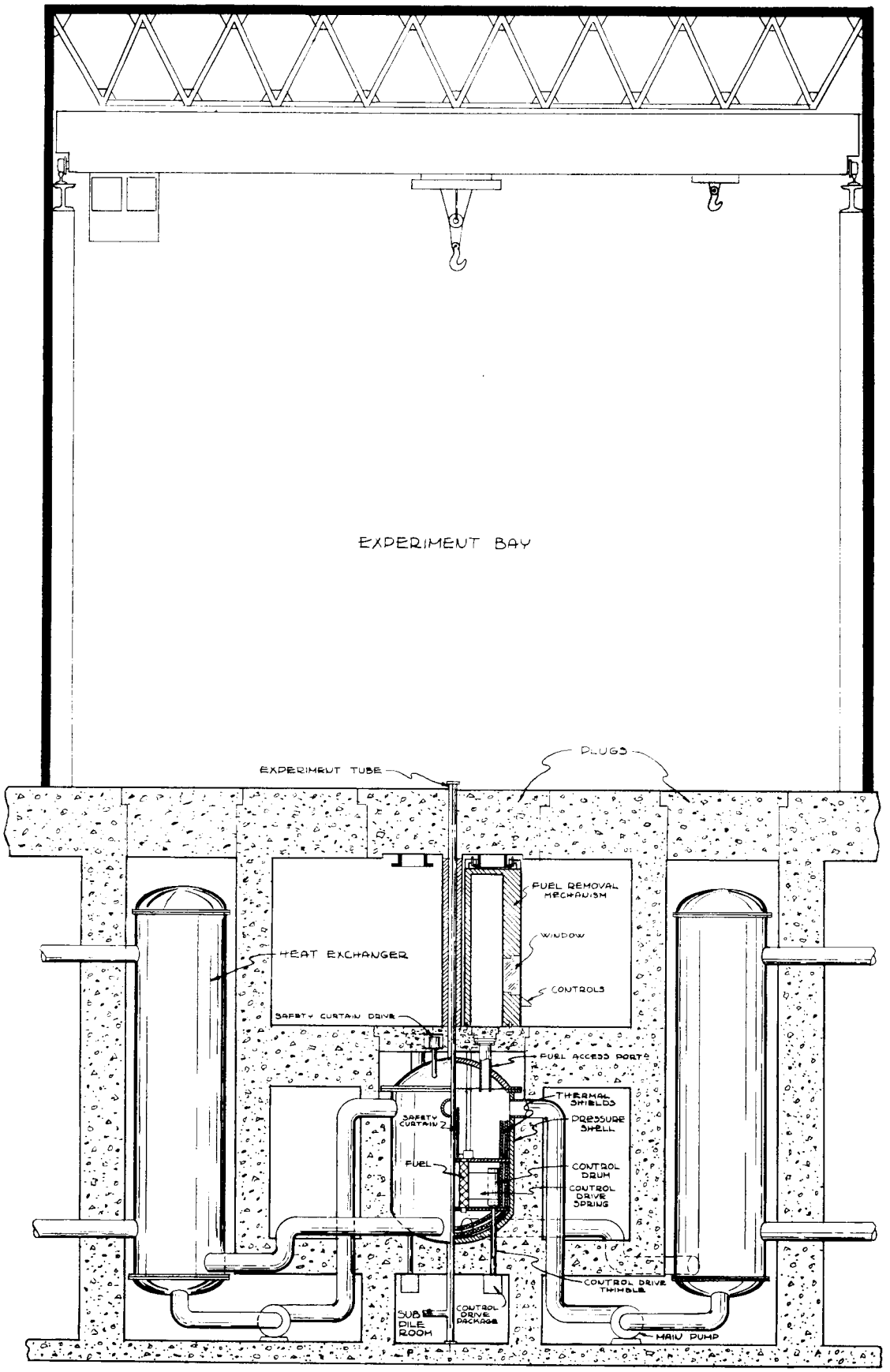

ADVANCED TEST REACTOR

ELEVATION

REACTOR BUILDING

0 1 2 3 4 5 10
scale — feet

C. W. GARRETT 8-15-57

UNCLASSIFIED
ORNL-LR-DWG 25085

Fig 1

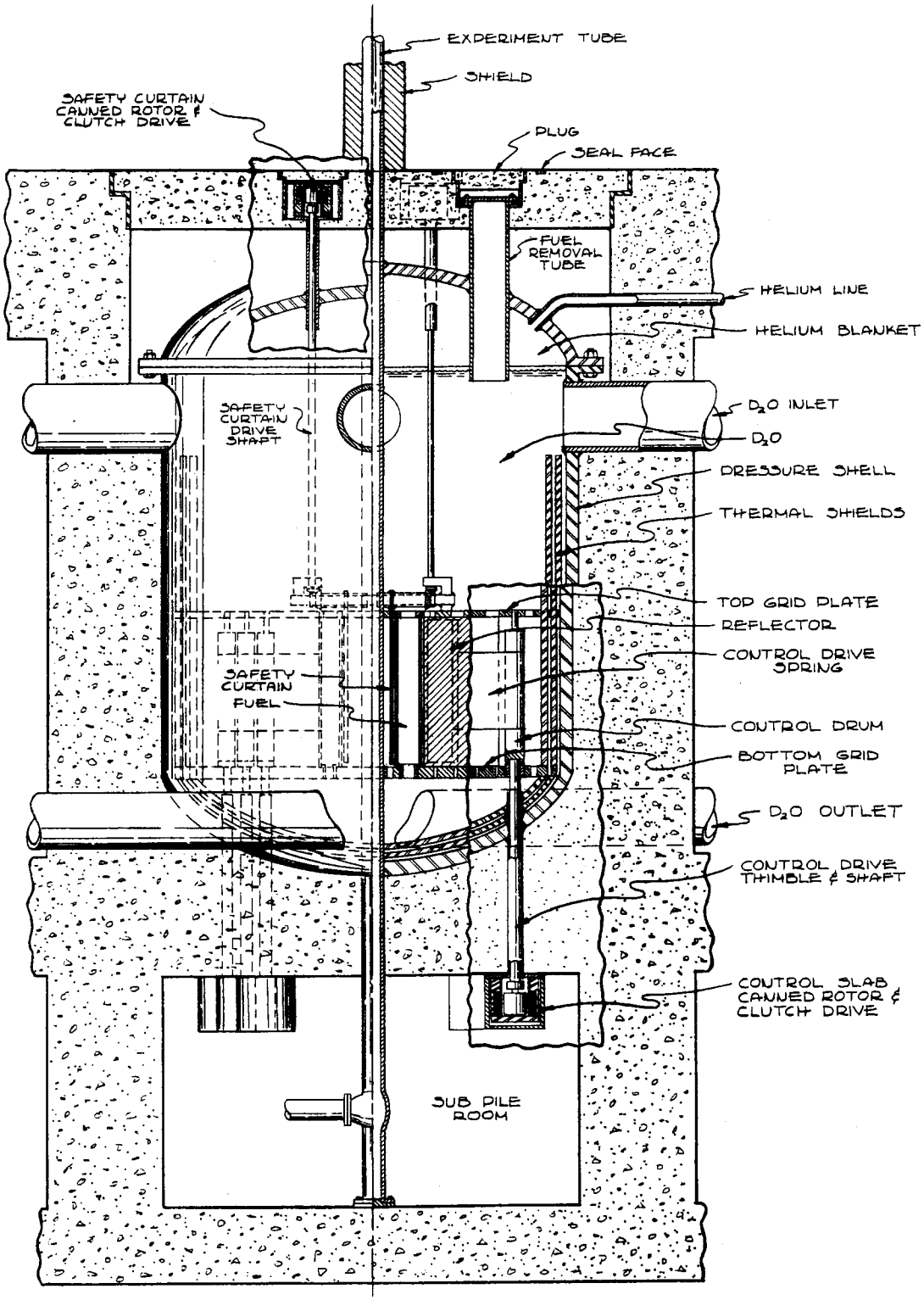

ADVANCED TEST REACTOR

ELEVATION

REACTOR TANK

0 ½ 1 2 3
scale — feet

C.W. GARRETT 8-17-57

UNCLASSIFIED
ORNL-LR-DWG 25086

Fig 2

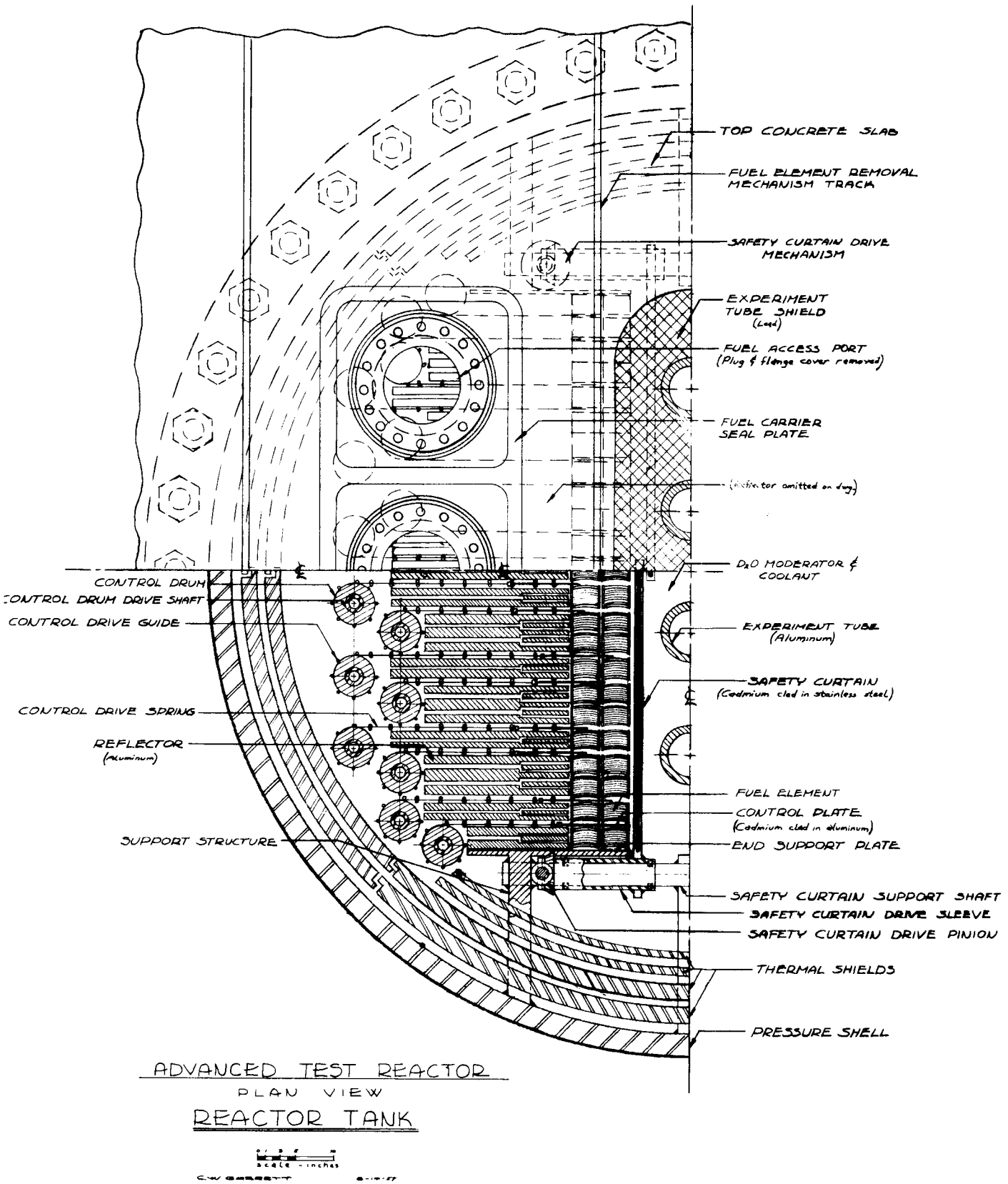

Fig 3

UNCLASSIFIED
ORNL-LR-DWG 25087

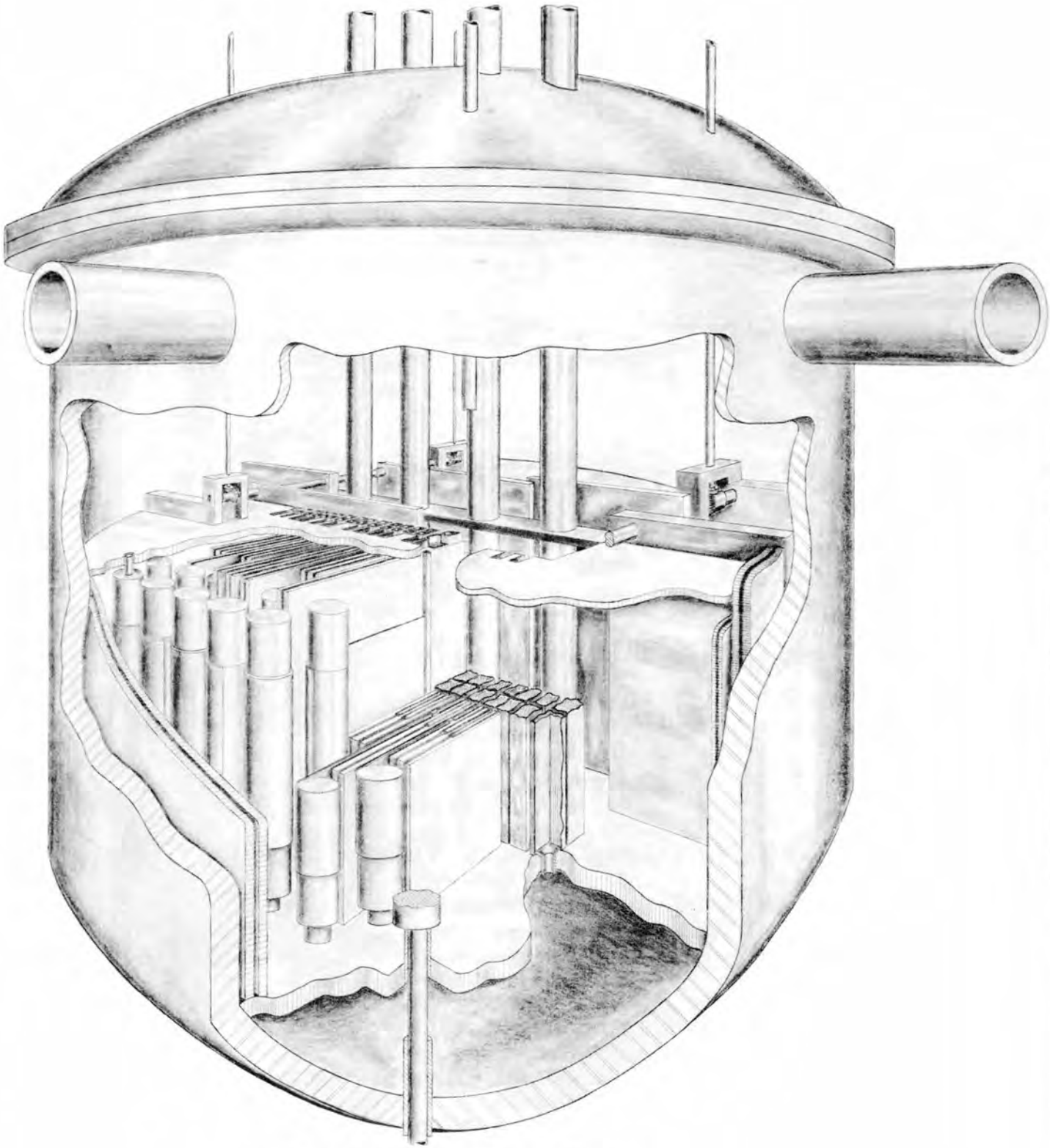

ADVANCED TEST REACTOR

ARTIST'S CONCEPTION

C.W. GARRETT 8-23-57

Fig 4

UNCLASSIFIED
ORNL-LR-DWG 25088

B. Reactor Test Region

The test region of the reactor occupies the space between the fuel slabs and has dimensions 40 cm wide by 180 cm long by 120 cm high. Experiment tubes will extend through this region as shown in Figures 1 and 2 and continue through the top and bottom heads of the reactor- containing vessel. In reality these tubes are through-tubes permitting experimental access at both the top and sub pile areas for locating test fuel elements or other specimens in the heart of the reactor. Possible choices for materials of construction are aluminum and hafnium-free zirconium. In any case, the material should have a low thermal-neutron absorption cross section so that maximum flux can be delivered to the experiments. For this study it was assumed that the tubes would be made of aluminum.

The tube walls need to be constructed for an outside pressure of at least 500 psi as this will be the pressure of the reactor vessel. Likewise, the conditions on the inside of the tube might also require pressure construction. Test fuel elements will produce large quantities of heat, and pressurized test systems could well be necessary to prevent vaporization of the coolant.

As will be discussed in Section IV, the test region has been planned to minimize distortion of the flux pattern at the experiment. The dimensions of the system have been chosen to permit thermal flux peaking in the experiment region. The clean and cold reactor will have about 30% excess reactivity available for experiments, burn-out, xenon over-ride, and thermal effects which can be satisfactorily controlled by absorbing curtains extending through the fuel region.

Fissionable material in the experiment region has a pronounced effect upon the multiplication factor and flux level at the experiment. In order to make calculations to show this effect with the three-group, three-region code, it was necessary to homogenize the experiment, through-tube and structural material into a central slab 7 cm thick by 180 cm long by 120 cm high; reflector savings were then applied

to the core region to account for the fast reflector effect. Noting that a concentration of 10×10^{19} U-235 atoms per cm^3 is the average concentration of a PWR seed element which contains approximately 2.4 kg of U-235 homogenized into a 6-foot long by 8-inch diameter pipe, the following tabulation of the effect of fissionable material in the test region on the multiplication constant and thermal flux at the surface of the experiment can be constructed:

TABLE 1

EFFECT ON MULTIPLICATION FACTOR AND EXPERIMENT ZONE THERMAL FLUX OF VARYING CONCENTRATIONS OF FISSIONABLE MATERIAL IN THE EXPERIMENT REGION

Fuel concentration in experiment, atoms U-235/cm^3	k_{eff}	Thermal flux* at a reactor power of 390 MW, n/cm^2-sec
0	1.29	2.48×10^{15}
1×10^{19}	1.179	1.165×10^{15}
2×10^{19}	1.209	1.135×10^{15}
3×10^{19}	1.238	1.097×10^{15}
4×10^{19}	1.266	1.061×10^{15}
6×10^{19}	1.306	0.994×10^{15}
9.18×10^{19}	1.354	0.893×10^{15}

* for a clean, cold reactor (does not include fission product and temperature effect:

It will be noticed that delivered fluxes of the magnitude of 10^{15} n/cm^2-sec can be attained with fuel concentrations as high as 4×10^{19} atoms of U-235/cm^3. Estimations have shown that the heat produced by U-235 concentrations of this magnitude will be quite large and create serious heat dissipation problems for the experimenter.

C. Reactor Core and Reflector

The fuel region of the reactor consists of two fuel slabs each being 20 cm thick

by 180 cm long by 120 cm high and separated by a 40 cm D_2O moderator gap containing the experiment region. Each slab contains 46 fuel elements of the MTR type; these are pictured in Figure 5.

Individual fuel elements are mounted in a grid plate which is supported by the vessel walls. This plate is fitted with orifices to distribute coolant between the fuel, reflector and moderator regions. As previously stated downflow of coolant is provided to minimize the danger of the fuel elements lifting out of the grid during operation. At appropriate points spacing of the fuel elements is adjusted to permit entry of control plates into the fuel zone.

Based upon the volume of the fuel region, the concentration of U-235 is 9.18×10^{19} atoms per cm^3 and the volume ratio of metal to water is 0.73. A detailed discussion of the calculations required in determining these numbers is included in Section IV. Engineering calculations were made to investigate the problems associated with heat removal, fuel zone temperatures, pressure drop, coolant velocities, etc., and these results are presented in Table 2. It may be pointed out that these results appear to describe a system which can be engineered by an extension of existing technology.

The outside 180 x 120 cm faces of the fuel slabs are covered by fast neutron reflectors consisting of aluminum plates which comprise 70% of the volume of this region; the remaining 30% is D_2O for cooling purposes. Of course, the function of the fast reflector is to return fast and epithermal leakage neutrons back through the core region into the central experiment region. Slowing down of these fast and epithermal neutrons shifts the flux peaking into the experiment zone. The scattering processes whereby fast and epithermal neutrons are reflected deposit heat in the aluminum reflector; however, as will be shown in Section III-G, heat removal is not a serious problem.

FIGURE 5

FUEL ELEMENT SKETCH

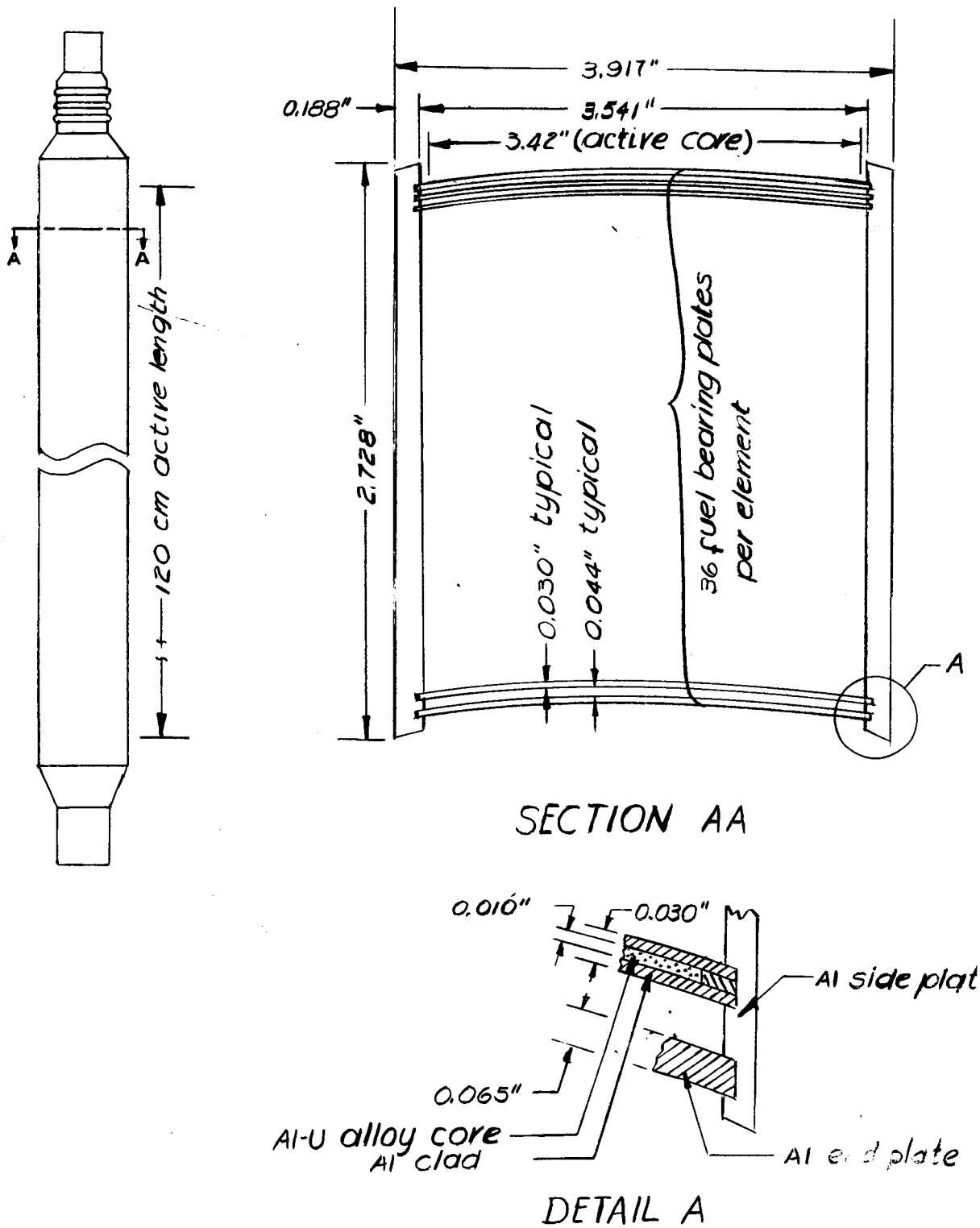

TABLE 2

SUMMARY OF DOUBLE-SLAB REACTOR CALCULATIONS

Nuclear Characteristics	Supercritical Calculations	k = 1
$\bar{\Phi}_{TH}$ in fuel (average)	2.97×10^{14}	2.13×10^{14}
$\hat{\Phi}_{TH}$ in fuel (peak)	8.4×10^{14}	7.25×10^{14}
$\hat{\Phi}_{TH}$ in experiment region	2.48×10^{15}	2.48×10^{15}
Total power for unperturbed peak flux of 2.48×10^{15}	500 MW	390.6 MW
k_{eff} (at start-up)	1.30	
δk (temperature effect)	5%	
δk (steady state fission-product poisoning)	5%	
δk (fuel burn-up)	8%	
δk (experiment effect, Xe over-ride and burn-up)	12%	
Core lifetime	12 days	
Fuel Element Characteristics		
Active length	47.3 in	
Width	3.917 in	
Depth	2.728 in	
No. fuel bearing plates per element	36	
No. fuel elements in core (46 per slab)	92	
Surface area for heat transfer in core	7704 ft^2	
U-Al fuel alloy composition	12.5% wt. U	
Metal-to-water ratio	0.73	
Fuel element type	MTR	
Loading mass for k = 1.30	30.9 kg U-235	
Fuel plate thickness	0.030 in	

Table 2 (continued)

Fuel alloy thickness	0.010 in
Al clad thickness	0.010 in
Geometry	
Core configuration	double slab
Slab length	180 cm
Slab thickness	20 cm
Slab height	120 cm
Distance between slabs	40 cm
Moderator-reflector between slabs	D_2O
Fast reflector on outside 120 cm x 180 cm faces of slabs	70% Vol. Al 30% Vol. D_2O
Reflector on other faces of fuel slabs	D_2O
Thermal Characteristics	
Average heat flux	210,430 BTU/hr-ft^2 66.4 watts/cm^2
Maximum heat flux	775,000 BTU/hr-ft^2 245 watts/cm^2
Average power density (homogenized core)	53.14×10^6 BTU/hr-ft^3 550 watts/cm^3
Maximum power density(homogenized core)	196×10^6 BTU/hr-ft^3 2029 watts/cm^3
Average power density (heterogeneous core)	50.5×10^7 BTU/hr-ft^3 5230 watts/cm^3
Maximum power density (heterogeneous core)	186.5×10^7 BTU/hr-ft^3 19,310 watts/cm^3
Maximum temperature of fuel element surface	464°F
Mixed mean temperature of D_2O coolant leaving core	204.5°F

Table 2 (continued)

Temperature of D_2O coolant entering core and fast reflector	$120^{\circ}F$
Temperature of D_2O coolant leaving fast reflector	$170^{\circ}F$
Temperature of D_2O coolant going to heat exchangers	$203^{\circ}F$
<u>Coolant Flow Characteristics</u>	
Flow rate through core	33,800 GPM
Flow rate through fast reflector	3,100 GPM
Total flow rate through system	36,900 GPM
Velocity through core	21 ft/sec
Pressure drop through core	40 psi
Total pressure drop through system	ca. 62 psi
Flow channel cross sectional area in core	3.58 ft^2
Estimated pumping power	1360 HP
Estimated flow rate of secondary coolant (river water)	114,000 GPM

D. Shutdown and Control System

Owing to the high thermal peaking in the D_2O region contained between the fuel slabs, this region is chosen for the safety shutdown elements. Two cadmium curtains, placed so that each fuel region has a curtain of cadmium between it and the central moderating region to prevent thermalized neutrons from being reflected back into the fuel and to prevent coupling between the two fuel regions, form the nuclear portion of the safety shutdown system. This mechanism is shown in Figure 6. Each curtain is made of two sheets of cadmium jacketed in stainless steel with an overall size of 2 cm x 120 cm x 92 cm and is pivoted at the outside upper corners. These sheets are rotated upward through 90° for complete withdrawal. The insertion

ORNL-LR-Dwg.-26595
UNCLASSIFIED

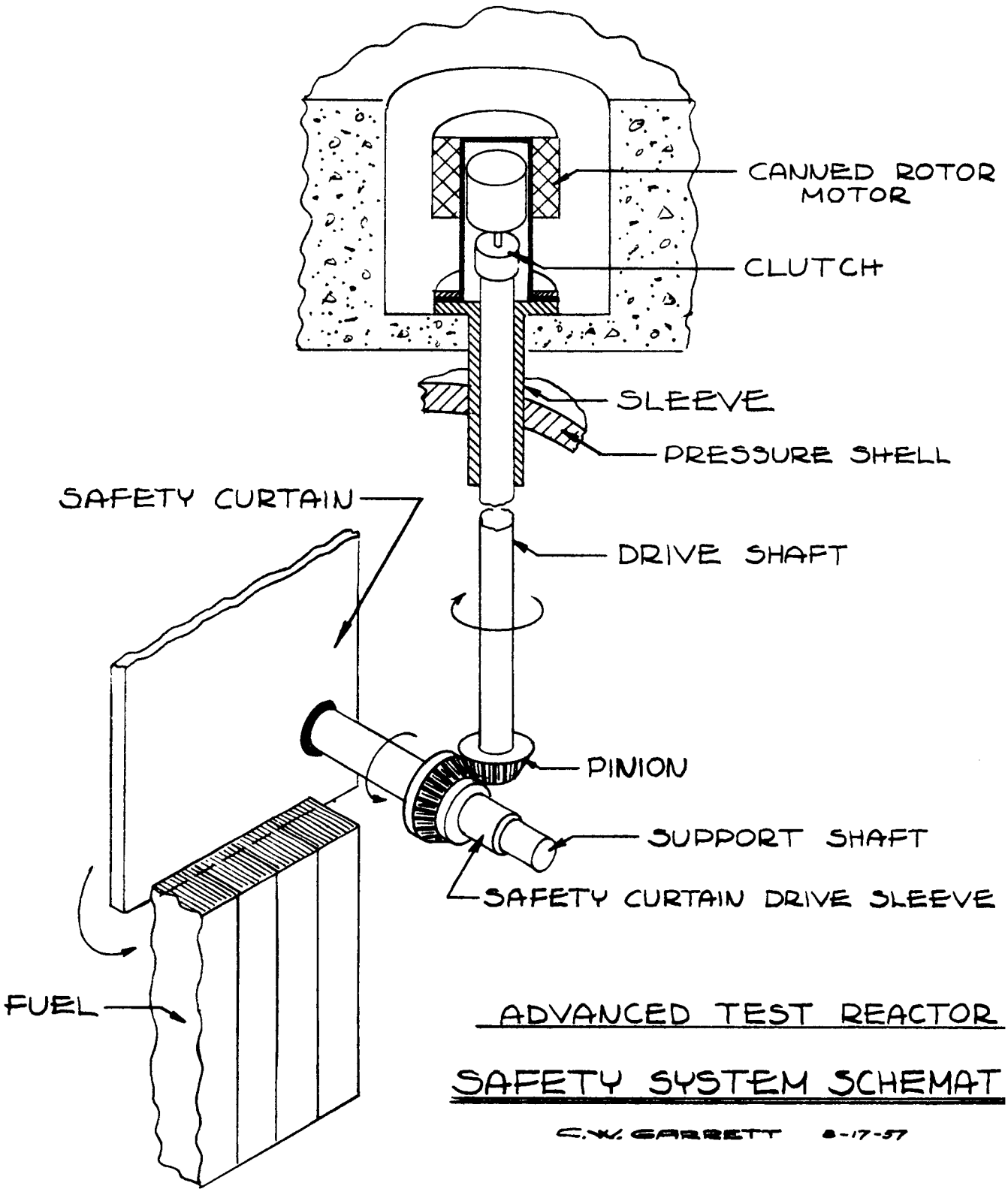

Fig 6

is by gravity plus help from down flow of the D_2O coolant with an insertion time of less than 0.4 sec. When the control elements are fully inserted the entire face of the fuel zone is covered by a curtain between the fuel and the D_2O. Each blade has a volume of 21,600 cm^3 and a mass of 173 kg. The torque exerted in the fully withdrawn position is 10.4×10^6 gm-cm.

To make an estimate of the change in k when the position is changed from withdrawn-fully to inserted-fully, the following procedure is followed in making nuclear calculations on the ORACLE using the 3G3R code. It is assumed that the effect of the cadmium curtain on k is the same as poisoning the central region for thermal neutrons. The calculations are made with and without fuel in the test region and show the curtains to be capable of shutting down the reactor with the highest fuel concentration ever likely to be tested in the central region.

The torque to remove the blades is supplied by canned motors to eliminate a mechanical seal in the head of the pressure tank. In order to allow faster insertion times the shaft is declutched between the reduction gears and the blade shaft. The high power at which the reactor operates makes a disaster so potentially costly and dangerous that the greatest possible care must be taken when the safety instrumentation is selected to actuate the safety curtains.

The shim and regulation system is designed to achieve not only shimming and regulation but, in addition, to provide flux shaping throughout the horizontal length without distrubing the flux pattern in the vertical direction. Figure 3 shows where the sixteen elements are located in the reactor. The elements are blades of cadmium jacketed with stainless steel with dimensions of 0.75 cm x 22 cm x 120 cm. These slabs move laterally in 1.27 cm wide slots in the fuel zone. The drive mechanism (Figures 3 and 7) is an adaptation of one designed at Argonne National Laboratory for use on the Argonaut.[19] It is believed that enough

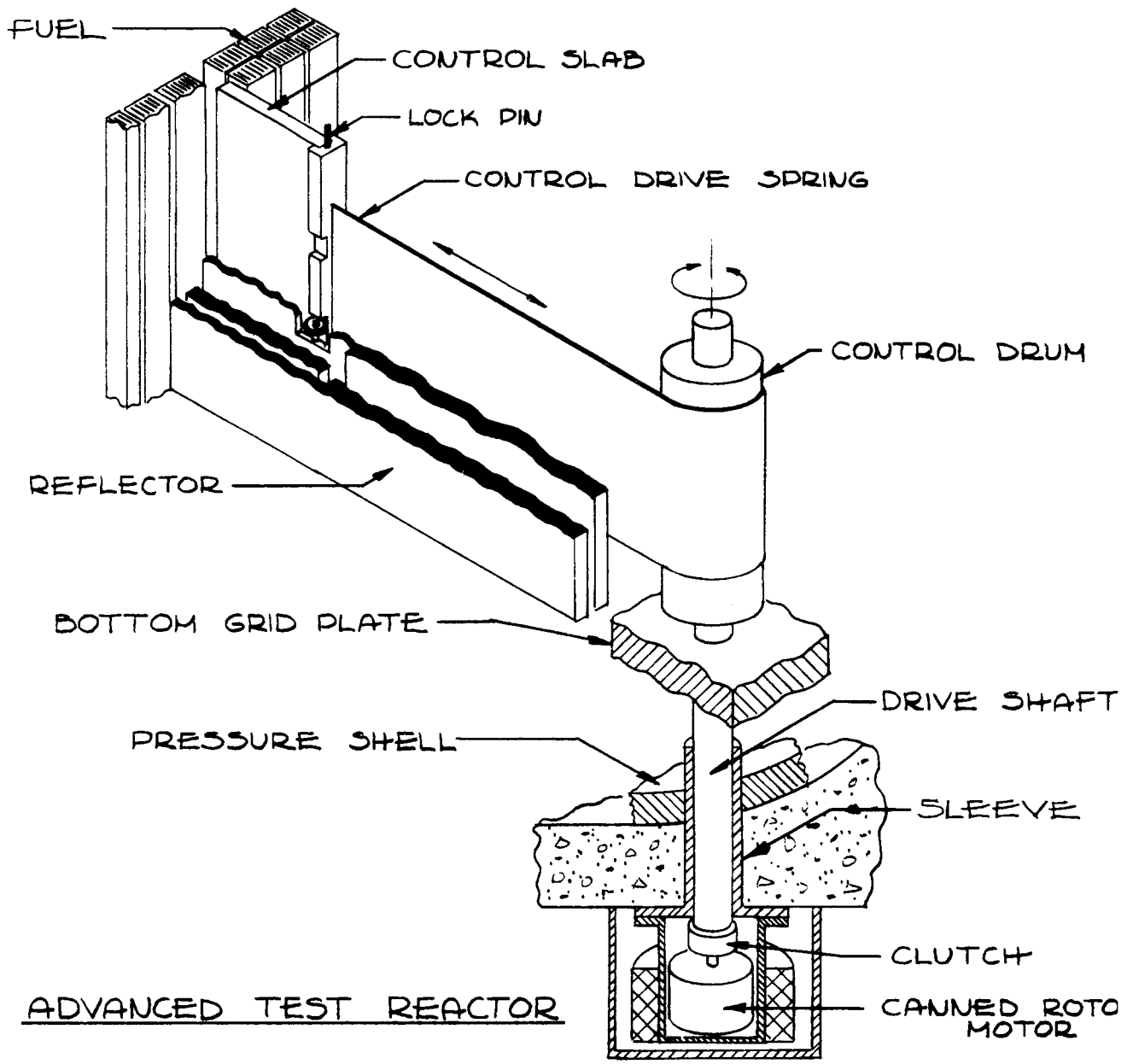

ADVANCED TEST REACTOR

CONTROL SYSTEM SCHEMATIC

C.W. GARRETT 8-18-57

Fig 7

experience has been gained with drives of this design to predict reliable service in this application. The stainless steel sheathed cadmium control elements are attached by disconnects to spring steel strips running through the aluminum reflector to aluminum drums 6.5 inches in diameter. The steel strips are wound on the aluminum drums in withdrawing the elements from the slots in the fuel. The torques for turning the drums are furnished by canned motors operating from the subpile room. When the shaft is declutched the steel strips serve as powerful springs for driving the blades into their fully-inserted positions. Snubbers are built inside the drums and use D_2O as the snubbing fluid. The same handling equipment can be used for changing both the fuel elements and the control blades so that the comparatively frequent changes of every three or four months of the cadmium plates can be made as easily as possible.

The value of $\frac{\Delta k}{k}$ for all rods inserted is estimated by homogenizing the effective cross-sectional area of the cadmium into the fuel zone for a basic case of $k = 1.298$. A plot is shown in Figure 8. No practical way is found to calculate the worth of the cadmium rods; however, experienced personnel[32] have expressed an opinion that the sixteen sheets of cadmium will furnish ample poisoning to give a $\frac{\Delta k}{k}$ large enough for all loadings and experiments planned. This, of course, needs experimental verification. If the cadmium does not give enough change in k from the withdrawn to the inserted position of the elements, then the cadmium should be replaced by a rare earth having a high epithermal cross section as well as a high thermal cross section. With the elements fully inserted, each fuel slab is divided into six compartments 6.93 cm x 20 cm and seventeen compartments 3.46 cm x 20 cm. These are far below critical size when each is considered as a system uncoupled from the others.

E. Reactor Fuel Handling

Replacement of the ninety-two fuel elements every two weeks and the control

FIGURE 8

Effect of the Mass of Cadmium in
Fuel Region on Multiplication Constant

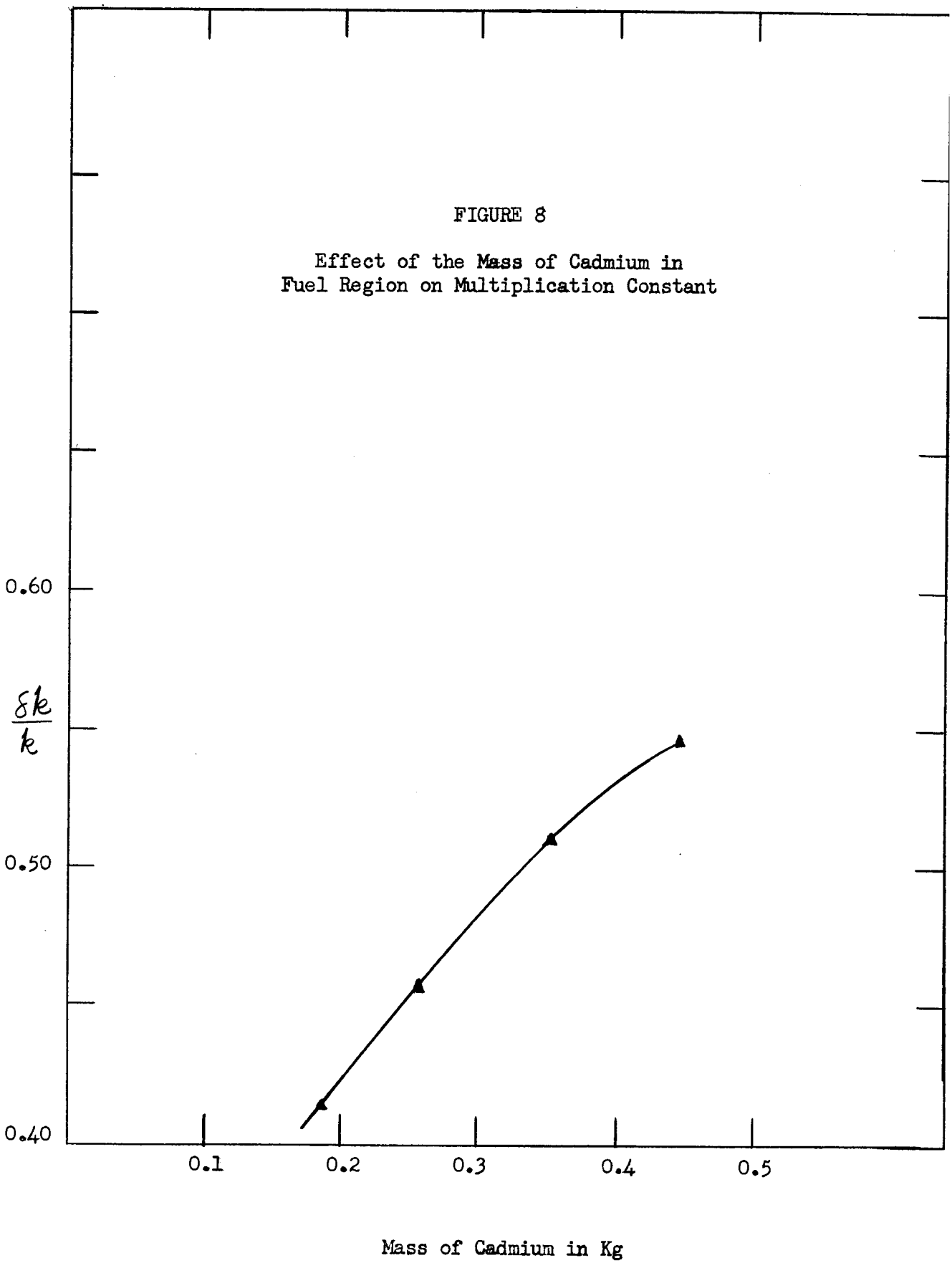

plates at about two-month intervals poses an awkward problem due to the possibility of contaminating the D_2O during the handling procedures. This danger can be circumvented, however, by the use of an indexing system and remote handling equipment which can be operated through seals. This type of equipment is already devised for other reactors and should not be an insurmountable problem for this case.

Although several types of handling systems were discussed by this study group, none were pursued in sufficient detail to warrant consideration here. Some necessary requirements of the handling equipment other than sufficient shielding are listed below.

1. The equipment must be capable of being permanently or temporarily sealed to an opening in the reactor top to protect the D_2O during handling.
2. An indexing system must be provided to properly position the equipment for removal and replacement of any desired core and reflector component.
3. A cooling system must be provided to keep the spent elements from melting due to fission product heating during transit.
4. A transfer from D_2O cooling of the removed element to H_2O cooling must be provided, possibly by an intermediate period of cooling by dry air or nitrogen.
5. An H_2O cooled storage must be provided to allow fission product partial decay prior to reprocessing of the elements.

F. Heat Production in the Central D_2O Region

The average heat distribution in the central D_2O region is depicted in Figure 9. Two sources of heat were considered; neutron elastic scattering and fission gammas. The calculations leading to this result appear in Appendix C.

The total heat produced in the central D_2O region is 9.3 MW which is 1.9 percent of the total power being generated in the reactor.

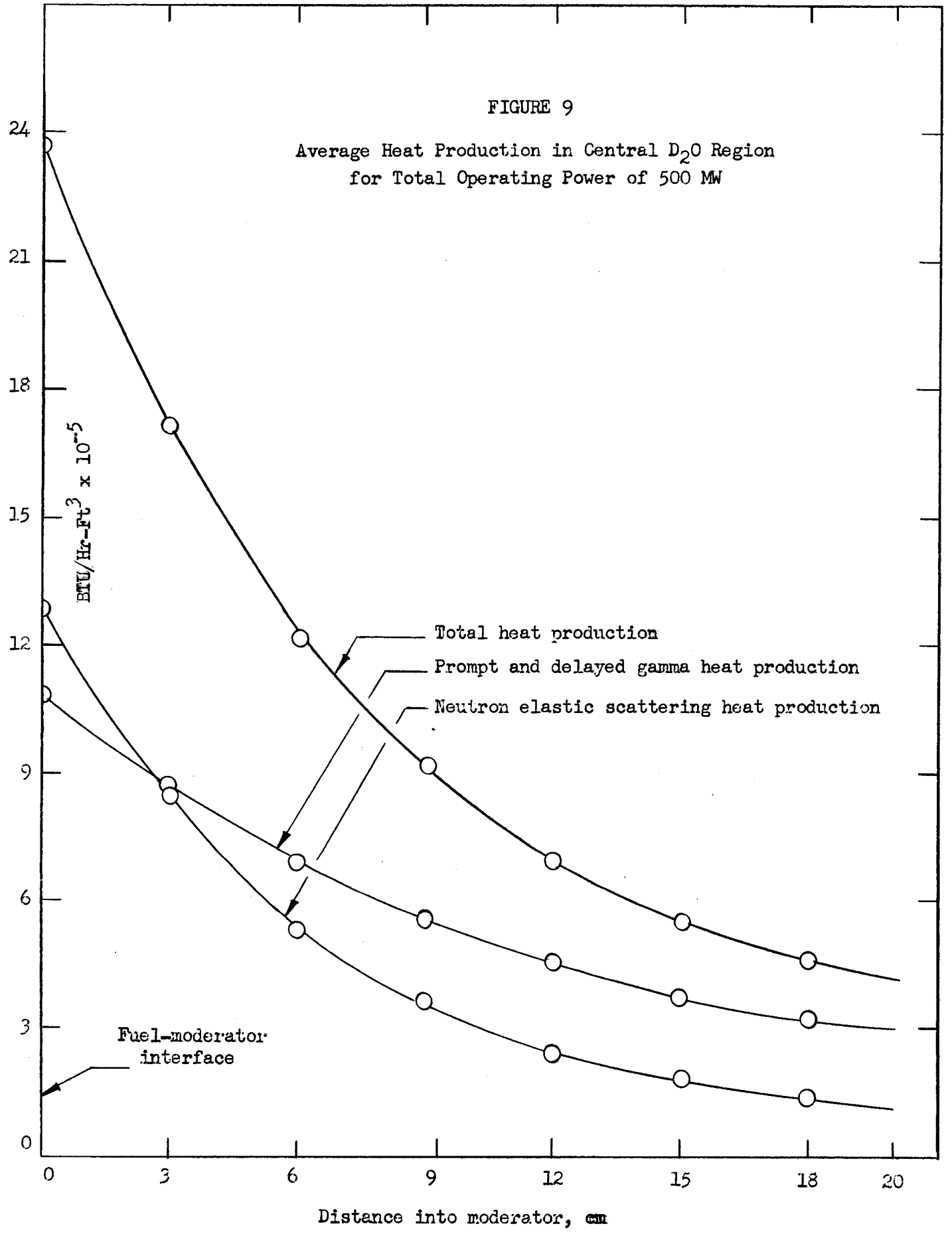
FIGURE 9
Average Heat Production in Central D_2O Region
for Total Operating Power of 500 MW
BTU/Hr-Ft^3 x 10^{-5}
24
21
18
15
12
9
6
3
0
Total heat production
Prompt and delayed gamma heat production
Neutron elastic scattering heat production
Fuel-moderator interface
0
3
6
9
12
15
18
20
Distance into moderator, cm

G. Heat Production and Heat Transfer in the Aluminum-D_2O Reflector

It has been shown that improved nuclear performance can be achieved by using an aluminum fast reflector in preference to a D_2O reflector. The ideal arrangement would be to use a solid block of aluminum as the fast reflector and have no neutron moderating material present. However, it is known that substantial quantities of heat will be deposited in the fast reflector by penetrating neutrons and gamma rays and that successful removal of this heat will require flowing a coolant through the reflector. Consequently the fast reflector is designed as laminated layers of aluminum and heavy water and so arranged that the aluminum layers are thinest where the heat production is the greatest.

The heat distribution in the reflector was obtained by considering the reflector as a homogeneous mixture of 70% aluminum and 30% D_2O and calculating the heat deposited from fission gammas, capture gammas and elastically scattered neutrons. The heat resulting from neutron captures was found to be negligible.

Figure 10 shows the contribution from each of the above sources as well as the total heat distribution throughout each reflector. The total heat produced in each reflector was calculated to be 6.75 MW which is 2.7% of the total heat produced in the reactor. The calculations which led to the above results are presented in Appendix B.

An estimate of the coolant flow rate required to limit the maximum hot-spot temperature rise in the reflector to less than 220°F is given in Appendix B. The maximum hot-spot occurs at the interface between the core and reflector. At this location, aluminum slabs 2.5 cm thick are separated by a D_2O coolant gap of 1 cm. The coolant velocity required at this location to keep the temperature rise within allowable limits was found to be 20 ft/sec. At other locations within the reflector the coolant velocities can be lowered appropriately.

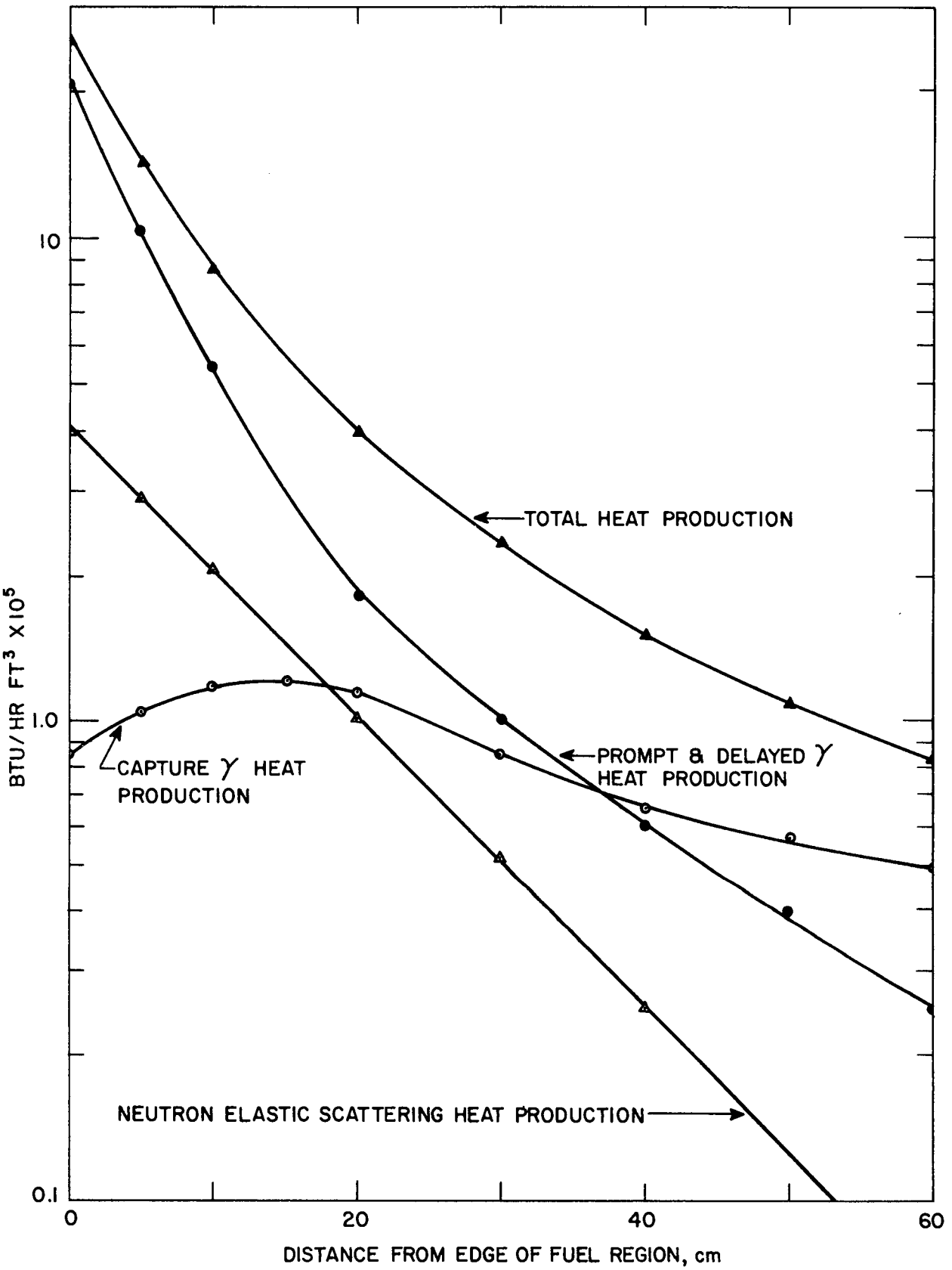

Fig. 10. Average Heat Distribution in Homogenized Side Reflectors. Reflector composition: 70% Al, 30% D_2O; Based on total operating power of 500 mw.

This investigation has been directed toward determining the feasibility of removing heat deposited in the fast reflector. Insufficient time was available to permit optimization of the reflector design, and a more detailed analysis should be made before selecting the final composition.

IV. REACTOR CORE ANALYSIS

A. General

The limiting criteria which establish the basis for this design study are listed in Section I-B. In addition, certain other limitations were adopted very early in the study. The combination of these forms the basis for the design of the reactor core. The criteria thus established are:

1. Total reactor thermal power should not exceed 500 megawatts.
2. The reactor should be designed to deliver a thermal flux not less than 1×10^{15} to four fuel experiments housed in 20 centimeter diameter test holes.
3. Core life should exceed seven days.
4. The core should be heterogeneous.
5. The fuel should be fully enriched U^{235} in the form of a uranium-aluminum alloy.
6. The fuel element structural material should be aluminum.
7. D_2O should be used as coolant and moderator.

It is seen that the materials to be used in the core are chosen; the problem remaining is the selection of a suitable concentration for the materials and the choice of a geometry and dimensions which will provide for the delivery of the required flux to the experiments within the limits of power and core life listed.

B. The Power Equation and its Implications

The general power equation for the fuel zone of a reactor is

$$P = \omega \int_{\text{Fuel}} \int_{\text{Energy}} \Sigma_f(E, \underline{r})\, \phi(E, \underline{r})\, dE\, d^3r \qquad \text{IV-1}$$

where P is the power generated in megawatts;

ω is a power conversion constant, generally taken as 3.23×10^{-16} megawatts/fission;

$\Sigma_f(E, \underline{r})$ is the macroscopic fission cross-section as a function of space and neutron energy expressed in cm^{-1};

$\phi(E, \underline{r})$ is the neutron track-length or flux as a function of space and energy.

If it is assumed that the fuel is homogeneously distributed, equation IV-1 reduces to

$$P = \omega \int_{Fuel} \left[\Sigma_{f_1} \phi_1(\underline{r}) + \Sigma_{f_2} \phi_2(\underline{r}) + \Sigma_{f_3} \phi_3(\underline{r}) \right] d^3 r \qquad \text{IV-2}$$

for the special case of three neutron energy groups. Σ_{f_i} is now the appropriately flux-averaged fission cross section for the i-th group and ϕ_1, ϕ_2, and ϕ_3 denote the fast, intermediate and thermal track-lengths. In terms of average track-lengths, equation IV-2 becomes

$$P = \omega \left(\Sigma_{f_1} \bar{\phi}_{1F} + \Sigma_{f_2} \bar{\phi}_{2F} + \Sigma_{f_3} \bar{\phi}_{3F} \right) V_F \qquad \text{IV-3}$$

where V_F is the volume of the fuel region, and the subscript F on $\bar{\phi}$ also denotes the fuel region. For 500 megawatts power, equation IV-3 may be rewritten as

$$\phi_{3F} = \frac{1.174 \times 10^{16}}{RM}. \qquad \text{IV-4}$$

Where M is the mass of U^{235} in the reactor in kilograms.

$$R \equiv 1 + \frac{\Sigma_{f_1} \bar{\phi}_{1F} + \Sigma_{f_2} \bar{\phi}_{2F}}{\Sigma_{f_3} \bar{\phi}_{3F}},$$

and it is assumed that the average thermal fission cross section of U^{235} is 515 barns. As a consequence of equation IV-4, it is seen that one or both of

two conditions must be satisfied in order for a 500 megawatt reactor to deliver an experiment flux greater than 10^{15}. This high flux may be obtained by minimizing the mass of fuel in the reactor or by creating a high flux at the experiment while keeping the average fluxes in the fuel low. In view of the latter possibility, let a peaking factor, Pe, be defined by

$$Pe \equiv \frac{\hat{\Phi}_{3E}}{\bar{\Phi}_{3F}}$$

where $\hat{\Phi}_{3E}$ is the peak thermal flux in the experiment region and

$\bar{\Phi}_{3F}$ is the average thermal flux in the fuel.

If this identity is substituted in equation IV-4, the result is

$$\hat{\Phi}_{3E} = 1.174 \times 10^{16} \frac{Pe}{RM} \qquad \text{IV-5}$$

The peak flux in the experiment region of the reactor is thus shown to be directly porportional to the quantity Pe/RM. Consequently, this quantity will be designated as "core effectiveness" and used as a parameter by which the worth of various core configurations may be compared.

C. Core Geometry

Traditionally the best shape for a nuclear reactor is that of a sphere. Cylinders are considered second in desirability while the rectangular parallepiped or, more simply, slab geometry is third. This ranking is based upon the desirability of obtaining a minimum surface to volume ratio since this condition provides minimum probability of neutron leakage. Design deviations from this ranking are usually predicted upon the practical difficulties encountered in arranging for heat transfer, control, fuel placement, etc.

There are, however, certain special considerations which affect the choice of basic geometry for this reactor which do not fall into the categories mentioned above. Four experiment facilities are desired and it seems likely that these

must be placed inside the fuel zone in order to obtain the desired experiment flux. In addition, a minimum of inter-experiment flux perturbation is desirable, so that the facilities must be separated from one another as much as possible. If a spherical core is eliminated as impractical, the problem is reduced to choosing between two geometries, the cylinder and the slab. The possible arrangement of the experiments and fuel for each of these geometries is shown in Figure 11.

It is seen that the choice between the two geometries may depend upon:

1. The minimum experiment spacing. The spacing which will produce equal interaction may be different for the two cases.
2. Central region volume required. When the experiment positions have been chosen, there still remains a choice of the optimum distance between experiment and fuel. The volume of the inner region will help to determine the amount of fuel required to produce the desired reactivity.
3. The flux peaking achievable. In the slab geometry the experiments are on the centerline in one dimension and will benefit automatically from the high flux produced at the center of a multiplying system. In the cylinder, the experiments are off-center, but are surrounded by fuel.
4. Perturbation produced by the experiments. It is likely that the introduction of experiments will depress the flux somewhat differently in the two arrangements.

In the time available for this study, it was not possible to consider quantitatively all of the above questions. One attempt was made to compare the two systems directly by means of three-group, three-region calculations using the ORACLE[5]. The two cores considered each contained 18.55 kg of U^{235} and were 180 centimeters in height. A fuel concentration of 9.18×10^{19} U-235 atoms per cm^3 and a metal-to-water ratio of .73 were used on the basis of the results of a

FIGURE 11

Comparison of Cylindrical and Slab Geometries

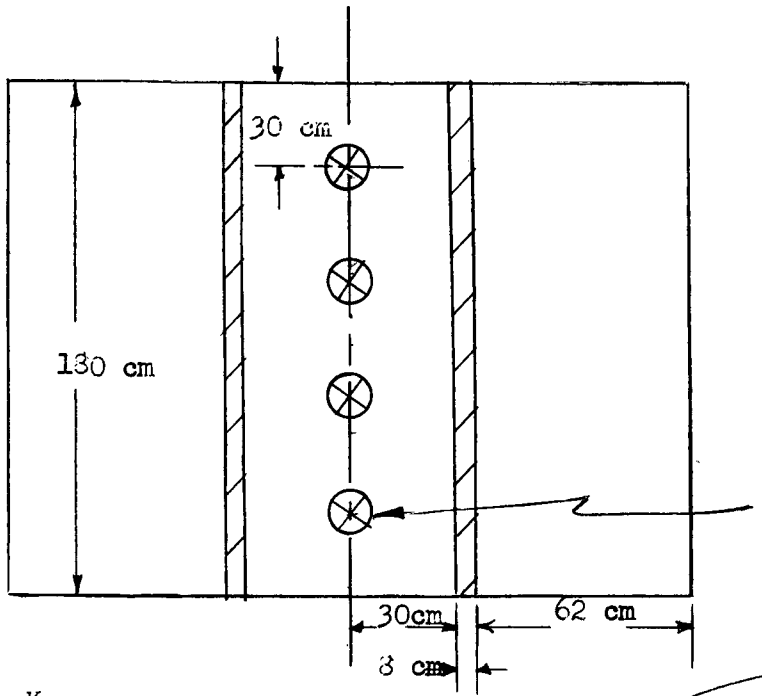

Slab

Pe/RM = .0732

k_{eff} = 1.12

Loading = 18.55 Kg

4 20-cm dia. experiment tubes 40 cm apart

Key

fuel region

moderator region

contemplated experiment locations

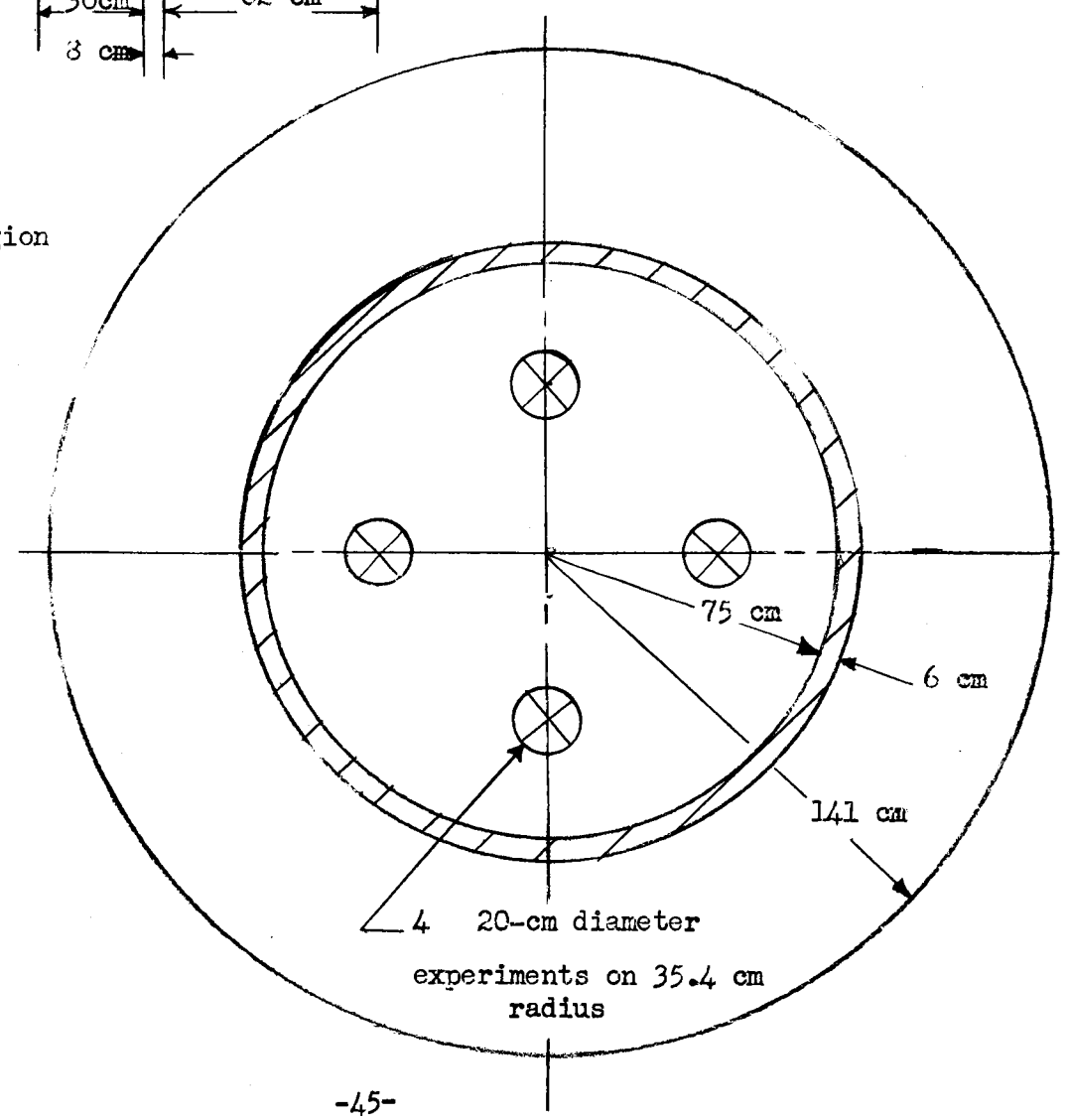

Cylinder

Pe/RM = .0596

k_{eff} = 1.08

Loading = 18.55 Kg

previous study[1]. The absorbing characteristics of the experiments were simulated by using group constants for 30% aluminum, 70% D_2O in the central region. Both systems used D_2O reflectors. Reflector savings of 20 centimeters was assumed for the directions not computed. The results of the computations and dimensions used are shown in Figure 11. Although the slab geometry appears superior both in reactivity and in core effectiveness, it is not certain that a valid comparison of the two geometries has been made. However, on the basis of these results, it was decided to restrict further calculations to the slab geometry for fuel concentrations in the 10^{19} atoms U-235 per cm^3 range. Several additional cylinder calculations were made using more dilute fuel and a slightly different arrangement of the fuel and experiments. These calculations are discussed in detail in Section IV-E.

For the more concentrated fuel loadings, calculational attention was directed toward the slab geometry. Early calculations indicated that experiment fluxes of the order of 10^{15} could probably not be achieved over a 180 cm high core. The core height was therefore changed to 120 cm without any attempt at optimization of this dimension since it was believed that the optimum length would depend to a great extent upon the axial flux variation in the experiments. However, 120 centimeters is considered to be adequate, although it is recognized that a greater core height might be desirable. Except where specified, all slab geometry calculations discussed in the following sections are for a reactor height of 120 centimeters, and reflector savings of 40 centimeters (20 centimeters per side) added to these dimensions. The effect upon the reactor of the value of reflector savings used is discussed in the following section. See Appendix A for information regarding the three-group constants used in the calculations.

D. Heavily-Loaded Slab Geometry Calculations

Notation: Before entering into a full-scale discussion of the results of the many three-group, three-region ORACLE calculations performed for the slab geometry type reactor, a short deviation to define the notational conventions to be used is considered desirable. First, unless otherwise specified, all calculations refer to the X-direction dimension of the reactor as illustrated in Figure 12. The reactor is considered as bare in the Y and Z directions for computational purposes. Reflector savings are added to the core dimensions as specified in Section IV-C.

Dimensions used are to be interpreted as referring to the half-reactor from the centerline out. For instance, a region 2 thickness of 20 centimeters means that the total region 2 volume in the reactor is 40 cm x 120 cm x 180 cm. Flux plots will be shown from the centerline out.

Core effectiveness, Pe/RM, which is used extensively as a measure of reactor worth was derived and discussed briefly in Section IV-B. In this connection it should be noted that Pe as used in this section is computed on the basis of X-direction peaking only and may be thought of as measuring the thermal flux in the experiment zone at those points where the Y and Z components of the flux are equal to their average value. ϕ_{ij} refers to the flux of the i-th group in the j-th region; for example, ϕ_{12} denotes the fast group flux in region 2.

Fuel concentrations are given in terms of homogenization throughout the fuel region. M/W is used in the conventional sense as metal to water volume ratio.

Choice of Reflector: Although it is generally recognized that use of D_2O as a reflector material will minimize the probability of neutron leakage from a reactor and thus reduce the critical mass for a given core size, it was considered possible that D_2O was not the best reflector for a high flux reactor design. An additional virtue of D_2O reflection for a power reactor is the reduction of the

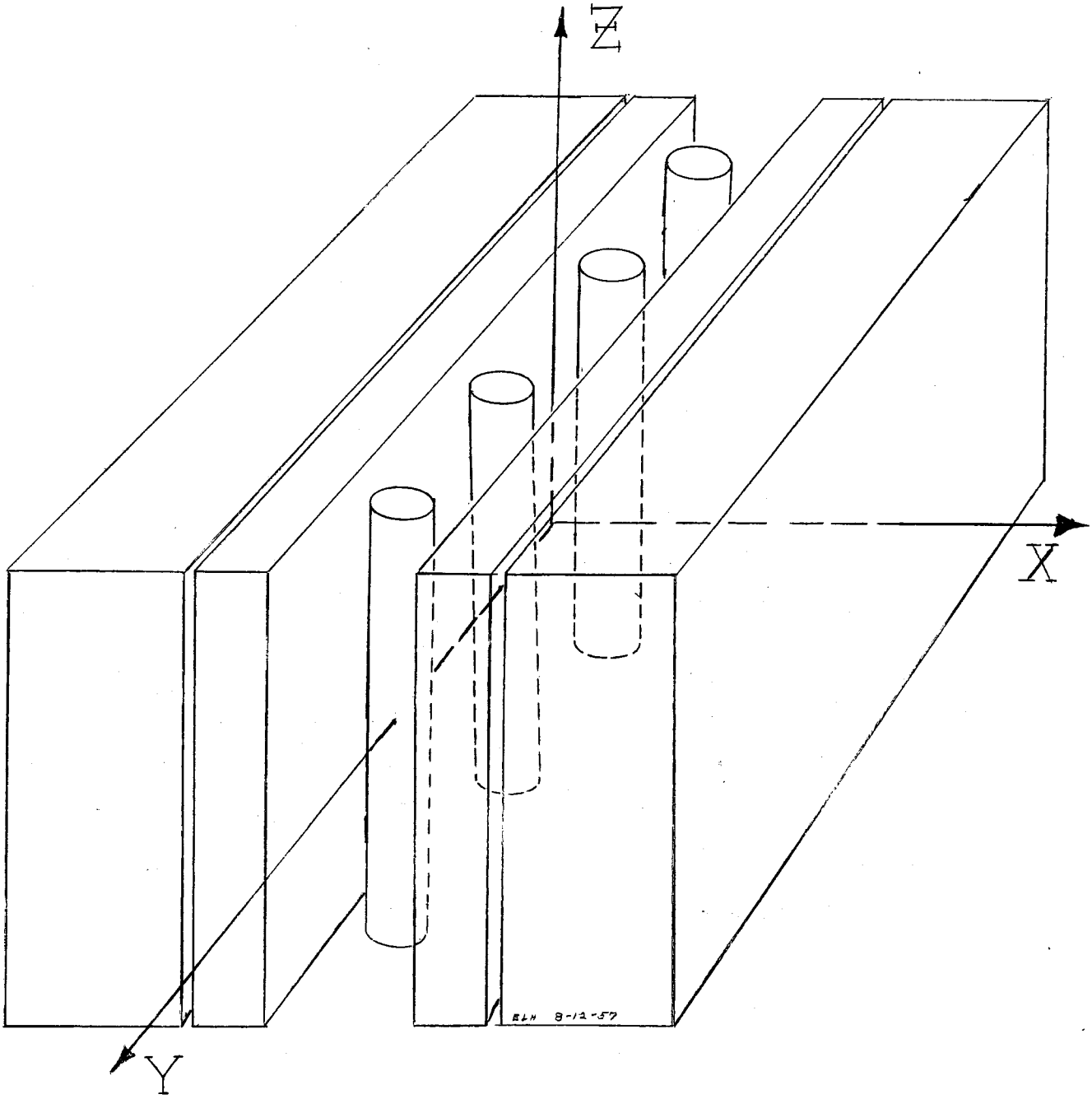

FIGURE 12

Illustration of Dimensional Notation

peak to average flux ratio, thereby increasing the usefulness of fuel near the edge of the core. However, since a high-peaked thermal flux in the center of the reactor is desired in this reactor, consideration was given to other types of reflectors. If a material could be employed which would reflect fast and intermediate neutrons back through the core into the D_2O region at the center of the reactor, there to be thermalized, a higher peak thermal flux might result. It would be desirable from a critical loading viewpoint for the reflector to return as m thermal neutrons as possible while at the same time retaining its fast neutron reflective properties. What is desired, then, is a reflector with a large elastic scattering cross-section, large atomic mass (to reduce the energy loss per collision) and low absorption and inelastic scattering cross-sections. Unfortunately a material which satisfies all of these requirements perfectly does not exist. However, aluminum and zirconium, alone or in combination with D_2O as a coolant, are outstanding candidates. The properties of the reactor with constant fuel mass for various types of reflectors are pictured in Figure 13.

It is seen that the requirements of reactivity and high Pe/RM are in direct opposition. For this reason, it was considered desirable to study aluminum, zirconium, and D_2O reflectors in greater detail in order to determine which would be more suitable. Since a coolant must be provided for the metallic reflectors, 30 volume percent of D_2O was included for the calculation of the group constants. It is emphasized that this percentage is probably not an optimum value, but was chosen on the basis of approximate calculations which indicated that the heat produced in the reflector could easily be removed at a metal-to-water ratio of 7/3.

Values of k_{eff} versus fuel mass for each reflector type are plotted in Figure 14. Pe/RM versus fuel zone thickness is shown in Figure 15. The same quantities as a function of U-235 number density for constant fuel region thickness are shown in Figures 16 and 17. Typical flux plots for each type of reflector are presented

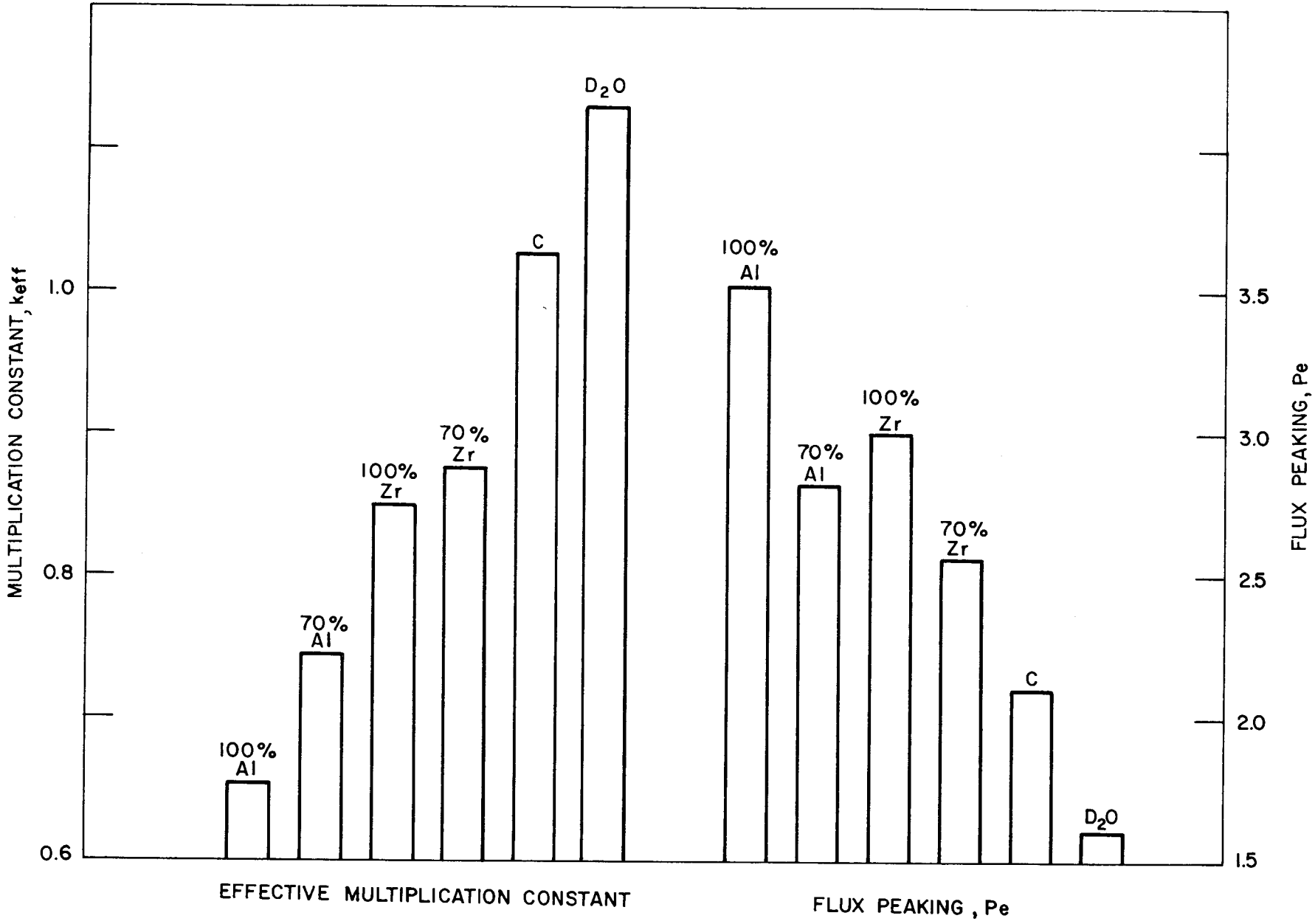

Fig. 13. Effect of Various Reflectors on Reactivity and Flux Peaking.

ORNL-LR-Dwg.-26598
UNCLASSIFIED

ORNL-LR-Dwg.-26599
UNCLASSIFIED

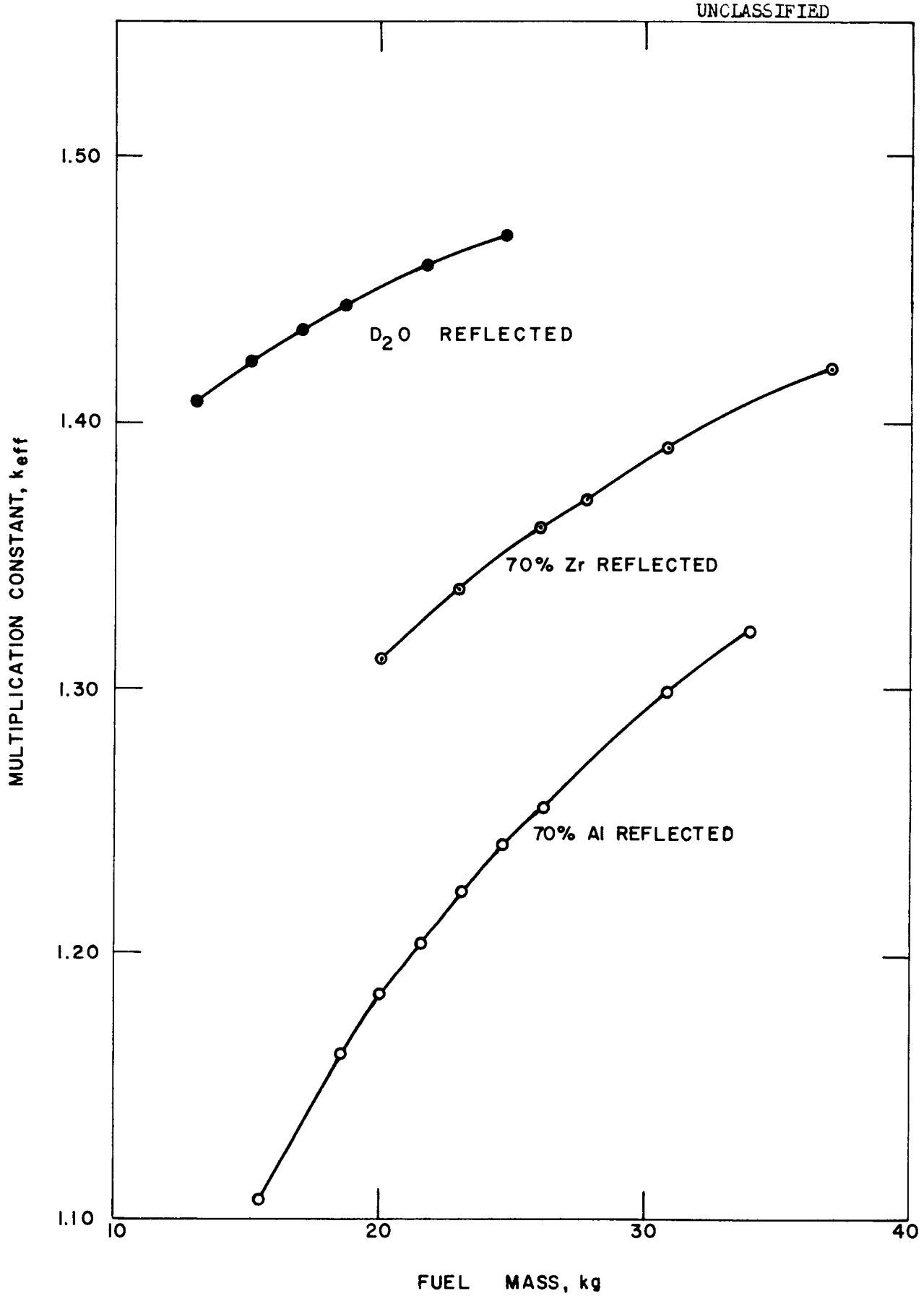

Fig. 14. Multiplication Constant (k_{eff}) vs Fuel Loading for Three Types of Reflectors.

ORNL-LR-Dwg. -26600
UNCLASSIFIED

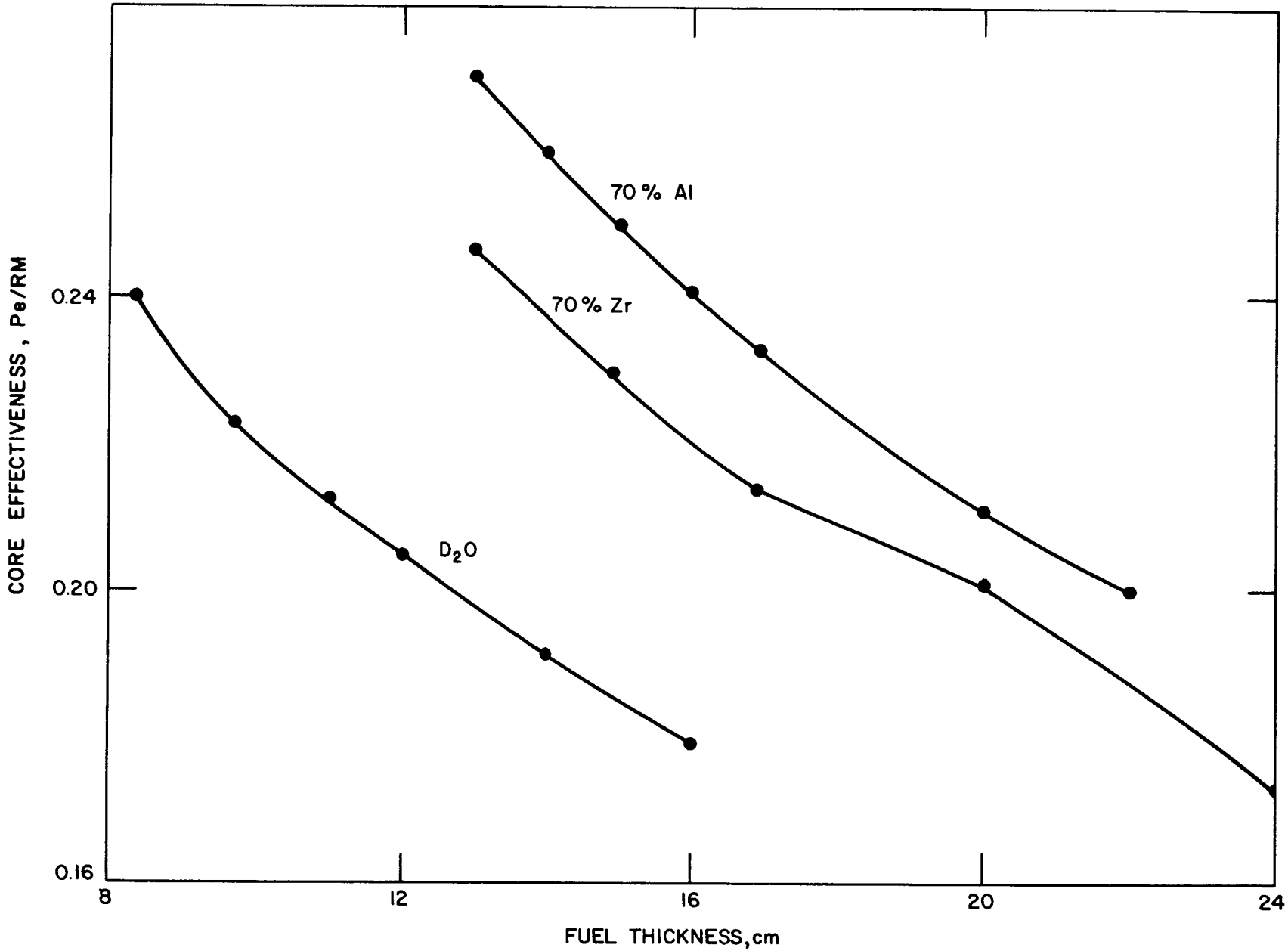

Fig. 15. Core Effectiveness (Pe/RM) vs Fuel Thickness for Various Reflectors, $Nu = 9.18 \times 10^{19}$.

ORNL-LR-Dwg.-26601
UNCLASSIFIED

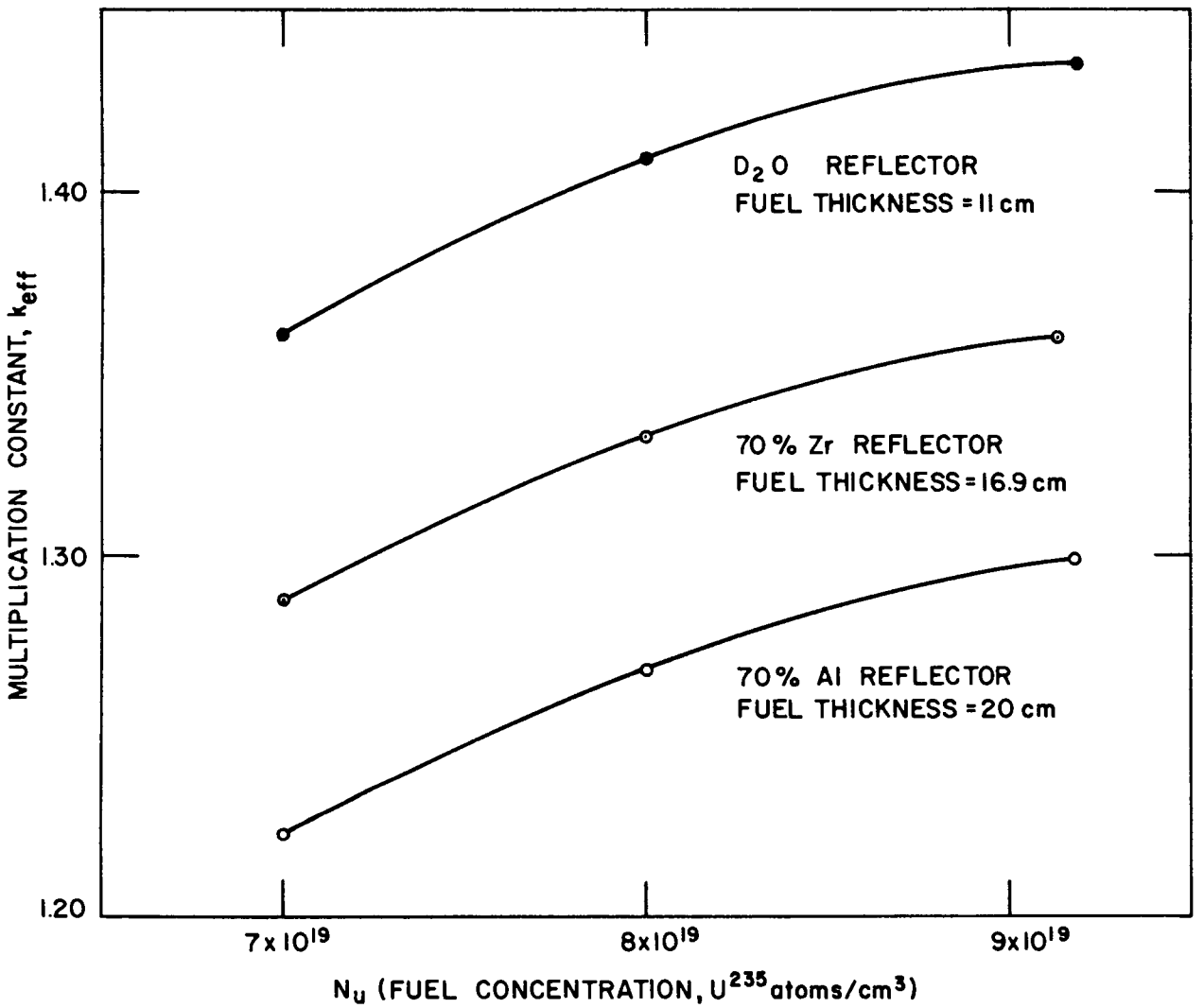

Fig. 16. Multiplication Constant vs Fuel Concentration for Typical Fuel Zone Thickness for Three Types of Reflectors.

ORNL-LR-Dwg.-26602
UNCLASSIFIED

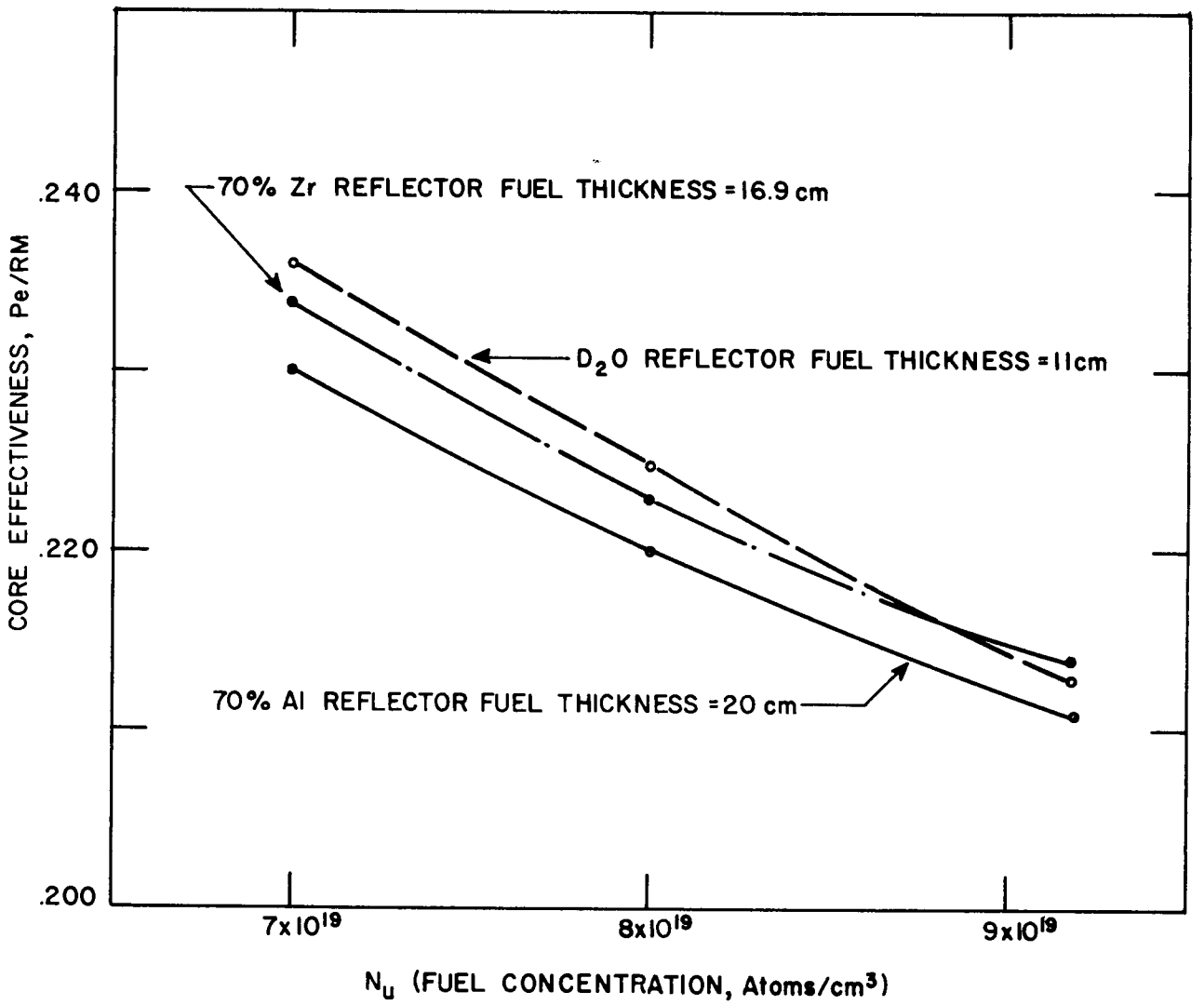

Fig. 17. Core Effectiveness (Pe/RM) vs Fuel Concentration for Three Types of Reflectors for Typical, Constant Fuel Zone Thickness.

in Figures 18, 19 and 20. It is seen that the same considerations which were evident in Figure 13 still apply. That is, for a given U-235 loading, the use of a D_2O reflector will produce the largest k_{eff}, but the lowest Pe/RM. From these results, the following general statements may be inferred either directly or by extrapolation:

1. In terms of nuclear considerations only any one of the three reflector types might be used to produce the desired experiment flux.
2. For a given k_{eff}, the highest value of Pe/RM would probably be obtained by D_2O reflection.
3. For a given k_{eff}, the largest $\delta k/\delta M$, hence shortest core life, would be obtained with D_2O reflection.
4. For a given flux at the reactor centerline, the lowest power density, both peak and average, is obtained by aluminum reflection. See Figure 21.
5. The lowest peak to average power density ratio is obtained by D_2O reflection.

Since it was not considered possible to spend more time in detailed analysis of the merits of the three types of reflectors, the aluminum reflector was chosen for further study primarily because of considerations 3 and 4. Approximate calculations indicated that core heat removal would probably be a very difficult problem and might in consequence be the determining factor in reflector choice. It was not clearly established that an insufficient core life would result from the use of D_2O reflection, but this might also be a limiting factor. Many considerations were not taken into account explicitly in comparing the three systems. These include:

1. Initial costs.
2. Maintenance and replacement costs.
3. Interference with the design of other parts of the reactor.
4. Fuel processing costs.

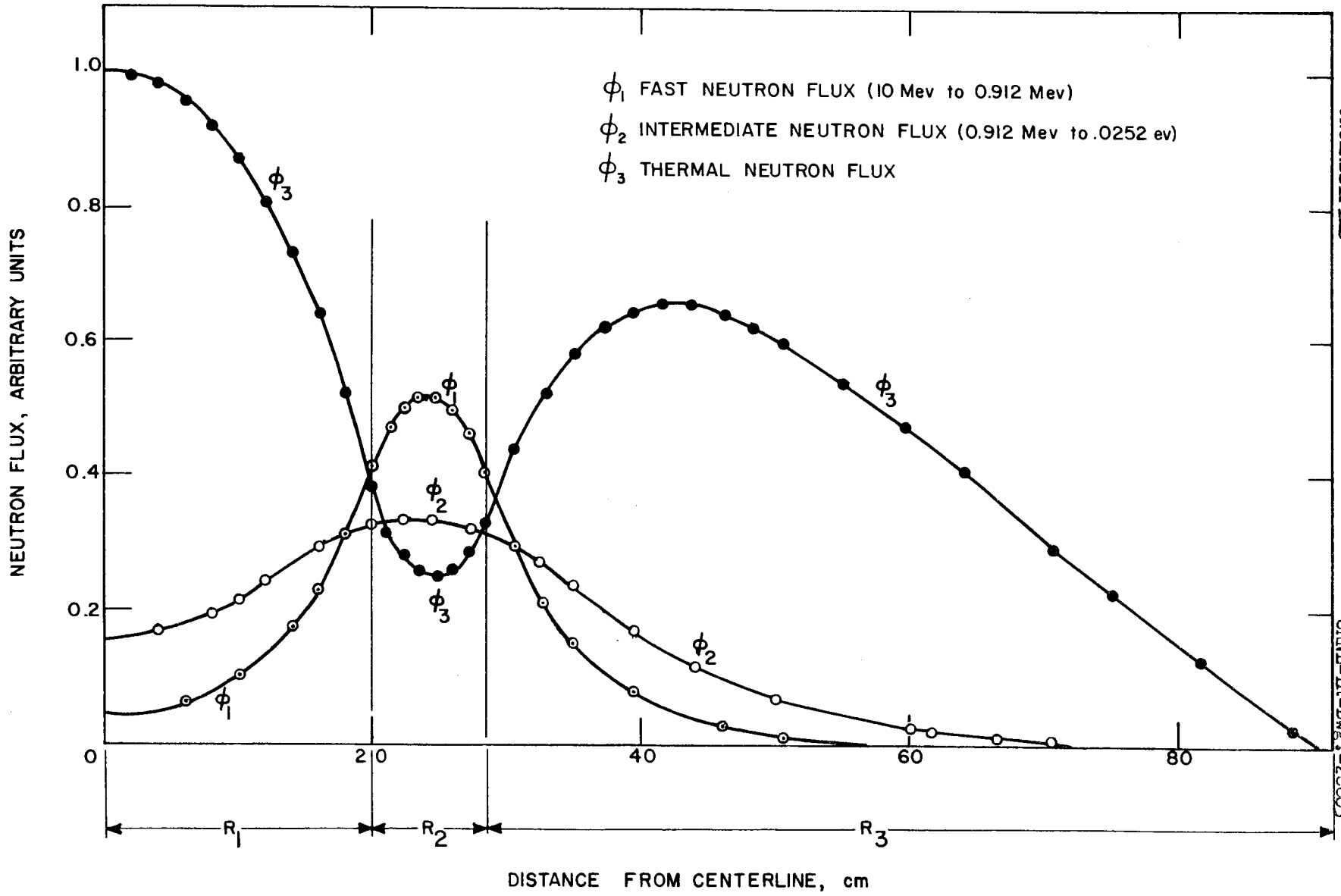

Fig. 18. Typical Flux for a D_2O Reflected Core, k_{eff} = 1.42

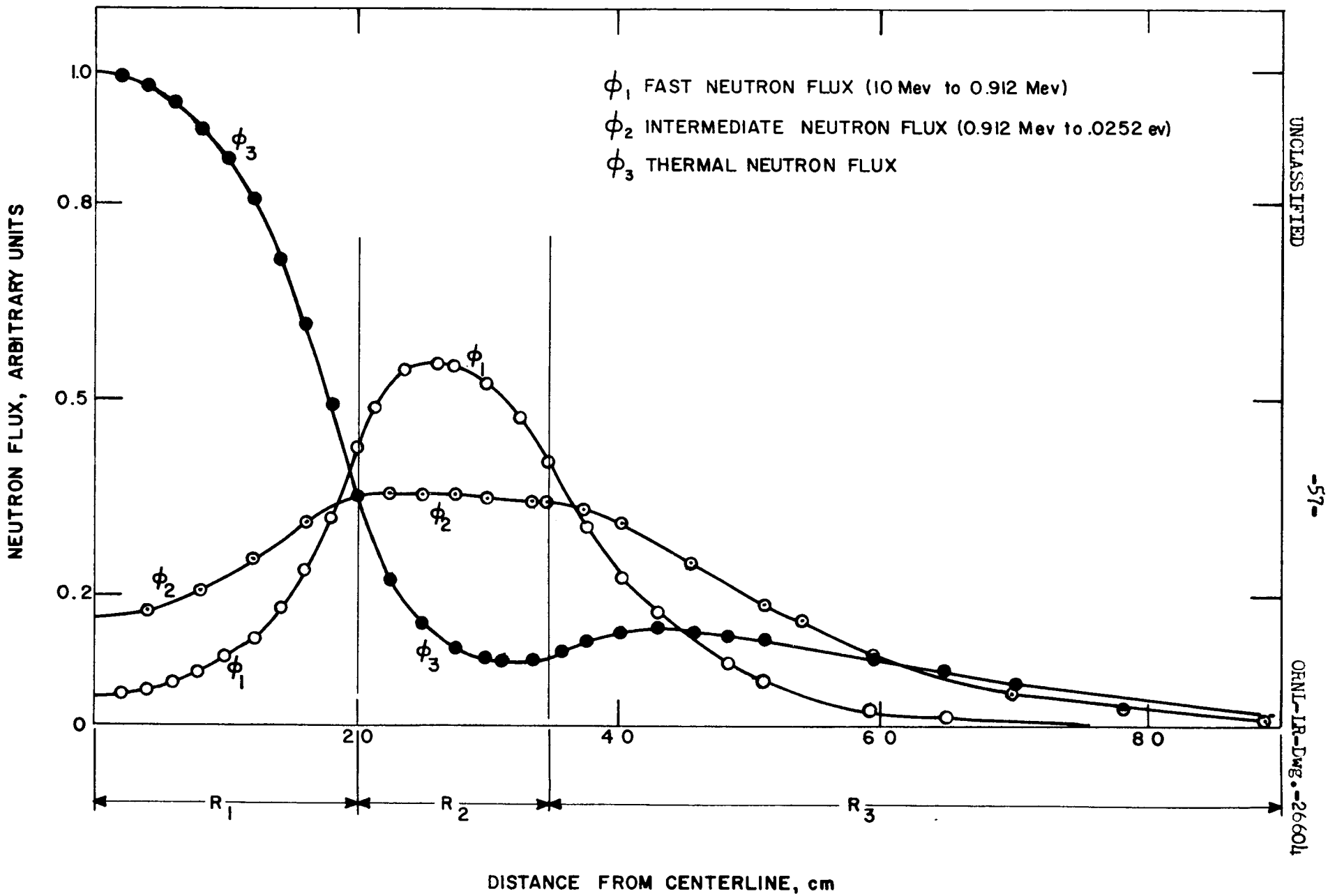

Fig. 19. Typical Flux Plot for a 70% Zirconium Reflected Core, $k_{eff} = 1.34$

UNCLASSIFIED

ORNL-LR-Dwg.-26604

ORNL-LR-Dwg.-26605
UNCLASSIFIED

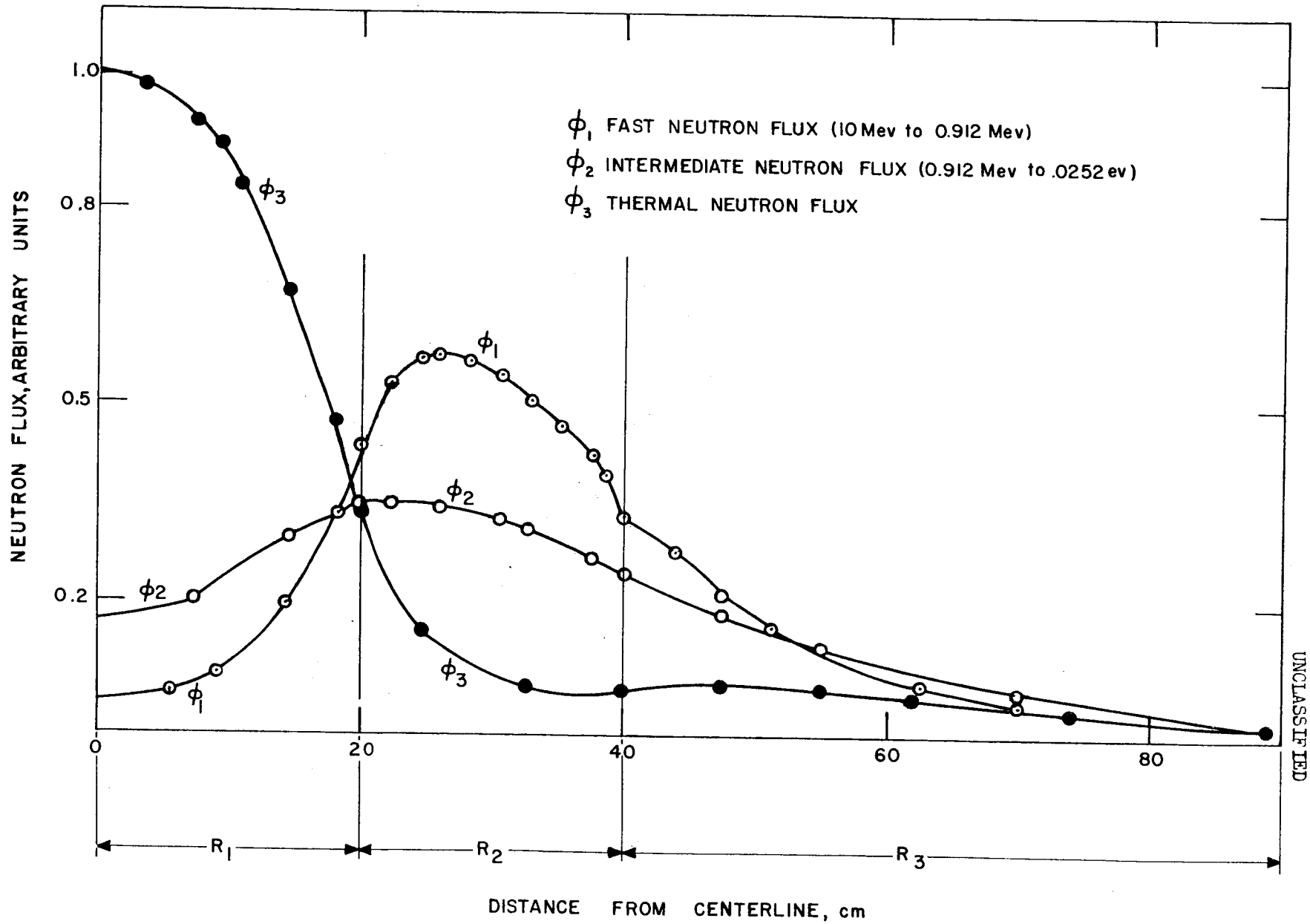

Fig. 20. Typical Flux Plot for 70% Al Reflected Core, $k_{eff} = 1.30$

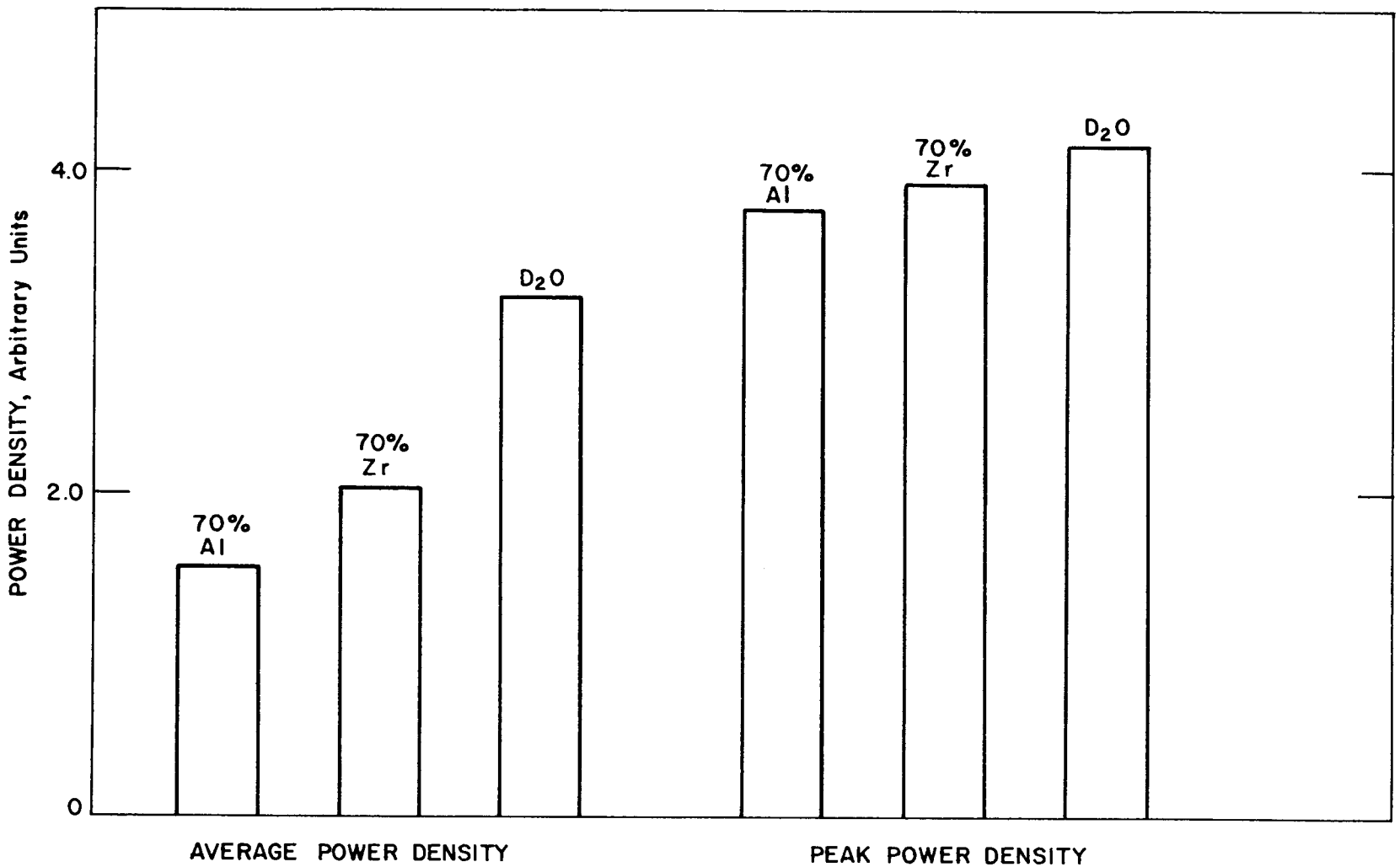

Fig. 21. Peak and Average Power Densities Required to Deliver Equal Experiment Fluxes for Various Types of Reflectors, $N_u = 9.18 \times 10^{19}$

ORNL-LR-Dwg.-26606
UNCLASSIFIED

5. Relative validity of the calculated results. See Section IV-E.

Item 4 above, while perhaps the greatest economic discrepancy between the systems, is not as large a factor as might be expected. While it is true that approximately three times as much fuel is required per core loading for the aluminum reflected reactor, it is also true that the average core life of the aluminum reflected reactor is considerably longer than that of a D_2O reflected reactor. This increase in life is a consequence of lower loss in reactivity per kilogram burned and of the better xenon overide characteristics of the aluminum-reflected reactor (since it operates at a much lower flux). Xenon poisoning calculations are discussed in Appendix D-3.

Zirconium reflection, which occupies the middle ground between the aluminum and D_2O systems, might well prove desirable if heat transfer problems can be overcome. Other questionable factors are the high cost and limited availability of hafnium-free zirconium.

Choice of Fuel Zone Parameters: Once the choice of reflector material is made, it becomes desirable to optimize the region 1 and region 2 parameters for the system. It should be pointed out, however, that the parameters for a given region are not independent of those chosen for the other two regions. This statement applies most obviously to the choice of fuel zone thickness, which is very much dependent upon the type of reflector material chosen. It is considered likely that the same condition applies to the choice of all other core parameters. Conversely, of course, the choice of fuel zone parameters may also affect the relative performance of the various reflector types. However, a complete analysis of all variables was not possible in the limited time available for this study. It does appear that variables for the regions not under study were fortunately chosen at or near their optimum values, so that results for the parameters of a given region are considered to be reasonably valid.

Region 2 variables include thickness, metal-to-water ratio, and fuel concentration. The effect of fuel zone thickness upon k_{eff}, Pe, and Pe/RM is shown in Figure 22. It is seen that the choice of thickness depends primarily upon the k_{eff} desired for the reactor. A thickness of twenty centimeters was chosen to produce a k_{eff} of 1.3, since approximate calculations indicated that some 30% excess reactivity would be necessary to counteract the effects of temperature, burnout, fission product poisoning, and possible experiment poisoning. If a lower value of k_{eff} could be used some slight gain in flux delivered to the experiment zone could be achieved by reducing either the fuel thickness or concentration.

The effect of varying fuel concentration upon k_{eff} and Pe/RM is shown in Figure 23. Since there were a limited number of concentrations for which three-group constants were available, a concentration of 9.18×10^{19} atoms per cubic centimeter was chosen from these values. The results of previous calculations[1] indicated that this concentration might be an upper limit because of metallurgical and heat transfer limitations. Thus, this parameter is to be considered as optimized to an approximate degree only. It is quite likely that another concentration near this value might prove more desirable.

The same limitation applies to the value of metal to water ratio, which was chosen to be .73. The variation in k_{eff} and Pe/RM as a function of this parameter are shown in Figure 24. However, only a very few cases were computed. The actual optimum value of this parameter will depend upon a detailed analysis of both nuclear and heat transfer properties. Such an analysis would require much more time than was available for this study.

<u>Region 1 Parameters</u>: The central zone of the reactor was considered to contain four experiment tubes 20 centimeters in diameter surrounded by a large volume of D_2O which serves as a source of <u>thermal</u> neutrons. Variables in this region include

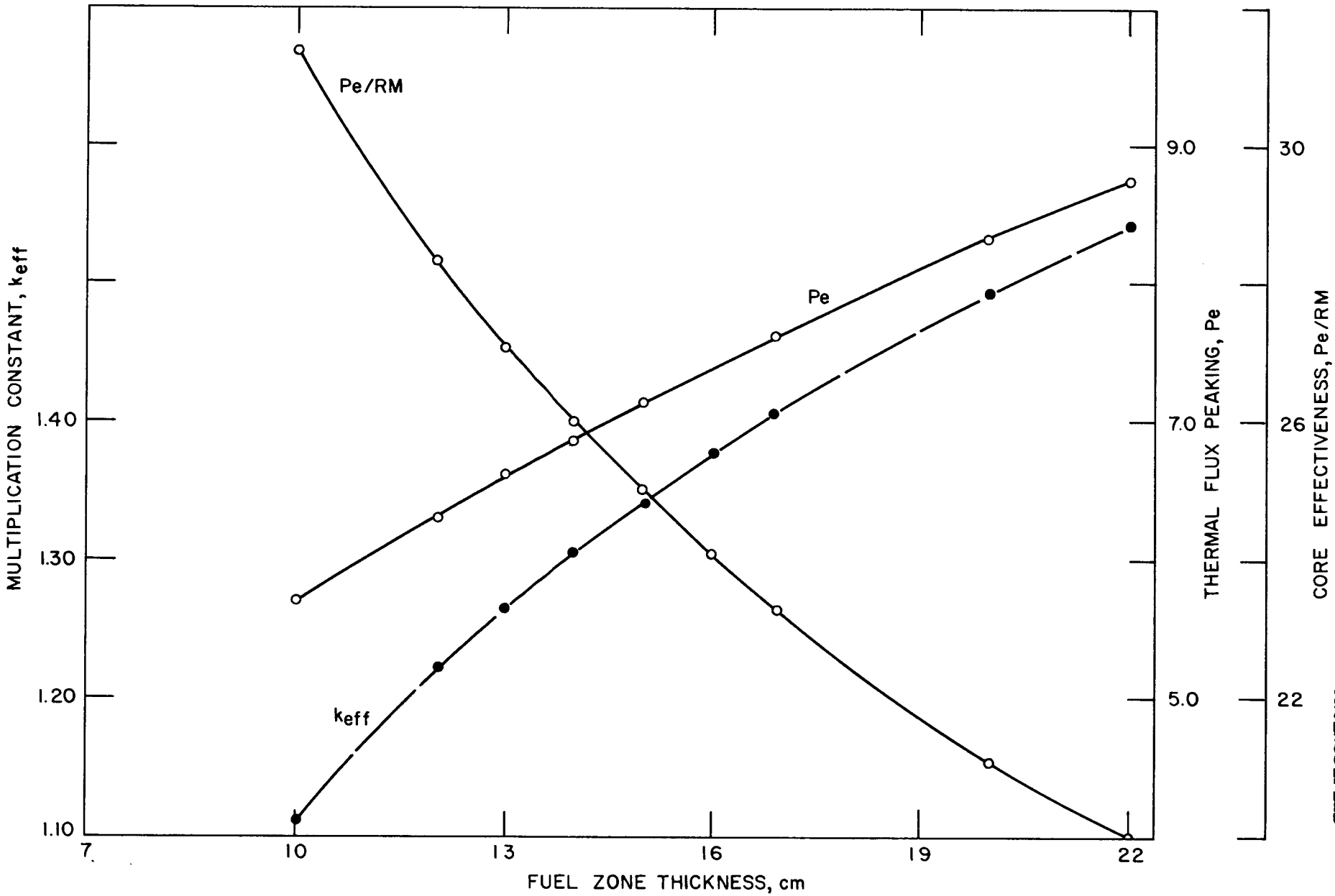

Fig. 22. Multiplication Constant, Flux Peaking and Core Effectiveness vs Fuel Thickness for a 70% Al. Reflected Reactor, $N_u = 9.18 \times 10^{19}$.

ORNL-LR-Dwg.-26607
UNCLASSIFIED

ORNL-LR-Dwg.-26608
UNCLASSIFIED

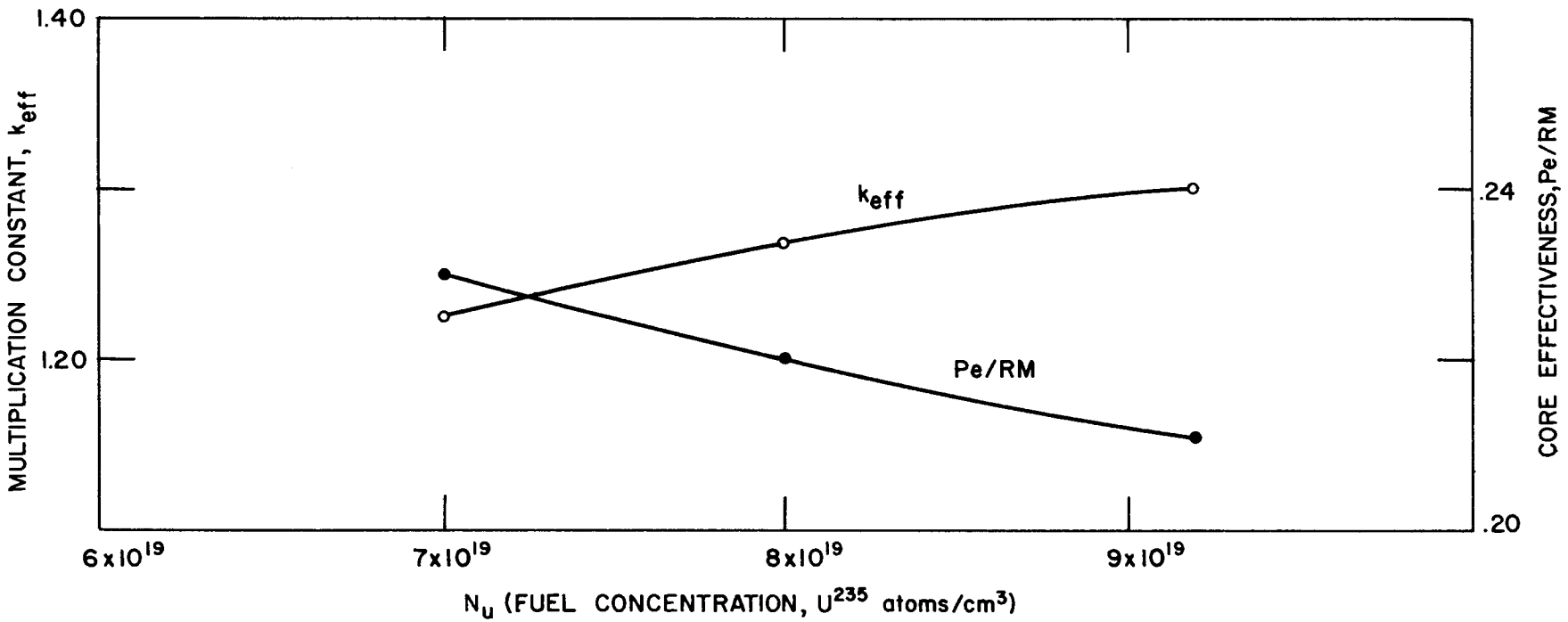

Fig. 23. Multiplication Constant and Core Effectiveness vs Fuel Concentration for a 70% Al Reflector, Fuel zone thickness = 20 cm.

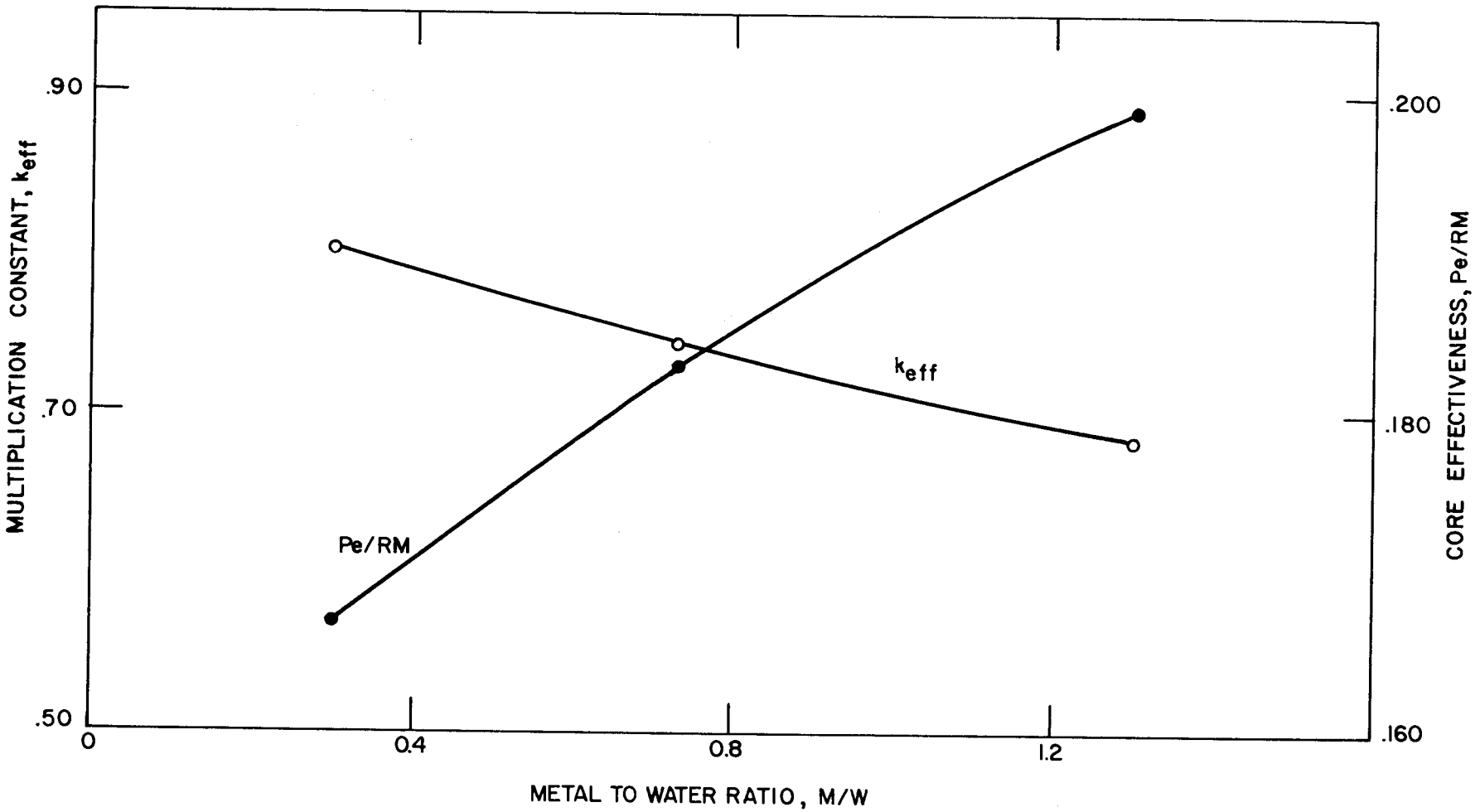

Fig. 24. Multiplication Constant and Core Effectiveness vs Metal/Water Ratio. Fuel thickness = 8 cm - N_u = 9.18 x 10^{19}.

ORNL-LR-Dwg.-26609
UNCLASSIFIED

D_2O thickness and the concentration of fissionable material plus other neutron absorbers in the experiments. Since the actual geometry of this region could not be treated with the one-dimensional code available, it was necessary to attempt some approximation which would give reasonably valid results. As a first approximation, the region was considered to be filled with D_2O. Fluxes calculated in this manner were considered to be "unperturbed" fluxes, i.e., fluxes which would exist if the experiments and their housings were not in place. A second approximation used was the replacement of the four experiment cylinders with a slab of equal volume across the center of the reactor. This method is considered to give good values for the flux delivered to the edge of the experiments[17]. The slab thickness used was seven centimeters (3.5 centimeters on either side of the centerline). Additional calculations were made with greater thicknesses to determine the importanc of this parameter to the results. In order to make these calculations, it was necessary to replace the aluminum reflector with an equivalent thickness of fuel. For this purpose, the extrapolation distance for the fast flux, 14.3 centimeters, was taken as reflector savings. A two-region machine calculation with D_2O in region 1 resulted in a k_{eff} of 1.29 for this (34.3 cm) thickness of fuel compared to a value of 1.30 obtained from the three-region calculation.

The experiments for which calculations were made contained aluminum, D_2O, and various concentrations of U-235. A metal-to-water ratio of .73 was used. In an effort to simulate the effect of structural material on the neutron economy, the thermal absorption cross section of the aluminum was tripled for all of these calculations.

The effect of region 1 thickness on k_{eff} and Pe/RM is shown in Figure 25 for a D_2O-filled central region. A peak value of Pe/RM of 0.22 is achieved at 26 centimete: with, however, appreciable loss in reactivity from the values obtained at smaller

ORNL-LR-Dwg.-26610
UNCLASSIFIED

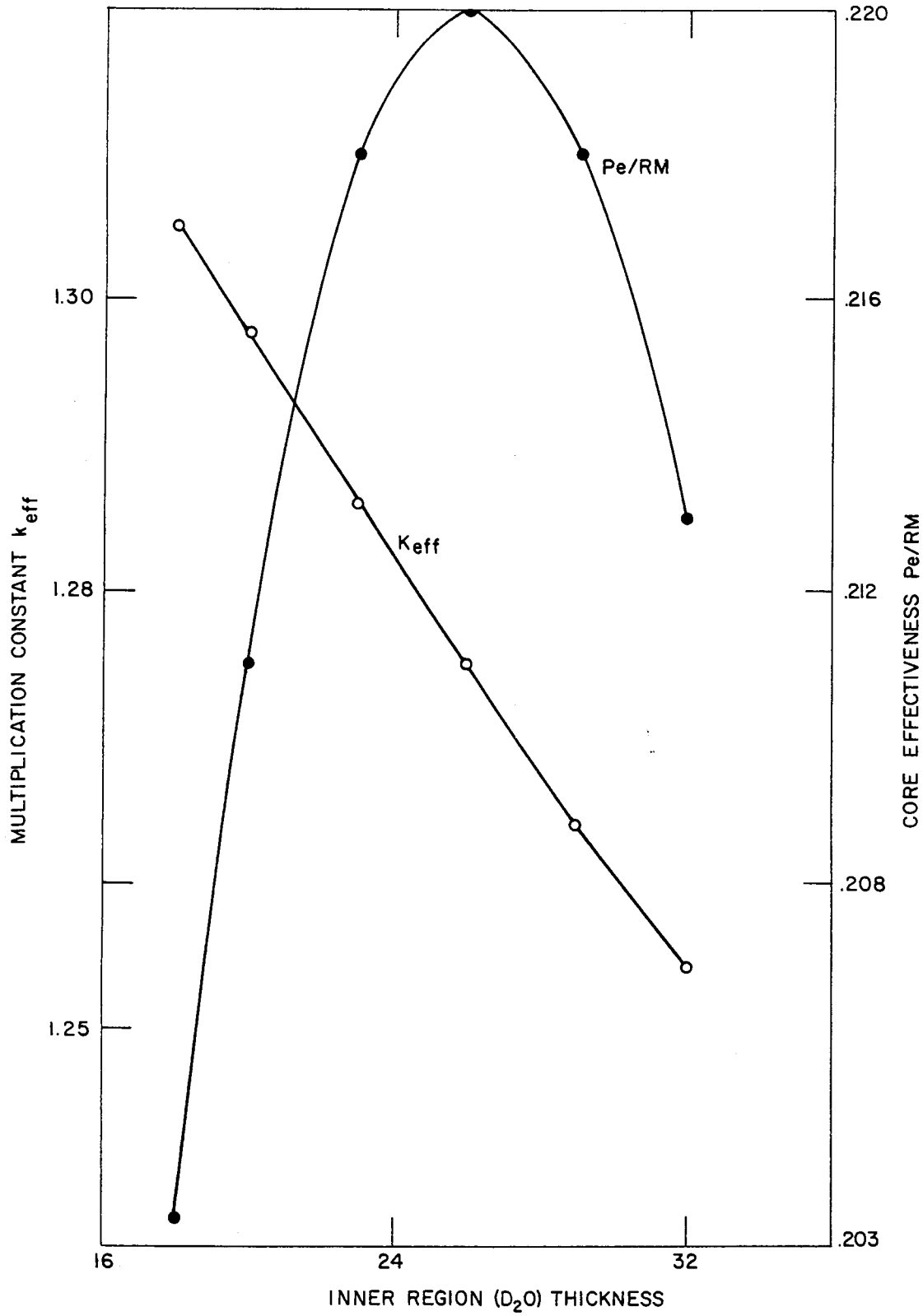

Fig. 25. Multiplication Constant and Core Effectiveness vs R_1 Thickness.

thicknesses. The effect of D_2O thickness variation with an experiment containing 4×10^{19} uranium atoms/cc in place is shown in Figure 26. Values of Pe/RM shown were calculated in terms of the thermal flux at the edge of the experiment and normalized to the value obtained with D_2O in the central region. A good agreement in optimum thickness with and without the experiment is shown.

Since there is a loss in k_{eff} as the center region thickness increases, it was considered desirable to compare the values of Pe/RM for various central region thicknesses at constant k_{eff}. For this purpose values of $\delta k/\delta M$ obtained from Figure 14 were used to correct Pe/RM to a k_{eff} of 1.29. These results indicated that an optimum thickness for constant k_{eff} was approximately 20 centimeters. Therefore, twenty centimeters was chosen as the region 1 thickness.

Pe/RM and k_{eff} as a function of U-235 concentration in the experiment slab are plotted in Figure 27. Relative core effectiveness, Pe/R, as a function of the thickness of the experiment slab is plotted in Figure 28 for an experiment concentration of 4×10^{19} U-235 atoms/cm^3.

Temperature Effect Calculations: To determine the effect of temperature upon the advanced engineering test reactor (double-slab configuration), calculations using the 3-group, 3-region ORACLE code were performed. Utilizing the group constants for various temperatures that are given in Appendix A, Table 7, on group constants, for the D_2O reflector, fuel region and fast reflector, the effects of temperature upon the multiplication factor are summarized in Figures 29, 30, 31 and 32.

As can be seen from Figure 29, variation of the fast neutron reflector temperatur has very little effect upon the multiplication factor of the reactor. Figure 32 shows that variation of the D_2O reflector temperature has only slightly more effect upon the multiplication factor while both Figures 30 and 31 evidence the large

ORNL-LR-Dwg.-26611
UNCLASSIFIED

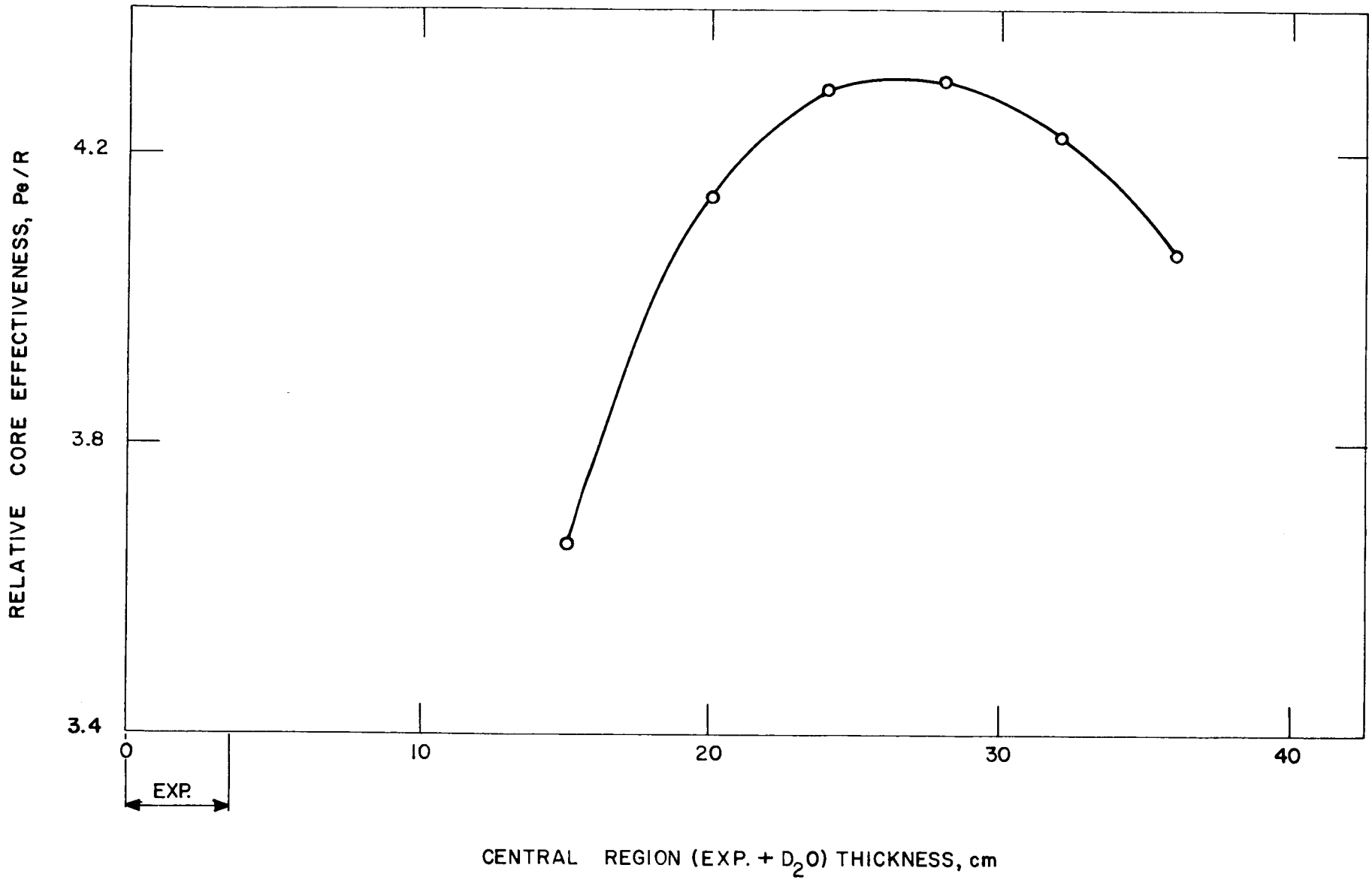

Fig. 26. Relative Core Effectiveness (Pe/R) vs Exp. (3.5 cm) + D_2O Thickness, Experiment $N_u = 4 \times 10^{19}$

ORNL-LR-Dwg.-26612
UNCLASSIFIED

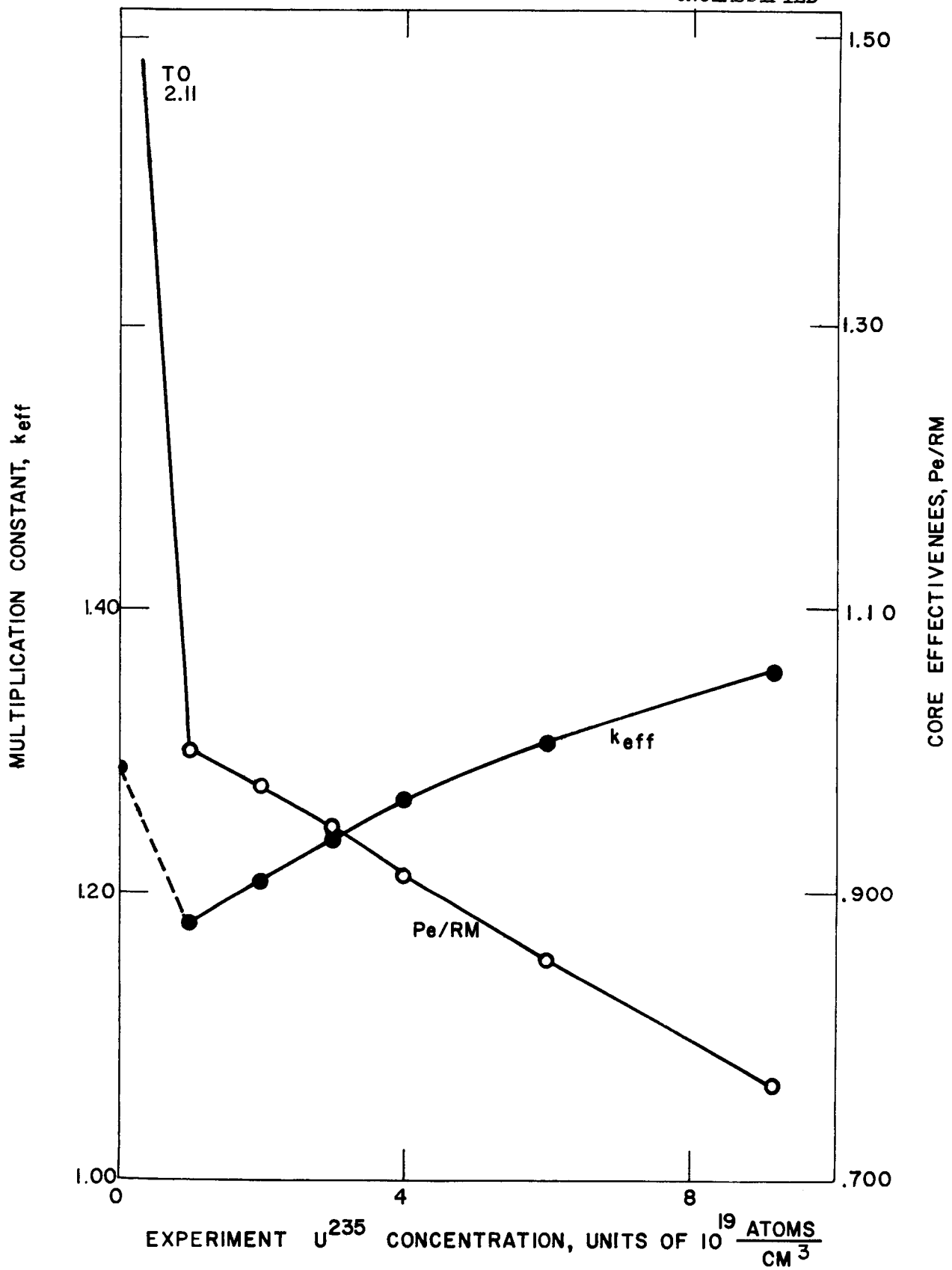

Fig. 27. Multiplication Constant and Core Effectiveness as a Function of Experiment U^{235} Concentration

ORNL-LR-Dwg.-26613
UNCLASSIFIED

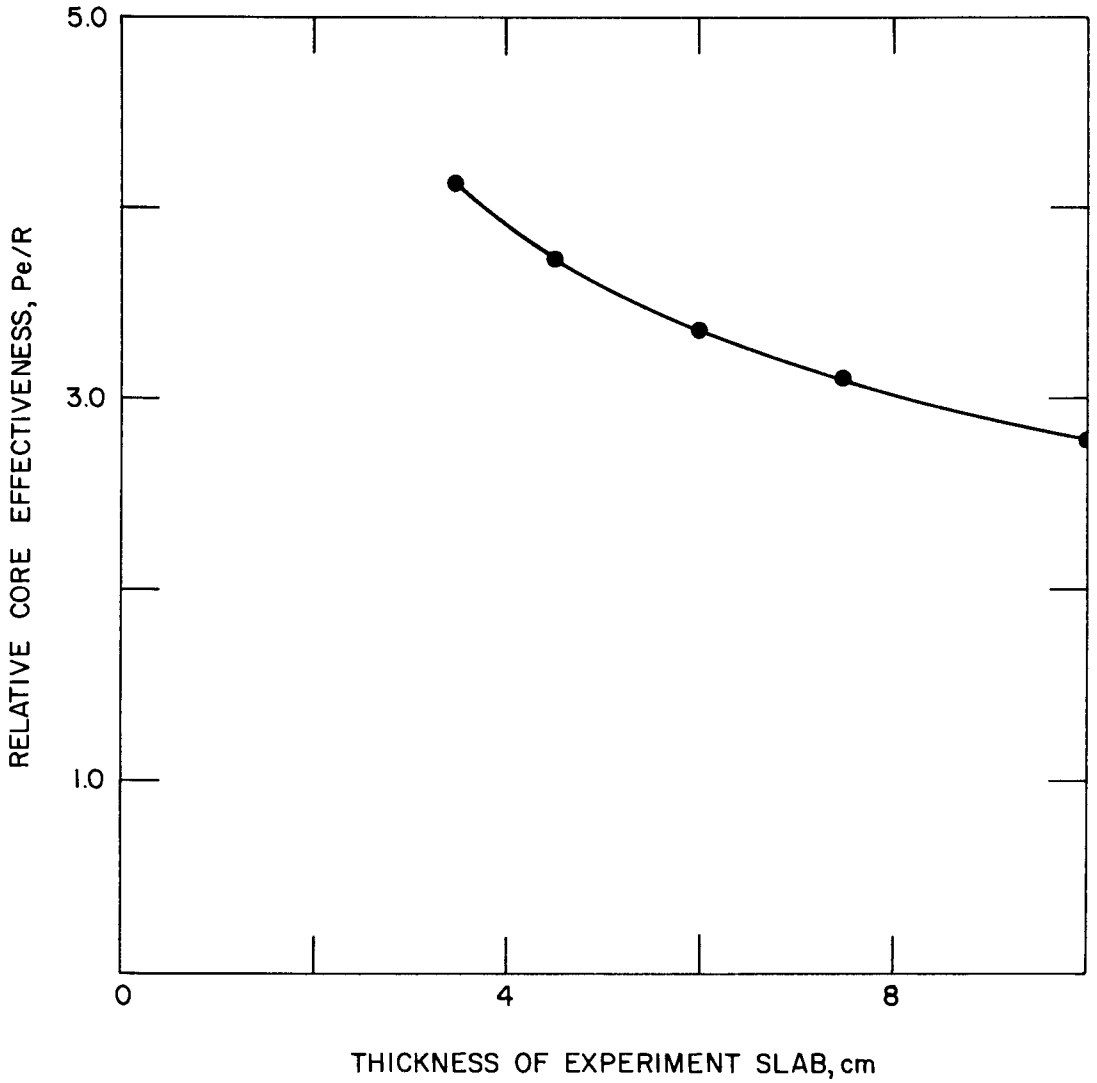

Fig. 28. Relative Core Effectiveness (Pe/R) as a Function of Experimental Slab Thickness (Experiment $N_u = 4 \times 10^{19}$)

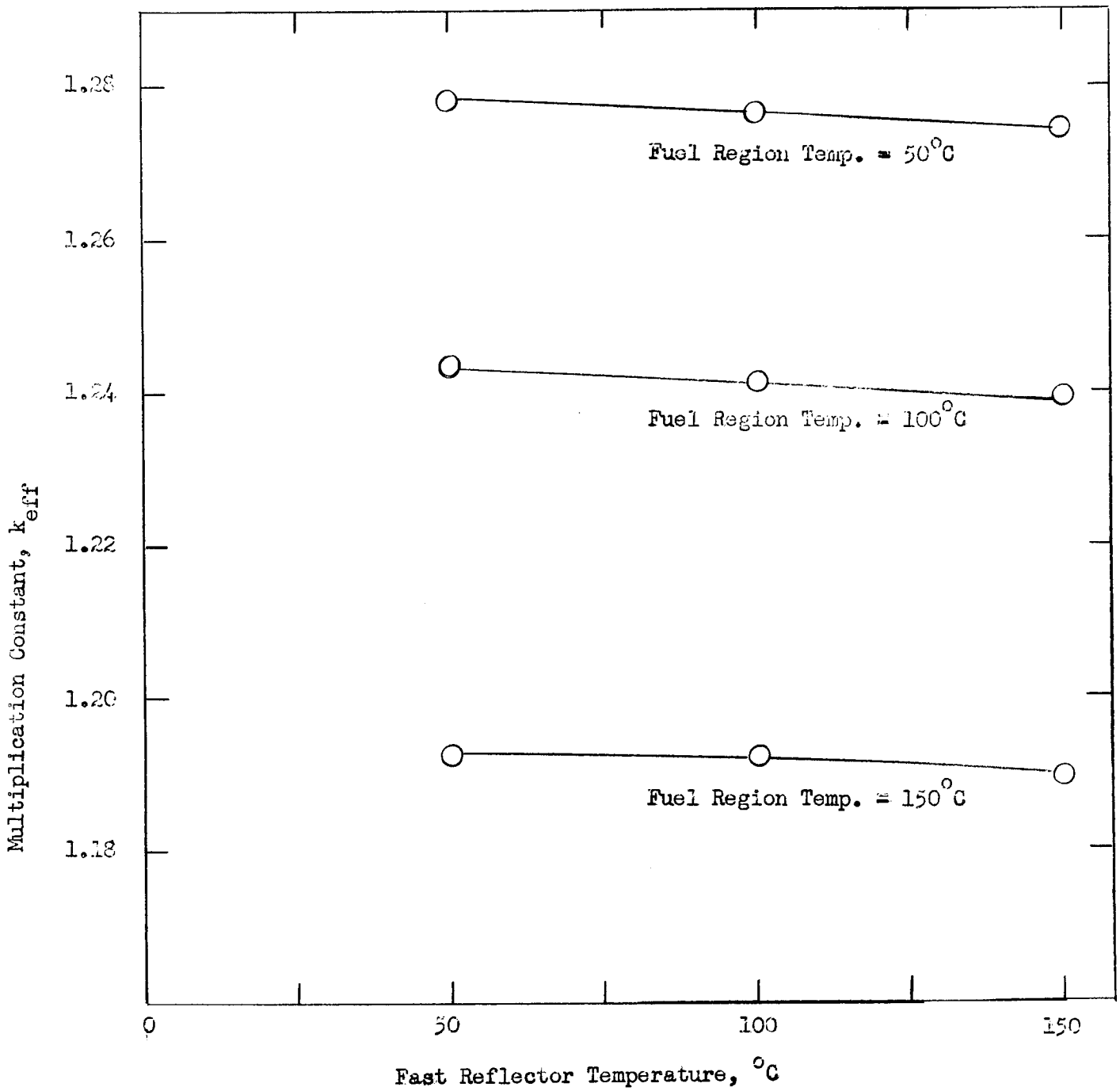

FIGURE 29

Results of Temperature Coefficient Calculations for Constant D_2O Reflector Temperature of 50°C

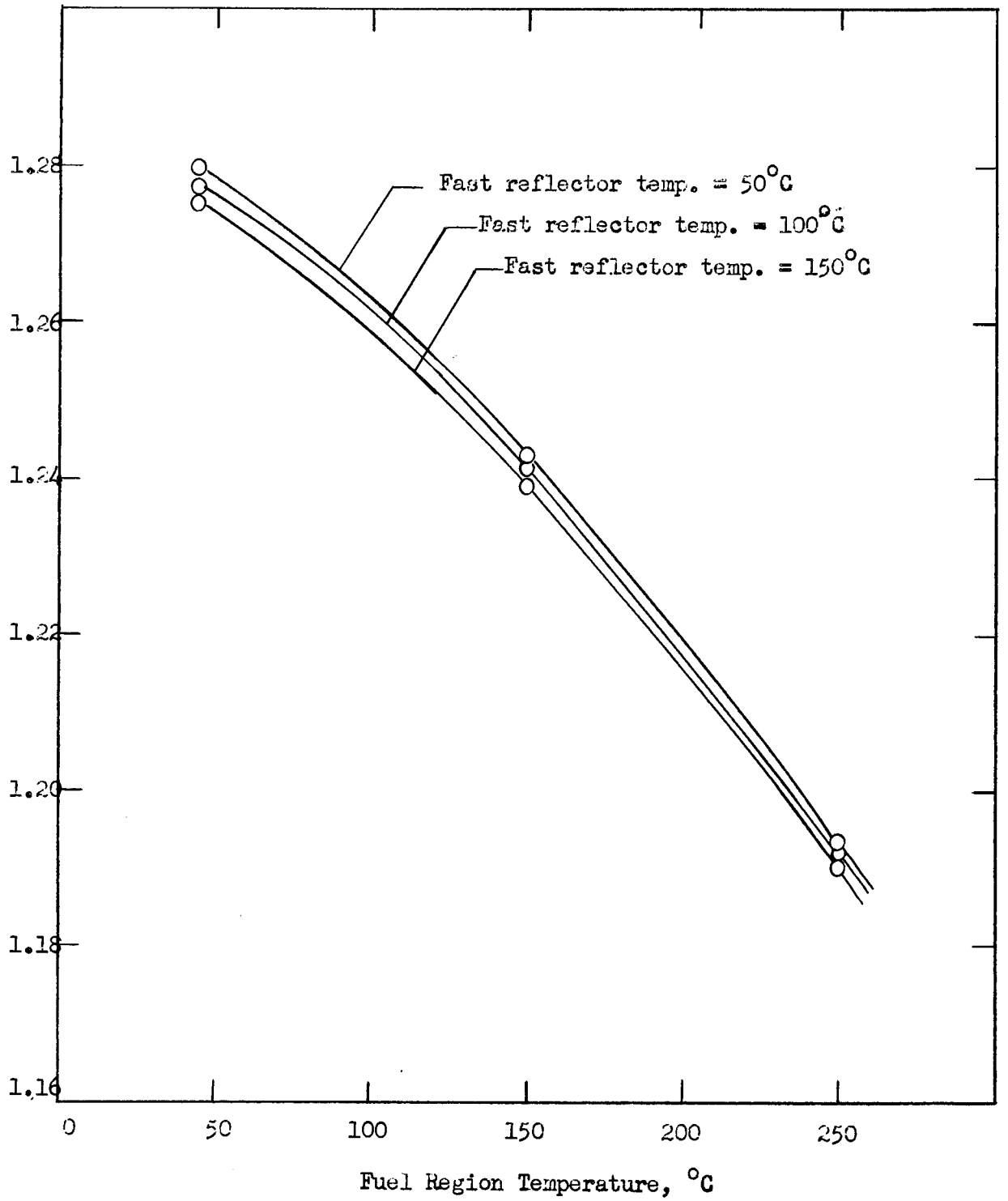

FIGURE 30

Results of Temperature Coefficient Calculations for Constant D_2O Reflector Temperature of 50°C

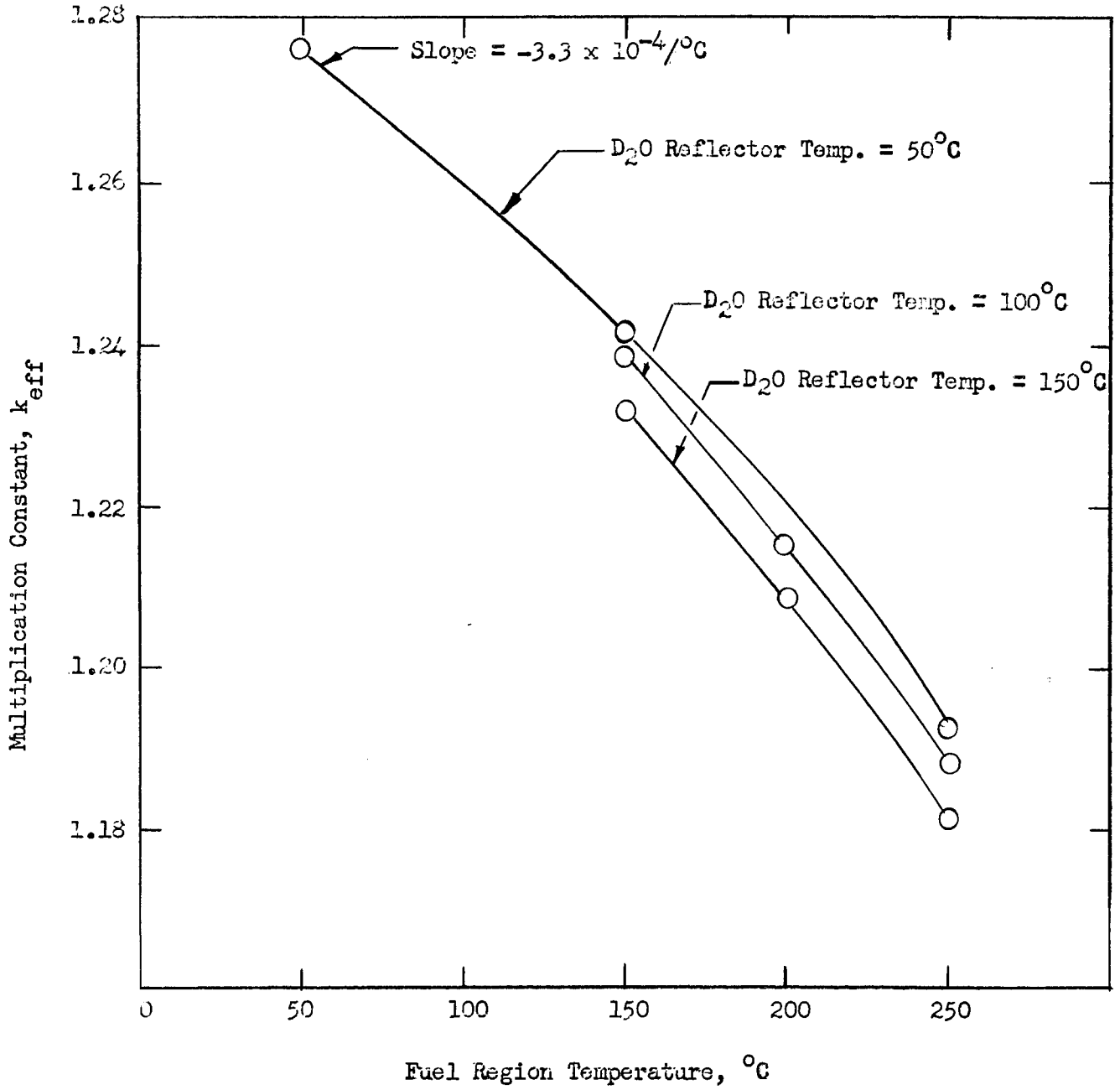

FIGURE 31

Results of Temperature Coefficient Calculations for Constant Fast Reflector Temperature of $100^{\circ}C$

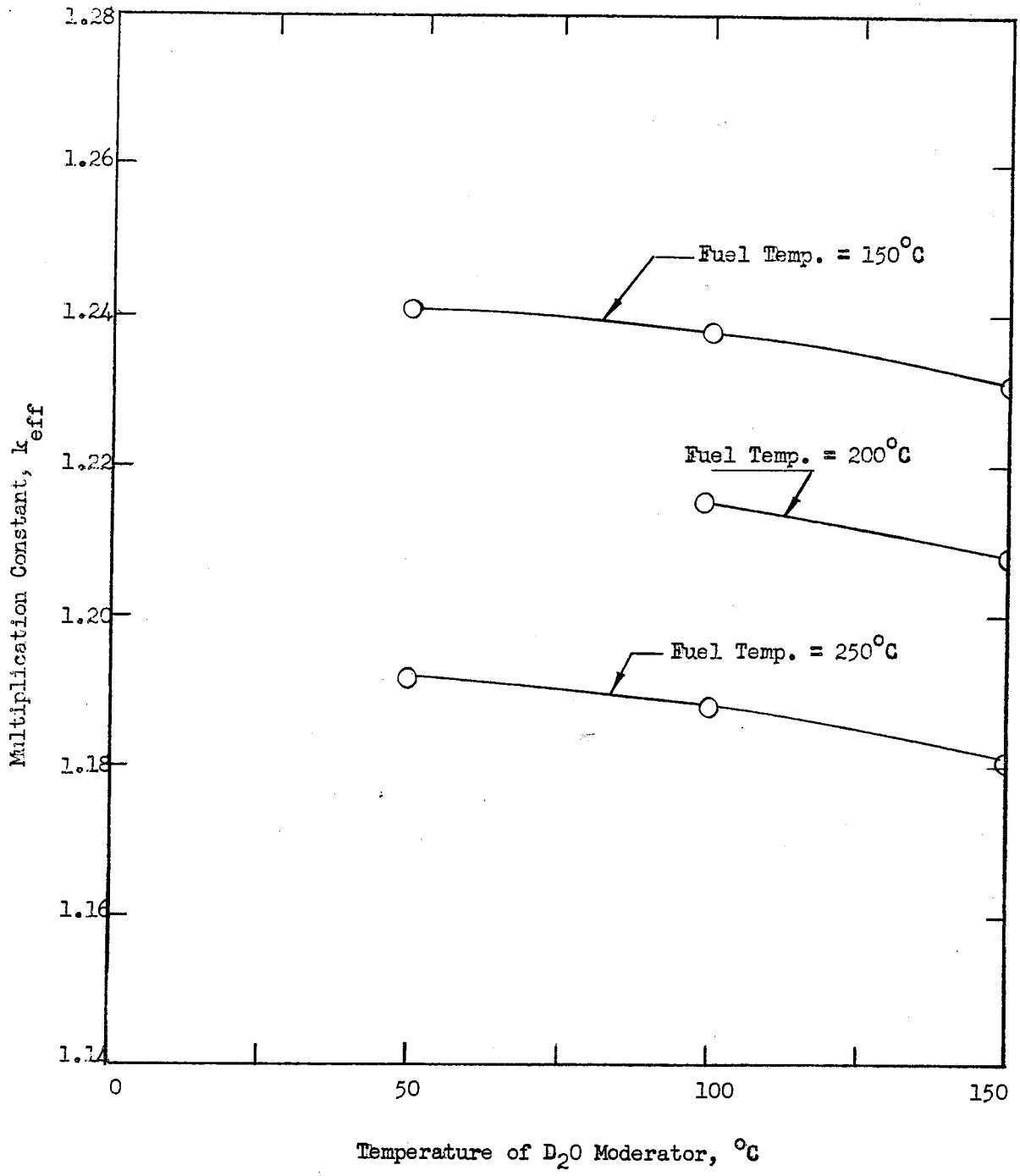

FIGURE 32

Results of Temperature Coefficient Calculations for Constant Fast Reflector Temperature of 100°C

effect upon the multiplication factor of a change in fuel region temperature.

This result is a very desirable one from a safety standpoint since increases in power are almost immediately reflected as increases in temperature of the fuel region. The temperature coefficient at startup is determined to be about -3.3×10^{-4} $\delta k/k/^{\circ}C$, which, while probably higher than will be realized, indicates a very safe reactor from the standpoint of temperature. Other sections of this report show that sufficient excess k is available to override the loss in k obtained in going to operating temperature from the clean, cold condition.

Miscellaneous Calculations: In this category are included reflector thickness calculations, Y and Z flux traverse calculations, and effect of reflector savings calculations. Xenon poisoning and burn-out effects are included in Appendix D-1 and D-3. In order to determine the size of reflector needed on the various faces of the core, three-group, three-region machine calculations were made for several reflector thicknesses. The results of these calculations are shown in Figure 33 for a D_2O reflector and Figure 34 for a 70% Al - 30% D_2O reflector. On the basis of these results, minimum reflector thicknesses of 60 centimeters were considered effectively infinite in both cases.

An attempt was made to obtain Y-and Z-direction flux traverses through the fuel region for use in heat transfer calculations. It is considered that the results are only approximate since no account could be taken of the extreme heterogeneity of the reactor in the X-direction. Traverses obtained using 20 centimeters reflector savings in the X-direction (core thickness of 60 centimeters) are plotted in Figures 35 and 36.

It was necessary throughout the calculations to use some value for the reflector savings obtained from effectively infinite D_2O reflectors on four sides of the reactor. From the data presented for lower U-235 concentration[31], it was estimated that 20 centimeters would be a reasonable estimate of the savings for a U-235

ORNL-LR-Dwg.-26614
UNCLASSIFIED

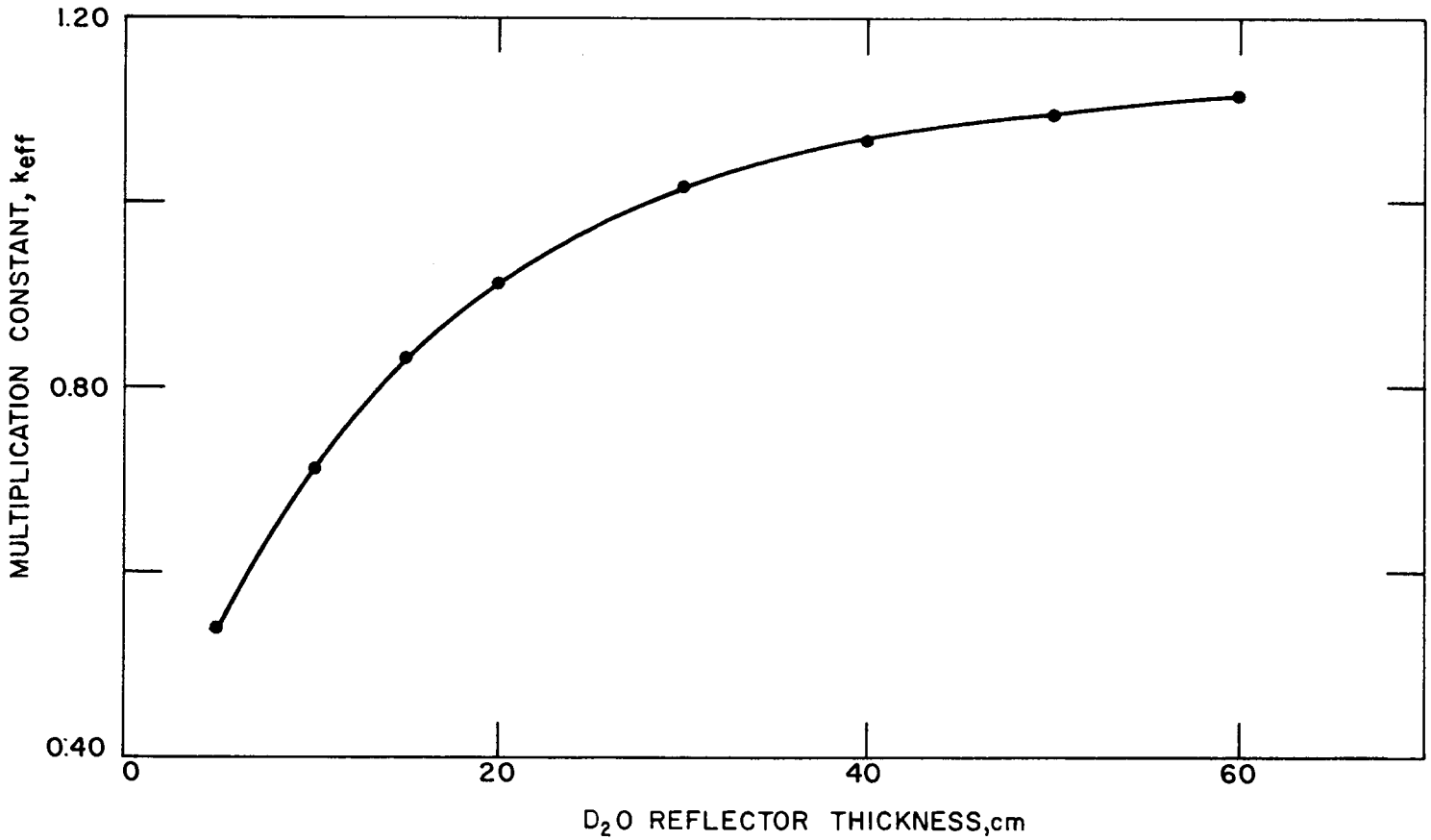

Fig. 33. Multiplication Constant vs D_2O Reflector Thickness.

ORNL-LR-Dwg.-26615
UNCLASSIFIED

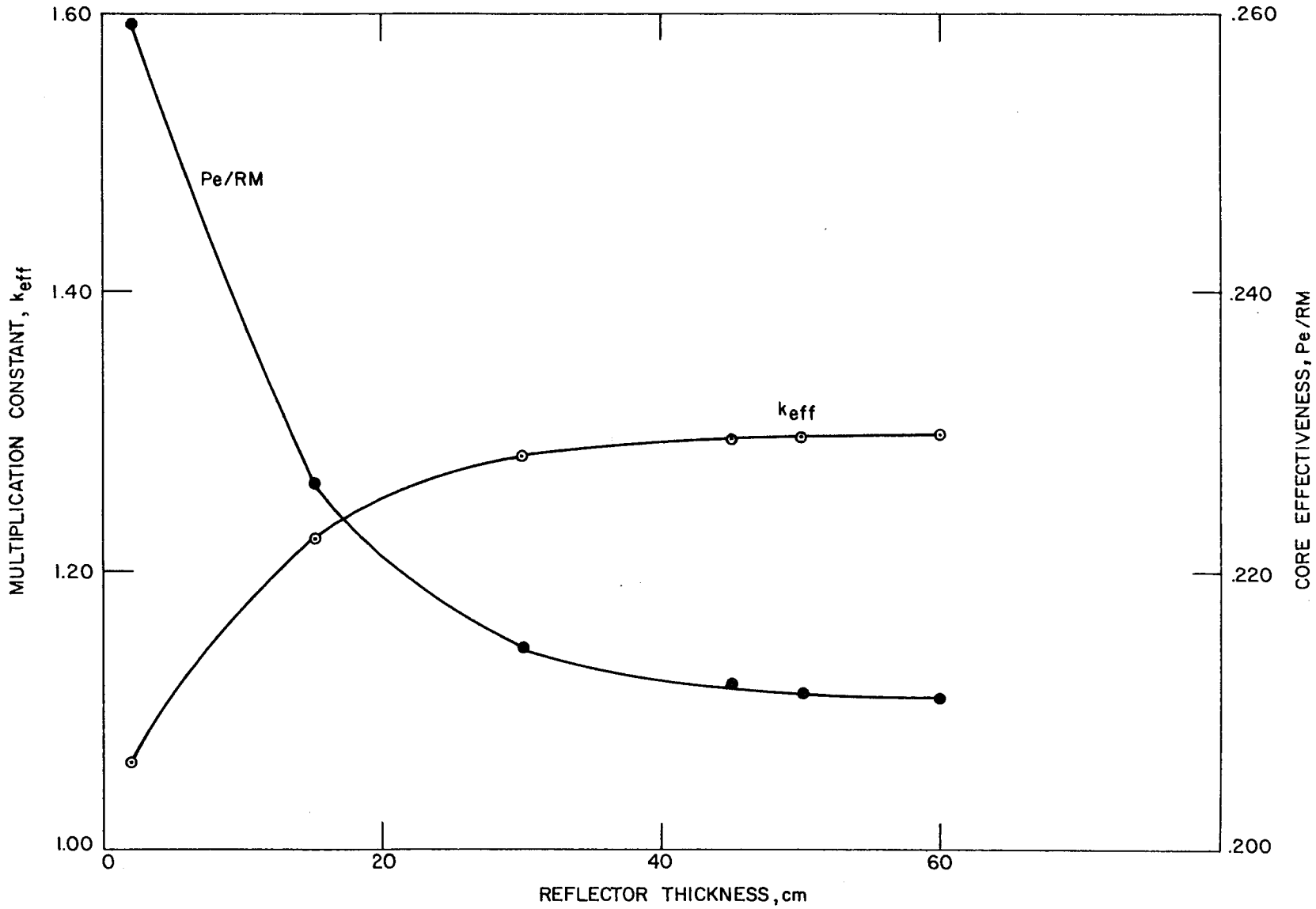

Fig. 34. Multiplication Constant and Core Effectiveness vs Thickness of 70% Aluminum Reflector.

ORNL-LR-Dwg.-26616
UNCLASSIFIED

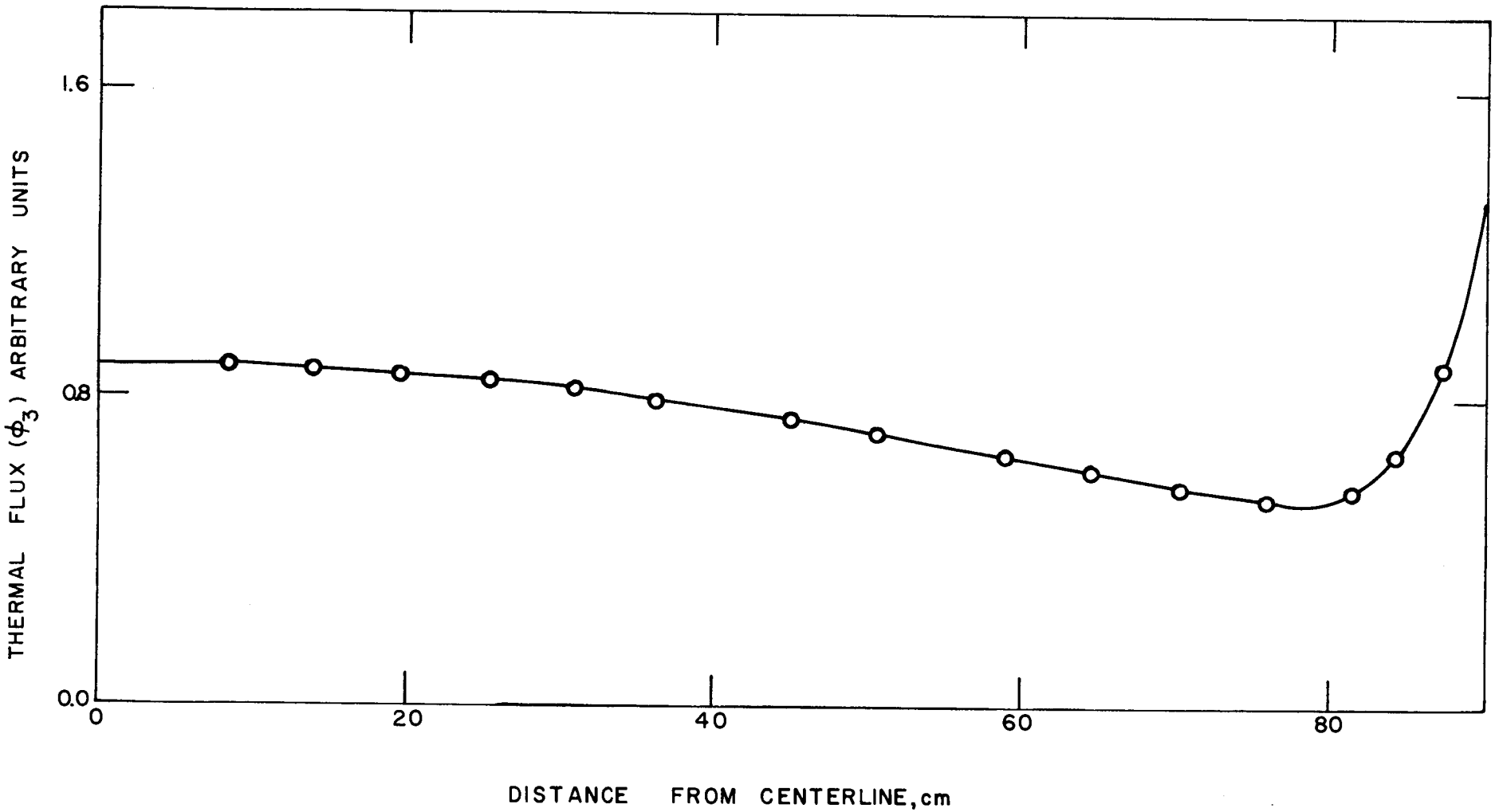

Fig. 35. Thermal Flux in the Fuel Zone — Y Traverse

ORNL-LR-Dwg.-26617
UNCLASSIFIED

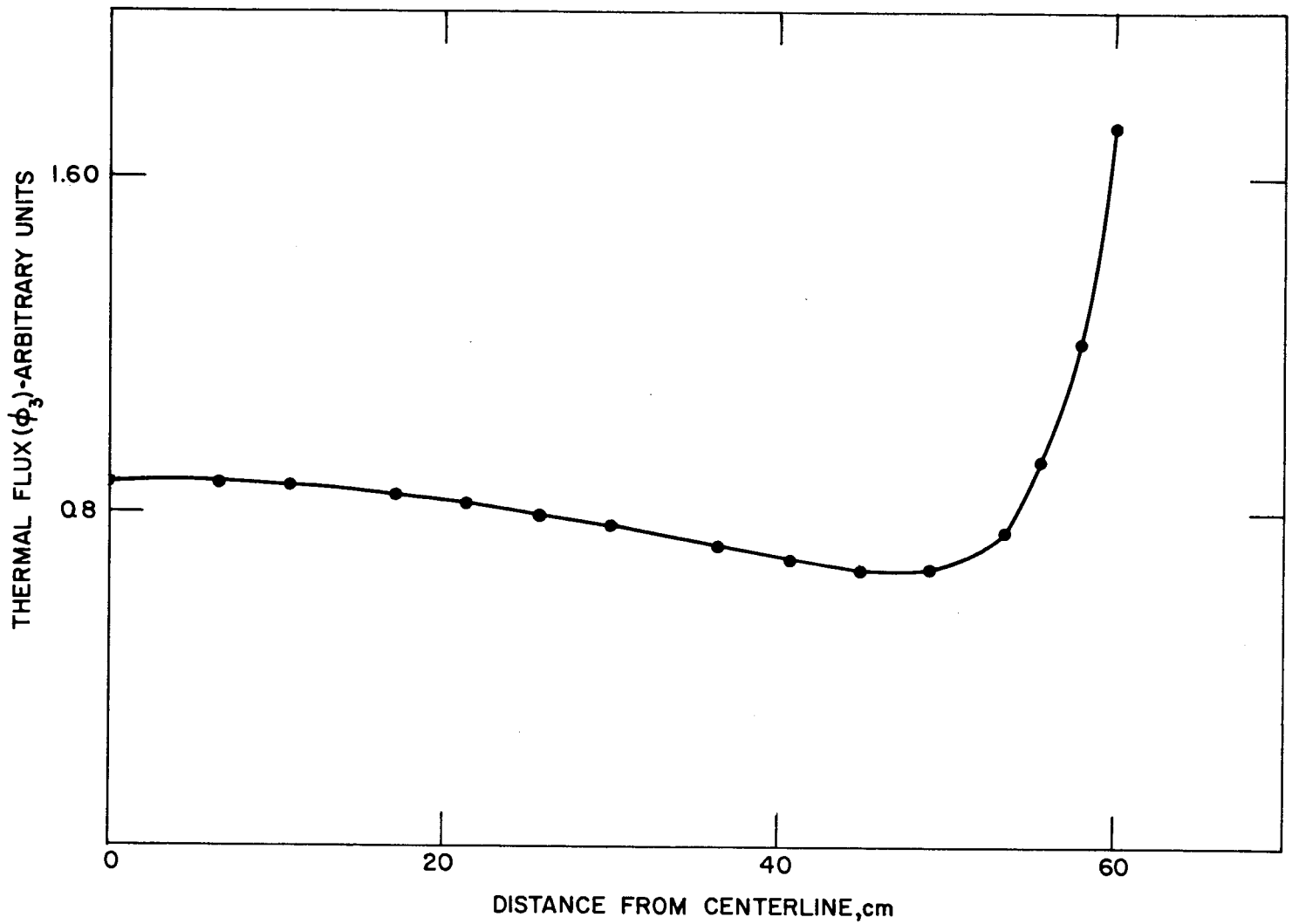

Fig. 36. Thermal Flux in the Fuel: Z – Traverse.

concentration of 9.18×10^{19} atoms/cm^3 used in this reactor. Unfortunately, the validity of this estimate was not verified during this study, although some of the results previously discussed indicate D_2O reflector savings are between 25 and 30 centimeters on the X-face of the reactor. A bare reactor with a fuel thickness of 34.3 cm produces a k_{eff} of 1.29 while a D_2O reflected reactor with a fuel thickness of 8.4 cm has a k_{eff} of 1.42. However, it is expected that D_2O reflection on the other side may have a different effect. Since this question was not resolved, it is considered desirable to exhibit the effect of the value of reflector savings upon the characteristics of the reactor. This data is presented in Figure 37.

E. Lightly-Loaded Cylindrical Cores

In the process of arriving at the particular core for the reactor, a good deal of consideration was given to lightly-loaded D_2O moderated, D_2O cooled, enriched-fuel cylindrical cores. These merited consideration since one of the methods of obtaining a high neutron flux with low power output is to operate with a low concentration of fissionable material in a low-neutron absorbing medium. Such systems must be relatively large to reduce neutron leakage and because of their relatively low critical masses must either be refueled frequently or have initially large multiplication constants to have a reasonable core cycle time.

Critical calculations by one-speed diffusion theory methods were made for two D_2O-moderated, D_2O-cooled, bare cylindrical cores containing aluminum-clad, enriched uranium-aluminum alloy fuel elements sheathed in aluminum tubes. A 10-foot high, 10-foot diameter core required 6.6 Kg of 90% enriched uranium for criticality and 17.4 Kg for $k = 1.30$. A 6-foot high, 10-foot diameter core required 5.5 Kg of 90% enriched uranium and 11.1 Kg for $k = 1.30$.

In order to operate such reactors with experiments in place and allow for temperature effects and fission-product poisoning, a minimum clean, cold k of about

ORNL-LR-Dwg.-26618
UNCLASSIFIED

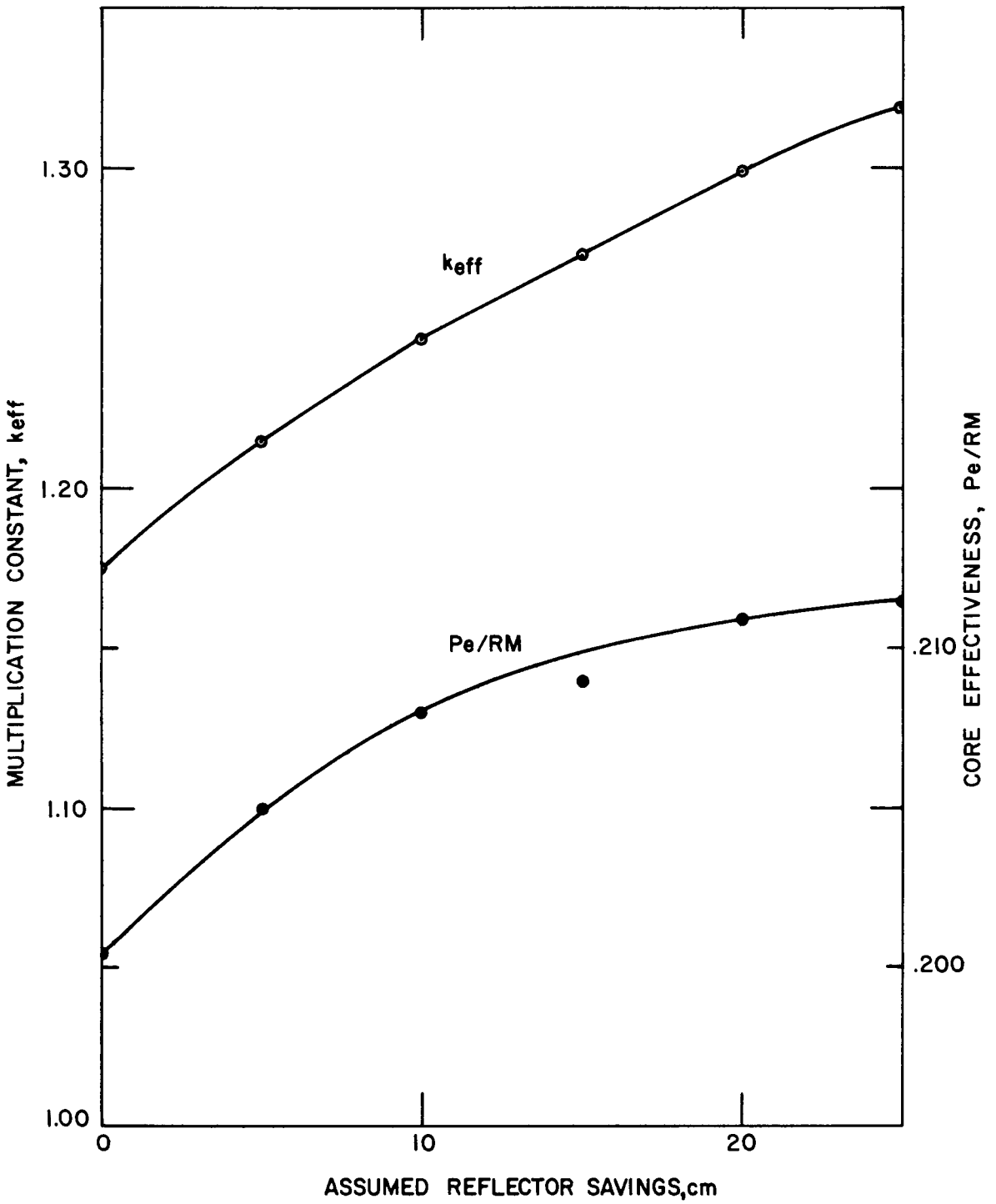

Fig. 37. Multiplication Constant and Core Effectiveness as a Function of Reflector Savings in the Y and Z Directions.

1.2 will be required leaving only about 0.1 k for burnup if the clean cold k is 1.3. The value of 0.1 k excess represents about 1.4 kg of U-235. If the reactor is to operate at a power level of 500 MW in order to provide an initial average thermal neutron flux of 10^{15}, the burnup rate of U-235 will be about 600 grams per day giving the reactor a cycle time of only 2.3 days for a heterogeneous system.

It is possible that such short cycle time would not be a hindrance to many experiments; however, experiments demanding longer run-times would be greatly inconvenienced. Also, it is possible that refueling during operation could be accomplished to allow almost continuous operation of the core; however, such a procedure could introduce a variety of hazards both to the reactor and to personnel. Although a homogeneous reactor core could solve the refueling problem, the technology is not sufficiently advanced to provide a high-flux testing reactor within the limitations imposed upon this study.

Some of the results of calculations for the lightly-loaded 6-foot high, 10-foot diameter cylinder may be of interest and are included. Figures 38 and 38a show neutron flux plots through an experiment (PWR seed element) placed at different distances from the reactor center and for a D_2O filled region surrounding the experiment as obtained from ORACLE calculations. The lack of an $r-\theta$ (two-dimensional) code for the calculations forced some severe approximations to be imposed, so that it is felt that the flux depressions indicated may be somewhat exaggerated. The plot is actually that for an annular region of the experiment constituents surrounding a lightly-loaded core and, in turn, surrounded by a lightly-loaded outer region. For the real case, the experiments would be in the form of 10-inch diameter cylinders placed the equivalent distance from the core. Although some exaggeration of the flux depression no doubt exists, the low thermal neutron source strength per unit volume leads to the conclusion that severe flux depressions

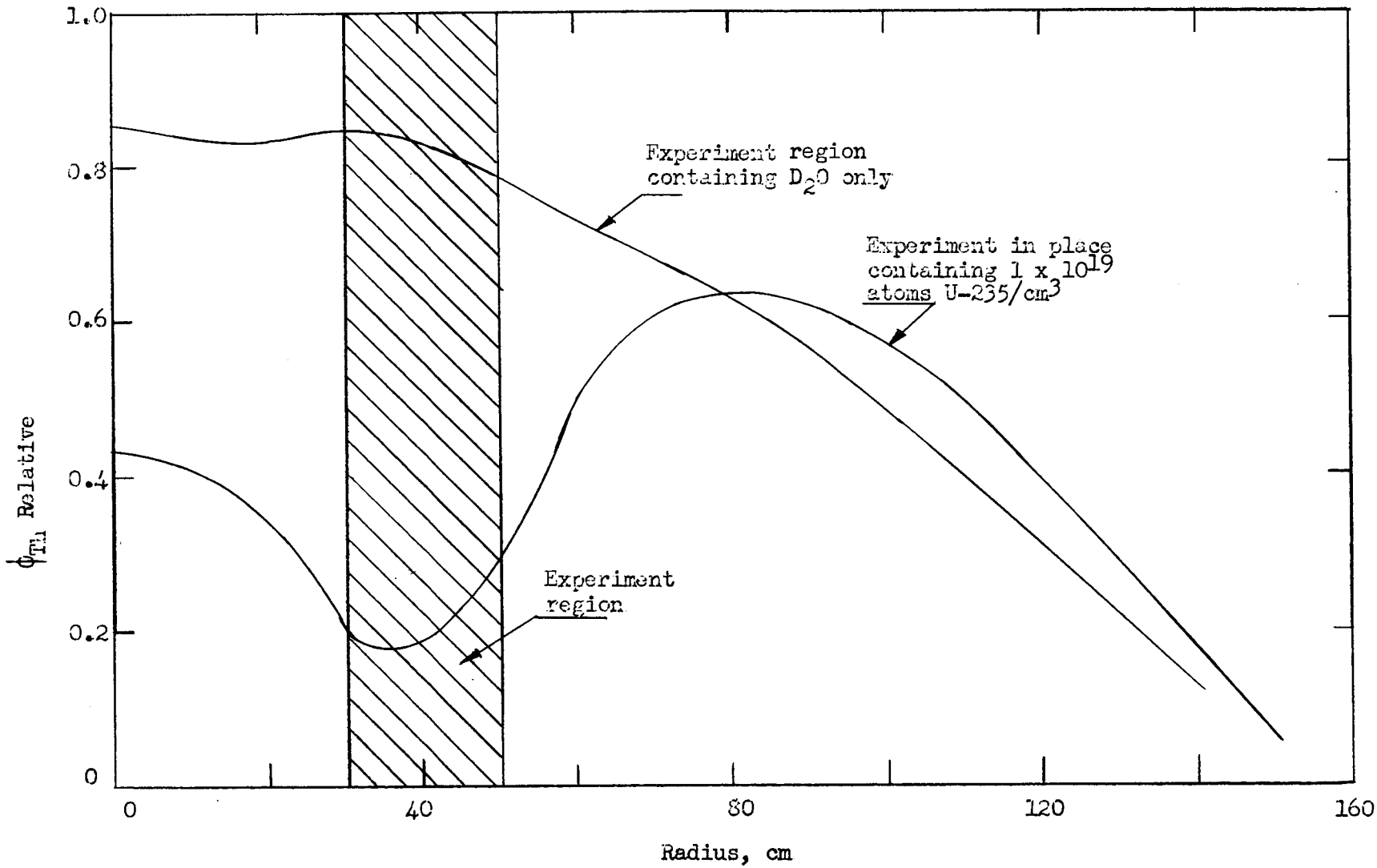

FIGURE 38

Effect of Experiment Absorbers on Thermal Flux for Experiment at 40 cm Radius

Reactor size = 10 ft Dia. x 6 ft High

Fuel Concentration = 2 x 10^{18} atoms U-235/cm^3

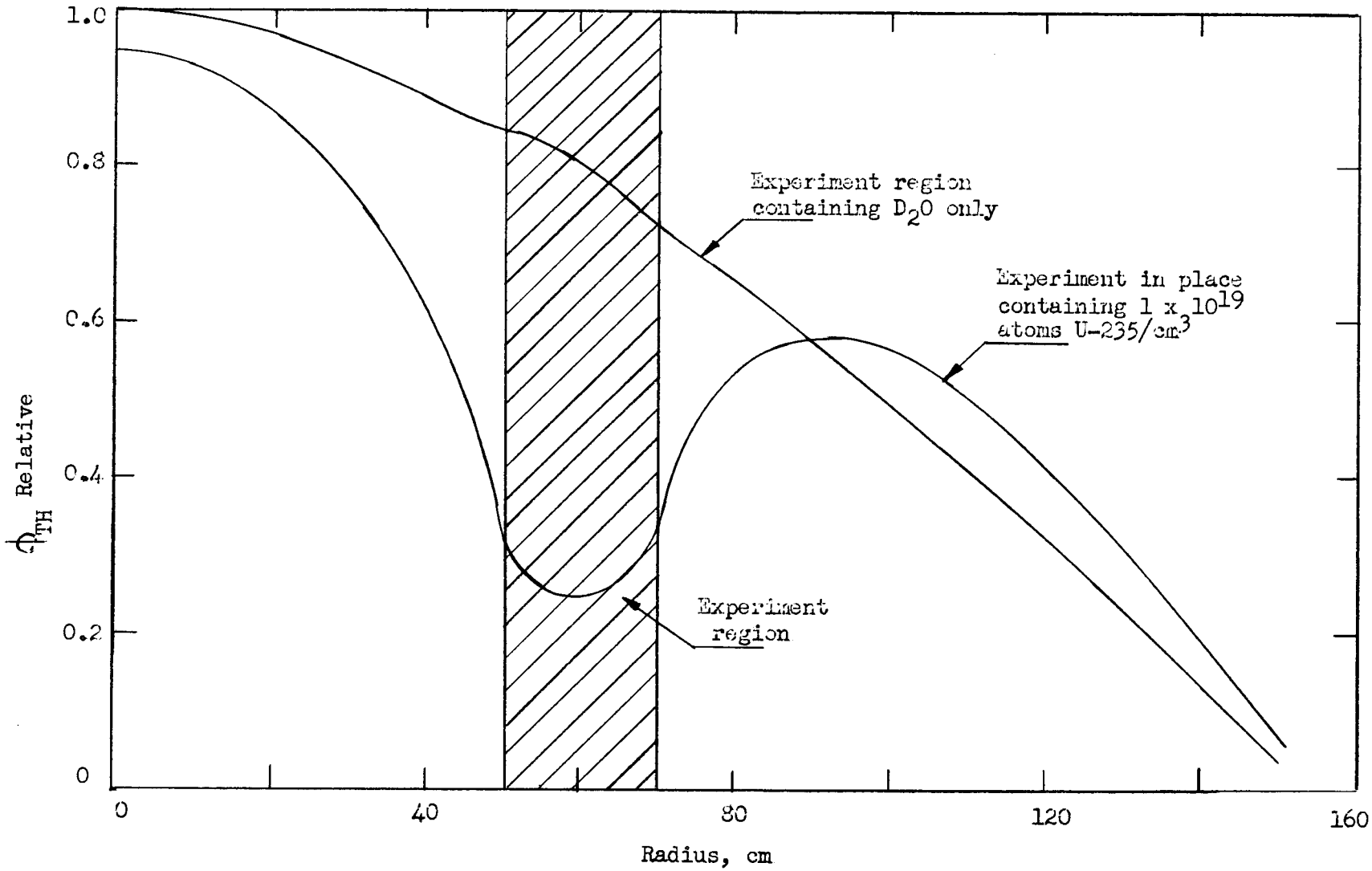

FIGURE 38a

Effect of Experiment Absorbers on Thermal Flux for Experiment at 60 cm Radius

Reactor Size = 10 ft dia x 6 ft high
Fuel Concentration = 2 x 10^{18} atoms U-235/cm^3

will, in reality, be caused by putting large-sized, neutron-absorbing experiments into this type of reactor.

Table 3 lists results of one-speed, diffusion theory hand calculations for the 6-foot high, 10-foot diameter bare cylinder. Some of these data are plotted in Figure 39.

The lightly loaded cores have some advantages which may overshadow their disadvantages to a great extent and should warrant consideration in a more thorough study. These are:

1. Lower fuel inventory.
2. Possibly better isolation of experiments from each other.
3. Lower power density which could eliminate pressurization.

F. Validity of the Calculations

Throughout Sections III and IV calculational results have been presented with few comments regarding their validity. In this section an effort will be made to point out such flaws in the calculations as are known to the authors. Undoubtedly, there are many others.

Reactor (and many other) calculations depart from reality in somewhat the following manner:

1. A physical model is chosen.
2. The physical model is replaced by a mathematical model.
3. The mathematical model is replaced by an approximate, but more tractable, model.
4. The problem is solved analytically or approximately, by machine or by hand, using input data constructed from "basic" constants based upon experimental results.

Comments regarding the approximations introduced in steps 1, 2, and 3 are,

TABLE 3

ONE-SPEED DIFFUSION THEORY RESULTS

Diameter = 10 ft.
Height = 6 ft.
Vol. = 1.16×10^{7} cc
$N^{AL} = 1.69 \times 10^{21}$ atoms/cc
$N^{D_2O} = 3.23 \times 10^{22}$ atoms/cc

U-235 atoms/cm^3	Loading Mass, kg	$\nu\Sigma_f$, cm^{-1}	Σ_a, cm^{-1}	k_∞	L^2, cm^2	$L^2B_g^2$	k	$\bar{\phi}$ n/cm^2-sec
1.2×10^{18}	5.46	1.71×10^{-3}	1.294×10^{-3}	1.32	618	.335	.99	1.9×10^{15}
1.3×10^{18}	5.92	1.855	1.363	1.36	587	.318	1.03	1.75
1.4×10^{18}	6.37	1.997	1.432	1.39	558	.302	1.07	1.63
1.5×10^{18}	6.83	2.14	1.501	1.42	532	.288	1.10	1.52
1.6×10^{18}	7.28	2.28	1.57	1.47	509	.276	1.15	1.42
1.7×10^{18}	7.74	2.425	1.638	1.48	488	.265	1.17	1.34
1.8×10^{18}	8.20	2.565	1.708	1.50	468	.254	1.19	1.26
1.9×10^{18}	8.65	2.71	1.777	1.52	450	.244	1.22	1.20
2.0×10^{18}	9.10	2.855	1.847	1.54	433	.235	1.25	1.14
2.1×10^{18}	9.55	3.00	1.919	1.57	417	.227	1.28	1.09
2.2×10^{18}	10.0	3.14	1.984	1.58	403	.218	1.30	1.03

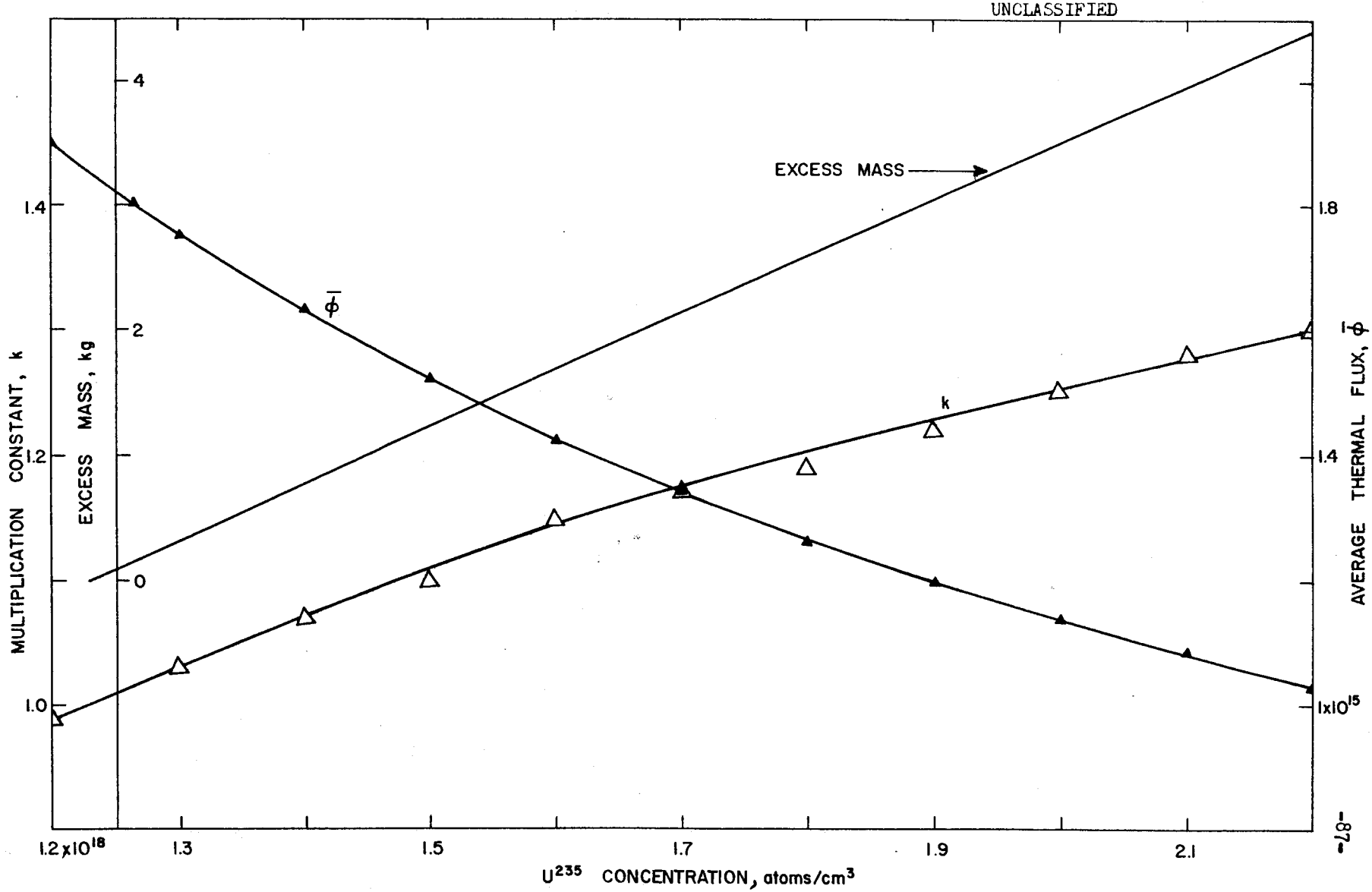

Fig. 39. One- Speed Diffusion Theory Results.

in general, beyond the scope of this report except where obvious discrepancies have been introduced by the choice of a calculational model to represent the reactor under consideration. Likewise, the "basic" constants used can not be questioned herein, except where the absence of exact data has forced the use of extrapolation or guess work.

The model employed for most of the nuclear calculations is based upon three-group diffusion theory, employing the basic assumptions that the flux is separable in space and energy and that the spatial component is separable into the usual orthogonal coordinates. Differential equations are replaced by difference equations and the latter are solved by machine iteration. One-dimensional, three-region computation is provided; finiteness in other dimensions is accounted for by introduction of a neutron leakage cross-section for each group ($D_i B_i^2$) into the differential equations[5].

It is clear that the assumption of spatial separability of the flux is rather invalid for many of the cases which were computed. The magnitude of the error thus introduced is not known. In many cases, flux plots which were somewhat distorted were used for computation of Pe/RM because the reactor multiplication constant was not unity. This distortion occurs because in order to make the computation, the machine code changes ν, the number of neutrons produced per fission, until the multiplication constant is unity. It is believed that for the "supercritical" reactors on which most of the results are based, that the calculated Pe/RM is conservative (erroneously small). This belief is sustained by the results of a calculation made during a study of the control system. For this calculation, the thermal absorption cross-section of the fuel region was increased to correspond to the insertion of control plates into the core. The flux peaking ratio increased from 8.35 to 11.37 at a k_{eff} of 0.997. This increase

is somewhat greater than might be expected on the basis of the increased "blackness" of the fuel zone only. However, even though all results may be conservative, the presence of any distortion certainly restricts the validity of comparison of the core effectiveness of reactors which have differing values of k_{eff}. This type of comparison was used for instance, in evaluating the characteristics of the different reflectors.

As mentioned previously, there is some question regarding the value of reflector savings which should be added to the Y and Z dimensions for computation in the X-direction. Even if values were chosen which were accurate in terms of reactivity, these might not produce the correct flux pictures.

Another questionable aspect of the calculations is the validity of the three-group constants used as inputs for the machine calculations. These constants depend, with varying degrees of sensitivity upon the validity of the energy spectrum and flux averaging procedures used in their calculation. The details of the methods employed are included in Appendix A. Many of the constants used were not prepared during this study, but were taken directly from an earlier report[1].

In addition to these considerations, there exists always the possibility of human error in the preparation of input data and the interpretation of results. Every attempt has been made to limit this possibility; however, experience indicates that such errors are nearly impossible to eliminate.

BIBLIOGRAPHY

1. Cheverton, R. D., et al
   High Flux Research Reactor
   ORNL CF 56-8-206

2. Link, L. E., et al
   The Mighty Mouse Reactor Preliminary Design Study
   ANL-5688

3. Aeronutronic Systems, Inc.
   A Selection Study for an Advanced Engineering Test Reactor
   U-047

4. Alexander, J. H. and Given, N. D.
   The Eyewash Program for UNIVAC
   ORNL-1925

5. Bate, R. R., Einstein, L. T. and Kinney, W. E.
   Description and Operating Manual for the Three-Group, Three-Region Reactor Code for ORACLE
   ORNL CF 55-1-76

6. Bolger, J. C., et al
   Feasibility Study of a Superflux Reactor
   MIT Practice School Report KT-262

7. Elgert, O. J., et al
   Preliminary Investigations for an Advanced Engineering Test Reactor
   Internuclear Co.
   Internuc-9 and addendum

8. Hughes, D. J. and Harvey, J. A.
   Neutron Cross Sections
   BNL-325

9. Hughes, D. J. and Schwartz, R. B.
   Neutron Cross Sections
   BNL-325 Supplement No. 1

10. Kasten, P. R.
    Aqueous Homogeneous Research Reactor - Feasibility Study
    ORNL-2256

11. Kitzes, A. E.
    A Discussion of Liquid Metals as Pile Coolants
    ORNL-360

12. Laurence, G. C. and Ward, A. G.
    Some Calculations on Heat Production and Shielding for NRU
    RDP-44

13. McAdams, W. H.
Heat Transmission, third edition
McGraw-Hill Book Co., Inc., New York

14. Mallon, R. G., et al
Conceptual Design of an Advanced Engineering Test Reactor
ASTRA-200 E 1.1
NYO-4849

15. Nelson, C. A.
USAEC and Atomic Energy of Canada Limited Meeting July 7 and 8, 1953, Held at Savannah River Plant
WASH-348

16. Sisman, O., Brundage, W. E. and Parkinson, W. W.
A Fluoride Fuel In-Pile Loop Experiment
ORNL-1965

17. Charpie, R. A.
Private Communication

18. Webster, J. W.
Practical Reactor Theory
ORNL-1631

19. Lennox, D. H. and Kelber, C. N.
Summary Report on the Hazards of the Argonaut Reactor
ANL-5647

20. Tonks, L.
The Thermal Test Reactor of the Knolls Atomic Power Laboratory
AECD-3530

21. Sampson, J. B., Robb, W. L., Stehn, J. R. and Davidson, J. K.
Poisoning in Thermal Reactors Due to Stable Fission Products
KAPL-1226

22. Hurwitz, H., Nims, J. B. and Storm, M. L.
Multigroup Treatments of Gamma Ray Absorption
KAPL-753

23. Alexander, L. G.
The Integral Spectrum Method for Gamma Heating Calculations in Nuclear Reactors
ORNL CF 56-11-82

24. Beck, C. K.
Nuclear Reactors for Research
D. Van Nostrand Co., Princeton, N. J. (1957)

25. Gamble, R. L.
Prompt Fission Gamma Rays from Uranium-235
Ph.D. Dissertation, June 1955, University of Texas, Austin, Texas

26. Rockwell, T.
Reactor Shielding Design Manual
D. Van Nostrand Co., Princeton, N. J. (1956)

27. Goldstein, H. and Wilkins, J. E.
Calculations of the Penetration of Gamma Rays
NYO-3075

28. Mittleman, P. S. and Liedtke, R. A.
Gamma Rays from Thermal Neutron Capture
Nucleonics 13, No. 5, 50 (1955)

29. Moteff, J.
Miscellaneous Data for Shielding Calculations
APEX-176

30. Jahnke, E. and Emde, F.
Tables of Functions
B. G. Teubner, Leipzig and Berlin, (1940)

31. The Reactor Handbook
Technical Information Service
U. S. Atomic Energy Commission

32. Callihan, A. D.
Personal Communication

33. Nestor, C. W.
Personal Communication

34. Ward, A. G.
The Problem of Flux Instability in Large Power Reactors
AECL-345, CRRP-657

35. C.R.C. Standard Mathematical Tables
Chemical Rubber Publishing Co., Cleveland, Ohio (1956)

APPENDIX A

THREE-GROUP CONSTANTS

Input data required for the ORACLE three-group, three region code used extensively in these calculations necessitated the use of group constants which had been appropriately averaged over the chosen energy groups. The basic information for preparing group constants is microscopic cross sections given as a function of energy or lethargy. The data of Nestor[33] provided the majority of the values given in Table 4 for thirty lethargy groups; however, microscopic absorption cross sections for some of the high energy groups were calculated from the data of Hughes[9]. These were:

1. $\bar{\sigma}_a$ of Al for lethargy groups 1 through 11
2. $\bar{\sigma}_a$ of Fe for lethargy groups 1 through 2
3. $\bar{\sigma}_a$ of O_2 for lethargy groups 1 through 8
4. $\bar{\sigma}_a$ of Zr for lethargy groups 1 through 12

These thirty-group cross sections - $\bar{\sigma}_a$, $\bar{\sigma}_{tr}$, $\bar{\sigma}_f$, and $\xi\bar{\sigma}_t$ - were averaged into two fast groups which included lethargy groups 1 through 7 and lethargy groups 8 through 30, and these were designated as the fast and epithermal groups respectively. The energy ranges covered by these groups were 10 Mev - 9.118 Kev and 9.118 Kev - 0.0252 ev; the fast group was thus chosen to include the entire fission spectrum. All neutrons of energy below 0.0252 ev were included in the thermal group. For shorthand notation throughout the calculations, the fast, epithermal and thermal groups were designated as groups 1, 2 and 3 respectively.

The method of obtaining three-group constants from the available thirty-

group constants is given by Webster[18] and is a flux-averaging procedure. In this method the individual macroscopic cross sections are multiplied by a weighting function for the particular group, and these values are summed over the groups for which the average is desired. This sum is then divided by a summation of the weighting functions, and the result is a flux-averaged cross section. Expressed mathematically for the average absorption cross section of the fast group, this becomes

$$\bar{\Sigma}_{a_i} = \frac{\sum_{i=1}^{7} \phi_i \, \Delta u_i \, \Sigma_{a_i}}{\sum_{i=1}^{7} \phi_i \, \Delta u_i} \qquad \text{A-1}$$

$\bar{\Sigma}_{a_i}$ = the macroscopic absorption cross section for the ith lethargy group

$\sum_{j=1}^{n} \Sigma_{a_i}^{j}$, j = 1, 2, . . . n atomic species.

Δu_i = the lethargy width of the ith lethargy group.

ϕ_i = the neutron flux associated with ith lethargy group.

The ϕ_i for use in Equation A-1 above is obtained from the often used approximation

$$\phi_i \cong \frac{q_i}{\xi_i \, \Sigma_{t_i}} \qquad \text{A-2}$$

q_i = slowing down density in ith group.

$\xi \Sigma_{t_i} = \sum_{j=1}^{n} \xi_i^{j} \, \Sigma_{t_i}^{j}$, j = 1, 2, . . . n nuclear species.

$\xi = 1 + \frac{\alpha \ln \alpha}{1 - \alpha}$, $\alpha = \left(\frac{A-1}{A+1}\right)^2$, A = atomic mass of species.

Σ_{t_i} = total macroscopic cross section for ith group.

The q_i is obtained from the recursion formula given by Webster[18], page 44, Equation 2.99:

$$q_i = \frac{q_{i-1}(1 - C_{N_i}) + \nu Z_i}{1 + C_{N_i}} \qquad A-3$$

This formula gives q(u) at $u = u_i$ in terms of the value at $u = u_{i-1}$ starting with $q_0 = 0$ and

$$C_{N_i} = \left[\frac{B^2}{3\xi\Sigma_{ti}\Sigma_{tri}} + \frac{\Sigma_{ai}}{\xi\Sigma_{ti}}\right]\left[\frac{u_i - u_{i-1}}{2}\right] \qquad A-4$$

B^2 = geometric buckling chosen to account for buckling in all directions

Σ_{ti} = total macroscopic total cross section for ith lethargy group

$= \sum_{j=1}^{n} \Sigma_{ti}^{j}$, j = 1, 2, ...n atomic species.

Σ_{tri} = total transport macroscopic cross section for ith lethargy group = $\sum_{j=1}^{n} \Sigma_{tri}^{j}$, j = 1, 2, . . . n atomic species.

$\frac{u_i - u_{i-1}}{2}$ = average lethargy in ith lethargy group.

$$Z_i = \int_{u_{i-1}}^{u_i} f(u)\,du \qquad A-5$$

$f(u)$ = fraction of fission neutrons born into unit lethargy about u.

The above sequence of calculations illustrates the method used to obtain Σ_{a_1}. To obtain the values for $\xi\Sigma_{t_1}$, $\nu\Sigma_{f_1}$, and Σ_{tr_1} , exactly the same sequence of computation is followed starting with the following equations corresponding to A-1 for Σ_{a_1} .

$$\Sigma_{tr_1} = \frac{\sum_{i=1}^{7} \phi_i \Delta u_i \Sigma_{tr_i}}{\sum_{i=1}^{7} \phi_i \Delta u_i} \qquad A-6$$

$$\xi \Sigma_{t_1} = \frac{\sum_{i=1}^{7} \phi_i \Delta u_i \xi \Sigma_{t_i}}{\sum_{i=1}^{7} \phi_i \Delta u_i} \qquad A-7$$

$$\nu \Sigma_{f_1} = \frac{\sum_{i=1}^{7} \phi_i \Delta u_i \nu \Sigma_{f_i}}{\sum_{i=1}^{7} \phi_i \Delta u_i} \qquad A-8$$

For the epithermal or second group exactly the same sequence of calculations is carried through using groups 8 through 30 of the thirty group cross sections to obtain Σ_{a_2} , $\xi \Sigma_{t_2}$, Σ_{tr_2} , and $\nu \Sigma_{f_2}$. For computed values of these quantities see Tables 5, 7 and 8.

The age, τ , required for the calculation of removal cross section, is

$$\tau = \int_0^{u} \frac{1}{3 \Sigma_{tr_1} \xi \Sigma_1} \, du \qquad A-9$$

The thirty group constants are averaged for values of τ. The formulae used for the averaging for τ_1 and τ_2 are

$$\tau_1 = \sum_{i=1}^{7} \frac{F_i \Delta u_i}{3 \Sigma_{tr_i} \xi \Sigma_{t_i}} \qquad A-10$$

$$\tau_2 = \sum_{i=8}^{30} \frac{F_i \, \Delta u_i}{3 \Sigma_{tr_i} \, \xi \, \Sigma_{t_i}} \qquad A\text{-}11$$

F_i = fraction of neutrons born above of ith group and all other symbols have the same meaning as before.

Transfer cross sections, Σ_{x_1}, and Σ_{x_2}, are found by subtracting the absorption cross sections from the removal cross sections. Their values are given by A-12 and A-13 below.

$$\Sigma_{x_1} = \frac{D_1}{\tau_1} - \Sigma_{a_1} \qquad A\text{-}12$$

$$\Sigma_{x_2} = \frac{D_2}{\tau_2} - \Sigma_{a_2} \qquad A\text{-}13$$

Σ_{x_1} = macroscopic transfer cross section for fast group.

Σ_{x_2} = macroscopic transfer cross section for epithermal group.

$$D_1 = \frac{1}{3 \Sigma_{tr_1}} \qquad A\text{-}14$$

$$D_2 = \frac{1}{3 \Sigma_{tr_2}} \qquad A\text{-}15$$

Tables 5, 7 and 8 list computed values of group constants D_1, D_2, Σ_{x_1}, and Σ_{x_2} for several water to metal ratios, geometric bucklings and uranium concentrations.

The thermal cross sections were corrected to new temperatures by considering the thermal flux to be Maxwellian and adjusting the average by the square root of the temperature ratio. For a change in reactor temperature the epithermal and fast cross sections are computed by correcting only for density changes in the reactor materials.

TABLE 4

MICROSCOPIC CROSS SECTIONS OF ELEMENTS

(All values expressed in barns)

Energy Group	Lethargy Interval, ΔU	Aluminum			Deuterium			Iron		
		$\bar{\sigma}_a$	$3\bar{\sigma}_{tr}$	$\xi\bar{\sigma}_t$	$\bar{\sigma}_a$	$3\bar{\sigma}_{tr}$	$\xi\bar{\sigma}_t$	$\bar{\sigma}_a$	$3\bar{\sigma}_{tr}$	$\xi\bar{\sigma}_t$
1	0.5	0.111	6.62	0.17	-	2.33	0.99	0.14	8.54	0.10
2	0.5	0.025	7.33	0.19	-	3.26	1.39	0.08	8.86	0.10
3	0.5	0.004	7.91	0.20	-	4.37	1.78	0.04	8.44	0.09
4	0.5	0	8.18	0.18	-	5.40	2.12	0.04	6.96	0.08
5	0.5	0	7.13	0.26	-	6.19	2.36	0.04	6.91	0.09
6	1.5	0.001	12.06	0.39	-	6.89	2.53	0.05	9.32	0.12
7	3.0	0.003	11.81	0.13	-	6.97	2.53	0.05	14.19	0.25
8	3.0	0.01	4.62	0.11	-	6.97	2.53	0.05	19.85	0.29
9	1.4	0.01	4.51	0.11	-	6.97	2.53	0.04	29.62	0.38
10	1.2	0.01	4.51	0.11	-	6.97	2.53	0.05	32.56	0.39
11	0.8	0.01	4.51	0.11	-	6.97	2.53	0.08	33.37	0.40
12	0.4	0.01	4.50	0.11	-	6.97	2.53	0.10	32.95	0.39
13	0.8	0.01	4.49	0.11	-	6.97	2.53	0.14	32.93	0.41
14	1.2	0.02	4.46	0.11	-	6.97	2.53	0.24	33.62	0.41
15	0.4	0.03	4.43	0.11	-	6.97	2.53	0.35	34.43	0.41
16	0.4	0.04	4.41	0.11	-	7.05	2.60	0.43	32.72	0.40
17	0.4	0.04	4.39	0.11	-	7.23	2.63	0.53	32.34	0.41
18	0.4	0.05	4.36	0.11	-	7.35	2.71	0.65	32.39	0.41
19	0.2	0.06	4.33	0.11	-	7.52	2.76	0.76	32.30	0.41
20	0.2	0.07	4.31	0.11	-	7.71	2.86	0.84	32.31	0.41
21	0.2	0.08	4.28	0.11	-	7.97	2.92	0.93	32.21	0.42
22	0.2	0.09	4.26	0.11	-	8.12	2.95	1.02	32.26	0.42
23	0.2	0.10	4.23	0.11	-	8.21	3.02	1.14	32.21	0.43
24	0.2	0.11	4.19	0.11	-	8.49	3.15	1.26	32.15	0.43
25	0.2	0.12	4.16	0.11	-	8.85	3.25	1.39	32.46	0.44
26	0.2	0.13	4.12	0.11	-	9.03	3.31	1.55	32.69	0.45
27	0.2	0.15	4.08	0.11	-	9.23	3.44	1.70	32.72	0.45
28	0.2	0.17	4.03	0.11	-	9.65	3.57	1.87	32.67	0.46
29	0.2	0.18	3.98	0.11	-	9.87	3.61	2.08	32.37	0.46
30	0.2	0.20	3.92	0.11	-	10.22	3.75	2.30	31.93	0.47

TABLE 4 (Con'd)

Energy Group	Lethargy Interval, ΔU	Uranium-235				Oxygen			Zirconium		
		$\bar{\sigma}_a$	$3\bar{\sigma}_{tr}$	$\bar{\sigma}_f$	$\xi\bar{\sigma}_t$	$\bar{\sigma}_a$	$3\bar{\sigma}_{tr}$	$\xi\bar{\sigma}_t$	$\bar{\sigma}_a$	$3\bar{\sigma}_{tr}$	$\xi\bar{\sigma}_t$
1	0.5	1.32	18.63	1.30	0.06	0.02	2.87	0.12	0.49	9.97	0.07
2	0.5	1.32	20.04	1.30	0.06	0.067	4.63	0.29	0.45	10.14	0.07
3	0.5	1.34	20.39	1.30	0.06	0	4.03	0.13	0.29	11.15	0.08
4	0.5	1.36	20.04	1.30	0.06	0	4.67	0.41	0	13.74	0.11
5	0.5	1.39	17.83	1.32	0.06	0	12.93	0.37	0	18.95	0.14
6	1.5	1.59	24.14	1.50	0.11	0	11.58	0.45	0	24.83	0.19
7	3.0	2.76	37.00	2.39	0.12	0	10.71	0.45	0	26.49	0.19
8	3.0	8.88	29.16	6.51	0.22	-	10.71	0.45	0	28.98	0.24
9	1.4	24.69	24.71	17.35	0.34	-	10.71	0.45	0	34.59	0.27
10	1.2	44.58	23.99	31.06	0.52	-	10.71	0.45	0	38.46	0.29
11	0.8	59.75	23.99	41.44	0.59	-	10.71	0.45	0	41.06	0.30
12	0.4	64.33	23.99	45.17	0.61	-	10.71	0.45	0	41.66	0.30
13	0.8	87.62	23.99	41.99	0.22	-	10.71	0.45	0.01	41.65	0.30
14	1.2	24.37	23.99	14.91	0.28	-	10.71	0.45	0.01	41.98	0.31
15	0.4	80.74	23.99	61.91	0.58	-	10.71	0.45	0.02	42.20	0.31
16	0.4	63.16	23.99	54.12	0.63	-	10.71	0.45	0.03	43.31	0.31
17	0.4	89.00	23.99	76.66	1.07	-	10.71	0.45	0.04	42.46	0.31
18	0.4	184.66	23.99	147.83	1.99	-	10.74	0.45	0.04	42.43	0.31
19	0.2	230.33	23.99	184.83	1.94	-	10.85	0.45	0.05	42.41	0.31
20	0.2	221.50	23.99	180.00	1.95	-	10.92	0.46	0.06	42.39	0.31
21	0.2	230.00	23.99	190.33	2.03	-	10.98	0.46	0.06	42.37	0.31
22	0.2	246.33	24.24	205.33	2.20	-	11.06	0.46	0.07	42.35	0.31
23	0.2	267.83	24.54	223.90	2.41	-	11.14	0.46	0.08	42.32	0.31
24	0.2	298.33	24.59	249.33	2.73	-	11.20	0.47	0.09	42.35	0.31
25	0.2	337.66	24.59	282.16	3.08	-	11.27	0.47	0.10	42.84	0.32
26	0.2	380.00	24.59	320.00	3.42	-	11.73	0.47	0.11	43.35	0.32
27	0.2	428.33	24.59	360.00	3.83	-	11.54	0.48	0.12	44.20	0.33
28	0.2	475.83	24.59	405.00	4.30	-	11.61	0.48	0.14	43.25	0.31
29	0.2	535.00	24.59	455.00	4.80	-	11.84	0.49	0.15	42.31	0.35
30	0.2	600.83	24.59	510.00	5.43	-	11.93	0.51	0.17	46.93	0.33

TABLE 5

THREE GROUP CONSTANTS FOR VARIOUS URANIUM CONCENTRATIONS, BUCKLINGS AND METAL-TO-WATER RATIOS

	(a)	(a)	(a)	(b)
B_g^2, cm^{-2}	3.54×10^{-4}	3.54×10^{-4}	3.54×10^{-4}	9.86×10^{-4}
N_{235}, atoms/cm^3	0.5×10^{18}	1×10^{18}	2×10^{18}	2×10^{18}
N_{Al}, atoms, cm^3	3.59×10^{20}	7.18×10^{20}	14.36×10^{20}	14.36×10^{20}
N_{D_2O}, atoms/cm^3	3.3×10^{22}	3.28×10^{22}	3.25×10^{22}	3.25×10^{22}
M/W, $\frac{\text{Vol. of Metal}}{\text{Vol. of Water}}$	0.006	0.012	0.024	0.024
Σa_1, cm^{-1}	2.49×10^{-6}	4.54×10^{-6}	8.78×10^{-6}	8.8×10^{-6}
Σa_2, cm^{-1}	5.29×10^{-5}	1.11×10^{-4}	2.23×10^{-4}	2.21×10^{-4}
Σa_3, cm^{-1}	4.80×10^{-4}	8.96×10^{-4}	1.73×10^{-3}	1.73×10^{-3}
Σx_1, cm^{-1}	3.42×10^{-2}	3.42×10^{-2}	3.44×10^{-2}	3.40×10^{-2}
Σx_2, cm^{-1}	1.37×10^{-2}	1.49×10^{-2}	1.45×10^{-2}	1.45×10^{-2}
D_1, cm	1.29	1.275	1.286	1.27
D_2, cm	1.19	1.223	1.207	1.20
D_3, cm	0.874	0.874	0.874	0.874
$\nu\Sigma_{f_1}$, cm^{-1}	2.44×10^{-6}	4.84×10^{-6}	9.73×10^{-6}	9.75×10^{-6}
$\nu\Sigma_{f_2}$, cm^{-1}	8.65×10^{-5}	1.72×10^{-4}	3.42×10^{-4}	3.39×10^{-4}
$\nu\Sigma_{f_3}$, cm^{-1}	7.15×10^{-4}	1.43×10^{-3}	2.86×10^{-3}	2.86×10^{-3}

Table 5 continued

	(c)	(c)		
B_g^2, cm^{-2}	5.43×10^{-4}	5.43×10^{-4}	-	-
N_{235}, atoms/cm^3	2×10^{18}	1.75×10^{18}	1×10^{19}	2×10^{19}
N_{Al}, atoms, cm^3	14.36×10^{20}	12.6×10^{20}	2.55×10^{22}	2.55×10^{22}
N_{D_2O}, atoms/cm^3	3.25×10^{22}	3.26×10^{22}	1.92×10^{22}	1.92×10^{22}
M/W, $\frac{\text{Vol. of Metal}}{\text{Vol. of Water}}$	0.024	0.021	0.73	0.73
Σ_{a_1}, cm^{-1}	8.99×10^{-6}	7.87×10^{-6}	117×10^{-6}	138×10^{-6}
Σ_{a_2}, cm^{-1}	2.23×10^{-4}	1.95×10^{-4}	15.9×10^{-4}	24.25×10^{-4}
Σ_{a_3}, cm^{-1}	1.73×10^{-3}	1.52×10^{-3}	11.1×10^{-3}	17×10^{-3}
Σ_{x_1}, cm^{-1}	3.40×10^{-2}	3.41×10^{-2}	1.386×10^{-2}	1.396×10^{-2}
Σ_{x_2}, cm^{-1}	1.45×10^{-2}	1.48×10^{-2}	1.099×10^{-2}	1.112×10^{-2}
D_1, cm	1.271	1.277	1.38	1.385
D_2, cm	1.206	1.21	1.66	1.66
D_3, cm	0.874	0.874	1.255	1.23
$\nu\Sigma_{f_1}$, cm^{-1}	9.91×10^{-6}	8.68×10^{-6}	48×10^{-6}	96×10^{-6}
$\nu\Sigma_{f_2}$, cm^{-1}	3.43×10^{-4}	3.00×10^{-4}	13.2×10^{-4}	26.4×10^{-4}
$\nu\Sigma_{f_3}$, cm^{-1}	2.86×10^{-3}	2.50×10^{-3}	12.2×10^{-3}	24.4×10^{-3}

Note: Columns for which no buckling is listed were obtained from EYEWASH code calculations as reported by R. D. Cheverton[1], Table IV, page 148.

Table 5 continued

B_g^2, cm^{-2}				
N_{235}, atoms/cm^3	3×10^{19}	4×10^{19}	5×10^{19}	6×10^{19}
N_{Al}, atoms, cm^3	2.55×10^{22}	2.55×10^{22}	2.55×10^{22}	2.55×10^{22}
N_{D_2O}, atoms/cm^3	1.92×10^{22}	1.92×10^{22}	1.92×10^{22}	1.92×10^{22}
M/W, $\frac{\text{Vol. of Metal}}{\text{Vol. of Water}}$	0.73	0.73	0.73	0.73
Σ_{a_1}, cm^{-1}	160.6×10^{-6}	182.6×10^{-6}	204.7×10^{-6}	225.5×10^{-6}
Σ_{a_2}, cm^{-1}	29.87×10^{-4}	38.49×10^{-4}	46.4×10^{-4}	48.19×10^{-4}
Σ_{a_3}, cm^{-1}	22.8×10^{-3}	28.84×10^{-3}	34.6×10^{-3}	40.66×10^{-3}
Σ_{x_1}, cm^{-1}	1.406×10^{-2}	1.356×10^{-2}	1.414×10^{-2}	1.363×10^{-2}
Σ_{x_2}, cm^{-1}	1.11×10^{-2}	1.082×10^{-2}	1.101×10^{-2}	1.089×10^{-2}
D_1, cm	1.391	1.391	1.39	1.392
D_2, cm	1.652	1.671	1.642	1.674
D_3, cm	1.20	1.175	1.15	1.136
$\nu\Sigma_{f_1}$, cm^{-1}	144×10^{-6}	192.8×10^{-6}	240×10^{-6}	288×10^{-6}
$\nu\Sigma_{f_2}$, cm^{-1}	39.5×10^{-4}	59.75×10^{-4}	65.9×10^{-4}	78.9×10^{-4}
$\nu\Sigma_{f_3}$, cm^{-1}	36.6×10^{-3}	49.6×10^{-3}	61.0×10^{-3}	74.4×10^{-3}

Table 5 continued

B_g^2, cm^{-2}	—	—	—	—
N_{235}, atoms/cm^3	7×10^{19}	8×10^{19}	9.18×10^{19}	12×10^{19}
N_{Al}, atoms, cm^3	2.55×10^{22}	2.55×10^{22}	2.55×10^{22}	2.55×10^{22}
N_{D_2O}, atoms/cm^3	1.92×10^{22}	1.92×10^{22}	1.92×10^{22}	1.92×10^{22}
M/W, $\frac{\text{Vol. to Metal}}{\text{Vol. to Water}}$	0.73	0.73	0.73	0.73
Σ_{a_1}, cm^{-1}	269.5×10^{-6}	269.3×10^{-6}	295.2×10^{-6}	357×10^{-6}
Σ_{a_2}, cm^{-1}	54.31×10^{-4}	62.14×10^{-4}	70.36×10^{-4}	90.03×10^{-4}
Σ_{a_3}, cm^{-1}	46.4×10^{-3}	52.48×10^{-3}	59.45×10^{-3}	76.12×10^{-3}
Σ_{x_1}, cm^{-1}	1.422×10^{-2}	1.369×10^{-2}	1.372×10^{-2}	1.380×10^{-2}
Σ_{x_2}, cm^{-1}	1.104×10^{-2}	1.094×10^{-2}	1.097×10^{-2}	1.104×10^{-2}
D_1, cm	1.392	1.391	1.390	1.388
D_2, cm	1.639	1.673	1.672	1.670
D_3, cm	1.11	1.092	1.067	1.012
$\nu\Sigma_{f_1}$, cm^{-1}	336×10^{-6}	384×10^{-6}	430×10^{-6}	576×10^{-6}
$\nu\Sigma_{f_2}$, cm^{-1}	92.3×10^{-4}	105.2×10^{-4}	120.8×10^{-4}	158×10^{-4}
$\nu\Sigma_{f_3}$, cm^{-1}	85.4×10^{-3}	99.4×10^{-3}	113.8×10^{-3}	148.8×10^{-3}

Table 5 continued

		(d)
B_g^2, cm^{-2}	—	18.3×10^{-4}
N_{235}, atoms/cm^3	15×10^{19}	3.1×10^{18}
N_{Al}, atoms, cm^3	2.55×10^{22}	18×10^{20}
N_{D_2O}, atoms/cm^3	1.92×10^{22}	3.21×10^{22}
M/W, $\frac{\text{Vol. of Metal}}{\text{Vol. of Water}}$	0.73	0.03
Σ_{a_1}, cm^{-1}	422.8×10^{-6}	6.87×10^{-6}
Σ_{a_2}, cm^{-1}	110.9×10^{-4}	2.62×10^{-4}
Σ_{a_3}, cm^{-1}	93.84×10^{-3}	4.43×10^{-3}
Σ_{x_1}, cm^{-1}	1.389×10^{-2}	3.37×10^{-2}
Σ_{x_2}, cm^{-1}	1.111×10^{-2}	1.45×10^{-2}
D_1, cm	1.387	1.267
D_2, cm	1.667	1.206
D_3, cm	0.9592	0.874
$\nu\Sigma_{f_1}$, cm^{-1}	720×10^{-6}	15.03×10^{-6}
$\nu\Sigma_{f_2}$, cm^{-1}	197.2×10^{-4}	5.06×10^{-4}
$\nu\Sigma_{f_3}$, cm^{-1}	186×10^{-3}	4.43×10^{-3}

(a) cylindrical geometry 10' D x 10' H
(b) cylindrical geometry 6' D x 6' H
(c) cylindrical geometry 10' D x 6' H
(d) double slab geometry 180 cm x 180 cm x 150 cm

TABLE 6

WEIGHTING FUNCTIONS (= $\phi\Delta U$) FOR CALCULATING GROUP CONSTANTS

Group	ΔU	(a) $B_g^2 = 3.54 \times 10^{-4}$, $N_{235} = 0.5 \times 10^{18}$, $N_{Al} = 3.59 \times 10^{20}$, $N_{D_2O} = 3.3 \times 10^{22}$	(b) $B_g^2 = 3.54 \times 10^{-4}$, $N_{235} = 1 \times 10^{18}$, $N_{Al} = 7.18 \times 10^{20}$, $N_{D_2O} = 3.28 \times 10^{22}$	(c) $B_g^2 = 3.54 \times 10^{-4}$, $N_{235} = 2 \times 10^{18}$, $N_{Al} = 14.36 \times 10^{20}$, $N_{D_2O} = 3.25 \times 10^{22}$
1	0.5	0.185	0.186	0.187
2	0.5	0.875	0.879	0.883
3	0.5	2.278	2.294	2.309
4	0.5	3.572	3.603	3.632
5	0.5	4.721	4.783	4.843
6	1.5	17.106	17.279	17.464
7	3.0	39.110	39.540	39.971
8	3.0	39.528	39.99	40.377
9	1.4	18.383	18.59	18.767
10	1.2	15.710	15.88	16.028
11	0.8	10.451	10.56	10.655
12	0.4	5.215	5.28	5.32
13	0.8	10.407	10.52	10.61
14	1.2	16.763	15.70	15.86
15	0.4	5.18	5.24	5.28
16	0.4	5.07	5.12	5.13
17	0.4	5.01	5.06	5.07
18	0.4	4.97	5.02	5.06
19	0.2	2.43	2.49	2.47
20	0.2	2.36	2.38	2.39
21	0.2	2.25	2.29	2.29
22	0.2	2.23	2.26	2.26
23	0.2	2.18	2.21	2.22
24	0.2	2.10	2.12	2.12
25	0.2	2.03	2.05	2.06
26	0.2	2.00	2.02	2.03
27	0.2	1.92	1.94	1.95
28	0.2	1.86	1.88	1.88
29	0.2	1.84	1.85	1.85
30	0.2	1.77	1.78	1.78

(a) cylindrical geometry 10'D x 10'H
(b) cylindrical geometry 10'D x 10'H
(c) cylindrical geometry 10'D x 10'H

TABLE 6 (Continued)

Group	ΔU	(d) $B_g^2 = 5.43 \times 10^{-4}$, $N_{235} = 2 \times 10^{18}$, $N_{Al} = 14.36 \times 10^{20}$, $N_{D_2O} = 3.25 \times 10^{22}$	(e) $B_g^2 = 9.86 \times 10^{-4}$, $N_{235} = 2 \times 10^{18}$, $N_{Al} = 14.36 \times 10^{22}$, $N_{D_2O} = 3.25 \times 10^{22}$	(f) $B_g^2 = 18.3 \times 10^{-4}$, $N_{235} = 3.1 \times 10^{18}$, $N_{Al} = 18 \times 10^{20}$, $N_{D_2O} = 3.21 \times 10^{22}$	(g) $N_{235} = 6.9 \times 10^{19}$
1	0.5	0.186	0.185	0.183	0.7686
2	0.5	0.882	0.878	0.872	4.147
3	0.5	2.305	2.295	2.276	10.60
4	0.5	3.692	3.613	3.561	17.27
5	0.5	4.834	4.812	4.772	21.76
6	1.5	17.408	17.284	17.049	77.06
7	3.0	39.70	39.807	38.078	157.6
8	3.0	40.06	40.42	37.34	142.9
9	1.4	18.54	18.68	17.13	60.94
10	1.2	15.84	15.87	14.44	49.07
11	0.8	10.52	10.51	9.52	30.95
12	0.4	5.25	5.24	4.74	14.91
13	0.8	10.47	10.41	9.37	28.63
14	1.2	15.65	15.48	13.84	40.70
15	0.4	5.20	5.14	4.58	13.03
16	0.4	5.05	4.99	4.44	12.55
17	0.4	4.98	4.92	4.37	11.99
18	0.4	4.97	4.99	2.34	11.33
19	0.2	2.43	2.40	2.12	5.352
20	0.2	2.35	2.62	2.05	5.095
21	0.2	2.25	2.17	1.95	4.837
22	0.2	2.22	2.15	1.93	4.649
23	0.2	2.11	2.14	1.88	4.558
24	0.2	2.09	2.05	1.80	4.211
25	0.2	2.02	1.99	1.74	3.945
26	0.2	1.99	1.96	1.71	3.731
27	0.2	1.91	1.88	1.65	3.508
28	0.2	1.84	1.81	1.58	3.280
29	0.2	1.82	1.78	1.56	3.040
30	0.2	1.74	1.71	1.50	2.800

(d) cylindrical geometry 10'D x 6'H
(e) cylindrical geometry 6'D x 6'H
(f) double slab geometry 180 cm x 180 cm x 150 cm
(g) double slab geometry 180 cm x 120 cm x 150 cm; data from R. D. Cheverton[1], Table I, page 98.

TABLE 7

THREE GROUP CONSTANTS FOR SEVERAL MATERIALS

IN TEMPERATURE RANGE 25° - 150°C

	D_2O				Al			
T, °C	25	50	100	150	25	50	100	150
Σ_{a_1}	0	0	0	0	2.259×10^{-4}	2.255×10^{-4}	2.245×10^{-4}	2.238×10^{-4}
Σ_{a_2}	0	0	0	0	0.001867	0.001864	0.001856	0.001850
Σ_{a_3}	6.42×10^{-5}	6.33×10^{-5}	6.14×10^{-5}	5.87×10^{-5}	0.0123	0.01228	0.01223	0.01218
Σ_{x_1}	0.02752	0.02713	0.02631	0.02518	2.902×10^{-4}	2.897×10^{-4}	2.885×10^{-4}	2.875×10^{-4}
Σ_{x2}	0.01651	0.01628	0.01578	0.01511	0.003017	0.003012	0.002999	0.002989
D_1	1.321	1.333	1.374	1.436	1.533	1.536	1.542	1.547
D_2	1.203	1.214	1.251	1.308	3.713	3.721	3.735	3.748
D_3	0.874	0.882	0.909	0.950	4.262	4.272	4.288	4.302

Note: Data for T = 25°C obtained from R. D. Cheverton[1]
Tables 2 and 3, page 146-47.

TABLE 7 (Continued)

	70% vol. Al 30% vol. D_2O				C
T, °C	25	50	100	150	25
Σ_{a_1}	1.577×10^{-4}	1.578×10^{-4}	1.571×10^{-4}	1.567×10^{-4}	0
Σ_{a_2}	0.001303	0.001305	0.001299	0.001295	5×10^{-5}
Σ_{a_3}	0.008588	0.00861	0.00858	0.00854	0.000228
Σ_{x_1}	0.006134	0.00834	0.00809	0.00775	0.00924
Σ_{x_2}	0.006390	0.00699	0.00683	0.00662	0.00464
D_1	1.450	1.469	1.487	1.512	1.432
D_2	2.273	2.297	2.341	2.403	0.942
D_3	1.933	1.985	2.027	2.09	0.945

TABLE 8

THREE GROUP CONSTANTS FOR SEVERAL METAL-TO-WATER RATIOS AND SEVERAL URANIUM CONCENTRATIONS

(Data from Cheverton[1], Table 5, p. 151)

N_{235}, $\frac{\text{atoms}}{\text{cm}^3}$	9.18×10^{19}	5.5×10^{19}	9.18×10^{19}	15×10^{19}
N_{Al}, $\frac{\text{atoms}}{\text{cm}^3}$	1.32×10^{22}	3.41×10^{22}	3.41×10^{22}	3.41×10^{22}
N_{D_2O}, $\frac{\text{atoms}}{\text{cm}^3}$	2.55×10^{22}	1.44×10^{22}	1.44×10^{22}	1.44×10^{22}
M/W	0.3	1.30	1.30	1.30
Σ_{a_1}, cm^{-1}	0.0002524	0.0002462	0.0003628	0.0004544
Σ_{a_2}, cm^{-1}	0.006747	0.004685	0.007251	0.01131
Σ_{a_3}, cm^{-1}	0.05708	0.03946	0.06120	0.09560
Σ_{x_1}, cm^{-1}	0.01957	0.009615	0.00972	0.009854
Σ_{x_2}, cm^{-1}	0.01301	0.008703	0.008783	0.008910
D_1, cm	1.358	1.425	1.423	1.420
D_2, cm	1.421	1.939	1.935	1.930
D_3, cm	0.9376	1.377	1.262	1.115
$\nu\Sigma_{f_1}$, cm^{-1}	0.0004415	0.000264	0.000442	0.000720
$\nu\Sigma_{f_2}$, cm^{-1}	0.01207	0.00724	0.01208	0.0197
$\nu\Sigma_{f_3}$, cm^{-1}	0.1138	0.06825	0.1109	0.186

APPENDIX B

1. Heat Production in the Al-D_2O Fast Reflector

The methods used in calculating the contribution to the heat generated in the reflector from prompt and delayed gamma absorption, neutron elastic scattering and absorption of gammas from neutron capture mentioned previously in Section III-G is presented below.

Fission Gammas: The heat deposited in the reflector from prompt and delayed fission gammas originating in the core was calculated by means of the integral spectrum method as outlined by Hurwitz et al[22]. The basic assumptions of this method are that photons are degraded in energy but not deflected by scattering collisions; the spectrum of the photon flux does not vary appreciably with distance from the source. Application of the above assumptions leads to the following simple exponential attenuation equation[23].

$$G(\rho) = \int_{\text{all } \gamma \text{ sources}} \frac{S_\gamma \bar{E}_\gamma P_\Omega \bar{\mu}_{e,m}}{\rho^2} \exp\left[-\sum_{n=1}^{m} \bar{\mu}_{e,m} \rho_m\right] dV \qquad B-1$$

where G = heating rate at a point located a distance ρ from the source

S = gamma source strength, photons/sec

$\bar{E}$ = mean energy of photons, Mev/photon

P_Ω = angular distribution of photons

$\mu_{e,m}$ = mean energy absorption coefficient for medium m

ρ_m = path length through each medium

It is further assumed that the flux is uniform at its average value throughout the volume of the reactor. This assumption is reasonable throughout the length and height of the fuel slab but not throughout the thickness. However, the assumption leads to a conservative estimate of the heating and serves to offset the underestimate inherent in the integral spectrum assumption.

For a slab source with a uniform neutron flux, the contribution to the heating from fission gammas in the core is given[23] by

$$\delta G = \frac{\bar{\Phi}_n \bar{\Sigma}_f N_\gamma \bar{\Sigma}_\gamma \bar{\mu}_{e,R}}{2\bar{\mu}_{e,f}} \left[E_2(\mu_{e,R}\, a) - E_2(\bar{\mu}_{e,R}\, a + \bar{\mu}_{e,f}\, b) \right] \quad B$$

where $\Sigma_f \bar{\Phi}_n$ = average number of fissions per cm^3 per sec in core

N_γ = number of photons emitted per fission

$\bar{\mu}_{e,f}$ = mean energy absorption coefficient for the fuel

$\bar{\mu}_{e,R}$ = mean energy absorption coefficient for the reflector

a = distance from the core interface to the point being investigated for gamma heating

b = thickness of fuel region

$E_2(\xi) = \int_{\xi}^{\infty} \frac{e^{-t}\,dt}{t^2}$ = exponential integral of order two

The total heating rate, G, is obtained by summing the individual heating rates, δ G's, for each energy group. The prompt-gamma energy groups were taken from a breakdown of Gamble's "Energy Spectrum of Prompt Gamma Rays from Fission of U^{235}"[25] as given in Table 9.

TABLE 9

GAMBLE'S ENERGY SPECTRUM FOR FISSION GAMMAS

$\bar{E}$, Mev/photon	$\bar{N}_\gamma$, photons/fission	$N_\gamma \bar{E}_\gamma$, Mev
1	3.2	3.2
1.5	0.8	1.2
2.3	0.85	1.96
3.0	0.15	0.45
5.0	0.2	1.0
		7.81 Mev total.

According to Rockwell[26], at equilibrium the energy released by delayed gammas is approximately equal to that released by the prompt gammas, but the average energy per photon is 0.7 Mev. Hence, to account for the delayed gamma energy, the heating rate, δ G, was calculated for $\bar{E}$ = 0.7 Mev and N_γ = 11.2 photons per fission so that the total delayed gamma energy released per fission equaled the prompt gamma energy released per fission. The energy absorption coefficients used in the calculations are given in Table 10.

TABLE 10

GAMMA ENERGY ABSORPTION COEFFICIENTS

$\bar{E}_\gamma$, Mev	μ_{D_2O}, cm^{-1}	μ_{Al}, cm^{-1}	μ_U, cm^{-1}	μ_R, cm^{-1}	μ_f, cm^{-1}
1	0.0352	0.0729	1.049	0.0616	0.053
1.5	0.0308	0.0653	0.684	0.0548	0.047
2.3	0.0275	0.0594	0.566	0.0498	0.042
3.0	0.0253	0.0566	0.595	0.0473	0.0395
5.0	0.0218	0.0513	0.710	0.0425	0.036
.7	0.0362	0.0769	1.671	0.0648	0.0565

$$\mu_R = \mu_{D_2O} \frac{V_{D_2O}}{V_{TR}} + \mu_{Al} \frac{V_{Al}}{V_{TR}}$$

$$\mu_f = \mu_{D_2O} \frac{V_{D_2O}}{V_{Tf}} + \mu_{Al} \frac{V_{Al}}{V_{Tf}} + \mu_U \frac{V_U}{V_{Tf}}$$

where $\frac{V_{D_2O}}{V_{TR}} = \frac{\text{Volume of } D_2O}{\text{Total volume of reflector}} = 0.3$

$\frac{V_{Al}}{V_{TR}} = \frac{\text{Volume of aluminum}}{\text{Total volume of reflector}} = 0.7$

$\frac{V_{D_2O}}{V_{Tf}} = \frac{\text{Volume of } D_2O}{\text{Total volume of fuel}} = 0.577$

$\frac{V_{Al}}{V_{Tf}} = \frac{\text{Volume of aluminum}}{\text{Total volume of fuel}} = 0.421$

$\frac{V_U}{V_{Tf}} = \frac{\text{Volume of uranium}}{\text{Total volume of fuel}} = 1.92 \times 10^{-3}$

It will be noted that this method of evaluating μ_R and μ_f assumes that the reflector and fuel are homogeneous mixtures of D_2O and the respective metals in these regions.

The average number of fission per cm^3 per sec is the product of the average effective thermal flux in the fuel, $\bar{\phi}_n$, and the macroscopic fission cross section for the fuel, Σ_f .

$$\bar{\phi}_n = 4 \times 10^{15}$$

$$\Sigma_f = N_u \sigma_f^u = 9.18 \times 10^{19} \times 515 \times 10^{-24}$$

$$\Sigma_f \bar{\phi}_n = 4 \times 10^{15} \times 9.18 \times 10^{19} \times 515 \times 10^{-24}$$

Evaluating Equation B-2 for each energy group using the constants given above led to the results indicated in Figure 10.

Neutron Elastic Scattering: The heating due to elastic scattering of fast neutrons is given by

$$G_{ne}(x) = \int_{E_n=0.01}^{\infty} \delta_{ne} E_n \phi_n(x, E_n) \Sigma_{ne}(E_n) \, dE_n \qquad B-3$$

By considering the contribution from the fast group only, the equation reduces to:

$$G_{ne}(x) = \delta_{ne} \bar{E}_1 \phi_1(x) \Sigma_{ne_1} \qquad B-4$$

where δ_{ne} = average fraction of the kinetic energy of the incident neutron appearing as kinetic energy of the target nucleus after an elastic scattering collision.

$\bar{E}_1$ = average energy of the fast neutron group - Mev

$\phi_1(x)$ = fast group flux, $\frac{\text{neutron-cm}}{\text{cm}^3\text{-sec}}$, obtained from the flux plot in Figure 20 and based upon an unperturbed flux at the center of the D_2O region of 2.5×10^{15}.

Σ_{ne_1} = macroscopic neutron elastic scattering cross section for the fast group, cm^{-1}.

G_{ne} must be summed with respect to all kinds of atoms present.

By summing isotropic scattering in the center of mass

$$\delta_{ne} = \frac{1}{2}\left[1 - \left(\frac{M-1}{M+1}\right)^2\right] \qquad B-5$$

where M = mass number.

The constants used in the above calculation were as follows:

TABLE 11

NEUTRON ELASTIC SCATTERING CONSTANTS

Atomic Species	$\bar{\sigma}_{ne}$, barns	Σ_{ne_1}, cm^{-1}	δ_{ne}
Deuterium	2.1	0.0411	0.445
Oxygen	2.5	0.0249	0.105
Aluminum	1.9	0.08	0.08

The average energy of the fast group was calculated by weighting each energy interval in the fast group with the flux for that interval. Using the values listed in Appendix A, the average weighted energy of the fast group was found to be 1.1 Mev. The fast flux at each point considered was obtained from the reflector flux plot in Figure 20.

Capture Gammas: The heat produced as a result of capture gammas in the reflector was calculated through the use of build-up factors in accordance with the method of Goldstein and Wilkins[27]. Application of this method yields the following equation for the geometry shown in Figure 40.

$$G(x,a) = \int_E \int_{x=0}^{a} \int_{y=0}^{\infty} \int_{\psi=0}^{2\pi} \Sigma_a \phi(x) N_\gamma(E) P(E)\, dE\, dy\; y\, d\psi\, dx' \frac{B_a(E,R)\, e^{-\mu_t R}\, \mu_e(E) E}{4\pi R^2} \qquad (B-6)$$

$\phi(x)$ = thermal neutron flux in the reflector, $\frac{\text{neutrons cm}}{\text{cm}^3 \text{ sec}}$

Σ_a = macroscopic absorption cross section for aluminum, cm^{-1}

N_γ = number of photons produced per neutron captured

P(E) = spectral distribution of the photons

Ba(E,R) = NDA "energy absorption build-up factor"

μ_t = total cross section (absorption plus scattering) in aluminum

μ_e = energy absorption coefficient, cm^{-1}

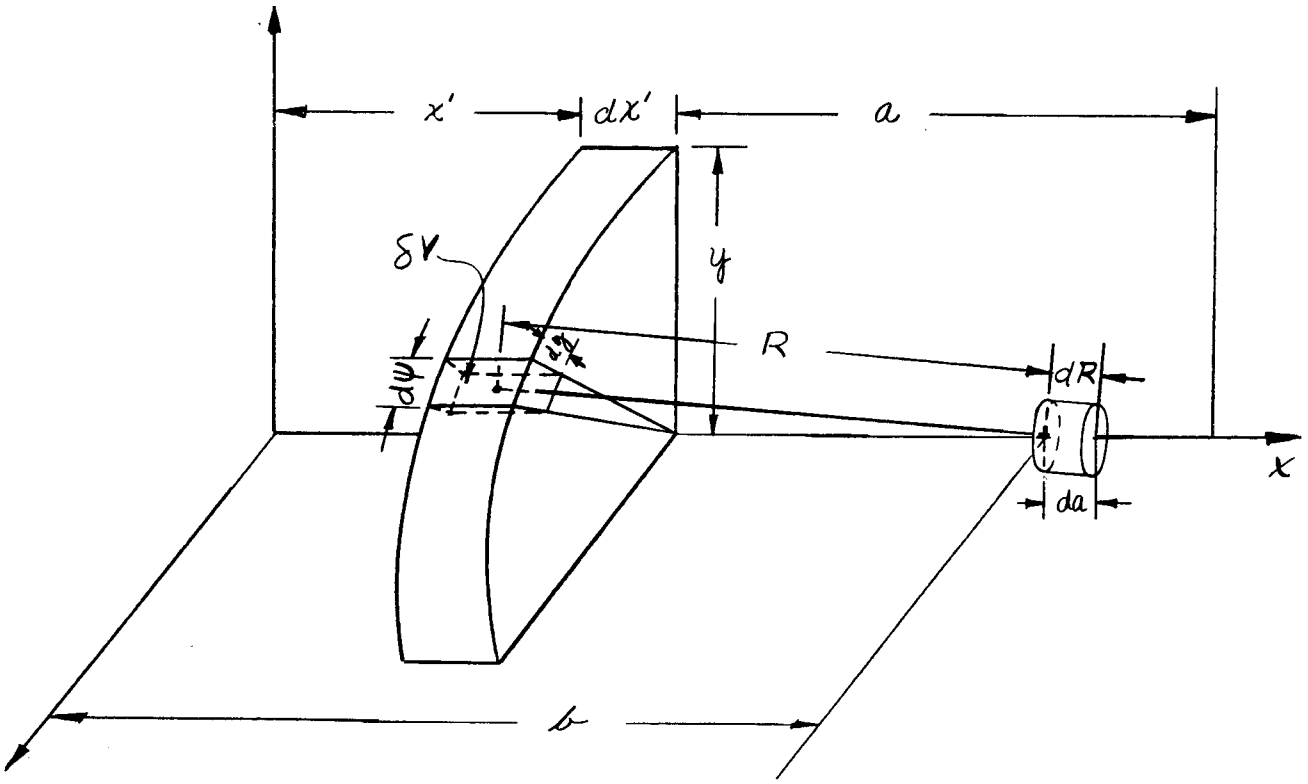

FIGURE 40

Dimensional Notation for Capture Gamma Heating
(a = reflector thickness)

From the above figure:

$$R^2 = y^2 + (b-x')^2$$

$$RdR = ydy$$

By making the above substitutions and integrating over ψ, the equation for any specified energy increment Δ E about E becomes:

$$G(x,a) = \frac{\Sigma_a N_r \mu_e E}{2} \int_{x'=0}^{a} \int_{R=b-x'}^{\infty} \frac{\phi(x')\, dR\, e^{-\mu_t R}}{R} B_a(E,R)\, dx' \qquad B-7$$

By assuming a linear build-up of the form:

$$Ba = 1 + m(E)\ \mu_t(E)\ R$$

the equation then becomes:

$$G(x,a) = \frac{\Sigma_a N_r \mu_e E}{2} \int_{x'=0}^{a} \int_{R=b-x'}^{\infty} \frac{\phi_n(x')(1+m\mu_t R)}{R} e^{-\mu_t R}\, dR\, dx'$$

$$= \frac{\Sigma_a N_r \mu_e E}{2} \int_{x'=0}^{a} \phi_n(x')\, dx' \int_{R=b-x'}^{\infty} \left(\frac{e^{-\mu_t R}}{R} + m\mu_t e^{-\mu_t R} \right) dR \qquad B-8$$

If the thermal neutron flux in the reflector is anything but a constant, the above equation cannot be easily integrated. Numerical integration was therefore employed to solve the equation. The final equation is thus:

$$G(b) = \frac{\Sigma_a N_r \mu_e E}{2} \sum_{i=1}^{n} \phi_{ni}\, \Delta x_i \left\{ E_1\left[\mu_t (b - x_i')\right] + m e^{-\mu_t (b - x_i')} \right\} \qquad B-9$$

where $E_1[\mu_t(b-x_i')$ is an exponential integral of order one and argument $\mu_t(b-x_i')$.

$\phi_{ni}\Delta x_i$ was obtained by dividing the reflector flux plot shown in Figure 20 into six increments of Δx and using the average ϕ for each increment.

The energy groups considered were taken from the energy spectrum for capture gammas in aluminum[28].

TABLE 12

ENERGY SPECTRUM FOR CAPTURE-GAMMAS IN ALUMINUM

Energy Intervals, Mev	1-3	3-5	5-7	>7
Photons/100 captures	13	77	21	37

Other values used in the equations were:

TABLE 13

CONSTANTS FOR CALCULATING CAPTURE-GAMMA HEATING

E, Mev	μ_t^{Al*}, cm^{-1}	μ_e^{Al*}, cm^{-1}	m(E)[29]
2	0.0815	0.0435	0.85
4	0.0586	0.0378	0.55
6	0.0504	0.036	0.40
7.5	0.0473	0.0352	0.33

$$\Sigma_a^{Al} = 0.7 \times 6.02 \times 10^{22} \times 0.215 \times 10^{-24} = 0.00863 \text{ cm}^{-1}$$

* Values based upon a mixture density of aluminum of 1.89 gm/cm^3.

The total heat produced in each reflector is:

$$Q = \int_{Vol.} G_T \, dV$$

$$= \int_{x=0}^{60} \int_{y=0}^{180} \int_{z=0}^{120} (24.7 e^{-0.127x} + 1.97) \, dx \, dy \, dz$$

$$= 180 \times 120 \left[\frac{24.7}{0.127} \quad e^{-0.127x} + 1.97\ x \right]_0^{60}$$

$$= 180 \times 120 \left[195\ (1-e^{-7.62}) + 1.97\ (60) \right]$$

$$= 6.75 \times 10^6 \text{ watts}$$

$$Q = 6.75 \text{ MW.}$$

Percent of total power produced in the reflector =

$$100 \times \frac{6.75}{250} = 2.7\%$$

2. <u>Heat Transfer Calculations for the Aluminum Reflector</u>

An upper limit for the coolant velocity required to limit the maximum hot-spot temperature rise in the reflector to 220°F was obtained by examining the heat equations for the maximum hot-spot channel. The hot-spot channel was first oriented 90° with respect to its actual position in order to display the point of maximum heat production which occurs at the fuel-reflector interface. This procedure leads to an overestimate of the temperature rise but does represent an upper limit.

Figure 41 illustrates this condition and represents the pertinent dimensions at this location.

The total heat produced in a slab is given by:

$$q_p = \int_x \int_y \int_z q(x)\, dx\, dy\, dz$$

The average production curve in Figure 10 can be represented to a close approximation by

$$q(x) = 24.7\ e^{-0.127x} + 1.97\ x \quad (\text{watts/cm}^3) \qquad \text{B-10}$$

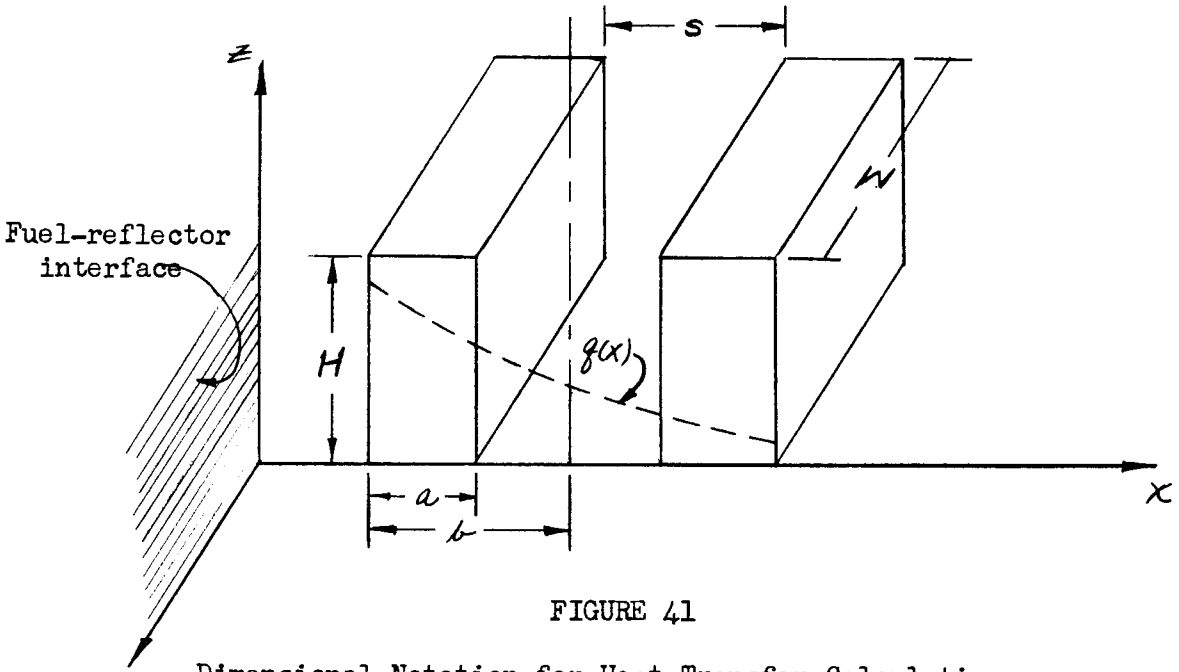

FIGURE 41

Dimensional Notation for Heat Transfer Calculations

a = 2.5 cm
s = 1 cm
b = 3 cm
H = 120 cm
W = unit length

Hence the average heat produced in the slab nearest the core is

$$q_P = \int_{x=1}^{3.5} \int_{y=0}^{w} \int_{z=0}^{H} (24.7\, e^{-0.127x} + 1.97x)\, dx\, dy\, dz \quad . \; . \; . \qquad \text{B-11}$$

$$= WH \left[\frac{24.7}{.127} \left(e^{-0.127} - e^{-0.127(3.5)}\right) + 1.97(2.5) \right]$$

$$= WH \left[195\,(0.88 - 0.64) + 4.92 \right]$$

$$= 51.7\ WH\ , \text{ watts}$$

$$= 3.41 \times 51.7\ WH = 176\ WH\ , \text{ BTU/hr}$$

The maximum heat produced in this slab was approximated by multiplying the average value by the ratio of peak to average thermal flux in the Y-direction and this product by the ratio of peak to average thermal flux in the Z-direction. This gives

$$q_{P_{max}} = 176\ WH \times 1.2 \times 1.2$$
$$= 254\ WH,\ BTU/hr$$

By neglecting any heat conduction in the Y-direction and assuming the temperature drop through the aluminum in the X-direction is negligible compared to the film drop, the heat conducted into the coolant is given by

$$q_c = h\ A_c \left[T_s\ (H) - T_f\ (H) \right] \qquad \text{B-12}$$

where T_s = surface temperature of the slab, ^oF

T_f = mixed mean temperature of the fluid, ^oF

A_c = area of heat conduction = 2 HW, cm^2

The heat removed by the coolant flow in the channel is given by

$$q_R = \rho_{D_2O}\ A_{D_2O}\ v\ C_p \left[T_f\ (H) - T_f\ (O) \right] \qquad \text{B-13}$$

ρ_{D_2O} = density of D_2O = 67.8 lb/ft^3

A_{D_2O} = cross sectional area of D_2O channel = S W, cm^2

v = velocity of D_2O, ft/sec

C_p = heat capacity = $1\ \frac{BTU}{lb\ ^oF}$

Under equilibrium conditions $q_P = q_C = q_R$.

$$2hWH \left[T_s(H) - T_f(H) \right] = 254\ W\ H \qquad \text{B-14}$$

$$\rho_{D_2O}\ S\ W\ v\ C_p \left[T_f(H) - T_f(o) \right] = 254\ W\ H \qquad \text{B-15}$$

$$T_s(H) - T_f(o) = \left[T_s(H) - T_f(H) \right] + \left[T_f(H) - T_f(o) \right]$$

$$= \frac{254}{2h} + \frac{254\ H}{\rho_{D_2O}\ S\ v\ C_p}$$

$$T_s(H) - T_f(o) = 254 \left[\frac{1}{2h} + \frac{H}{\rho_{H_2O} S V C_p} \right] \qquad \text{B-16}$$

The film coefficient, h, is obtained from

$$\frac{hD}{k} = 0.023 \left(\frac{DV\rho}{\mu}\right)^{0.8} \left(\frac{C_p \mu}{k}\right)^{0.4}$$

D = hydraulic diameter $\cong$ 2 S = 0.0328 ft.

μ = 0.968 lb/hr-ft

k = 0.378 BTU/hr-ft^2 ^oF/ft.

Assume V = 20 ft/sec = 72,000 ft/hr

$$\frac{hD}{k} = 0.023 \left(\frac{0.0656 \times 72{,}000 \times 68.7}{0.968}\right)^{0.8} \left(\frac{0.968}{0.378}\right)^{0.4}$$

$$h = 0.378 \times 0.023 \left(\frac{0.0656 \times 72{,}000 \times 68.7}{0.968}\right)^{0.8} \left(\frac{0.968}{0.378}\right)^{0.4}$$

$$h = 795 \text{ BTU/hr ft}^2\ ^oF$$

Substituting these values into Equation B-16 gives

$$T_s(H) - T_f(o) = 254 \left[\frac{1}{2 \times 795} + \frac{120}{1 \times 67.8 \times 7200} \right] \times 960 \frac{cm^2}{ft^2}$$

$$= (254)(0.00087)(960)$$

$$T_s(H) - T_f(o) = 212^oF.$$

This calculation shows that a coolant velocity of 20 ft/sec flowing through the one-centimeter coolant gap is sufficient to keep the maximum hot-spot temperature rise below 220°F.

APPENDIX C

1. Calculations of Heat Production in the Central D_2O Region

The same equations that were developed for the fast neutron reflector (Appendix B) were used in calculating the heat produced in the central D_2O region by fission gammas and neutron elastic scattering collisions. For the heat produced by neutron elastic scattering

$$G_{ne}(x) = \sum_{i=0}^{n} \delta_{ne_i} \bar{E}_1 \bar{\phi}_1(x) \Sigma_{ne_i} \qquad \text{C-1}$$

n = number of different atomic species present

δ_{ne} for deuterium = 0.445

δ_{ne} for oxygen = 0.105

$\bar{E}_1$ = 1.1 Mev

$\bar{\phi}_1(x)$ is obtained from the flux plot in Figure 20 and is based upon an unperturbed flux delivered to the experiment of 2.5×10^{15} neutrons/cm^{2}sec

$\Sigma_{ne_D} = 6.64 \times 10^{22} \times 2.1 \times 10^{-24} = 0.1392$

$\Sigma_{ne_O} = 3.32 \times 10^{22} \times 2.5 \times 10^{-24} = 0.083$

For the heat produced by fission gammas all constants remain the same as for the fast reflector expect μ_R. The following values were used for μ_R in the moderator region:

TABLE 14

GAMMA ABSORPTION COEFFICIENTS FOR D_2O

$\bar{E}_\gamma$,Mev	$\mu_R = \mu_{D_2O}$,cm^{-1}
1	0.0352
1.5	0.0308
2.3	0.0275
3.0	0.0253
5.0	0.0218
0.7	0.0363

The results of this calculation are graphically presented in Figure 9.

APPENDIX D

1. Fuel Burnup
2. Xenon-135 Concentration
3. Xenon-135 Poisoning
4. Samarium Concentration
5. Samarium Poisoning
6. Total Fission Product Poisoning
7. Xenon Over-ride
8. Xenon Instability

1. Fuel Burnup

If, as in most experiment reactors, the neutron flux is held as nearly constant as possible throughout the run cycle, the fuel depletion will be exponential and the average concentration at anytime will be

$$N_u(t) = N_{u_o} e^{-\bar{\Phi}\sigma_a^f t} \quad . \qquad \text{D-1}$$

N_{u_o} is the startup fuel concentration, and σ_a^f if the microscopic neutron absorption cross section for the fuel. $\bar{\Phi}$ is the average neutron flux, and t is the operating time.

If the power level is held constant so that the fission rate per cm^3 is constant, then

$$N_u(t) = N_{u_o} - N_{u_o} \bar{\Phi}_o \sigma_a^f t = N_{u_o} \left[1 - \bar{\Phi}_o \sigma_a^f t\right] \qquad \text{D-2}$$

$\bar{\Phi}_o$ is the initial average neutron flux. In this case $\bar{\Phi}$ must rise as the fuel depletes as shown by the following equation:

$$\bar{\Phi}(t) = \frac{N_{u_o} \bar{\Phi}_o \sigma_a^f}{N_{u_o} \left[1 - \bar{\Phi}_o \sigma_a^f t\right] \sigma_a^f} = \frac{\bar{\Phi}_o}{\left[1 - \bar{\Phi}_o \sigma_a^f t\right]} \quad . \qquad \text{D-3}$$

These conditions are graphically shown in Figures 42 and 43.

2. Xenon Concentration

Derivation of Equations: I. Precursor Concentration (I^{135}):

$$\frac{dN_I}{dt} = -\lambda N_I - \Phi\sigma_a^I N_I + F_I \Phi \sigma_f N_u \qquad \text{D-4}$$

Φ = neutrons/cm^2-sec (assumed constant)

F_I = fission yeild of I^{135}

N_u = U^{235} concentration (varying slowly with time)

σ_f = microscopic fission cross section of U^{235}

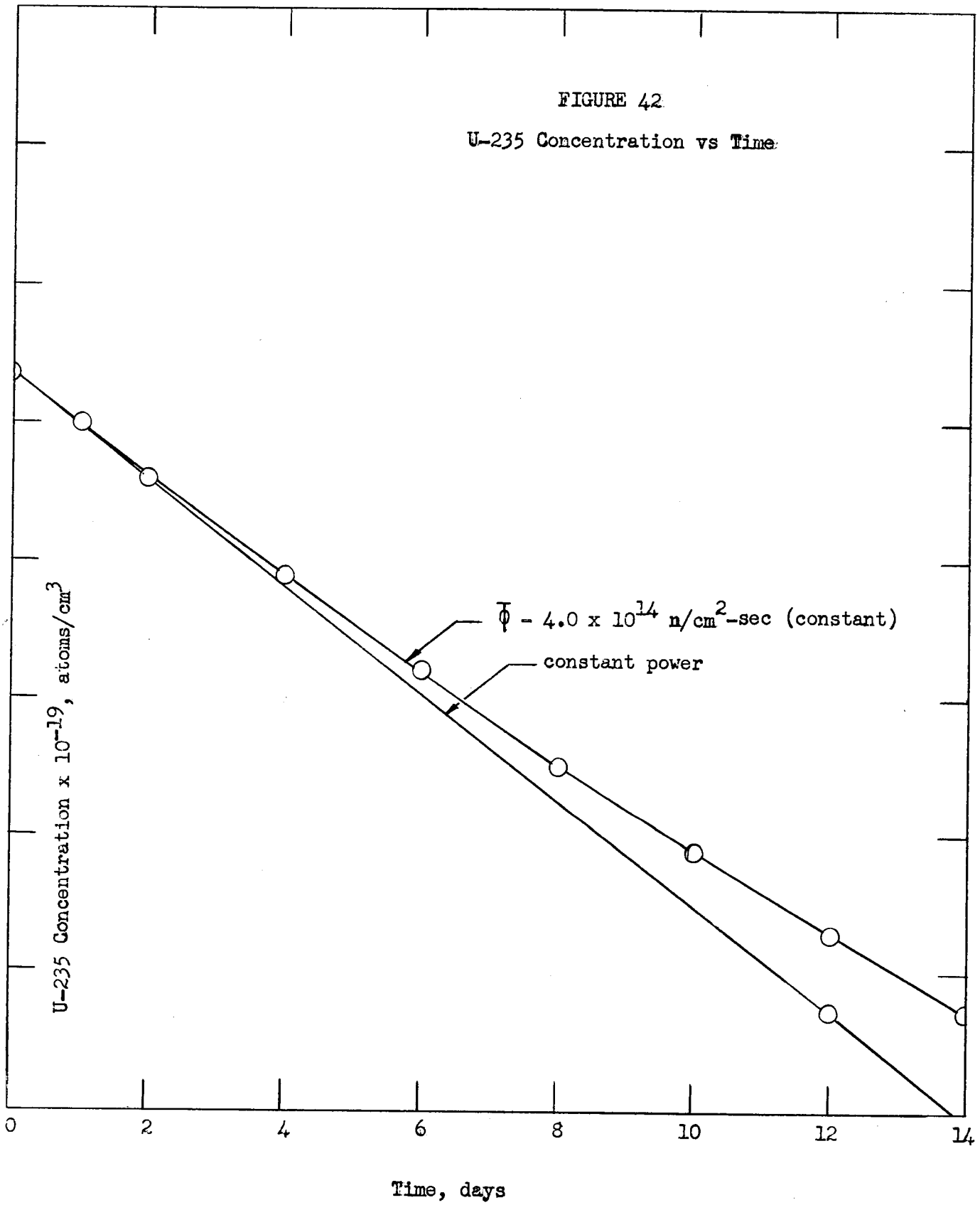

FIGURE 42

U-235 Concentration vs Time

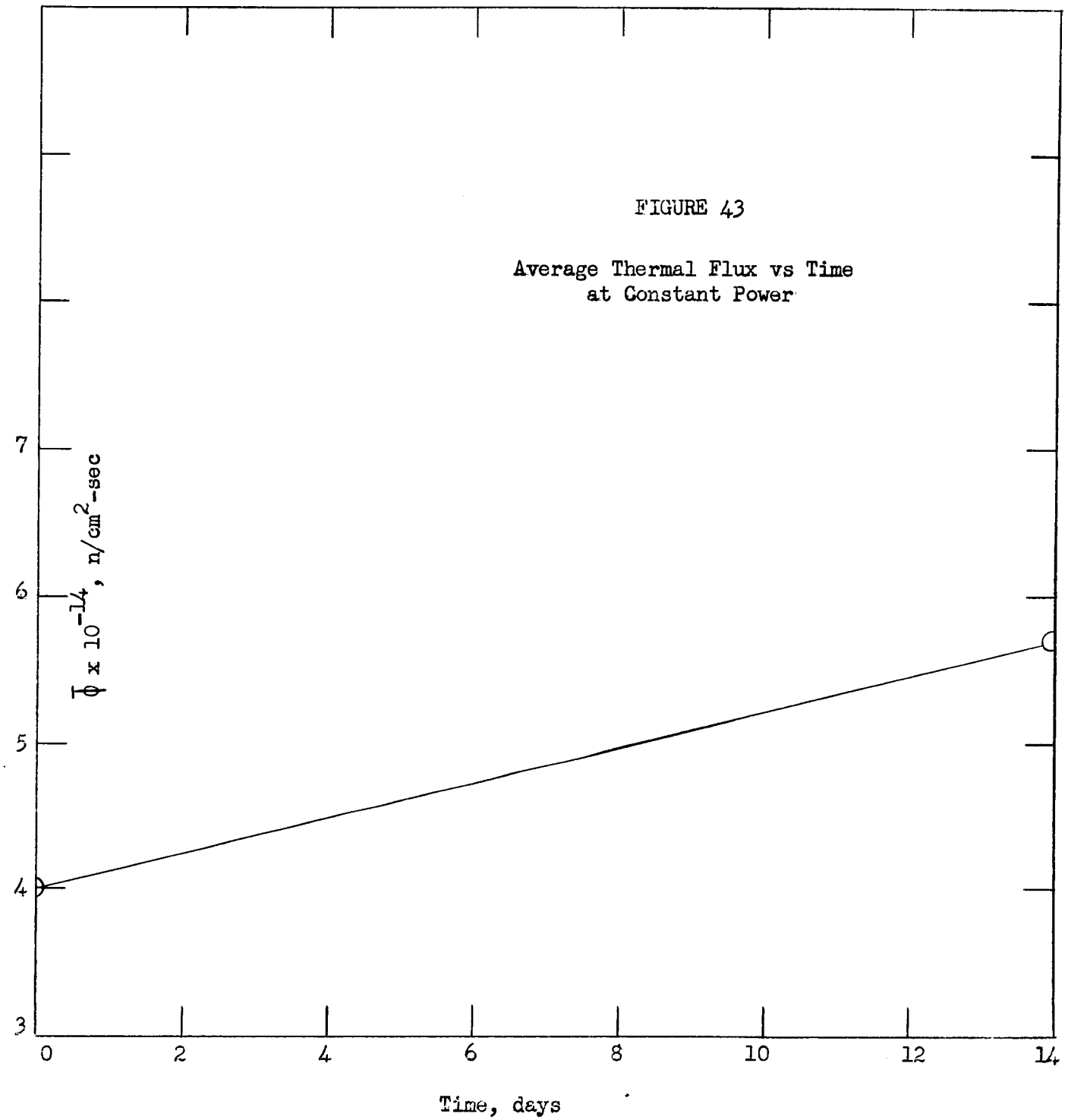

FIGURE 43

Average Thermal Flux vs Time
at Constant Power

σ_a^I = microscopic neutron absorption cross section of I^{135}

N_I = concentration of I^{135} at time t

λ_I = I^{135} decay constant

$$\frac{dN_I}{dt} + (\lambda_I + \Phi\sigma_a^I)\, N_I = F_I \Phi \sigma_f N_u \qquad \text{D-5}$$

$$(t) = F_I \Phi \sigma_f N_u\, e^{-(\lambda_I + \Phi\sigma_a^I)t} \int e^{(\lambda_I + \Phi\sigma_a^I)t'} dt' + C\, e^{-(\lambda_I + \Phi\sigma_a^I)\, t} \qquad \text{D-6}$$

$$N_I(t) = \frac{F_I \Phi \sigma_f N_u}{\lambda_I + \Phi\sigma_a^I} + C\, e^{-(\lambda_I + \Phi\sigma_a^I)\, t} \qquad \text{D-7}$$

When t = 0, $N_I = N_{Io}$; therefore,

$$C = N_{Io} - \frac{F_I \Phi \sigma_f N_u}{\lambda_I + \Phi\sigma_a^I}$$

$$N_I(t) = \frac{F_I \Phi \sigma_a^I N_u}{\lambda_I + \Phi\sigma_a^I} \left[1 + e^{-(\lambda_I + \Phi\sigma_a^I)\, t}\right] + N_{Io}\, e^{-(\lambda_I + \Phi\sigma_a^I)\, t} \qquad \text{D-8}$$

When $t \to \infty$,

$$N_I(\infty) = \frac{F_I \Phi \sigma_f N_u}{\lambda_I + \Phi\sigma_a{}^I}$$

If N_u is being depleted slowly with respect to the half life of I^{135},

$$N_I(t) = \frac{F_I \Phi \sigma_f N_{uo}\, e^{-(\Phi\sigma_a^f\, t)}}{\lambda_I + \Phi\sigma_a^I} \left[1 - e^{-(\lambda_I + \Phi\sigma_a^I)\, t}\right] + N_{Io}\, e^{-(\lambda_I + \Phi\sigma_a^I)\, t} \qquad \text{D-9}$$

At saturation

$$N_I(t) = \frac{F_I \Phi \sigma_f N_{uo}\, e^{-\Phi\sigma_a^f\, t}}{\lambda_I + \Phi\sigma_a^I} \qquad \text{D-10}$$

II. Xenon Concentration (Xe^{135}):

$$\frac{dN_{Xe}}{dt} = -\lambda_{Xe} N_{Xe} - \Phi\sigma_{a_{Xe}} + N_I \lambda_I + F_{Xe} \Phi \sigma_f N_u \qquad \text{D-11}$$

N_{Xe} = concentration of Xe^{135} at any time t

λ_{Xe} = decay constant for Xe^{135}

Φ = neutrons/cm^2-sec (assumed constant)

$\sigma_{a_{Xe}}$ = neutron absorption cross section for Xe^{135}

N_I = concentration of I^{135} at any time t

λ_I = decay constant for I^{135}

F_{Xe} = direct fission yield of Xe^{135}

σ_f = U^{235} fission cross section

N_u = U^{235} concentration (assumed slowly varying)

The I^{135} concentration has been shown to be

$$N_I(t) = \frac{F_I \Phi \sigma_f N_u}{\lambda_I + \Phi \sigma_a{}^I} \left[1 - e^{-(\lambda_I + \Phi \sigma_a^I)\, t}\right] + N_{Io}\, e^{-(\lambda_I + \Phi \sigma_a^I)\, t}$$

$$N_{Xe}(t) = e^{-(\lambda_{Xe} + \Phi \sigma_a{}^{Xe})\, t} \int \left\{ \frac{F_I \Phi \sigma_f N_u \lambda_I}{\lambda_I + \Phi \sigma_a^I} \left[1 - e^{-(\lambda_I + \Phi \sigma_a^I)\, t'}\right] \right.$$

$$\left. + N_{Io} \lambda_I\, e^{-(\lambda_I + \Phi \sigma_a^I)\, t'} + F_{Xe} \Phi \sigma_f N_u \right\} e^{(\lambda_{Xe} + \Phi \sigma_a^{Xe})\, t''}\, dt'$$

$$- C\, e^{-(\lambda_{Xe} + \Phi \sigma_a^{Xe})\, t} \qquad \text{D-12}$$

$$N_{Xe}(t) = \frac{F_I \Phi \sigma_f N_u \lambda_I}{(\lambda_I + \Phi \sigma_a^I)(\lambda_{Xe} + \Phi \sigma_a^{Xe})} - \frac{F_I \Phi \sigma_f N_u \lambda_I\, e^{-(\lambda_I + \Phi \sigma_a^I)\, t}}{(\lambda_I + \Phi \sigma_a^I)(\lambda_{Xe} + \Phi \sigma_a^{Xe} - \lambda_I - \Phi \sigma_a^I)}$$

$$+ \frac{N_{Io} \lambda_I\, e^{-(\lambda_I + \Phi \sigma_a^I)\, t}}{(\lambda_{Xe} + \Phi \sigma_a^{Xe} - \lambda_I - \Phi \sigma_a^I)} + \frac{F_{Xe} \Phi \sigma_f N_u}{\lambda_{Xe} + \Phi \sigma_a^{Xe}} + C\, e^{-(\lambda_{Xe} + \Phi \sigma_a^{Xe})\, t} \qquad \text{D-13}$$

Let $a = F_I \Phi \sigma_f N_u \lambda_I$

$b = N_{Io} \lambda_I$

$c = F_{Xe} \Phi \sigma_f N_u$

$$d = \lambda_I + \Phi\sigma_a^I$$

$$g = \lambda_{Xe} + \Phi\sigma_a^{Xe} - \lambda_I - \Phi\sigma_a^I = h - d$$

$$h = \lambda_{Xe} + \Phi\sigma_a^{Xe}$$

By applying the initial conditions that at $t = 0$, $N_{Xe} = N_{Xe_o}$

$$C = N_{Xe_o} + \frac{a}{dg} - \frac{a}{dh} - \frac{b}{g} - \frac{c}{h}$$

and the equation becomes

$$N_{Xe}(t) = \left[\frac{a}{dh} + \frac{c}{h}\right]\left[1 - e^{-ht}\right] + \left[\frac{a}{dg} - \frac{b}{g}\right]\left[e^{-ht} - e^{-dt}\right] + N_{Xe_o}\, e^{-ht} \qquad \text{D-14}$$

When $N_{Xe_o} = 0$ and $N_{I_o} = 0$, this reduces to

$$N_{Xe}(t) = \left[\frac{a}{dh} + \frac{c}{h}\right]\left[1 - e^{-ht}\right] + \frac{a}{dg}\left[e^{-ht} - e^{-dt}\right] \qquad \text{D-15}$$

When $t \rightarrow \infty$,

$$N_{Xe}(\infty) \rightleftharpoons \frac{a}{dh} + \frac{c}{h} \qquad \text{D-16}$$

For usage here $N_u(t) = N_{u_o}\, e^{-\Phi\sigma_a^f t}$ with reasonable accuracy although the derivations assumed N_u to be constant.

<u>a. Calculation of Maximum Xe^{135} Concentration versus Φ:</u>

$$N_{Xe} = \frac{a}{dh} + \frac{c}{h}$$

Using the following values for the constants,

$\sigma_a^I = 6.2 \times 10^{-24}$ cm^2 (corrected for thermal spectrum)

$\sigma_a^{Xe} = 2.7 \times 10^{-18}$ cm^2

$F_I = 0.056$ (ignoring 2-minute Te half life)

$F_{Xe} = 0.003$

$$\lambda_I = 2.88 \times 10^{-5}\ \text{sec}^{-1}$$

$$\lambda_{Xe} = 2.10 \times 10^{-5}\ \text{sec}^{-1}$$

$$\sigma_f = 5.15 \times 10^{-22}\ \text{cm}^2 \text{ (corrected for thermal spectrum)}$$

Sample calculation for $\Phi = 1 \times 10^{14}$ neutrons/cm^2-sec:

$$a = F_I \Phi \sigma_f N_u \lambda_I = 0.056 \times 10^{14} \times 5.15 \times 10^{-22} \times 2.88 \times 10^{-5}\ N_u$$

$$= 8.30 \times 10^{-14}\ N_u$$

$$c = F_{Xe} \Phi \sigma_f N_u = 0.003 \times 10^{14} \times 5.15 \times 10^{-22}\ N_u$$

$$= 1.55 \times 10^{-10}\ N_u$$

$$d = \lambda_I + \Phi \sigma_a^I = 2.88 \times 10^{-5} + 10^{14} \times 6.2 \times 10^{-24}$$

$$\cong 2.88 \times 10^{-5}$$

$$g = h - d = 2.62 \times 10^{-4}$$

$$h = \lambda_{Xe} + \Phi \sigma_a^{Xe} = 2.10 \times 10^{-5} + 10^{14} \times 2.7 \times 10^{-18}$$

$$= 2.91 \times 10^{-4}$$

$$N_{Xe}(\infty) = \frac{a}{dh} + \frac{c}{h} = \frac{8.30 \times 10^{-14}\ N_u}{2.88 \times 10^{-5} \times 2.91 \times 10^{-4}} + \frac{1.55 \times 10^{-10}\ N_u}{2.91 \times 10^{-4}} = 1.04 \times 10^{-5}\ N_u$$

TABLE 15

MAXIMUM Xe CONCENTRATIONS FOR SEVERAL FLUXES

Φ, neutrons/cm^2-sec	$N_{Xe}(\infty)$
1×10^{12}	$1.28 \times 10^{-6}\ N_u$
5×10^{12}	$4.40 \times 10^{-6}\ N_u$
1×10^{13}	$6.21 \times 10^{-6}\ N_u$
5×10^{13}	$9.74 \times 10^{-6}\ N_u$
1×10^{14}	$1.04 \times 10^{-5}\ N_u$
5×10^{14}	$1.11 \times 10^{-5}\ N_u$
1×10^{15}	$1.12 \times 10^{-5}\ N_u$
2×10^{15}	$1.12 \times 10^{-5}\ N_u$
4×10^{15}	$1.11 \times 10^{-5}\ N_u$
8×10^{15}	$1.11 \times 10^{-5}\ N_u$

These values are plotted in Figure 44.

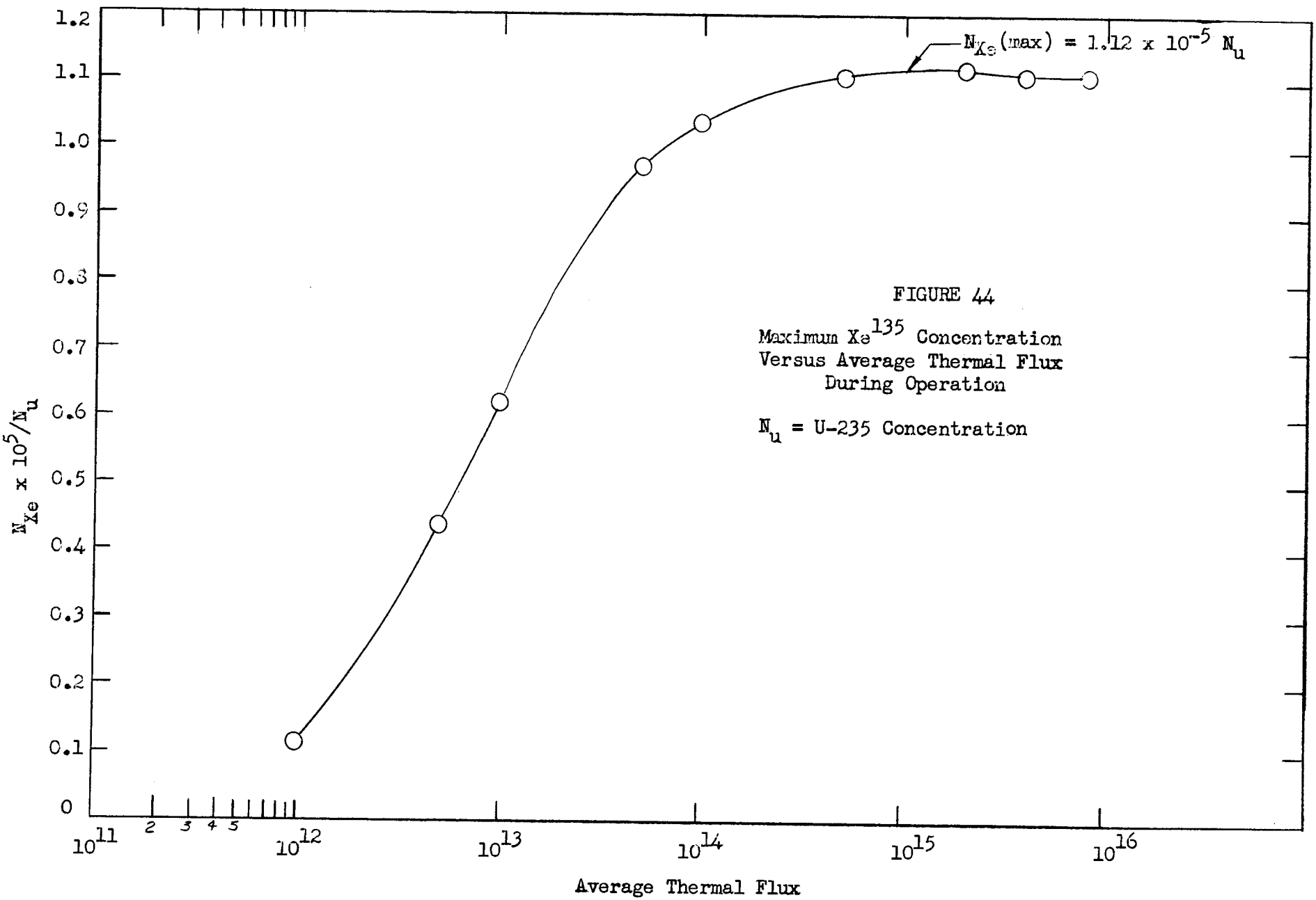

FIGURE 44

Maximum Xe^{135} Concentration Versus Average Thermal Flux During Operation

N_u = U-235 Concentration

b. Xe^{135} Growth After Clean and Cold Startup:

$$N_{Xe}(t) = \left[\frac{a}{dh} + \frac{c}{h}\right]\left[1 - e^{-ht}\right] + \frac{a}{dg}\left[e^{-ht} - e^{-dt}\right] \qquad \text{D-15}$$

Using $\Phi = 4 \times 10^{14}$ neutrons/cm^2 sec,

$$\frac{a}{dh} + \frac{c}{h} = 1.11 \times 10^{-5}\ N_u$$

$$\frac{a}{dg} = 1.08 \times 10^{-5}\ N_u$$

Sample calculation:

$$t = 1 \text{ hour} = 3.6 \times 10^3 \text{ sec}$$

$$N_{Xe} = 1.11 \times 10^{-5}\ N_u \left[1 - e^{-1.10 \times 10^{-3} t}\right] + 1.08 \times 10^{-5}\ N_u \left[e^{-1.10 \times 10^{-3} t} - e^{-2.88 \times 10^{-5} t}\right]$$

$$= 0.11 \times 10^{-5}\ N_u$$

Where $N_u(t) = N_{u_o}\ e^{-\Phi \sigma_a^f t}$

TABLE 16

Xe^{135} CONCENTRATION AS A FUNCTION OF REACTOR OPERATING TIME

		For $N_{u_o} = 9.18 \times 10^{19}$	
Time	N_{Xe}	N_{Xe}	Σ_a^{Xe}, cm^{-1}
1 hour	$0.11 \times 10^{-5}\ N_u$	1.01×10^{14}	2.73×10^{-4}
2 hours	$0.23 \times 10^{-5}\ N_u$	2.22×10^{14}	6.00×10^{-4}
4 hours	$0.40 \times 10^{-5}\ N_u$	3.66×10^{14}	9.80×10^{-4}
8 hours	$0.64 \times 10^{-5}\ N_u$	5.84×10^{14}	15.78×10^{-4}
16 hours	$0.91 \times 10^{-5}\ N_u$	8.25×10^{14}	22.30×10^{-4}
20 hours	$0.97 \times 10^{-5}\ N_u$	8.76×10^{14}	23.70×10^{-4}
32 hours	$1.07 \times 10^{-5}\ N_u$	9.60×10^{14}	25.75×10^{-4}
2 days	$1.10 \times 10^{-5}\ N_u$	9.70×10^{14}	26.18×10^{-4}
4 days	$1.11 \times 10^{-5}\ N_u$	9.35×10^{14}	25.25×10^{-4}
6 days	$1.11 \times 10^{-5}\ N_u$	8.98×10^{14}	24.25×10^{-4}
8 days	$1.11 \times 10^{-5}\ N_u$	8.61×10^{14}	23.30×10^{-4}
10 days	$1.11 \times 10^{-5}\ N_u$	8.25×10^{14}	22.30×10^{-4}
12 days	$1.11 \times 10^{-5}\ N_u$	7.81×10^{14}	21.13×10^{-4}
14 days	$1.11 \times 10^{-5}\ N_u$	7.60×10^{14}	20.53×10^{-4}

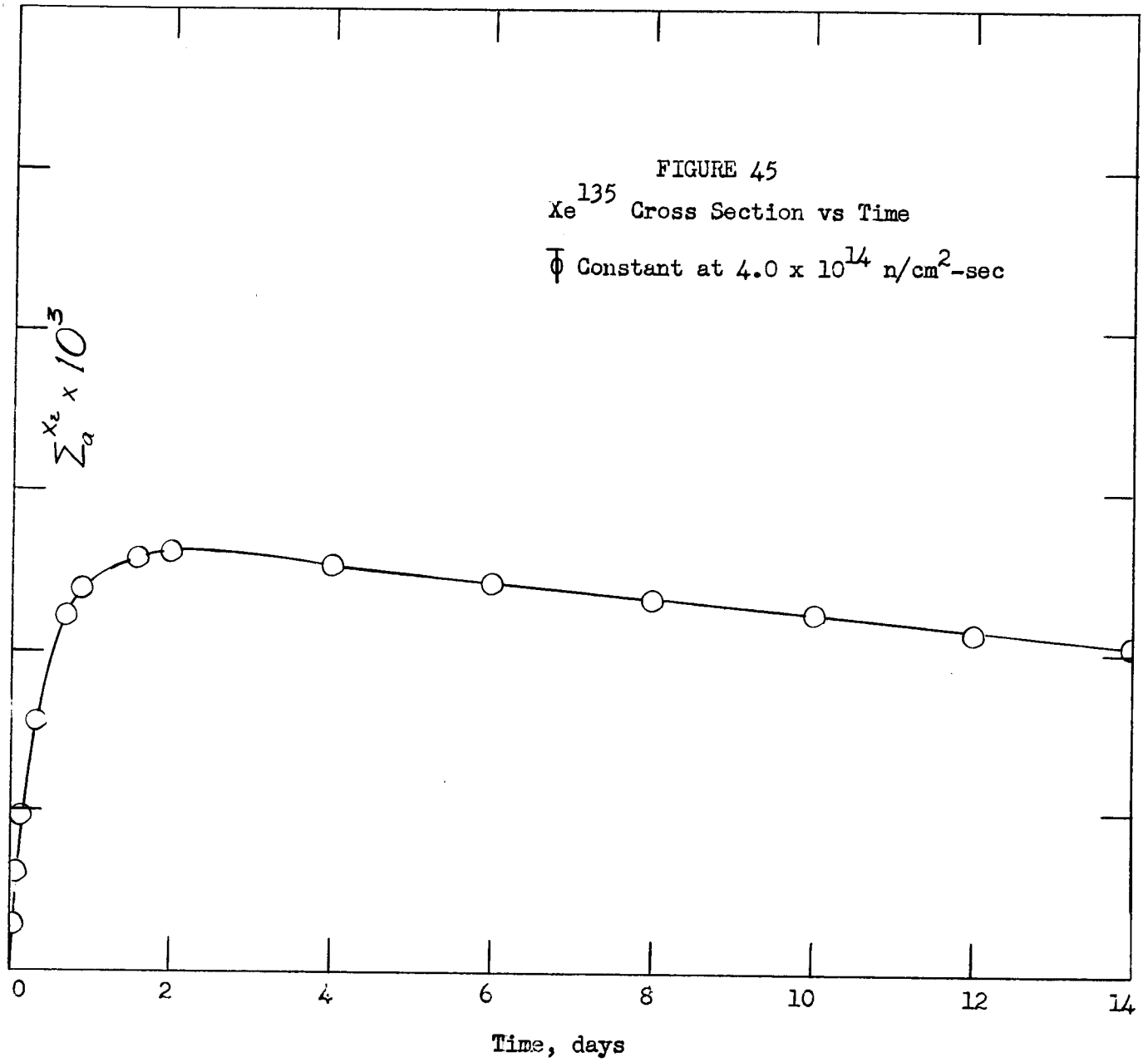

FIGURE 45

Xe^{135} Cross Section vs Time

Φ Constant at 4.0×10^{14} n/cm^2-sec

c. Xe^{135} Growth after Shutdown:

Derivation of equations:

$$\frac{dN_{Xe}}{dt} = -\lambda_{Xe}N_{Xe} + \lambda_I N_I \qquad \text{D-16}$$

$$\frac{dN_I}{dt} = -\lambda_I N_I$$

$$N_I(t) = N_{I_o}\, e^{-\lambda_I t}$$

$$N_{Xe}(t) = \lambda_I N_{I_o}\, e^{-\lambda_{Xe}t} \int e^{(\lambda_{Xe}-\lambda_I)\,t'}\, dt' + C\, e^{-\lambda_{Xe}t} = \frac{\lambda_I N_{I_o}\, e^{-\lambda_I t}}{\lambda_{Xe} - \lambda_I} + C\, e^{-\lambda_{Xe}t}$$

When $t = 0$, $N_{Xe} = N_{Xe_o}$

$$C = N_{Xe_o} + \frac{\lambda_I N_{I_o}}{\lambda_I - \lambda_{Xe}}$$

Therefore,

$$N_{Xe}(t) = \frac{\lambda_I N_{I_o}}{\lambda_I - \lambda_{Xe}} \left[e^{-\lambda_{Xe}t} - e^{-\lambda_I t} \right] + N_{Xe_o}\, e^{-\lambda_{Xe}t} \qquad \text{D-17}$$

N_{Xe_o} = Xe^{135} concentration at shutdown

N_{I_o} = I^{135} concentration at shutdown

Using $\Phi = 4 \times 10^{14}$ neutrons/cm^2 sec

$$N_{I_o} = 4.0 \times 10^{-4}\, N_u$$

$$N_{Xe_o} = 1.11 \times 10^{-5}\, N_u$$

$$N_{Xe}(t) = 1.48 \times 10^{-3}\, N_u \left[e^{-2.1\times10^{-5}t} - e^{-2.88\times10^{-5}t} \right] + 1.11\times10^{-5}\, N_u\, e^{-2.1\times10^{-5}t} \qquad \text{D-18}$$

Table 17

Xe^{135} GROWTH AND DECAY AFTER SHUTDOWN

Time after Shutdown	N_{Xe}
0 min	$1.11 \times 10^{-5}\ N_u$
10 min	$1.6 \times 10^{-5}\ N_u$
20 min	$2.3 \times 10^{-5}\ N_u$
40 min	$4.0 \times 10^{-5}\ N_u$
60 min	$4.8 \times 10^{-5}\ N_u$
2 hours	$7.8 \times 10^{-5}\ N_u$
4 hours	$12.4 \times 10^{-5}\ N_u$
8 hours	$16.7 \times 10^{-5}\ N_u$
10 hours	$17.3 \times 10^{-5}\ N_u$
11 hours	$17.6 \times 10^{-5}\ N_u$
12 hours	$17.3 \times 10^{-5}\ N_u$
14 hours	$17.0 \times 10^{-5}\ N_u$
16 hours	$16.1 \times 10^{-5}\ N_u$
20 hours	$14.1 \times 10^{-5}\ N_u$
30 hours	$8.7 \times 10^{-5}\ N_u$
40 hours	$4.8 \times 10^{-5}\ N_u$
50 hours	$2.5 \times 10^{-5}\ N_u$
60 hours	$1.3 \times 10^{-5}\ N_u$

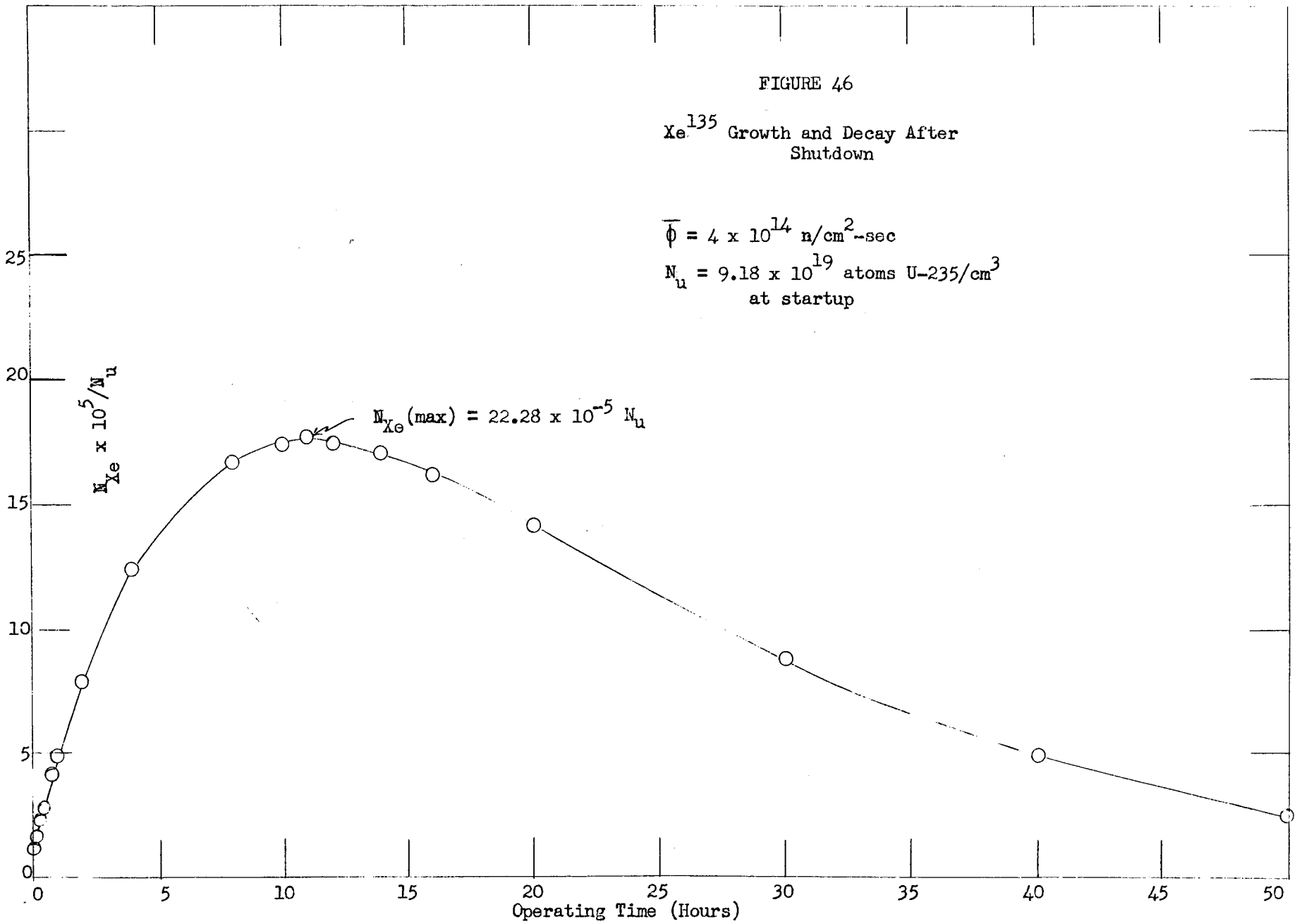

FIGURE 46

Xe^{135} Growth and Decay After Shutdown

$\overline{\phi} = 4 \times 10^{14}$ n/cm^2-sec

$N_u = 9.18 \times 10^{19}$ atoms U-235/cm^3 at startup

d. Time of Maximum Xe^{135} Concentration After Shutdown:

$$\frac{dN_{Xe}}{dt} = \frac{\lambda_I N_{I_o}}{\lambda_I - \lambda_{Xe}} \left[\lambda_I e^{-\lambda_I t} - \lambda_{Xe} e^{-\lambda_{Xe} t} \right] - N_{Xe_o} \lambda_{Xe} e^{-\lambda_{Xe} t}$$

Setting $\frac{dN_{Xe}}{dt} = 0$ and rearranging,

$$e^{-(\lambda_I - \lambda_{Xe}) t} = \frac{\lambda_{Xe}}{\lambda_I} + \frac{N_{Xe_o} \lambda_{Xe}}{N_{I_o} \lambda_I^2} \left[\lambda_I - \lambda_{Xe} \right]$$

Putting in values for the constants, there obtains

$$e^{-7.8 \times 10^{-6} t} = 0.7345$$

$$7.8 \times 10^{-6} t = 0.30856$$

$$t = 3.96 \times 10^4 \text{ sec}$$

$$= 11.0 \text{ hours}$$

3. Xe^{135} Poisoning

The reactivity, ρ, of a reactor is defined as

$$\rho \equiv \frac{k - 1}{k} \qquad \text{D-19}$$

$$k = k_o \frac{\Sigma_a^o}{\Sigma_a^o + \Sigma_a^P} \qquad \text{D-20}$$

where k = multiplication constant of the reactor after poison is introduced

k_o = multiplication constant for the clean, cold reactor

Σ_a^o = macroscopic absorption cross section for the clean, cold reactor

$= \Sigma_a^{fuel} + \Sigma_a^{other\ materials}$

$= 6.10 \times 10^{-22} N_u + 0.0048$

Σ_a^P = macroscopic absorption cross section of the poison introduced

Therefore,

$$= \frac{\frac{k_o \Sigma_a^o}{\Sigma_a^o + \Sigma_a^P} - 1}{\frac{k_o \Sigma_a^o}{\Sigma_a^o + \Sigma_a^P}} = \frac{k_o - 1}{k_o} - \frac{\Sigma_a^P}{\Sigma_a^o k_o} = \rho_o - \frac{\Sigma_a^P}{\Sigma_a^o k_o} \qquad \text{D-21}$$

where ρ_o = reactivity of the clean, cold reactor.

It follows, then, that

$$\rho(t) = \rho_o(t) - \frac{\Sigma_a^P(t)}{\Sigma_a^o(t)\, k_o(t)} \qquad \text{D-2}$$

TABLE 18

CHANGE OF REACTIVITY AND MULTIPLICATION CONSTANT DUE TO Xe^{135} AS A FUNCTION OF REACTOR OPERATING TIME

Time (Days)	Σ_a^o	k_o	ρ_o	Σ_a^{Xe}	ρ	$\Delta\rho$	k	$k_o - k$ (Due to Xe^{135})
0	0.05945	1.298	0.230	0	0.230	0	1.298	0
2	0.0584	1.292	0.226	0.00262	0.191	0.0347	1.238	0.054
4	0.0563	1.283	0.220	0.00253	0.185	0.0350	1.228	0.055
6	0.0542	1.272	0.214	0.00243	0.179	0.0352	1.219	0.053
8	0.0522	1.260	0.206	0.00233	0.171	0.0354	1.208	0.052
10	0.0502	1.247	0.198	0.00223	0.162	0.0356	1.193	0.054
12	0.0483	1.233	0.189	0.00211	0.154	0.0354	1.181	0.052

4. Samarium Concentration (Sm^{149} and Sm^{151}):

The following equations are derived assuming that beta decay of Sm^{151} (half life = 73 years) is negligible and that $\overline{\Phi}$ is constant:

$$\frac{dN}{dt} = -\Phi\sigma_a N + F\sigma_f^F N_u \Phi \qquad \text{D-23}$$

$$N = \frac{F\sigma_f^F N_u \Phi}{\Phi\sigma_a} + C\, e^{-\Phi\sigma_a t} \qquad \text{D-24}$$

At time $t = 0$, $N = N_o$ and

$$C = N_o - \frac{F\sigma_f^F N_u}{\sigma_a}$$

Therefore,

$$N(t) = \frac{F\sigma_f^F N_u}{\sigma_a}\left[1 - e^{-\Phi\sigma_a t}\right] + N_o\, e^{-\Phi\sigma_a t} \qquad \text{D-25}$$

$$\Sigma_a(t) = N(t)\,\sigma_a = F\sigma_f^F N_u\left[1 - e^{-\Phi\sigma_a t}\right] + N_o\sigma_a\, e^{-\Phi\sigma_a t} \qquad \text{D-26}$$

Where N = concentration of Sm atoms

F = fission yield of Sm

σ_f^F = fission cross section of U^{235}

N_u = concentration of U^{235} atoms = $N_{u_o}\, e^{-\Phi\sigma_a^F t}$

N_o = concentration of Sm atoms at initial time

σ_a = neutron absorption cross section of Sm

σ_a^F = neutron absorption cross section of U^{235}

N_{u_o} = U^{235} concentration at startup

Assuming a clean startup, $N_o \doteq 0$ and

$$\Sigma_a(t) = F\sigma_f^F N_{u_o}\, e^{-\Phi\sigma_a^F t}\left[1 - e^{-\Phi\sigma_a t}\right] \qquad \text{D-27}$$

Using $F(Sm^{149})$ = 0.0128

$F(Sm^{151})$ = 0.0049

σ_f^F = 5.15×10^{-22} cm^2 (corrected for thermal spectrum)

σ_a^F = 6.10×10^{-22} cm^2 (corrected for thermal spectrum)

$\sigma_a(Sm^{149})$ = 4.08×10^{-20} cm^2 (corrected for thermal spectrum)

$\sigma_a(Sm^{151})$ = 8.41×10^{-21} cm^2 (corrected for thermal spectrum)

N_{u_o} = 9.18×10^{19} atoms/cm^3

$\bar{\Phi}$ = 4.0×10^{14} neutrons/cm^2-sec (effective thermal)

The total absorption cross section for both isotopes is expressed as

$$\Sigma_a'(t) = N_{u_o}\sigma_f^F \; e^{-\Phi\sigma_a^F t} \left[F_{149}(1 - e^{-\Phi\sigma_a^{149} t}) + F_{151}(1 - e^{-\Phi\sigma_a^{151} t}) \right]$$

$$= 4.73 \times 10^{-2} \, e^{-2.44\times10^{-7} t} \left[1.28 \times 10^{-2}(1 - e^{-1.63\times10^{-5} t}) + 4.9 \times 10^{-3}(1 - e^{-3.36\times10^{-6}} \right.$$

$$= 8.37 \times 10^{-4} \, e^{-2.44\times10^{-7} t} - 6.05 \times 10^{-4} \, e^{-1.65\times10^{-5} t} - 2.32 \times 10^{-4} \, e^{-3.60\times10^{-6} t}$$

TABLE 19

Sm CROSS SECTION AS A FUNCTION OF OPERATING TIME

Time, days	Σ_a^{Sm}, cm^{-1}
0	0
0.5	3.35×10^{-4}
1	5.05×10^{-4}
2	6.41×10^{-4}
3	6.86×10^{-4}
4	7.00×10^{-4}
5	7.05×10^{-4}
6	7.03×10^{-4}
8	6.86×10^{-4}
10	6.68×10^{-4}
12	6.44×10^{-4}
14	6.19×10^{-4}

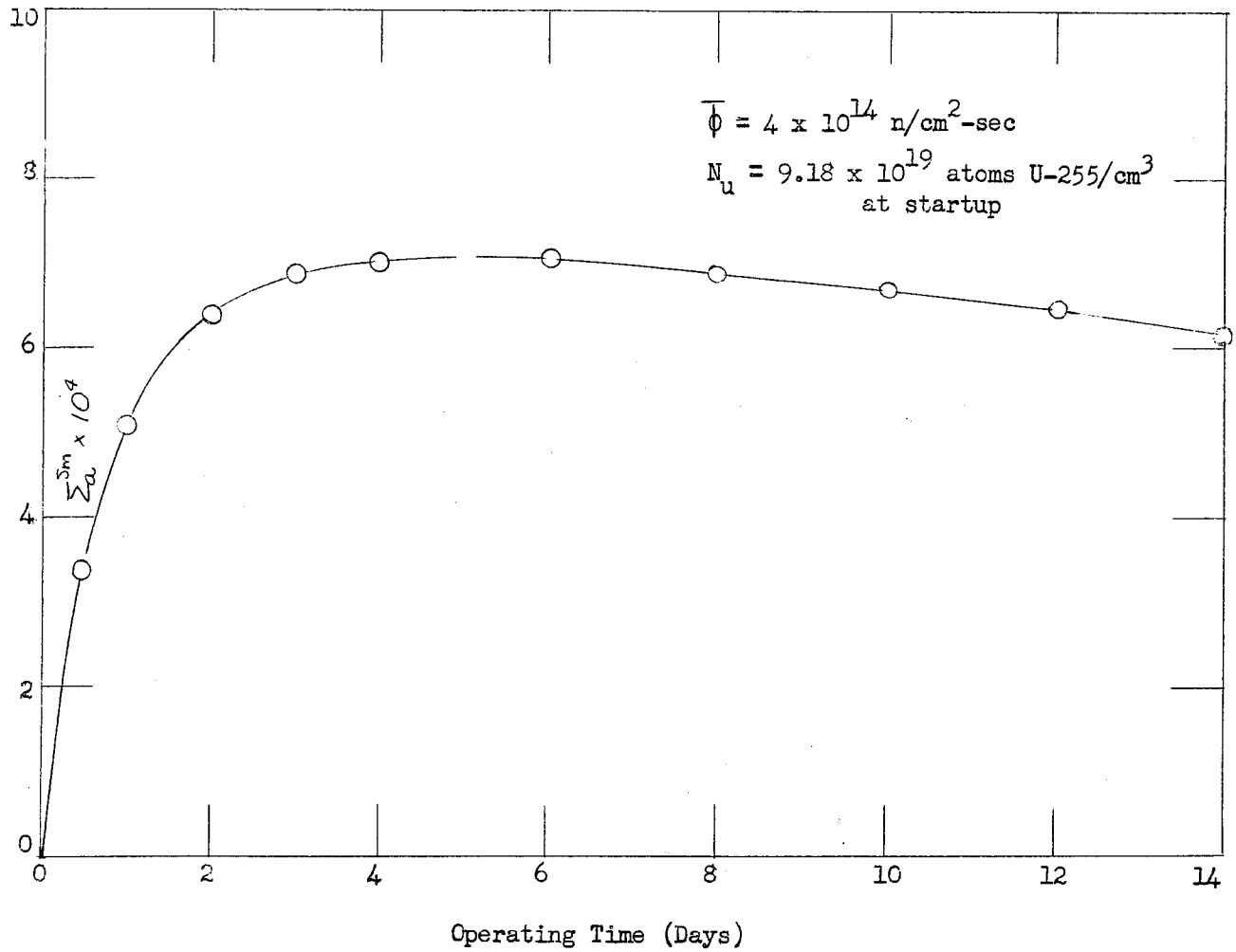

FIGURE 47. Samarium Cross Section Versus Operating Time

5. Samarium Poisoning:

The maximum samarium concentration occurs at about the fifth day of operation.

$$\Delta \rho = \rho - \rho_o = \frac{\Sigma_a^{Sm}}{\Sigma_a^o k_o} \qquad \text{D-28}$$

$$k \cong 1.277$$

$$\Sigma_a^{Sm} = 7.05 \times 10^{-4} \text{ cm}^{-1}$$

$$\Sigma_a^o = 0.0553$$

$$\Delta \rho = \frac{0.000705}{0.0553 \times 1.277} = 0.01$$

This is about 28.5% of the $\Delta \rho$ due to Xe^{135} which is about 0.0351 on the fifth day.

$$\rho = \rho_o - \frac{\Sigma_a^{Sm}}{\Sigma_a^o k_o}$$

$$= \frac{0.277}{1.277} - 0.10$$

$$= 0.207$$

$$k = \frac{1}{1 - \rho}$$

$$= \frac{1}{1 - 0.207}$$

$$= 1.260$$

$$k_o - k \cong 0.017 \text{ (loss of k due to Sm)}$$

6. Total Fission Product Poisoning:

From the data of Sampson[21] et al., a ratio of total long-lived fission product poisoning to samarium poisoning was estimated to be 1.23. This would indicate a $k_o - k$ of about 0.021. Xe^{135} brings this to about 0.076 as a maximum for total fission products.

7. Xenon Over-ride:

The length of a shutdown that can be tolerated and still leave sufficient

excess k to restart the reactor will vary with the time of operation. This shutdown time can be estimated by comparing the Xenon-135 growth curve with the available k curves. It will be assumed that arrangements can be made to take advantage of increased cooling at the time of such a shutdown, or rather that the reactor cools to nearly ambient temperature during the shutdown.

Defining Σ_a^{XeI} as increase in Xe^{135} cross section during the shutdown,

$$k'^c = \frac{1}{1 - \rho^{c'}} = 1 \text{ for criticality}$$

for this to be true, $\rho^{c'} = 0$

$$\rho^{c'} = \rho_c - \frac{\Sigma_a^{XeI}}{k^c \Sigma_a^c}$$

then $$\rho^c = \frac{\Sigma_a^{XeI}}{k^c \Sigma_a^c} \quad \text{and} \quad \Sigma_a^{XeI} = \rho^c k^c \Sigma_a^c$$

where ρ^c = reactivity of cold reactor with poisons at operating level

$$= \rho_o - \frac{\Sigma_a^P}{k_o \Sigma_a^o}$$

k^c = k of cold poisoned reactor = $\frac{1}{1 - \rho^c}$

Σ_a^c = absorption cross section of cold poisoned reactor (operating poisons)

$\rho^{c'}$ = reactivity of just critical reactor

TABLE 20

ALLOWABLE SHUTDOWN TIME FOR Xe^{135} OVER-RIDE AS A FUNCTION OF REACTOR OPERATING TIME FOR COLD REACTOR

Time (Days)	Σ_a^c	k^c	ρ^c	Σ_a^{XeI}	Allowable Shutdown Time
0	.05945	1.298	.230	---	---
2	.0618	1.221	.181	.0137	90 min
4	.0597	1.210	.173	.0125	81 min
6	.0575	1.200	.166	.0114	74 min
8	.0554	1.189	.158	.0104	68 min
10	.0533	1.175	.149	.0094	62 min
12	.0512	1.162	.140	.0083	55 min

The following values apply if the reactor remains at near operating temperature (the superscript, H, refers to hot-poisoned):

Table 21

Allowable Shutdown Time for Xe^{135} Over-ride as a Function of Reactor Operating Time for Hot Reactor

Time (Days)	Σ_a^c	k^{H*}	ρ^{H**}	Σ_a^{XeI}	Allowable Shutdown Time
0	.05945	1.259	.206	---	
2	.0618	1.182	.154	.0113	73 min
4	.0597	1.171	.146	.0102	66 min
6	.0575	1.161	.138	.0092	60 min
8	.0554	1.150	.130	.0083	54 min
10	.0533	1.136	.120	.0073	48 min
12	.0512	1.123	.109	.0063	41 min

* $k^H = k^c = \Delta k_T$

$\Delta k_T = (\text{temperature coefficient})(\text{temperature increase})$

$= -3.3 \times 10^{-4}\ k/^oC \times 75^o = -.039$

$** \rho^H = \frac{k^H - 1}{k^H}$

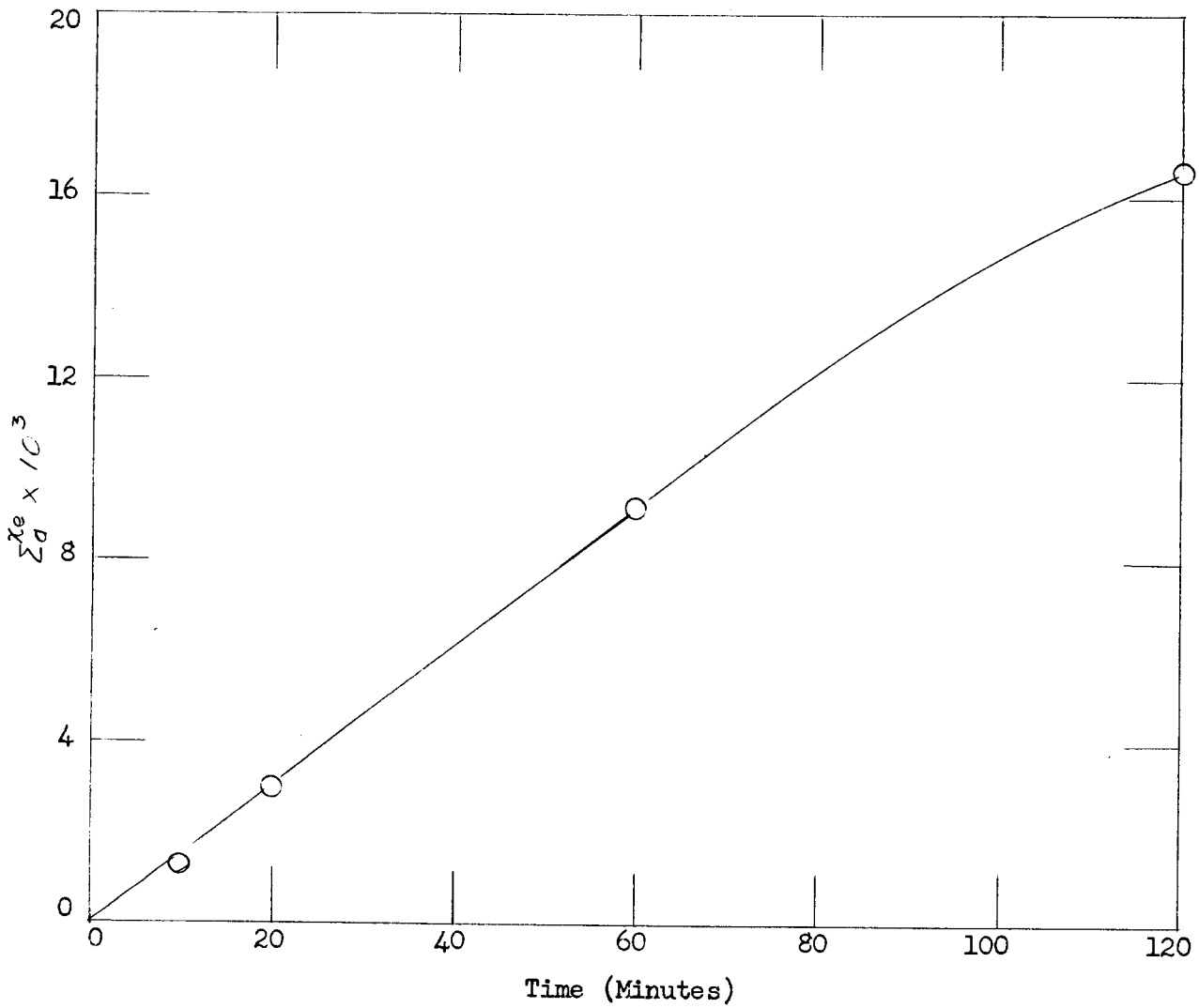

FIGURE 48

Increase in Xe^{135} Cross Section Following Shutdown

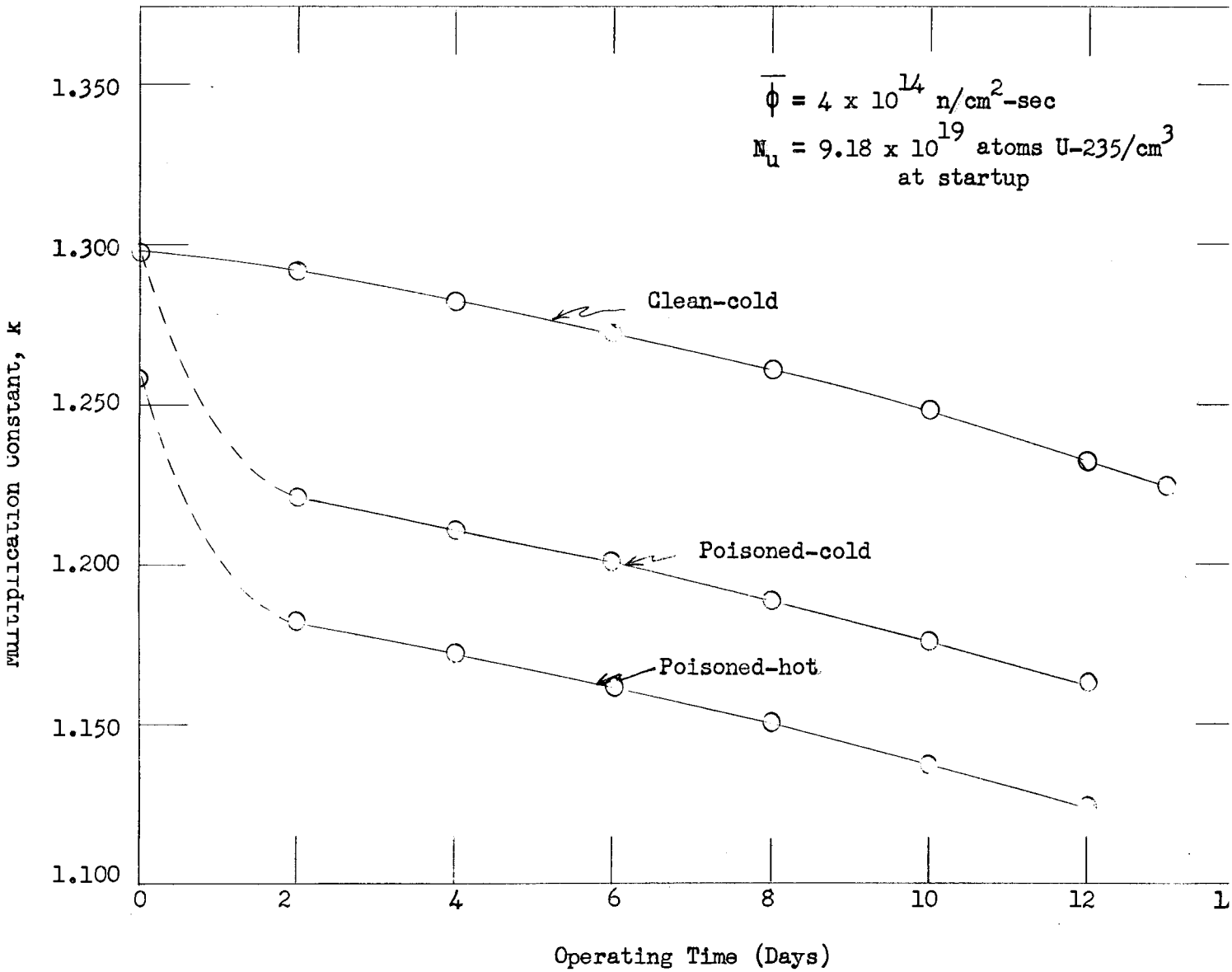

FIGURE 49

Multiplication Constant Versus Operating Time

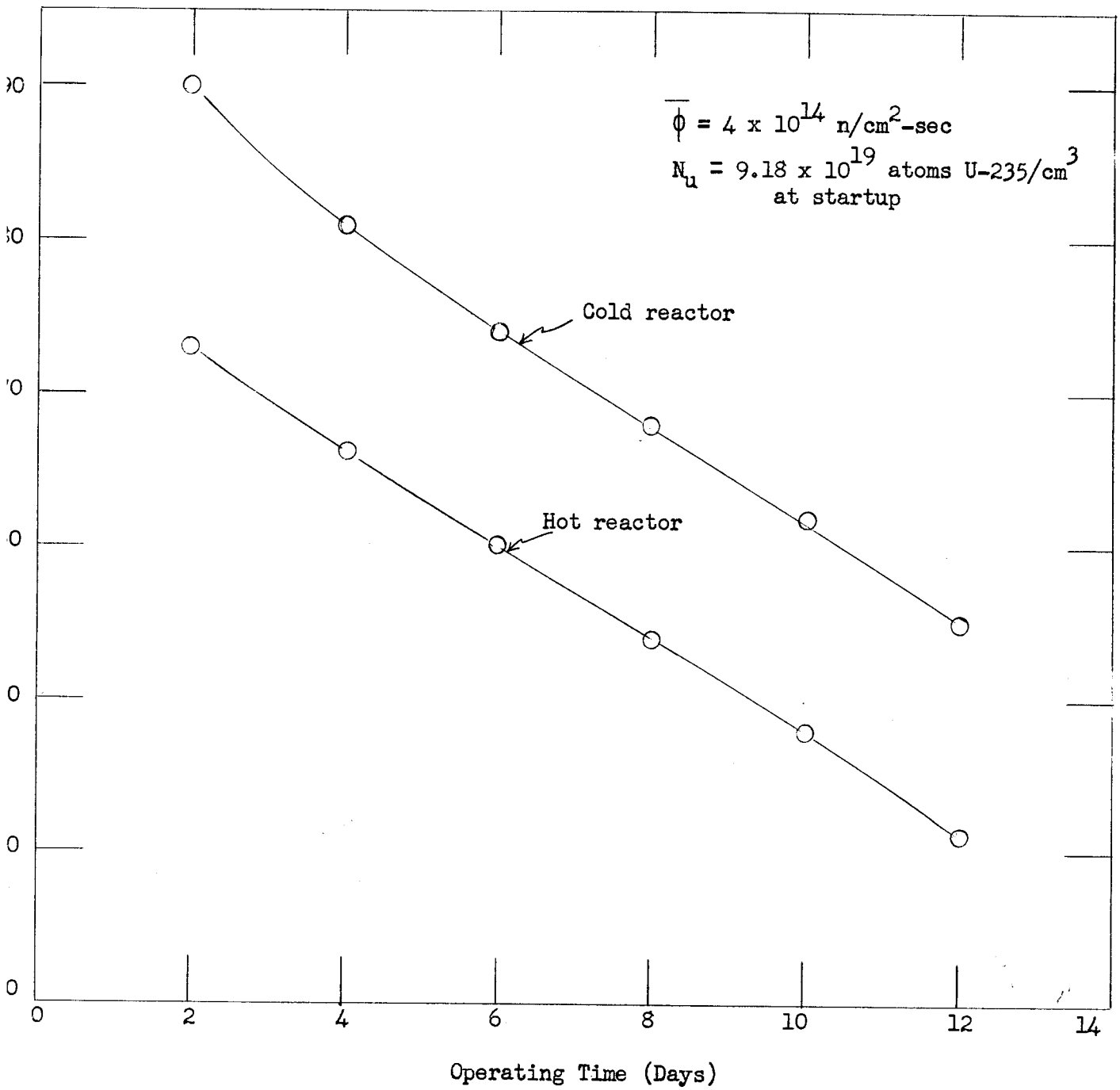

FIGURE 50

Allowable Length of Shutdown to Permit Restart Versus Time

8. Estimation of Change in Σ_a^{Xe} Due to Changes in Φ (Xe Instability):

The equation to be used is

$$\Sigma_a^{Xe}(t) = \sigma_a^{Xe}\left[\frac{a}{dh} + \frac{c}{h}\right]\left[1 - e^{-ht}\right] + \sigma_a^{Xe}\left[\frac{a}{dg} - \frac{b}{g}\right]\left[e^{-ht} - e^{-dt}\right] + \Sigma_{a_o}^{Xe}\, e^{-ht}$$

Where Σ_a^{Xe} = macroscopic cross section of Xe^{135} at the time of a step change in $\overline{\Phi}$

$$a = F_I \Phi_2 \sigma_f N_u \lambda_I$$

$$b = N_{I_o} \lambda_I$$

$$c = F_{Xe} \Phi_2 \sigma_f N_u$$

$$d = \lambda_I + \Phi_2 \sigma_a^I$$

$$g = \lambda_{Xe} + \Phi_2 \sigma_a^{Xe} - \lambda_I - \Phi_2 \sigma_a^I$$

$$h = \lambda_{Xe} + \Phi_2 \sigma_a^{Xe}$$

$$N_u = N_{u_o}\, e^{-\Phi_2 \sigma_a^F t}$$

The Xe^{135} concentration is at a maximum after two days of operation and for the particular reactor being considered the macroscopic absorption cross section is about 2.62×10^{-3} cm^{-1} at that time. This will be used as $\Sigma_{a_o}^{Xe}$ for this calculation.

Considering a plus 10% step change in $\overline{\Phi}$;

$$\Phi_1 = 4.0 \times 10^{14}$$

$$\Phi_2 = 4.4 \times 10^{14}$$

$$\sigma_a^{Xe} = 2.7 \times 10^{-18}\ cm^{+2}$$

$$N_{I_o} = 3.50 \times 10^{16}\ atoms/cm^3$$

$$a = 0.056 \times 4.4 \times 10^{14} \times 5.15 \times 10^{-22} \times 8.80 \times 10^{19}\, e^{-2.68 \times 10^{-7} t} \times 2.88 \times 10^{-}$$

$$= 3.22 \times 10^{7}\, e^{-2.68 \times 10^{-7} t}$$

$$b = 3.50 \times 10^{16} \times 2.88 \times 10^{-5}$$

$$= 1.03 \times 10^{12}$$

$$c = 0.003 \times 4.4 \times 10^{14} \times 5.15 \times 10^{-22} \times 8.80 \times 10^{19}\ e^{-2.68\times10^{-7}t}$$

$$= 5.98 \times 10^{10}\ e^{-2.68\times10^{-7}t}$$

$$d = 2.88 \times 10^{-5}$$

$$g = 2.10 \times 10^{-5} + 4.4 \times 10^{14} \times 2.7 \times 10^{-18} - 2.88 \times 10^{-5}$$

$$= 1.18 \times 10^{-3}$$

$$h = 2.10 \times 10^{-5} + 4.4 \times 10^{14} \times 2.7 \times 10^{-18}$$

$$= 1.21 \times 10^{-3}$$

$$\frac{a}{dg} - \frac{b}{g} = \frac{3.22 \times 10^{7}\ e^{-2.68\times10^{-7}t}}{2.88 \times 10^{-5} \times 1.118 \times 10^{-3}} - \frac{1.03 \times 10^{12}}{1.18 \times 10^{-3}}$$

$$= 9.47 \times 10^{14}\ e^{-2.68\times10^{-7}t} - 8.74 \times 10^{14}$$

For short term considerations $N_u \cong$ constant, then

$$\frac{a}{dh} + \frac{c}{h} = 9.74 \times 10^{14}$$

$$\frac{a}{dg} - \frac{b}{g} = 0.73 \times 10^{14}$$

$$\Sigma_a^{Xe}(t) = 2.63 \times 10^{-3} \left[1 - e^{-1.21\times10^{-3}t}\right] + 0.20 \times 10^{-3} \left[e^{-1.21\times10^{-3}t} - e^{-2.88\times10^{-5}t}\right] +$$

$$+ 2.62 \times 10^{-3}\ e^{-1.21\times10^{-3}t}$$

$$= 2.63 \times 10^{-3} + 0.19 \times 10^{-3}\ e^{-1.21\times10^{-3}t} - 0.20 \times 10^{-3}\ e^{-2.88\times10^{-5}t}$$

TABLE 22

EFFECT OF STEP CHANGES IN AVERAGE Φ ON Xe^{135} CROSS SECTION

Time, min	Σ_a^{Xe}, cm^{-1} (+ 10% step change in $\bar{\Phi}$ at t = 0)	Σ_a^{Xe}, cm^{-1} (+ 20% step change in $\bar{\Phi}$ at t = 0)	Σ_a^{Xe}, cm^{-1} (- 20% step change in $\bar{\Phi}$ at t = 0)
0	2.62×10^{-3}	2.62×10^{-3}	2.62×10^{-3}
1	2.61×10^{-3}	2.59×10^{-3}	2.64×10^{-3}
10	2.51×10^{-3}	2.41×10^{-3}	2.76×10^{-3}
20	5.47×10^{-3}	2.32×10^{-3}	2.85×10^{-3}
40	2.46×10^{-3}	2.27×10^{-3}	2.91×10^{-3}
60	2.45×10^{-3}	2.27×10^{-3}	2.93×10^{-3}

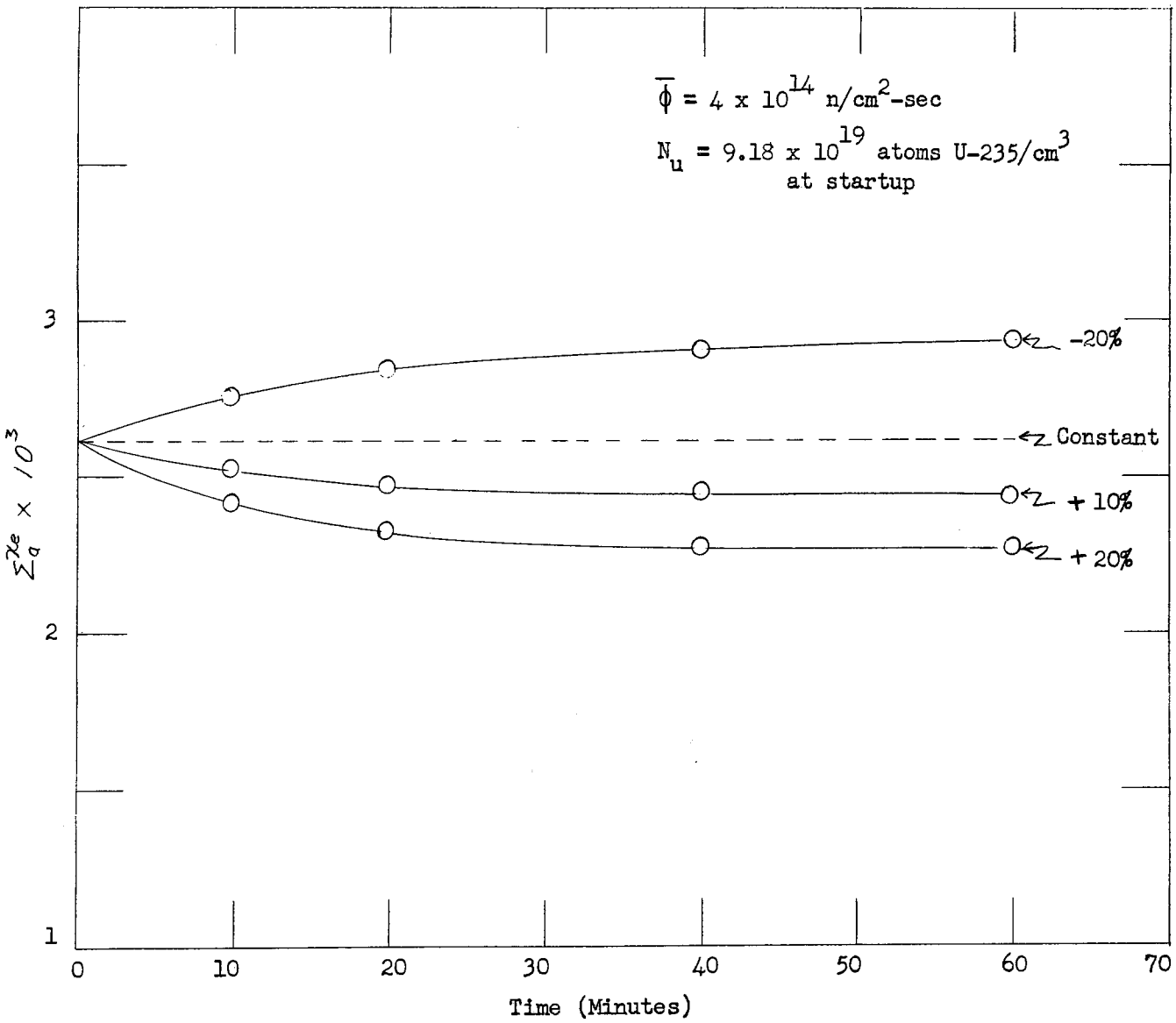

FIGURE 51

Change in Σ_a^{Xe} Versus Time Following

+ 10%, + 20% and - 20% Change in Average Flux

A criterion developed by A. G. Ward[34] indicates that in a high flux reactor a necessary condition for flux oscillations to occur due to xenon instability when there is a neutron perturbation is that

$$\frac{A}{K_j} > 1$$

where A = maximum local reactivity change due to Xe

$\cong$ 0.035 for this reactor

$K_j \cong M^2(B_0^2 - B_j^2)$

M^2 = migration area

B_0^2 = 0th mode buckling

B_j^2 = higher mode bucklings

For the double slab reactor

$$B_0^2 = \left(\frac{\pi}{108.6}\right)^2 + \left(\frac{\pi}{220}\right)^2 + \left(\frac{\pi}{160}\right)^2$$

$$= 1.43 \times 10^{-3}\ \text{cm}^{-2}$$

$$B_1^2 = 4\left(\frac{\pi}{108.6}\right)^2 + \left(\frac{\pi}{220}\right)^2 + \left(\frac{\pi}{160}\right)^2$$

$$= 3.93 \times 10^{-3}\ \text{cm}^{-2}$$

$$B_2^2 = \left(\frac{\pi}{108.6}\right)^2 + 4\left(\frac{\pi}{220}\right)^2 + \left(\frac{\pi}{160}\right)^2$$

$$= 2.04 \times 10^{-3}\ \text{cm}^{-2}$$

$$B_3^2 = \left(\frac{\pi}{108.6}\right)^2 + \left(\frac{\pi}{220}\right)^2 + 4\left(\frac{\pi}{160}\right)^2$$

$$= 2.58 \times 10^{-3}\ \text{cm}^{-2}$$

$$M^2 = 209\ \text{cm}^2$$

Therefore,

$$K_1 = 209\ [0.00143 - 0.00393] = -0.523$$

$$K_2 = 209\ [0.00143 - 0.00204] = -0.127$$

$$K_3 = 209\ [0.00143 - 0.00258] = -0.240$$

and

$$-\frac{A}{K_1} = 0.067$$

$$-\frac{A}{K_2} = 0.276$$

$$-\frac{A}{K_3} = 0.146$$

Since these are all less than unity and since higher modes should be less effective, the reactor is stable with respect to this type of oscillation by this criterion.

APPENDIX E

1. Fuel Element Calculation and Design

One of the prime considerations in a high-flux, high-power reactor of this type is the problem of heat removal. As pointed out in the preceeding sections, the fuel zone is relatively heavily loaded and in order to obtain experiment peak fluxes greater than 10^{15} neutrons/cm^{2}sec the average thermal flux in the fuel will be of the order 4×10^{14} neutrons/cm^{2}sec. Total power is directly proportional to the average flux. Nuclear considerations dictate the geometry and size of the system, and, if these require a compact fuel region, heat fluxes intolerable from an engineering viewpoint may result. Therefore, of supreme importance in reactor design is the choice of an adequate heat removal system of which the fuel element design is an integral part.

A basic requirement of such a fuel element is sufficient surface area to permit an acceptable heat flux. In obtaining this area there must be provided enough coolant flow capacity so that the maximum permissible surface temperature of the fuel plates is not exceeded. However, the choice of flow rate is not independent of other considerations. Flow velocities must be maintained within limits that will not cause intolerable pressure drops across the fuel element. At the same time the proper volumetric metal to water ratio and the fuel alloy composition must be consistent with nuclear and metallurgical requirements respectively.

After the nuclear calculations had been made and the core configuration had been decided, several heat transfer calculations were made to determine which type of fuel element, cylindrical or flat plate, would best fulfill the requirements. It became immediately apparent that, in order to keep heat fluxes below 500,000 BTU/hr-ft^2-$^\circ$F, the fuel element surface temperature would have to be above the atmospheric boiling point of the coolant and that pressurization would be necessary to prevent boiling in the fuel element flow channels. Individually pressurized

cylindrical fuel elements were first considered since this scheme would preclude pressurization of the large reactor tank and since a workable scheme for fuel changing that would minimize the opportunities for contamination of the D_2O coolant had been devised. Considerable effort was expended in this direction before it was decided that simultaneously meeting the metal to water ratio, geometry control problems and the requirements of the mathematical model used in the core analysis would require a more extensive analysis of the cylindrical fuel element than remaining time would permit. For this reason attention was directed toward modifying the design of the MTR type of fuel element to be used in a totally pressurized system.

Once the geometry of the fuel element had been determined, it was possible to choose locations for the control slabs and to calculate their worth in the reactor. Eighteen control plates are to be placed between the forty-six fuel elements per reactor slab as shown in Figure 3. Knowing the length of one reactor core slab, the allowance needed for the control plates, the number of fuel elements, and the clearance between adjacent fuel plates, the dimensions of the fuel plates were calculated as shown below. A sketch of the fuel element is shown in Figure 5.

$$\text{Depth of fuel element} = \frac{\text{length of core slab} - (\text{control rod allowances} + \text{fuel element spacing})}{\frac{1}{\text{number of rows}}\ (\text{number fuel elements per slab})}$$

$$= \frac{(70.9\ \text{in}) - [(8.0\ \text{in}) + 6(0.040\ \text{in})]}{\frac{1}{2}\ (46)}$$

$$= 2.728\ \text{in.}$$

$$\text{Width of fuel element} = \frac{\text{width core slab} - \text{clearance between fuel elements}}{2}$$

$$= \frac{7.874 \text{ in} - 0.040 \text{ in}}{2}$$

$$= 3.917 \text{ in.}$$

The fuel length in the fuel element is taken as the active height of the reactor core slab, 120 cm or 47.3 in. The thickness of the individual fuel plates comprising a fuel element was chosen as 0.030 in. This dimension is composed of an aluminum-uranium fuel alloy core 0.010 in. thick clad on each side by a 0.010 in thick aluminum sheet.

With these dimensions it was then possible to determine the number of plates that would give the proper volumetric metal to water ratio. The metal to water ratio was chosen from nuclear calculations to be 0.73. The volume of metal and number of fuel plates needed to give this ratio were obtained as follows:

$$\frac{M}{W} = \frac{V_m}{V_w} = \frac{V_T - V_w}{V_w} = \frac{V_T}{V_w} - 1$$

Rearranging and solving for V_w,

$$V_w = \frac{V_T}{1 + \frac{V_m}{V_w}}$$

$V_T \equiv$ volume of one fuel slab $= 7.87 \times 47.3 \times 70.9 \text{ in}^3$
$= 26{,}393 \text{ in}^3$

$V_m \equiv$ volume of metal

$V_w \equiv$ volume of D_2O

$$V_w = \frac{26,393}{1 + 0.73}$$

$$= 15,256 \text{ in}^3 \text{ (volume of } D_2O \text{ per slab)}$$

$$V_m = V_T - V_w$$

$$= 26,393 - 15,256$$

$$= 11,137 \text{ in}^3 \text{ (volume of metal per slab).}$$

This volume of metal can then be used to obtain the number of fuel plates per element.

$$\frac{M}{W} = 0.73 = \frac{\text{vol. of metal}}{\text{vol. of water}} = \frac{47.3 \times \text{unit vol. of metal per slab}}{47.3 \times \text{unit vol. of water per slab}}$$

$$\left\{\begin{matrix}\text{unit vol. of metal} \\ \text{per fuel element} \\ \text{assembly}\end{matrix}\right\} = \begin{matrix}\text{unit vol. of 2 side plates + unit vol. of 2 outside} \\ \text{fuel plates + unit vol. of n inside fuel plates}\end{matrix}$$

Assume the curved fuel plates are straight for dimension 3.541 in.

Unit volume of 2 side plates = $2(0.188)(2.728)(1) = 1.026 \text{ in}^3$

Unit volume of 2 outside fuel plates = $2(0.065)(3.541)(1) = 0.460 \text{ in}^3$

Unit volume of n inside fuel plates = $n(0.030)(3.541)(1) = 0.106\, n \text{ in}^3$

$$\left.\begin{matrix}\text{Unit volume of metal} \\ \text{per slab}\end{matrix}\right\} = 46\left[1.026 + 0.460 + 0.106\, n\right]$$

$$= 68.356 + 4.876\, n \text{ in}^3$$

$$\text{Unit volume of reactor slab} = \frac{26,393 \times 1}{47.3} = 558 \text{ in}^3$$

$$\frac{M}{W} = 0.73 = \frac{68.356 + 4.876\, n}{558 - (68.356 + 4.876\, n)}$$

$$n = 34.1$$

Since n must be a whole number

$n = 34$ = number of inside fuel plates per element

$N = (n + 2) = 36$ = number of total fuel plates per element

The spacing between the fuel plates can now be computed.

Spacing between fuel plates = S

$$S = \frac{\text{depth of fuel element} - 2(\text{thickness of outside fuel plates})}{\text{number of spacings}}$$

$$= \frac{(S - \text{end allowance}) - n(\text{thickness of inside fuel plates})}{\text{number of spacings}}$$

$$= \frac{2.728 - 2(0.065) - (S - 0.020) - 34(0.03)}{35}$$

Solving for S,

$S = 0.044$ in = spacing between fuel plates that is available for D_2O coolant flow.

2. Fuel Alloy Composition

It must now be determined if the 0.010 in fuel alloy with 0.010 in aluminum clad will give a fuel alloy composition within metallurgical limits.

U-235 loading = 30.9 kg

Total uranium loading $= \frac{30.9}{0.9} = 34.3$ kg (90% enriched)

Loading per fuel element $= \frac{34.300}{92} = 373.2 \frac{\text{gm of total U}}{\text{fuel element}}$

a = weight fraction of total uranium in fuel alloy

Density of fuel alloy $= \rho = \frac{\text{mass of fuel alloy}}{\text{vol. of fuel alloy}}$

$$= \frac{M}{V} = \frac{m^u + m^{Al}}{V^u + V^{Al}} = \frac{aM + (1-a)M}{V^u + V^{Al}}$$

$$m^u = aM = \frac{m^u}{V^u} V^u = \rho^u V^u$$

$$V^u = \frac{aM}{\rho^u}$$

Similarly $V^{Al} = \frac{(1-a)M}{Al}$

$$V^u + V^{Al} = V,$$

Substitute for V^u and V^{Al} from above to get

$$\frac{aM}{\rho u} + \frac{(1-a)M}{\rho Al} = V.$$

$$\left[\frac{a}{\rho u} + \frac{(1-a)}{\rho Al}\right]\rho = 1$$

$$\rho = \frac{1}{\left[\frac{a}{\rho u} \quad \frac{(1-a)}{\rho Al}\right]} = \text{density of fuel alloy.}$$

Volume of fuel alloy per fuel element = (Vol. of inside fuel plates) $\frac{\text{(fuel alloy thickness)}}{\text{(total plate thickness)}}$ +

+ (vol. of outside fuel plates) $\frac{\text{(fuel alloy thickness)}}{\text{(total plate thickness)}}$

$\frac{\text{Weight of total uranium per fuel element}}{\text{Weight fraction of total uranium}}$ = (density of fuel alloy) (vol. of fuel all per fuel elemen

= weight of fuel alloy per fuel element

$$\frac{373.2}{a} = \left[\frac{1}{\frac{a}{18.55} - \frac{(1-a)}{2.7}}\right]\left[(3.541)(0.030)(47.3)(34)\left(\frac{0.010}{0.030}\right) + (3.541)(0.065)(47.3)(2)\left(\frac{0.010}{0.065}\right)\right]\left[16.38\ \frac{cm^3}{in^3}\right]$$

Solving for a,

$$a = 0.125$$

$$= 12.5\% = \%\text{ by weight U in fuel alloy.}$$

This composition is well within metallurgical limits for U-Al alloys; the upper limit of composition is of the order of 25% weight uranium.

Total volume of fuel alloy = 92 (vol. of fuel alloy per fuel element)

$$= 92 \left[(3.541)(0.030)(47.3)(34)\left(\frac{0.010}{0.030}\right) + (3.541)(0.065)(47.3)(2)\left(\frac{0.010}{0.030}\right)\right]$$

$$= 92(60.296)$$

$$= 5547.2 \text{ in}^3$$

$$= 3.21 \text{ ft}^3$$

$$= 90{,}863 \text{ cm}^3$$

Total surface area of fuel plates = (92)(36)(area of one fuel plate)

$$= (92)(36)(2 \times 3.541 \times 47.3)$$

$$= 1{,}109{,}376 \text{ in}^2$$

$$= 7704 \text{ ft}^2 = \text{total fuel plate area of reactor}$$

APPENDIX F

1. Heat Production, Transfer and Removal Calculations

The initial approach to the heat transfer problem was to establish a substantially high D_2O coolant flow rate as the criterion for the system. For a given heat flux the flow rate will determine the maximum fuel plate temperature and therefore the pressurization, if any, for the system. The fuel plate temperature is inversely proportional to the velocity of the coolant; hence the maximum permissible flow rate was chosen as the design point. This flow rate was believed to be in the neighborhood of 30-40 ft/sec; a value of 35 ft/sec was chosen. This value, however, resulted in a pressure drop across the fuel element of about 104 psi. Since a pressure drop this great would probably be excessive for the current element design, it would require that the element be redesigned because the 0.030-inch fuel bearing plates would probably not be structually sound for a 104 psi differential. This calculation indicated that if an acceptable pressure drop was to be obtained across the fuel elements presently being considered, the coolant flow velocity must be reduced. A lower coolant flow rate, however, would lower the heat transfer rate from fuel to coolant and bring about an increase in fuel plate temperature. This would be accompanied by an increase in reactor tank pressure necessary to prevent boiling at the fuel plate surfaces. Therefore, the pressure drop across the fuel element became the new constraint on the system.

a. Surface Area Available for Heat Transfer:

Surface area per element $= 2NwL$

$$= (2)(36)(3.541)(47.3)$$

$$= 12{,}059 \text{ in}^2$$

$$= 83.74 \text{ ft}^2$$

Surface area per fuel slab = (46)(83.74)

$$= 3852 \text{ ft}^2$$

Total heat transfer area in reactor = (2)(3852)

$$= 7704 \text{ ft}^2$$

b. Average Heat Flux:

Assume that 95% of the reactor heat is released in the core.

Total power = P = 500 MW

$$\frac{q}{a} = \frac{0.95\ P}{A}$$

$$= \frac{500 \times 10^6 \times 0.95 \times 3.413}{7704}$$

$$= 210{,}430 \text{ BTU/hr-ft}^2$$

$$= 66.4 \text{ watts/cm}^2 = \text{average heat flux}$$

c. Power Density Calculations:

Power density calculations were made for two different cases:

1. The reactor core was considered as a completely homogenized region.
2. The reactor core was considered as a heterogeneous system, and the fissions were confined to the volume of fuel alloy.

Homogeneous Case

Assume 95% of the power is released in the core.

$$\text{Average power density} = \frac{(\text{reactor power})(0.95)}{\text{core volume}}$$

$$= \frac{500 \times 10^6 \times 0.95 \times 3.413 \times 1728}{7.87 \times 47.3 \times 70.9}$$

$$= 53.14 \times 10^6 \ \frac{\text{BTU}}{\text{hr-ft}^3}$$

$$= 550 \text{ watts/cm}^3$$

$$\text{Maximum power density} = \left(\frac{P}{V}\right)_{\max\ x,y,z} = \omega\left(\overline{\Sigma_f \Phi}\right)_{\max\ x,y,z}$$

$$\omega = 3.23 \times 10^{-16} \text{ megawatts-sec/fission}$$

From nuclear calculations obtained with the aid of the ORACLE, it can be shown that the fission rate density, $(\Sigma_f\Phi)_{max\ x;\ avg.\ y,z} = 436.9 \times 10^{11}$ fission/cm^3-sec as shown in Table 23 and Figures 52, 53 and 54. The following cross sections are recorded in Appendix A, Table 5:

$\nu\Sigma_{f_1} = 0.000430\ cm^{-1}$ $\nu\Sigma_{f_2} = 0.01208\ cm^{-1}$

$\Sigma_{f_1} = 0.000175\ cm^{-1}$ $\Sigma_{f_2} = 0.004911\ cm^{-1}$

$\nu\Sigma_{f_3} = 0.1138\ cm^{-1}$

$\Sigma_{f_3} = 0.04626\ cm^{-1}$

Peak thermal flux in experiment region = $2.5 \times 10^{15}\ \frac{\text{neutrons}}{cm^2\text{-sec}}$

TABLE 23

FISSION RATE DENSITIES IN CORE

x, cm	$\bar{\Sigma}_{f_1}\bar{\Phi}_{12}$	$\bar{\Sigma}_{f_2}\bar{\Phi}_{22}$	$\bar{\Sigma}_{f_3}\bar{\Phi}_{32}$	$q_p=\sum\bar{\Sigma}_{fi}\bar{\Phi}_{ij}$, $\frac{\text{fissions}}{cm^3\text{-sec}}$
20.00	1.90×10^{11}	42.0×10^{11}	393.0×10^{11}	436.9×10^{11}
22.35	2.33×10^{11}	42.2×10^{11}	255.5×10^{11}	300.0×10^{11}
24.71	2.49×10^{11}	42.2×10^{11}	176.5×10^{11}	221.2×10^{11}
27.06	2.51×10^{11}	41.6×10^{11}	131.0×10^{11}	175.1×10^{11}
29.41	2.43×10^{11}	40.6×10^{11}	104.3×10^{11}	147.3×10^{11}
31.76	2.31×10^{11}	38.9×10^{11}	88.8×10^{11}	130.0×10^{11}
34.12	2.14×10^{11}	36.8×10^{11}	80.0×10^{11}	118.9×10^{11}
36.47	1.95×10^{11}	34.2×10^{11}	76.7×10^{11}	112.9×10^{11}
38.82	1.72×10^{11}	31.3×10^{11}	79.2×10^{11}	112.2×10^{11}
40.00	1.59×10^{11}	29.8×10^{11}	83.4×10^{11}	114.8×10^{11}

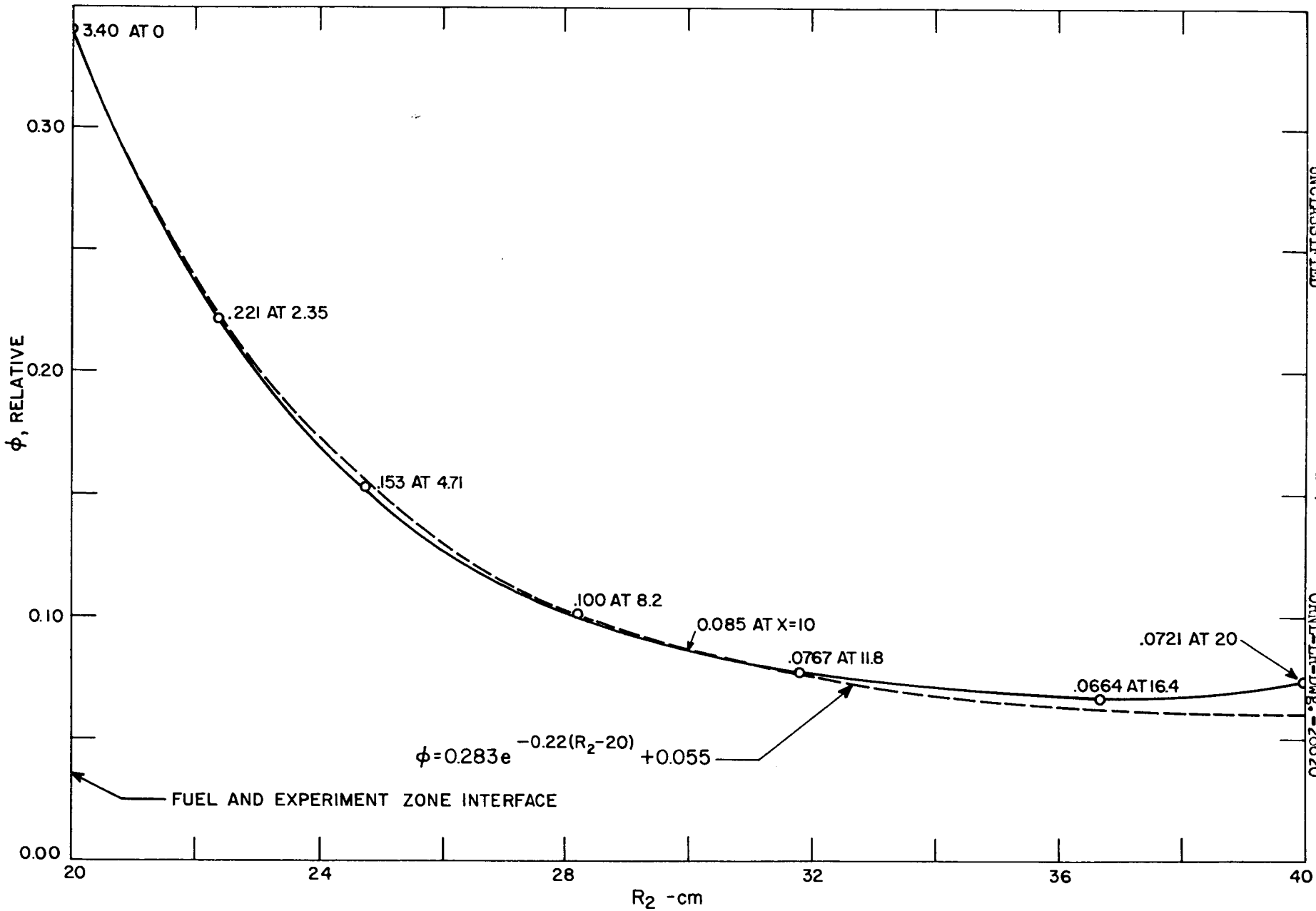

Fig. 52. Thermal Flux vs R_2.
R_2 = distance from reactor center line in X-direction.

UNCLASSIFIED

ORNL-LR-Dwg. -26620

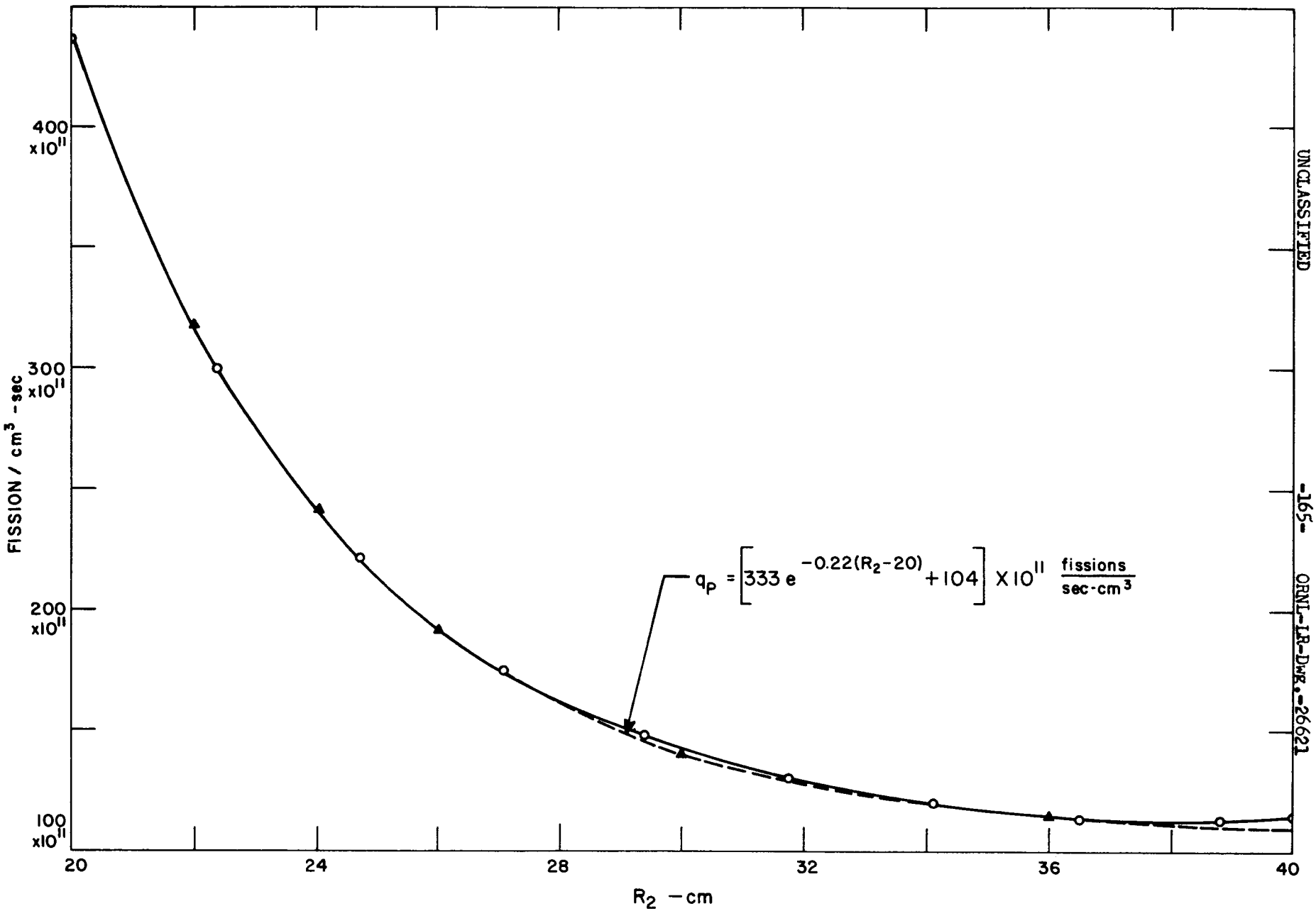

Fig. 53. Fission Rate Density vs R_2. At a line where $\phi(z)$ & $\phi(v)$ are at average value.

UNCLASSIFIED

ORNL-LR-DWG.-26621

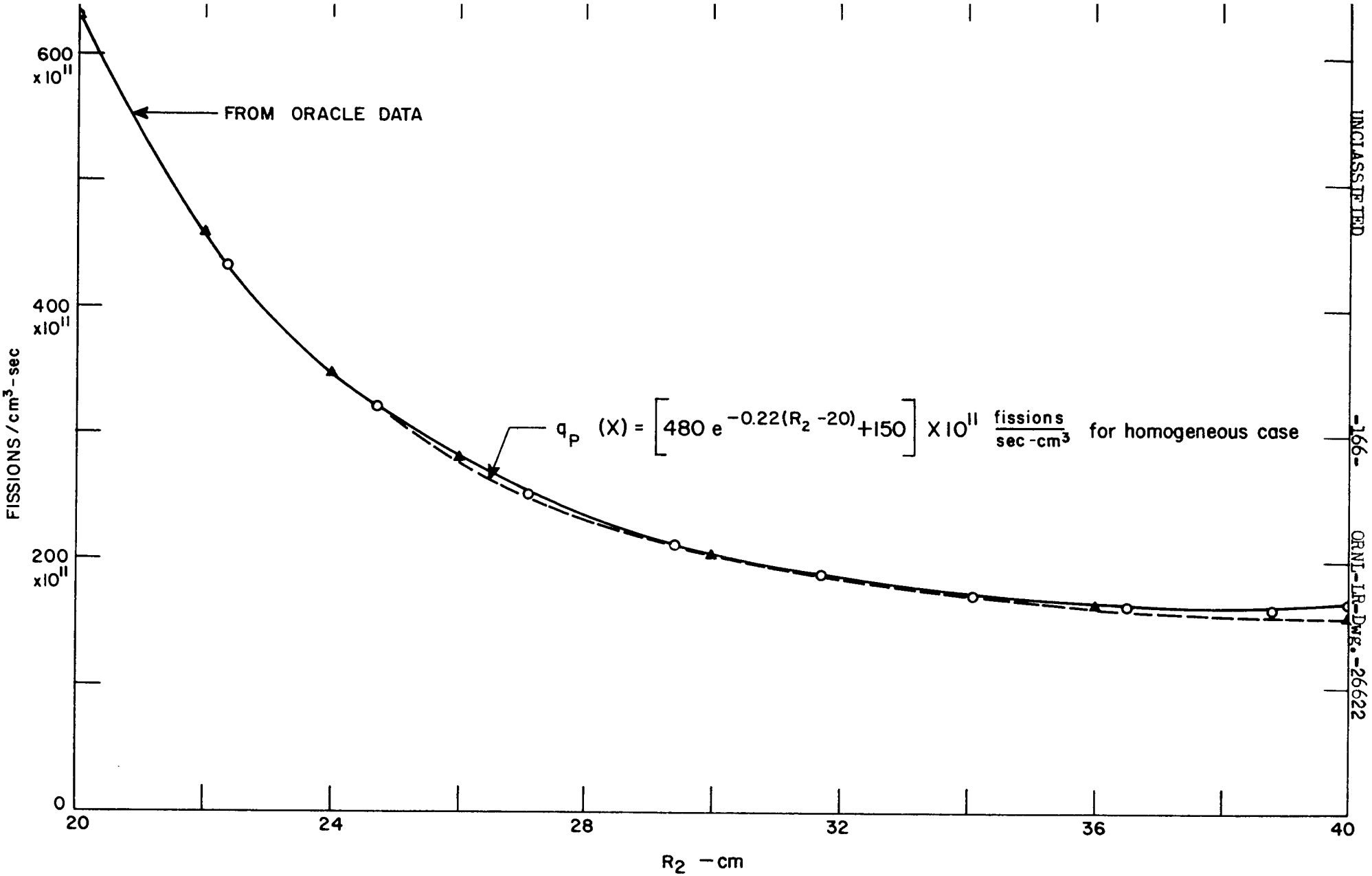

Fig. 54. Fission Rate Density vs R_2. At center of reactor, assuming $= \frac{\hat{\phi}(z)}{\bar{\phi}(z)} = \frac{\hat{\phi}(y)}{\bar{\phi}(y)} = 1.2$

UNCLASSIFIED

ORNL-LR-Dwg.-26622

$(\Sigma_f\Phi)_{max\ x;\ avg.\ y,z}$ represents a maximum fission rate density in the x-direction (7.87-inch dimension) and average values in the y- and z-directions (70.9-inch and 47.3-inch dimensions respectively). It can be shown that the ratio of peak to average flux in the y- and z-directions is

$$\frac{\hat{\Phi}(y)}{\bar{\Phi}(y)} \cong \frac{\hat{\Phi}(z)}{\bar{\Phi}(z)} \cong 1.2$$

$$\begin{aligned}
\text{Therefore } (\Sigma_f\Phi)_{max\ x,y,z} &= (1.2)^2\ (\Sigma_f\Phi)_{max\ x;\ avg.\ y,z} \\
&= (1.2)^2\ (436.9 \times 10^{11}) \\
&\doteq 629 \times 10^{11} \text{ fissions/cm}^3\text{-sec} \\
&= \text{maximum fission rate density}
\end{aligned}$$

$$\left(\frac{P}{V}\right)_{max\ x,y,z} = \omega'(\Sigma_f\Phi)_{max\ x,y,z} = \frac{629 \times 10^{11}}{3.1 \times 10^{10}} = 2029\ \frac{\text{watts}}{\text{cm}^3}$$

$$= 196 \times 10^6\ \frac{\text{BTU}}{\text{hr-ft}^3}$$

$$\omega' = \frac{\text{watt-sec}}{3.1 \times 10^{10} \text{ fissions}}$$

<u>Heterogeneous Case</u>

$$\begin{aligned}
\text{Average power density} &= \frac{0.95\ P}{\text{volume of fuel alloy}} \\
&= \frac{0.95 \times 500 \times 10^6}{90{,}863} \\
&= 5230 \text{ watts/cm}^3 \\
&= 50.5 \times 10^7 \text{ BTU/hr-ft}^3
\end{aligned}$$

The volume of fuel alloy was calculated above in Appendix E, Section 2.

The maximum power density is taken to be at the center of the side of the reactor core slab facing the experiment region. Since the reactor is symmetrical about the experiment cells, there will be two of these maximum power density regions. In order to get a better estimate of the maximum power density in the actual reactor

core it is necessary to "dehomogenize" the core. This is accomplished by assuming the maximum fission rate in the "dehomogenized" (heterogeneous) core is the same as in the homogenized core. It is then assumed that the maximum fission rate density occurs in the same size volume but of different geometries.

Power of reactor = $\omega \Sigma_f \Phi V$

$$\omega = \frac{\text{watt-sec}}{3.1 \times 10^{10} \text{ fissions}}$$

$\Sigma_f \Phi$ = fission rate density

V = volume of fuel

Since $P_{homo} = P_{het}$,

$$\omega(\Sigma_f\Phi)_{homo} V_{homo} = \omega(\Sigma_f\Phi)_{het} V_{het}$$

$$(\Sigma_f\Phi)_{het} = (\Sigma_f\Phi)_{homo} \frac{V_{homo}}{V_{het}}$$

$$\text{Maximum power density} = \left(\frac{P}{V}\right)_{max}$$

$$\left(\frac{P}{V_{het}}\right)_{max} = \omega(\Sigma_f\Phi)^{max}_{het}$$

$$= \omega(\Sigma_f\Phi)^{max}_{homo} \frac{V_{homo}}{V_{het}}$$

$$= \frac{\text{watt-sec}}{3.1 \times 10^{10} \text{ fissions}} \times 629 \times \frac{10^{11} \text{ fissions}}{\text{sec-cm}^3} \times \frac{864{,}000 \text{ cm}^3}{90{,}863 \text{ cm}^3}$$

$$= 19{,}310 \frac{\text{watts}}{\text{cm}^3} \text{ (This is per cm}^3 \text{ of } \underline{\text{fuel}} \ \underline{\text{alloy}}.)$$

$$= 1865 \times 10^6 \text{ BTU/hr ft}^3$$

$$\text{Maximum fission rate} = (\Sigma_f\Phi)^{max}_{het}$$

$$= (\Sigma_f\Phi)^{max}_{homo} \frac{V_{homo}}{V_{het}}$$

$$= 629 \times 10^{11} \frac{\text{fissions}}{\text{sec-cm}^3} \times \frac{864{,}000 \text{ cm}^3}{90{,}863 \text{ cm}^3}$$

$$= 5986 \times 10^{11} \frac{\text{fissions}}{\text{cm}^3\text{-sec}}$$

d. Maximum Heat Flux Per Unit Area:

Assume that the maximum power density occurs within one fuel plate.

$$\frac{\text{Surface area}}{\text{volume of fuel}} = \frac{\text{area of fuel plates in one fuel element}}{\text{volume of fuel alloy in one fuel element}}$$

$$= \frac{2(3.541\text{x}47.3\ \text{in}^2)(2.54\ \text{cm/in})^2}{987.6\ \text{cm}^3}$$

$$= 78.74\ \text{cm}^2/\text{cm}^3$$

$$q'' = \frac{\left(\frac{P}{V_{het}}\right)_{max}}{\frac{\text{area}}{\text{volume}}} = \frac{\text{maximum heat flux}}{\text{area}}$$

$$= \frac{19{,}310\ \text{watts/cm}^3}{78.74\ \text{cm}^2/\text{cm}^3}$$

$$= 245\ \text{watts/cm}^2$$

$$= 775{,}000\ \text{BTU/hr-ft}^2$$

2. D_2O Coolant Flow and Temperature Calculations:

The coolant flow pattern is presented schematically in Figure 55.

a. Core Region:

Flow area of core = (area of one coolant channel)(no. of channels)

$$= \left(\frac{0.044\text{x}3.541}{144}\right)(92\text{x}36)$$

$$= 3.58\ \text{ft}^2$$

Based on MTR data,[24] it has been assumed that the present fuel element design will permit a 40 psi pressure drop, and this value is used to determine a coolant velocity. It so happens that the pressure drop, friction factor, velocity and Reynolds number are inter-related such that it is not possible to solve for the velocity directly. Therefore a velocity has to be assumed and a calculation made to check the accuracy of the estimate. New estimates and further calculations are then made if necessary.

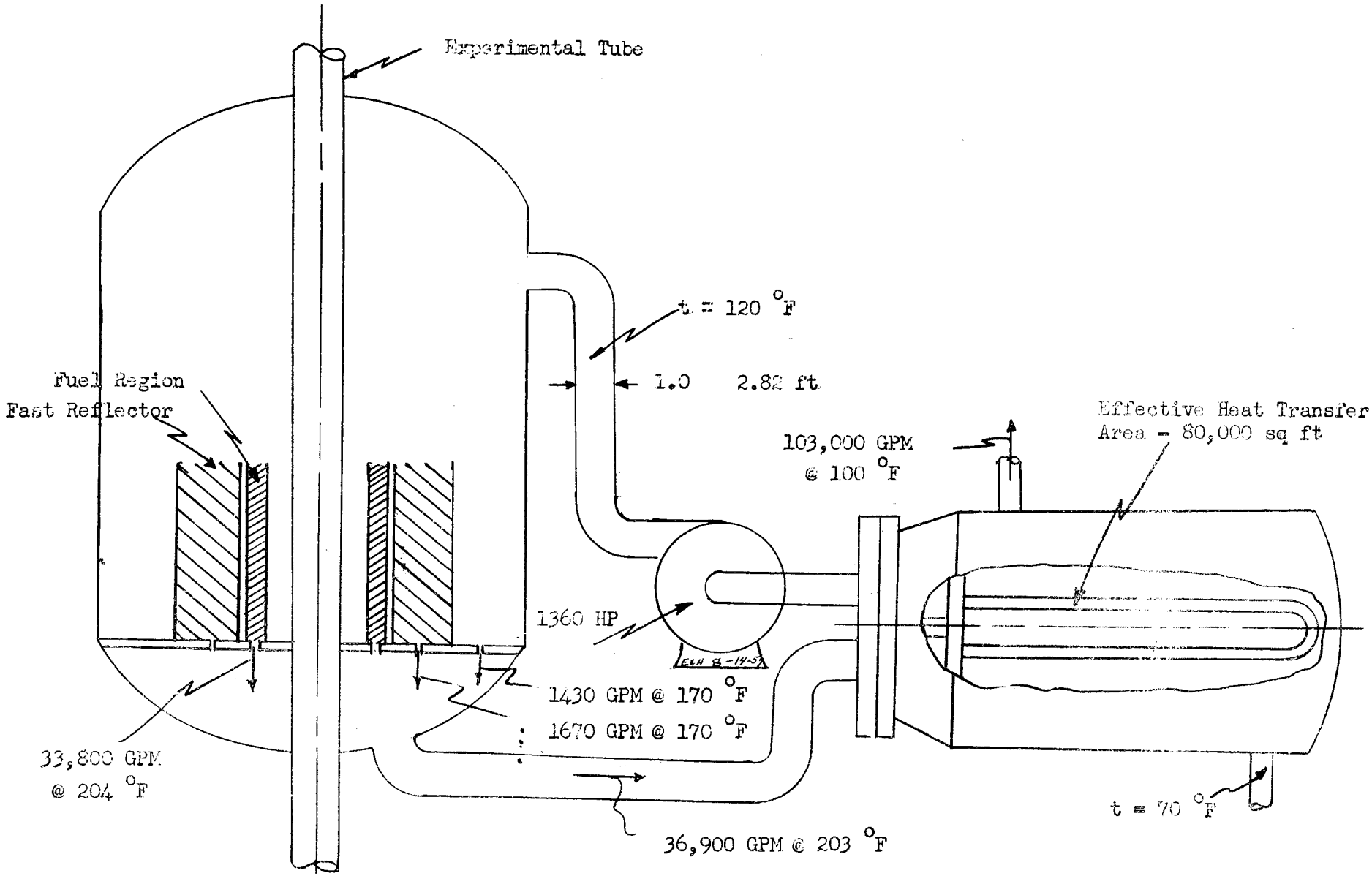
Experimental Tube
t = 120 °F
1.0
2.82 ft
Fuel Region
Fast Reflector
103,000 GPM
@ 100 °F
Effective Heat Transfer
Area - 80,000 sq ft
1360 HP
1430 GPM @ 170 °F
1670 GPM @ 170 °F
33,800 GPM
@ 204 °F
36,900 GPM @ 203 °F
t = 70 °F

For turbulent flow the pressure drop can be expressed as

$$\Delta p = \frac{2fu^2L\rho}{144\ g_cD_e}$$

solving for u, the velocity,

$$u = \left[\frac{\Delta p\ g_cD_e(144)}{2L\rho}\right]^{\frac{1}{2}} \frac{1}{f^{\frac{1}{2}}}$$

Let $\Delta p = 40$ psi

$$u = \left[\frac{40 \times 32.2 \times 0.0869 \times 144}{2 \times 4 \times 68 \times 12}\right]^{\frac{1}{2}} \frac{1}{f^{\frac{1}{2}}}$$

$$= \frac{1.57}{f^{\frac{1}{2}}}$$

Assume $u = 21.0$ ft/sec.

$$Re = \frac{D_e u \rho}{\mu}$$

$$= \frac{0.0869 \times 68 \times 3600}{12 \times 1.14}\ u$$

$$= 1555\ u$$

Therefore $Re = 1555 \times 21.0$

$$= 32{,}600$$

For which $f = 0.0058$

The value of f is now used to determine the corresponding velocity.

$$u = \frac{1.57}{f^{\frac{1}{2}}}$$

$$= \frac{1.57}{(0.0058)^{\frac{1}{2}}}$$

$$= 20.6 \text{ ft/sec.}$$

This corresponds favorably with the assumed value. Hence the flow velocity through the core for a 40 psi pressure drop will be about 21 ft/sec.

Volume Flow Rate of D_2O Through Core

$$V_c = (\text{Area})(\text{velocity})$$

$$= 3.58\ ft^2 \times 21\ \frac{ft}{sec} \times \frac{60\ sec}{min} \times 7.48\ \frac{gal}{ft^3}$$

$$= 33{,}800\ gpm$$

$$= 1.92 \times 10^7\ \frac{lbs}{hr}$$

Average D_2O Temperature Change Through Core

$$\Delta T = T_2 - 120 = \frac{q}{W\ C_p}$$

$T_2 \equiv$ core outlet D_2O temperature

$120°F \equiv$ core inlet D_2O temperature

$q = 500 \times 10^6 \times 0.95$ watts

$W = 1.92 \times 10^7$ lbs/hr

$C_p = 1$ BTU/lb-°F

$$\Delta T = \frac{500 \times 10^6 \times 0.95 \times 3.413}{1.92 \times 10^7 \times 1}$$

$$= 84.5°F$$

$$T_2 = \Delta T + 120$$

$$= 84.5 + 120$$

$$= 204.5°F$$

b. Fast Reflector Region

Flow area of fast reflector = 2(reflector area per slab)(water: metal ratio)

$$= (2)(60 \times 180\ cm^2)\ \frac{1}{(2.54)^2(144)}\ (0.3)$$

$$= 6.98\ ft^2$$

Volume Flow Rate of D_2O Through Fast Reflector

It will be assumed that the coolant flow in the fast reflector can be orificed to provide a control over both the distribution and the quantity of coolant. If this is the case, the outlet temperature of the coolant can be fixed. Most efficient use will be made of the coolant when it is allowed to accrue a substantial temperature rise since this is the condition that will necessitate pumping the least volume. If it is assumed that the fast reflector outlet coolant temperature is 170°F (50°F rise) and that 5% of the reactor heat is released in the reflector,

$$W = \frac{q}{C_p \, \Delta T}$$

$$= \frac{500 \times 10^6 \times 0.05 \times 3.413}{1 \times 50}$$

$$= 1.71 \times 10^6 \text{ lbs/hr}$$

$$= 3100 \text{ gpm}$$

c. Reactor Tank Region:

The total D_2O flow rate through the reactor tank is:

D_2O circulating through core	=	33,800 gpm
D_2O circulating through fast reflector	=	3,100 gpm
Total D_2O circulating rate	=	36,900 gpm
	=	2.04×10^7 lbs/hr

Average Temperature of D_2O Leaving Reactor Tank

$$\Delta T = T_2 - 120 = \frac{q}{W \, C_p}$$

$$T_2 = \frac{q}{W \, C_p} + 120$$

$$= \frac{500 \times 10^6 \times 3.413}{2.04 \times 10^7 \times 1} + 120$$

$$= 203°F$$

3. Heat Transfer Coefficients:

a. Film Transfer Coefficient, h, for D_2O:

$$\frac{hD_e}{k} = 0.023 \left(\frac{D_e u \rho}{\mu}\right)^{0.8} \left(\frac{C_p \mu}{k}\right)^{0.4}$$

$$h = 0.023 \frac{k}{D_e} \left(\frac{D_e u \rho}{\mu}\right)^{0.8} \left(\frac{C_p \mu}{k}\right)^{0.4}$$

$k = 0.38$ BTU-ft/hr-ft^2-°F

$D_e = 0.0869$ in

$\rho = 68$ lb/ft^3

$\mu = 1.14$ lb/ft-hr

$C_p = 1$ BTU/lb-°F

$u = 21$ ft/sec

$$h = \frac{(0.023)(38)(12)}{0.0869} \left[\frac{(0.0869)(21)(3600)(68)}{(12)(1.14)}\right]^{0.8} \left[\frac{(1.0)(1.14)}{0.38}\right]^{0.4}$$

$h = 7750$ BTU/hr-ft^2-°F

b. Fuel Plate Wall Transfer Coefficient, h_w:

Assume no temperature drop across fuel alloy - aluminum clad interface.

$$h_w = \frac{k_{Al}}{\frac{t_{avg}}{2}}$$

$$k_{Al} = 118 \frac{\text{BTU-ft}}{\text{hr-ft}^2\text{-°F}}$$

$$\frac{t_{avg}}{2} = \frac{1}{2}(\text{fuel plate thickness}) = 0.015 \text{ in}$$

$$h_w = \frac{118 \times 12}{0.015}$$

$$= 94{,}400 \frac{\text{BTU}}{\text{hr-ft}^2\text{-°F}}$$

c. Overall Heat Transfer Coefficient, U:

$$U = \frac{1}{\frac{1}{h} + \frac{1}{h_w}}$$

$$= \frac{1}{\frac{1}{7750} + \frac{1}{94{,}400}}$$

$$= 7150 \text{ BTU/hr-ft}^2\text{-}^\circ\text{F}$$

$$= 7.69 \text{ BTU/hr-cm}^2\text{-}^\circ\text{F}$$

4. Fuel Plate Temperatures:

These calculations are intended to determine the maximum fuel plate centerline and surface temperatures that will result during steady state operation at design power. Assumptions, necessary to facilitate the calculations, are made with the thought in mind of yielding a conservative estimate.

The approach will be to take the unit volume of reactor containing the maximum power density in the y- and z-directions but following the fission rate distribution in the x-direction and consider a fuel plate as producing heat accordingly throughout its entire volume. The heat will be assumed to leave the fuel plate by conduction only through the 0.010-inch aluminum clad into the D_2O coolant channel and not to have any lateral or longitudinal flow in the plate. A sketch of the fuel plate and D_2O channel is shown in Figure 56.

If a thin strip of the curved fuel plate is considered, the heat transfer problem can be reduced to that of a flat, thin plate generating heat uniformly at its center. It will later be shown that the temperature drop from the centerline of the plate to its surface is approximately 8°F, and hence the assumption that all heat is generated at the center seems to be valid. With these assumptions the fuel plate will have a temperature distribution that follows the maximum fission rate in the x-direction, and the rate of change of temperature will be zero at the center of the fuel plate and the center of the D_2O channel. That is

$$\frac{\partial T}{\partial x} = \left.\frac{\partial T}{\partial y}\right|_{y=0} = \left.\frac{\partial T}{\partial y}\right|_{y=\frac{1}{2}(t_p+t_c)} = 0 \quad .$$

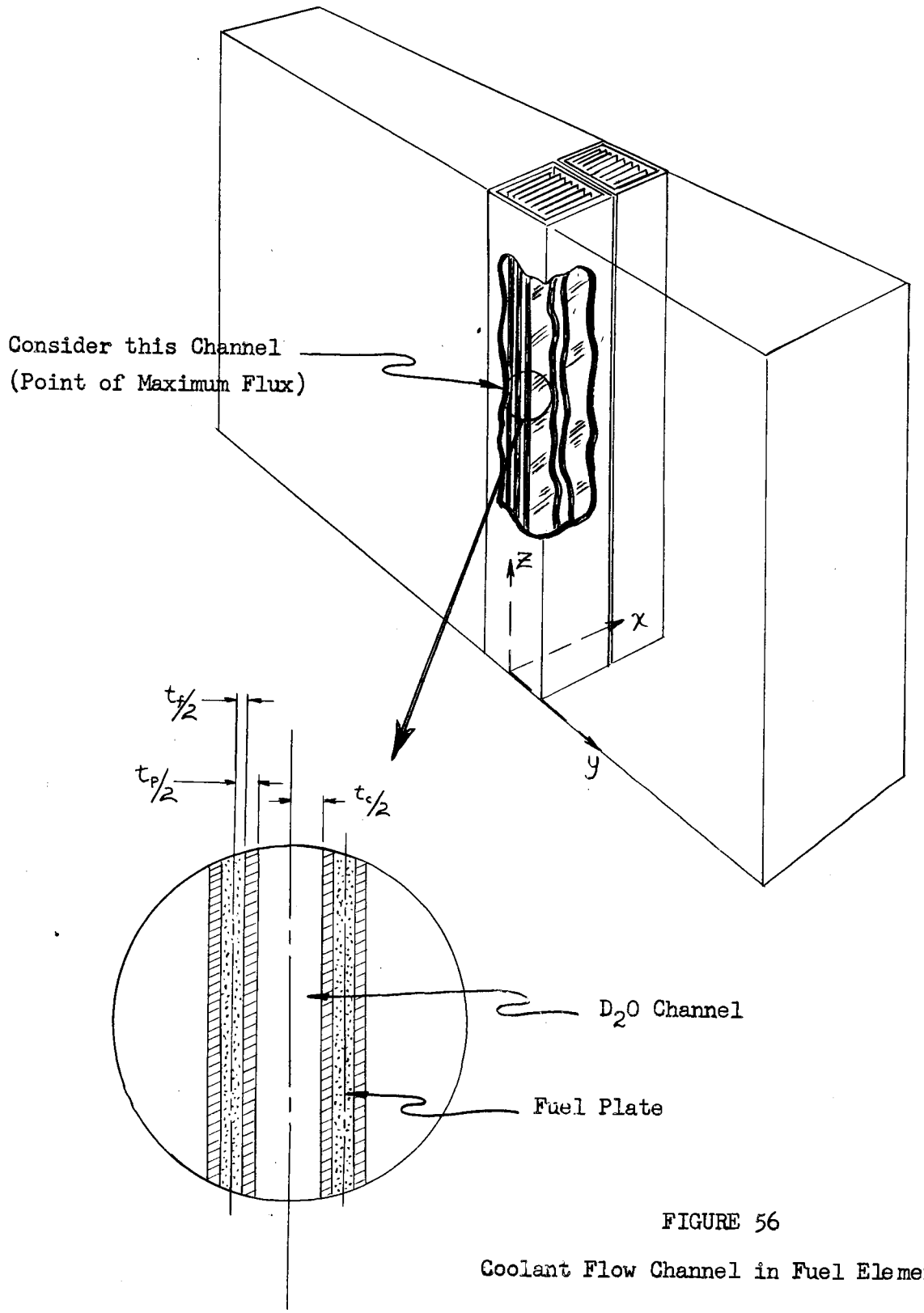

FIGURE 56

Coolant Flow Channel in Fuel Element

At steady state,

$$Q_P = Q_R = \Delta Q_c \quad . \qquad \text{F-1}$$

where $Q_P \equiv$ number of BTU/hr produced by fission in the plate

$Q_R \equiv$ number of BTU/hr removed from the plate

$\Delta Q_c \equiv$ number of BTU/hr absorbed by the coolant

Let $dQ_P = q_P dA$ F-2

$dQ_R = q_R dA = U \Delta T_P(z)\, dA$ F-3

$\Delta Q_c = q_c = WC_P \Delta T_c(z) = \rho v A_{D_2O} C_P \Delta T_c(z)$ F-4

where $dA = Wdz \equiv$ differential area of heat transfer

$W \equiv$ width of fuel plate

$dz \equiv$ height of dA

$q_P \equiv$ number of BTU/hr-ft^2 of heat transfer area produced by fission in the plate. (assumed constant)

$q_R \equiv$ number of BTU/hr-ft^2 of heat transfer area removed from the plate. (assumed constant)

$U \equiv$ overall heat transfer coefficient, $\frac{\text{BTU}}{\text{hr-ft}^2\text{-}^\circ\text{F}}$

$\Delta T(z) \equiv$ temperature difference between the centerline temperature of the plate, T_P, and the mean temperature of the coolant, T_c, at any particular height, z.

$q_c \equiv$ number of BTU/hr-ft^2 of coolant channel per °F absorbed by the coolant

$A_{D_2O} \equiv$ area of the coolant channel $= W \frac{t_c}{2}$

$\Delta T_c(z) \equiv$ temperature difference between the coolant at height $z \neq 0$, (T_c); and the coolant at height $z = 0$, (T_o).

$w \equiv$ mass flow rate of D_2O coolant

$\rho \equiv$ density of D_2O coolant

$C_P \equiv$ specific heat of D_2O at constant pressure; assumed constant with temperature change.

$v \equiv$ velocity of D_2O in the channel

From equation F-2

$$dQ_P = q_P W dz \qquad \text{F-5}$$

$$dQ_R = UW(T_P - T_c)_z \, dz \qquad \text{F-6}$$

$$\Delta Q_c = WC_P(T_c - T_o) \qquad \text{F-7}$$

From equations F-5, F-6 and F-7,

$$Q_P(z) = q_P W \int_0^z dz \qquad \text{F-8}$$

$$Q_R(z) = UW \int_0^z \left[T_P(z) - T_c(z) \right] dz \qquad \text{F-9}$$

$$\Delta Q_c(z) = wC_P \left[T_c(z) - T_o \right] \qquad \text{F-10}$$

For steady state conditions at any value of z,

$$Q_P(z) = Q_R(z) = \Delta Q_c$$

a. <u>Maximum Mixed Mean Temperature of Coolant at Core Outlet $(T_c)_{max}$:</u>

Equating the heat produced to the heat absorbed by the coolant, there obtains

$$Q_P(z) = \Delta Q_c \qquad \text{F-11}$$

$$\int_0^x Q_P(x)\, dx \int_0^z dz = wC_P \left[T_c(z) - T_o \right] \qquad \text{F-12}$$

Solving for $T_c(z)$,

$$T_c(z) = \frac{z \int_0^x q_P(x)\, dx}{w\, C_P} + T_o \qquad \text{F-13}$$

$T_c(z)$ is a maximum when z is a maximum.

T_o = 120°F = temperature of inlet coolant.

From Figure 54,

$$q_P = \omega \left[\Sigma_f \Phi(x) \right]_{homo} = \frac{\left[480\, e^{-0.22x} + 150 \right] (10^{11})}{3.1 \times 10^{10}}$$

Also

$$\left[q_P(x) \right]_{het} = \omega \frac{\left[\Sigma_f \Phi(x) \right]_{het}}{A_{het}} V_{het} \quad .$$

However it is known that for a given reactor power level the total fissions in the homogeneous case must equal the total fissions for the heterogeneous case.

$$\left[\Sigma_f\Phi(x)\right]_{het} dx = \left[\Sigma_f\Phi(x)\right]_{homo} \frac{V_{homo}}{V_{het}} dx$$

Therefore,

$$\int_0^x \left[q_P(x)\right]_{het} dx = \frac{\omega V_{het}}{A_{het}} \int_0^{x=(3.541)(2.54)} \left[\Sigma_f\Phi(x)\right]_{homo} \frac{V_{homo}}{V_{het}} dx$$

$$= \frac{\omega V_{homo}}{V_{het}} \int_0^{x=(3.541)(2.54)} \left[480\, e^{-0.22x} + 150\right] (10^{11})\, dx$$

$$= \frac{864{,}000 \times 10^{11}}{(3.1\times10^{10})(7.15\times10^{6})} \left[-\frac{480}{0.22} e^{-1.98} + (150)(3.541)(2.54) + \frac{480}{0.22}\right]$$

$$= 1255 \text{ watts/cm}$$

Equation F-13 becomes

$$T_c(z)_{max} = \frac{1255\, z_{max}}{\dot{W}\, C_P} + 120$$

$$= \frac{(1255)(120)(3.413)}{1.92 \times 10^{7} \times \frac{1}{36} \times \frac{1}{92} \times \frac{1}{2}} + 120$$

$$= 172 + 120$$

$$= 292°F$$ = maximum mixed mean temperature of D_2O at core outlet with $(q_P)_{x,y_{max}}$, z_{max}

If

$$\int_0^{x=(3.541)(2.54)} q_P(x)\, dx = (q_P)_{max\ x,y,z}\, W$$, i.e., the fission rate is a maximum and constant in the x-direction, then

$$T_c(z)_{max} = \frac{(q_P)_{max\ x,y,z}\ W\ z_{max}}{w\ C_P} + T_o$$

$$= \frac{\left(775{,}000\ \frac{BTU}{hr\text{-}ft^2}\right)(3.541x47.3\ in^2)\left(\frac{ft^2}{144in^2}\right)}{\left(1.92x10^7\ \frac{lb}{hr}x\frac{1}{36}x\frac{1}{92}x\frac{1}{2}\right)\left(1\frac{BTU}{lb\ ^\circ F}\right)} + 120$$

$$= 310 + 120$$

$$= 430^\circ F$$ = maximum mixed mean temperature of D_2O at core outlet with $(q_P)_{max\ x,y,z}$

b. Maximum Centerline Temperature, $T_{P_{max}}$, of Fuel Plate:

By equating the heat removed to that absorbed by the coolant, there results

$$Q_R(z) = \Delta Q_c(z)$$

$$U W \int_0^z \left[T_P(x,z) - T_c(x,z)\right] dz = wC_P\left[T_c(z) - T_o\right] \qquad \text{F-14}$$

By using equation F-12,

$$U\int_0^x dx \int_0^z \left[T_P(x,z) - T_c(x,z)\right] dz = \int_0^x q_P(x)\ dx \int_0^z dx$$

$$U\int_0^x \left[T_P(x,z) - T_c(x,z)\right] dx = \int_0^x q_P(x)\ dx$$

$$U\left[T_P(x,z) - T_c(x,z)\right] = q_P(x)$$

$$T_P(x,z) = \frac{q_P(x)}{U} + T_c(x,z)$$

$$= \frac{q_P(x)}{U} + \frac{zq_P(x)}{W(x)\ C_p} + T_o$$

$$= q_P(x)\left[\frac{1}{U} + \frac{z}{W(x)\ C_p}\right] + T_o \qquad \text{F-15}$$

Now $T_P(x,z)$ is a maximum when $x = 0$ and $z = 120$ cm. Consider a unit cell at $x = 0$, Δx in width, then

$$T_P(0, 120) = q_{P_{net}}(0) \left[\frac{1}{U} + \frac{120}{\frac{\dot{w}(\Delta x)\ C_p}{(3.541)(2.54)}} \right] + T_o$$

$$T_P(0, 120) \doteq \left(\frac{864{,}000}{7.15 \times 10^6} \right) (3.413) \left[\frac{480\ e^{-0.22(0)} + 150}{3.1 \times 10^{10}} \right] (10^{11}) \left[\frac{1}{7.69} + \frac{120}{322} \right] + 120$$

$$= 421 - 120$$

$$= 541°F = \text{maximum centerline temperature of hottest fuel plate}$$

Note that

$$U = 7150\ \text{BTU/hr-ft}^2\text{-°F}$$

$$= 7.69\ \text{BTU/hr-cm}^2\text{-°F}$$

$$\frac{\dot{w}(\Delta x)\ C_p}{(3.541)(2.54)} = \frac{1.92 \times 10^7 \times \frac{1}{36} \times \frac{1}{92} \times \frac{1}{2}}{(3.541)(2.54)}$$

$$= 322$$

c. Maximum Surface Temperature of Fuel Plate:

$T_P(x,z) - T_s(x,z)$ = Temperature difference between the centerline of fuel plate and its surface at any point (x,z) in the y-direction

$$\int_0^x q_P(x,z)\ dxdz = -k \int_0^x dA \frac{\partial T(x,z)}{\partial y} = -k \int_0^x dxdz \frac{\partial T(x,z)}{\partial y}$$

$$q_P(x,z) = \frac{k}{y} \left[T_P(x,z) - T_s(x,z) \right]$$

$\frac{\partial T(x,z)}{\partial y}$ is over a small increment and will be considered linear in y.

$$T_s(x,z) = -\frac{y}{k}\ q_P(x,z) + T_P(x,z) \qquad \text{F-16}$$

where

$$\frac{y}{k} = \frac{1}{h_w} = \frac{1}{94{,}400 \text{ BTU/hr-ft}^2\text{-}^\circ\text{F}}$$

But

$$T_{s_{max}}(x,z) = T_{s_{max}}(0, 120)$$

Also $y = 0.015$ in (half thickness of plate)

$$k = 118 \frac{\text{BTU-ft}}{\text{hr ft}^2\,^\circ\text{F}}$$

$$T_s(0, 120) = -\frac{1}{h_w} q_p(0, 120) + T_p(0, 120)$$

From Appendix F, Section 1d,

$$q_p(0, 120) = 775{,}000 \text{ BTU/hr-ft}^2$$

and from Appendix F, Section 4b,

$$T_p(0, 120) = 541^\circ\text{F}.$$

$$T_{s_{max}}(0, 120) = -\frac{775{,}000}{94{,}400} + 541$$

$$= -8.2 + 541$$

$$\cong 532.8^\circ\text{F}$$

If the average value of flux is used instead of the maximum in the z-direction, then

$$q_p(0, 120) = \frac{775{,}000}{1.2} = 646{,}000 \frac{\text{BTU}}{\text{hr ft}^2}$$

and

$$T_{s_{max}}(x,z) = q_p(x,z) \left[\frac{1}{U} + \frac{z}{\dot{w}(\Delta x)\ C_p} - \frac{1}{h_w}\right] + T_o$$

$$T_{s_{max}}(0, 120) = 646{,}000 \left[\frac{1}{7150} + \frac{3.94}{9800} - \frac{1}{94{,}400}\right] + 120$$

$$= 90.4 + 260 - 6.84 + 120$$

$$= 464^\circ\text{F}$$

This temperature corresponds to a saturation pressure of 490 psi.

Note that $z = 47.3 \text{ in} \times \frac{1}{12} = 3.94 \text{ ft}$

and $$W(\Delta x)\ C_p = \frac{1.92 \times 10^7 \times \frac{1}{36} \times \frac{1}{92} \quad \frac{1}{2}}{3.541 \times \frac{1}{12}}$$

$$= 9800$$

The value of $T_{s_{max}}(0, 120) = 464°F$ represents the maximum fuel plate surface temperature for a maximum power density in the x- and y-directions and

$$\left[47.3 \text{ in}\right] \left[\Sigma_f \Phi(z)\right] = \int_0^{47.3} \left[\Sigma_f \Phi(z)\right] dz$$

for the z-direction. It neglects any heat removed from the hot spot by conduction in the aluminum.

APPENDIX G

EXTERNAL CIRCUIT CALCULATIONS

1. Pressure Drop Calculations For External Circuit:

The following calculations are an estimate of the pressure drop through the external D_2O circulation system.

a. Pipe diameter:

Volume of D_2O per sec = pipe area x flow rate

$$V = Av$$

$$= \pi r^2 v$$

$$r = \left[\frac{V}{\pi v}\right]^{\frac{1}{2}}$$

$$V = 33{,}800 \text{ gal/min}$$

Assume $v = 10$ ft/sec = D_2O velocity in pipe

$$r = \left[\frac{33{,}800 \frac{\text{gal}}{\text{min}} \times 231 \frac{\text{in}^3}{\text{gal}}}{\pi \times 10 \frac{\text{ft}}{\text{sec}} \times 60 \frac{\text{sec}}{\text{min}} \times 1728 \frac{\text{in}^3}{\text{ft}^3}}\right]^{\frac{1}{2}} = 1.55 \text{ ft}$$

b. Pressure drop through pipe:

$$\Delta p = 2f \frac{u^2 L \rho}{144\, g_c\, D}, \text{ psi}$$

$$Re = \frac{Du\rho}{\mu}$$

$$u = 10 \text{ ft/sec}$$

$$D = 68 \text{ lb/ft}^3$$

$$\mu = 1.60 \frac{\text{lbs}}{\text{ft-hr}} \text{ at } 120°F$$

$$\mu = 0.66 \frac{\text{lbs}}{\text{ft-hr}} \text{ at } 240°F$$

$$Re_{120°F} = \frac{10 \frac{\text{ft}}{\text{sec}} \times 3.1 \text{ ft} \times 68 \frac{\text{lbs}}{\text{ft}^3} \times 3600 \frac{\text{sec}}{\text{hr}}}{1.60 \frac{\text{lbs}}{\text{ft-hr}}} = 4.74 \times 10^6$$

For this Re, $f_{120} = 0.0023$.

$$Re_{240°F} = \frac{10 \frac{\text{ft}}{\text{sec}} \times 3.1 \text{ ft} \times 68 \frac{\text{lbs}}{\text{ft}^3} \times 3600 \frac{\text{sec}}{\text{hr}}}{0.66 \frac{\text{lbs}}{\text{ft-hr}}} = 1.15 \times 10^7$$

For this Re, $f_{240} = 0.002$.

The length of pipe in the external circulation system will not be known until a complete design has been made. However, for purposes of this calculation, assume there is 100 feet of pipe. The temperature effect - as shown by the fact that $f_{120} \cong f_{240}$ - is small.

$$\Delta p = \frac{(2)(0.0023)(10)^2(100)(68)}{(32.2)(3.1)(144)} = 0.217 \text{ psi}$$

2. Heat Exchanger Calculations:

Before the total pressure drop through the external system can be calculated, the geometry of the heat exchanger must be known. This entails a calculation to determine the number and length of tubes.

a. Heat Transfer coefficient inside tubes:

$$\frac{hD}{k} = 0.023\left(\frac{Du\rho}{\mu}\right)^{0.8}\left(\frac{C_p\mu}{k}\right)^{0.4}$$

velocity = v = 10 ft/sec (assumed)

density = ρ = 68 lb/ft^3

viscosity = μ = 1.21 lb/ft-hr at 150°F

heat capacity = C_p = 1.0 BTU/lb-°F

thermal conductivity = k = $0.38 \frac{\text{BTU-ft}}{\text{hr-ft}^2\text{-°F}}$

diameter = D = 0.5 in = 0.0416 ft (assumed for inside diameter of tubes)

Flow area per tube = $\pi r^2 = \pi\left[\frac{0.5}{2}\right]^2$

= 0.196 in^2

For a flow rate of 33,800 gal/min at a velocity of 10 ft/sec the heat exchanger must have a cross section equivalent to that of the large conduit.

Area of large conduit = $\pi r^2 = \pi(1.55)^2$ = 7.55 ft^2

= 1090 in^2

Cross section area of heat exchanger = (No. tubes) (area per tube)

$$\text{No. tubes} = \frac{1090 \text{ in}^2}{0.196 \text{ in}^2} = 5500$$

$$h = \left(\frac{k}{D}\right)(0.023)\left(\frac{Du\rho}{\mu}\right)^{0.8}\left(\frac{C_p\mu}{k}\right)^{0.4}$$

$$= \frac{(0.38)(0.023)}{(0.0416)}\left[\frac{10 \times 3600 \times 0.0416 \times 68}{(1.21)}\right]^{0.8}\left[\frac{1 \times 1.21}{0.38}\right]^{0.4}$$

$$= (0.210)\,(8.42 \times 10^4)^{0.8}\,(3.18)^{0.4}$$

$$= 2910 \text{ BTU/hr ft}^2\ ^\circ\text{F}$$

b. Heat Transfer Coefficient Outside Tubes:

Assume outside diameter of tubes is 5/8 inch. Use correlation of McAdams[13], page 276, Figure 10-20.

$$X = \frac{D_o\, G_{max}}{\mu_f} = \frac{D_o\, u_{max}\, \rho}{\mu_f}$$

D_o = 0.625 in. = 0.0521 ft

u_{max} = 1 ft/sec (assumed)

ρ = 62.4 lb/ft^3

μ_f = 1.9 lb/ft-hr at 80°F

$$X = \frac{(0.625)\,(1)\,(62.4)\,(3600)}{(12)\,(1.9)} = 6150$$

From the plot on Figure 10-20,

$$\left(\frac{h_o D_o}{k_b}\right)\left(\frac{C_p\mu}{k}\right)_b^{-1/3}\left(\frac{\mu_s}{\mu_b}\right)^{0.14} = 60$$

$$h_o = \frac{(60)\left(\frac{C_p\mu}{k}\right)_b^{1/3}}{\left(\frac{D_o}{k_b}\right)\left(\frac{\mu_s}{\mu_b}\right)^{0.14}}$$

$$= \frac{(60)\left(\frac{1 \times 2.08}{0.38}\right)^{1/3}}{\left(\frac{0.521}{0.38}\right)\left(\frac{1.14}{2.08}\right)^{0.14}}$$

$$= 8.9 \text{ BTU/hr-ft}^2\text{-}^\circ\text{F}$$

c. Overall Heat Transfer Coefficient:

$$U = \frac{1}{\frac{1}{h} + \frac{x}{k_w} + \frac{1}{h_o} + \frac{1}{h_d}}$$

Assume a fouling factor such that $h_d = 1000 \frac{BTU}{hr\text{-}ft^2\text{-}°F}$

$$U = \frac{1}{\frac{1}{2910} + \frac{1/16}{12 \times 25} + \frac{1}{819} + \frac{1}{1000}}$$

$$= 360 \text{ BTU/hr-ft}^2\text{-°F}$$

3. Pressure Drop Across Heat Exchanger:

$$\Delta p = \frac{2f\, u^2\, L\, \rho}{144 g_c D} \quad \text{, psi}$$

The length, L, of the tubes in the heat exchanger is not known. This can be found by equating the heat production rate in the reactor to the rate at which heat is transferred to the cooling water. That is

$$q = U\, A\, \Delta T_L$$

A = total area of heat exchanger

= (area per foot) (length)

$= a\, L$

a = (mean area per tube per foot) (no. tubes)

$= (\pi D)(1)(5500)$

$= \pi\left(\frac{D_o + D_i}{2}\right)(5500)$

$= \left(\frac{\pi}{12}\right)\left(\frac{9}{16}\right)(5500)$

$= 816 \text{ ft}^2/\text{ft}$

$$A = a\, L = \frac{q}{U\, \Delta T_L}$$

$$L = \frac{q}{a\, U\, \Delta T_L}$$

$$\Delta T_L = \text{log mean temperature difference} = \frac{\left(T'_{D_2O} - T''_{H_2O}\right) - \left(T''_{D_2O} - T'_{H_2O}\right)}{\ln \dfrac{T'_{D_2O} - T''_{H_2O}}{T''_{D_2O} - T'_{H_2O}}}$$

where the several "T's" are defined by the following figure.

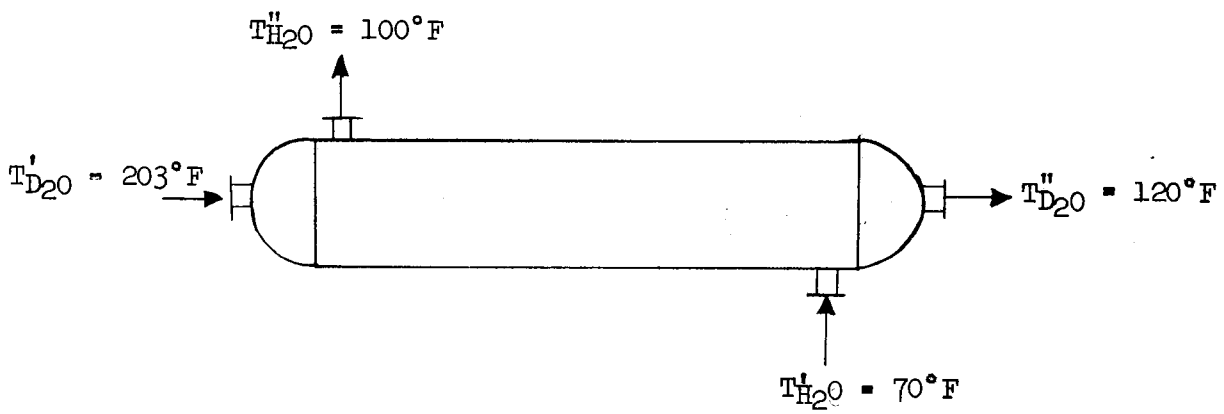

FIGURE 57

Temperature Identification for Heat Exchanger

$$\Delta T_L = \frac{(203-100) - (120-70)}{\ln \dfrac{203 - 100}{120 - 70}} = \frac{73}{\ln 3.43} = 59.2°F$$

$$L = \frac{500 \times 10^6 \times 3.413}{(816)(360)(59.2)} = 98.5 \text{ ft}$$

The exceptionally long length of this exchanger suggests that the chosen design parameters were not optimum. A more complete design would involve changing such parameters as fluid velocity in the tubes and the tube size to obtain a more

favorable geometry. In all probability such an exchanger would not be installed as a single unit but rather as two or more parallel exchangers.

For purposes of illustration, pressure drop calculations will be made on the above unit.

$$Re = \frac{Du\rho}{\mu} = \frac{(0.046)(10)(68)(3600)}{1.21} = 84,200$$

For this Re, f = 0.0047

$$\Delta p = \frac{(2)(0.0047)(10)^2(98.5)(68)}{(144)(32.2)(0.046)}$$

$$= 29.5 \text{ psi}$$

4. Total System Pressure Drop:

$$\Delta P_{total} = \Delta P_{reactor} + \Delta P_{pipe} + \Delta P_{exchanger}$$

$$= 40 + 0.217 + 29.5$$

$$= 69.7 \text{ psi}$$

5. Pumping Requirements:

Flow rate = 36,900 gal/min = 2.04×10^7 lb/hr

Work done = (mass flow rate) (head)

$$= (2.04 \times 10^7) \frac{(69.7 \times 144)}{68} \frac{1}{3600}$$

$$= 8.38 \times 10^5 \frac{\text{ft-lb}}{\text{sec}}$$

= 1524 horsepower

6. Cooling Water Requirements:

$$q = wC_p\Delta T$$

$$w = \frac{q}{C_p\Delta T} = \frac{500 \times 10^6 \times 3.413}{(1)(100 - 70)}$$

$$= 5.68 \times 10^7 \text{ lb/hr}$$

= 113,700 gal/min

APPENDIX H

Analysis of MTR plate-type element to determine the temperature distribution:

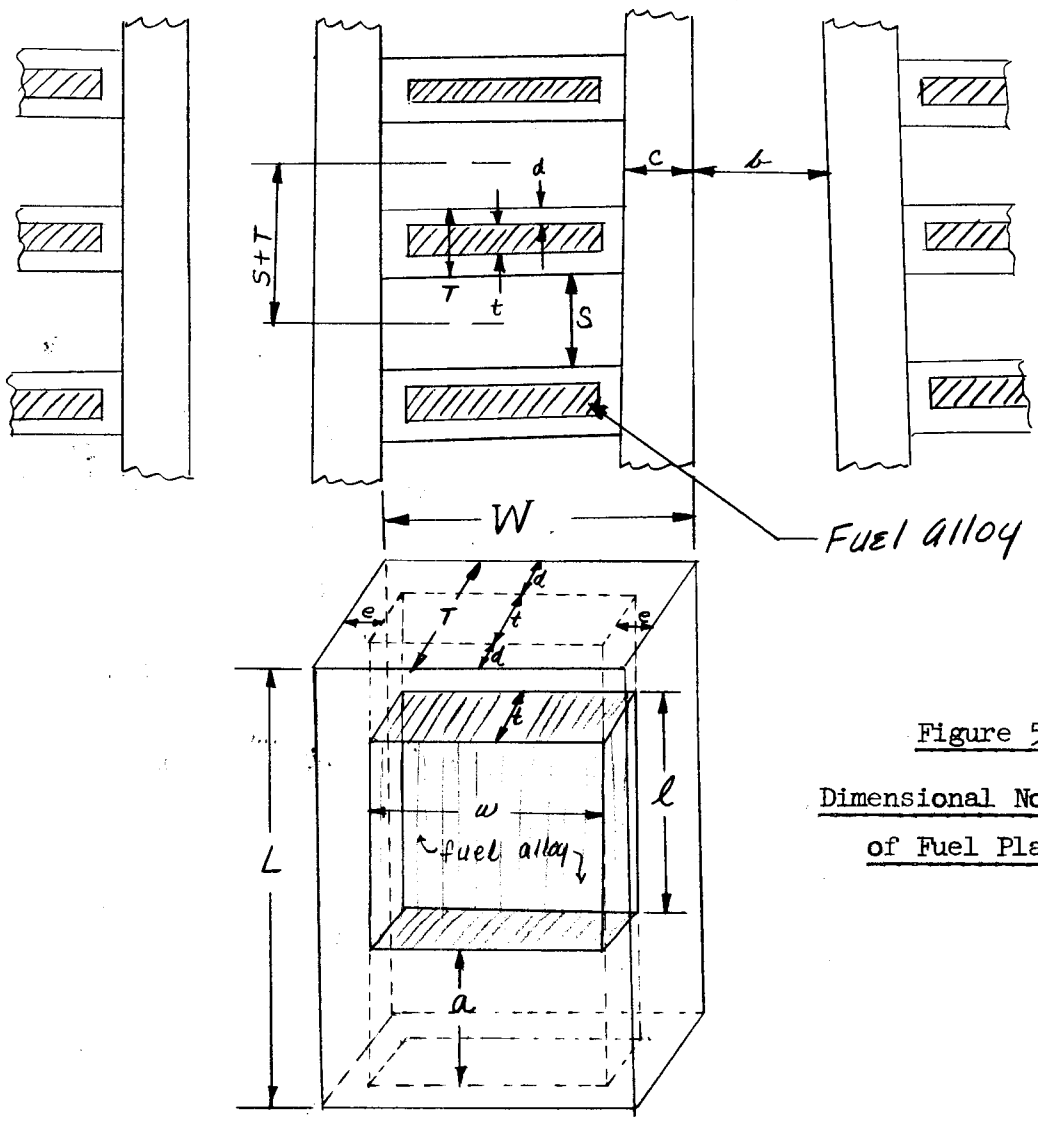

Figure 58

Dimensional Notation of Fuel Plate

$T = t + 2d$; $L = \ell + 2a$; $W = w + 2e$; $V_{fuel} = tw\ell$

$V_{A\ell\ clad} = TWL = tw\ell + 2(s+t)\ cL$

$V_{D_2O} = SWL + b(S+T)\ L$

$A_{D_2O} = SW + b(S+T)$ = cross sectional area of coolant channel

$A_{clad} = 2WL$ = heat transfer area (neglecting end leakage)

$\bar{\rho}_{fuel} = \dfrac{\text{wt. of fuel}}{\text{vol. of unit cell}} = \dfrac{\rho_{fuel}\,(wt\ell)}{(S+T)(W+2c+b)\,L}$ = average ρ of fuel in whole unit cell

$V_{cell} = L(S+T)(W+2c+b)$

x = % U^{235} in fuel alloy by volume

$100 - x$ = % $A\ell$ in fuel alloy by volume

$m_{235} = \rho_{235}\, V_{fuel}\, \dfrac{x}{100}$ where ρ_{235} = ρ of undiluted U^{235}

$\rho^{235}_{fuel} = \dfrac{m_{235}}{V_{fuel}} = \rho_{235}\,\dfrac{x}{100}$ = avg. ρ of fuel in fuel-alloy meat

$$\bar{\rho}_{fuel} = \left(\rho_{235}\right)\left(\frac{x}{100}\right)\frac{wt\ell}{(S+T)(W+2c+b)\,L}$$

<u>Metal-to-Water Ratio</u>

$V_{metal} = V_{fuel} + V_{A\ell\ clad} = tw\ell + TWL - tw\ell + 2(S+T)\,cL = TWL + 2(S+T)\,cL$

$V_{D_2O} = SWL + bL(S+T)$

$$\frac{V_m}{V_{D_2O}} = \frac{TWL + 2(S+T)\,cL}{SWL + bL(S+T)} = \frac{TW + 2c(S+T)}{SW + b(S+T)} = \frac{\text{cross section of metal}}{\text{cross section of water}}$$

$\bar{\Sigma}^{fuel}_f = \sigma^{235}_f\,\bar{N}_{235} = \dfrac{\sigma^{235}_f\ \text{Avog. No.}}{235}\,\bar{\rho}_{fuel}$ = macroscopic fission cross section in homogenized unit cell

$$= \frac{\sigma^{235}_f\ \text{Avog. No.}\ \rho_{235}}{235}\left[\frac{V_{235}}{V_m + V_{D_2O}}\right]$$

$$P_{cell} = \omega\bar{\Sigma}_f\bar{\rho}\bar{\Phi}_T V_{cell} = \left[\frac{\omega\,\sigma_f\ \text{Avog. No.}\ \rho_{235}}{235}\left(\frac{x}{100}\right)\frac{w + \ell}{(S+T)(W+2c+b)\,L}\right]\Big[TWL +$$

$$2(S+T)\,cL + SWL + bL(S+T)\Big]\,\bar{\Phi}_T$$

= cell power

$$\omega = 3.11 \times 10^{-6}\ \frac{\text{BTU/hr-ft}^3}{\text{fission/sec-cm}^3}$$

$$P_{cell} = \frac{\omega\sigma_f \text{ Avog. No.} \rho_{235} x}{23{,}500} \left[\frac{wt\ell}{W + 2c + b}\right] \left[\frac{W(S+T) + 2c(S+T) + b(S+T)}{(S+T)}\right] \bar{\Phi}_T$$

$$P_{cell} = \frac{\omega\sigma_f \text{ Avog. No.} \rho_{235} x}{23{,}500} \left[wt\ell\right] \bar{\Phi}_T$$

$$\mathcal{P}_{cell} = \frac{P_{cell}}{V_{cell}} = \frac{\omega\sigma_f \text{ Avog. No.} \rho_{235} x}{23{,}500} \left[wt\ell\right] \bar{\Phi}_T \left[\frac{1}{(W+2c+b)\ L(S+T)}\right]$$

= Average power density of cell

$$\mathcal{P}_{cell} = \frac{\omega\sigma_f \text{ Avog. No.} \rho_{235} x}{23{,}500} \left[\frac{wt\ell}{L(W+2c+b)\ (S+T)}\right] \bar{\Phi}_T$$

$$\mathcal{P}_{fuel} = \frac{P_{fuel}}{V_{fuel}} = \frac{\omega\sigma_f \rho_{235} x \text{ Avog. No.}}{23{,}500} \bar{\Phi}_T = \frac{\omega\sigma_f \rho_{235} f \text{ Avog. No.}}{235} \bar{\Phi}_T$$

where $\frac{x}{100} \equiv f$

$$\frac{A_{clad}}{V_{fuel}} = \frac{2WL}{twl} \longrightarrow \text{maximum, i.e., maximize e and a and minimize t}$$

$$\frac{n_{fuel}}{V_{fuel}} = \rho_{235} V_{fuel} \frac{x}{100} \left(\frac{1}{V_{fuel}}\right) = \frac{\rho_{235} x}{100} \longrightarrow \text{maximum, i.e., maximize x}$$

Define $N_{A\ell} \equiv$ total aluminum atoms in fuel cell

$$\Sigma_a^{A\ell} = \sigma_a^{A\ell} \frac{N_{A\ell}}{V_{cell}} = \sigma_a^{A\ell} \left[\frac{\text{Avog. No.} \rho_{A\ell}}{27}\right] \left[\frac{V_{A\ell}}{L(S+T)(W+2c+b)}\right] = \sigma_a^{A\ell} \frac{\text{Avog. No.}}{27} \rho_{A\ell} f_{A\ell}$$

where $f_{A\ell} \equiv$ volume fraction of $A\ell$

$$f_{A\ell} = \frac{TWL - twl + 2cL(S+T) + (1 - \frac{x}{100})\ twl}{L(S+T)(W+2c+b)} = \frac{TWL + 2cL(S+T) - \frac{x}{100}\ twl}{L(S+T)(W+2c+b)}$$

$$\Sigma_a^{A\ell} = \frac{\sigma_a^{A\ell} \text{Avog. No.} \rho_{a\ell}}{27} \left[\frac{TWL + 2cL(S+T) - \frac{x}{100}\ twl}{L(S+T)(W+2c+b)}\right] = \frac{\sigma_a^{A\ell} \text{Avog. No.} \rho_{a\ell}}{27} \left[\frac{V_{a\ell}}{V_m + V_{D2O}}\right]$$

$$\Sigma_a^{D2O} = \frac{(2\sigma_a^H + \sigma_a^O)\ \rho_{D2O}}{20} \left[\frac{1}{1 + \frac{V_m}{V_{D2O}}}\right]$$

$$\bar{\Sigma}_a^{235} = \frac{\sigma_a^{235} \text{ Avog. No. } \rho^{235}}{235} \left[\frac{V_{235}}{V_m + V_{D_2O}} \right]$$

$$\bar{\Sigma}_a^{238} = \frac{\sigma_a^{238} \text{ Avog. No. } \rho^{238}}{238} \left[\frac{V_{238}}{V_m + V_{D_2O}} \right]$$

Heat Production and Removal

Figure 59

Temperature Notation

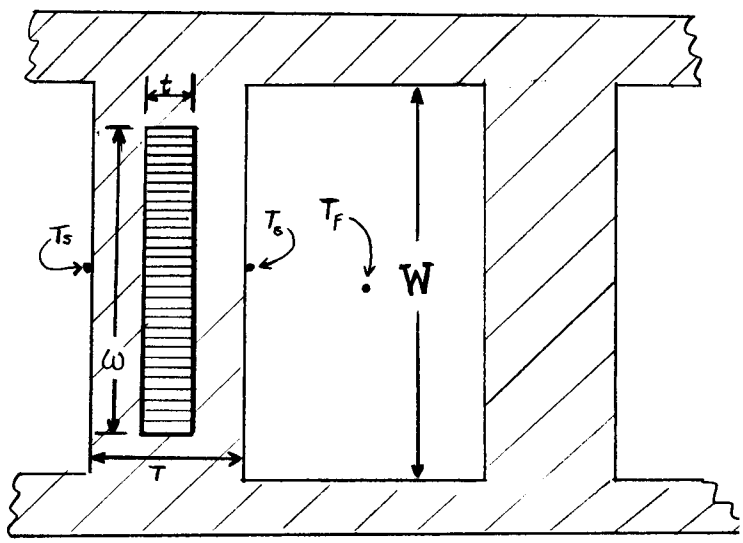

$q_P \equiv \frac{BTU}{hr}$ produced in cell by fission

$= \omega \bar{\Sigma}_f \Phi_T V_{cell}$

$q_R \equiv \frac{BTU}{hr}$ removed from cell

$= U A \Delta T$

where $U = \dfrac{1}{\dfrac{1}{h_{film}} + \dfrac{x}{k_{A\ell}}}$

= conductivity of element BTU/hr-ft^2-°F

A = surface area of cladding = 2WL

$\Delta T = \bar{T}_s - \bar{T}_f$

where $\bar{T}_s$ = mean temperature at outside of cladding

$\bar{T}_f$ = bulk mean temperature of coolant

$$dq_R = U\,dA\,\Delta T = U(2Wdz)(T_s - T_f)_z$$

This assumes no heat flux through ends and edge of element.

$$q_R = \int_{z=0}^{z=L} dq_R = \int_{z=0}^{L} U(2Wdx)\left[T_s(z) - T_f(z)\right]$$

$$= 2WU \int_{z=0}^{L} \left[T_s(z) - T_f(z)\right] dz$$

$$q_P = \int_{z=0}^{L} \omega\Sigma_f^{fuel}\,\Phi_T^{fuel}\,d\,V_{fuel}$$

$$= \int_{z=0}^{L} \omega\Sigma_f^{fuel}\,\Phi_T(z)\,wtdz = \omega\Sigma_f^{fuel}\,wt \int_{z=0}^{L} \Phi_T(z)\,dz$$

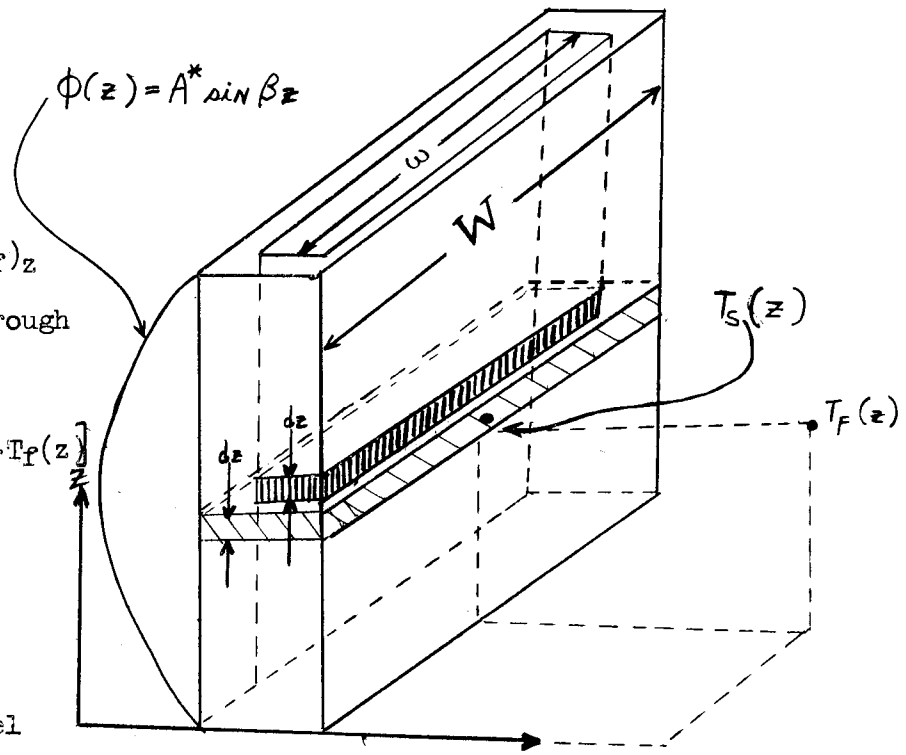

Figure 60

Dimensional Notation

Let $\Phi_T(z) \doteq A^* \sin\beta z$, i.e., assuming a cosine distribution along z-axis

where A^* = constant set by power level

$$\beta \cong \frac{\pi}{L}$$

$$q_P = \omega\Sigma_f^{fuel}\,wt\,A^* \int_{z=0}^{L} \sin\frac{\pi}{L}\,zdz$$

Note that $q_P = q_R = q_f$

where $q_f \equiv$ heat removed from channel by coolant

$$= A_{D_2O}\, \rho_{D_2O}\, v\, C_p \left[T_f(z) - T_f(0)\right]$$

where $A_{D_2O} \equiv$ area of coolant channel

$v \equiv$ coolant velocity

$\rho_{D_2O} \equiv$ mean density of coolant

$q_f = q_P$ at any given z

$$\rho_{D_2O}\, v\, C_p\, A_{D_2O} \left[T_f(z) - T_f(0)\right] = \omega\, \Sigma_f^{fuel}\, wt\, A^* \int_{z=0}^{z} \sin \frac{\pi}{L}\, z dz$$

Define $Q_o = \omega\, \Sigma_f^{fuel}\, wt\, A^*$

$$\rho_{D_2O}\, v\, C_p\, A_{D_2O} \left[T_f(z) - T_f(0)\right] = Q_o \int_{z=0}^{z} \sin \frac{\pi}{L}\, z dz = -Q_o \frac{L}{\pi} \cos \frac{\pi}{L}\, z$$

$$= \frac{Q_o}{\beta} \left[1 - \cos \frac{\pi}{L}\, z\right]$$

where $\beta \equiv \frac{\pi}{L}$

Solving for $\left[T_f(z) - T_f(0)\right]$

$$\boxed{T_f(z) - T_f(0) = \frac{Q_o}{\beta\, \rho_{D_2O}\, v\, C_p\, A_{D_2O}} \left[1 - \cos \frac{\pi}{L}\, z\right]}$$

$T_f(0) \equiv$ inlet temperature of D_2O

By equating the quantities q_R and q_P, there can be obtained an expression for the surface temperature, $T_s(z)$, of the element.

$q_R = q_P$

$$2\, W\, U \int_{z=0}^{z} \left[T_s(z) - T_f(z)\right] dz = Q_o \int_{z=0}^{z} \sin \frac{\pi}{L}\, z dz$$

$$2\,W\,U\left[T_s(z) - T_f(z)\right] = Q_o \sin\frac{\pi}{L} z$$

$$\boxed{T_s(z) - T_f(z) = \frac{Q_o}{2\,W\,U} \sin\frac{\pi}{L} z}$$

The constant, A^*, which appears in the constant Q_o can be obtained as follows:

$$d\,P_{cell} = \omega\,\Sigma_f^{fuel}\,\Phi_T(z)\,d\,V$$

$$P_{cell} = \omega\,\Sigma_f^{fuel} \int_{z=0}^{L} A^* \sin\frac{\pi}{L} z\,wt\,dz$$

$$P_{cell} = 2\omega\,\Sigma_f^{fuel}\,A^*\,wt\,\frac{L}{\pi}$$

$$\boxed{A^* = \frac{\pi\,P_{cell}}{2\,\omega\,\Sigma_f^{fuel}\,wt\,L}}$$

<u>Determining the maximum temperature of surface and the point at which it will occur</u>

$$q_R = 2\,W\,U \int_{z=0}^{L} \left[T_s(z) - T_f(z)\right] dz$$

$$= 2\,W\,U \int_{z=0}^{L} \left[\frac{Q_o}{2\,W\,U} \sin\frac{\pi}{L} z\right] dz = Q_o \int_{z=0}^{L} \sin\frac{\pi}{L} z\,dz$$

$$\boxed{q_R = -\frac{Q_o}{\beta} \cos\frac{\pi}{L} z \Big|_0^L = \frac{2\,Q_o}{\beta}}$$

$$T_s(z) = \frac{Q_o}{2\,W\,U} \sin\frac{\pi}{L} z + \frac{Q_o}{\beta\,\rho_{D_2O}\,v\,C_p\,A_{D_2O}} \left[1 - \cos\frac{\pi}{L} z\right] + T_f(0)$$

$$\boxed{T_s(z) = Q_o \left[\frac{\sin\frac{\pi}{L} z}{2\,W\,U} + \frac{1 - \cos\frac{\pi}{L} z}{\beta\,\rho_{D_2O}\,v\,C_p\,A_{D_2O}}\right] + T_f(0)}$$

$$\frac{dT_s(z)}{dz} = Q_o \left[\frac{(\pi/L) \cos \frac{\pi}{L} z_{max}}{2\,W\,U} + \frac{\frac{\pi}{L} \sin \frac{\pi}{L} z_{max}}{\beta\ \rho_{D_2O}\ v\ C_p\ A_{D_2O}} \right] = 0$$

$$\frac{\frac{\pi}{L} \cos \frac{\pi}{L} z_{max}}{2WU} + \frac{\frac{\pi}{L} \sin \frac{\pi}{L} z_{max}}{\beta\ \rho_{D_2O}\ v\ C_p\ A_{D_2O}} = 0$$

$$\left[\frac{\beta \rho_{D_2O}\ v\ C_p\ A_{D_2O}}{2\,W\,U} \right] \cos \frac{\pi}{L} z_{max} + \sin \frac{\pi}{L} z_{max} = 0$$

Define $\psi \equiv \beta\ \rho_{D_2O}\ v\ C_p\ A_{D_2O}$

$$\frac{\psi}{2WU} \cos \frac{\pi}{L} z_{max} + \sin \frac{\pi}{L} z_{max} = 0$$

$$\tan \frac{\pi}{L} z_{max} = - \frac{\psi}{2\,W\,U}$$

$$\boxed{z_{max} = \frac{L}{\pi} \tan^{-1}\left(-\frac{\psi}{2WU} \right)}$$

$$T_s(z_{max}) - T_f(z_{max}) = \frac{Q_o}{2\,W\,U} \sin \frac{\pi}{L} z_{max}$$

$$T_f(z_{max}) - T_f(o) = \frac{Q_o}{\beta\ \rho_{D_2O}\ v\ C_p\ A_{D_2O}} \left[1 - \cos \frac{\pi}{L} z_{max} \right]$$

$$T_s(z_{max}) - T_f(z_{max}) = T_s(z_{max}) - \left[T_f(z_{max} - T_f(o) + T_f(o) \right]$$

$$T_s(z_{max}) - \left[\frac{Q_o}{\beta\ \rho_{D_2O}\ v\ C_p\ A_{D_2O}} \left\{ 1 - \cos \frac{\pi}{L} z_{max} \right\} - T_f(o) = \frac{Q_o}{2\,W\,U} \sin \frac{\pi}{L} z_{max} \right]$$

$$\boxed{T_s(z_{max}) - T_f(o) = \frac{Q_o}{\beta\ \rho_{D_2O}\ C_p\ v\ A_{D_2O}} \left[1 - \cos \frac{\pi}{L} z_{max} \right] + \frac{Q_o}{2\,W\,U} \sin \frac{\pi}{L} z_{max}}$$

Define $\frac{\pi}{L} z \equiv \alpha$

$$\frac{\pi}{L} z_{max} \equiv \alpha_{max}$$

Then $$\tan \alpha_{max} = \frac{\sin \alpha_{max}}{\cos \alpha_{max}} = - \frac{\beta \rho_{D_2O} v C_p A_{D_2O}}{2 W U} = - \frac{\psi}{2 W U}$$

where $\psi \equiv \beta \rho_{D_2O} v C_p A_{D_2O}$

$$\cos \alpha_{max} = - \frac{2 W U}{\psi} \sin \alpha_{max}$$

$$T_s(z_{max}) - T_f(o) - \frac{Q_o}{\psi} = \frac{Q_o}{2 W U} \sin \alpha_{max} - \frac{Q_o}{\psi} \cos \alpha_{max}$$

$$\left[T_s(z_{max}) - T_f(o) - \frac{Q_o}{\psi} \right] \cos \alpha_{max} = \frac{Q_o}{2 W U} \sin \alpha_{max} \cos \alpha_{max} - \frac{Q_o}{\psi} \cos^2 \alpha_{max}$$

$$\left[T_s(z_{max}) - T_f(o) - \frac{Q_o}{\psi} \right] \cos \alpha_{max} = \frac{Q_o}{2 W U} \sin \alpha_{max} \left(- \frac{2 W U}{\psi} \sin \alpha_{max} \right) - \frac{Q_o}{\psi} \cos^2 \alpha_{max}$$

$$= - \frac{Q_o}{\psi} \left[\sin^2 \alpha_{max} + \cos^2 \alpha_{max} \right]$$

$$= - \frac{Q_o}{\psi}$$

$$\boxed{T_s(z_{max}) - T_f(o) = \frac{Q_o}{\psi} (1 - \sec \alpha_{max})}$$

<u>Temperature distribution along x-axis through fuel element given T_s and T_f</u>

$$dq_P = \omega \Sigma_f^{fuel} wt \, \Phi_T(z) \, dz$$

$$\frac{\partial^2 T_1}{\partial y^2} + \frac{dq_P/dV}{k_{fuel}} = 0$$

$$\frac{\partial^2 T_1}{\partial y^2} + \frac{\omega \Sigma_f^{fuel} wt \Phi_T(z) \, dz/twdz}{k_{fuel}} = 0$$

Let $q''' \equiv \omega \Sigma_f^{fuel} \Phi_T(z)$

$$\frac{\partial^2 T_1}{\partial y^2} - \frac{q'''}{k} = 0 \text{ for } 0 \leq y \leq \frac{t}{2}$$

$$\frac{dT_1}{dy} = - \frac{q''' y}{k_{fuel}} + C_1$$

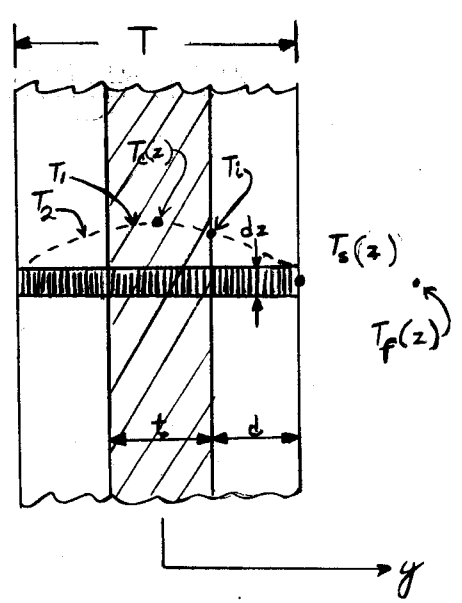

Figure 61

Temperature Distribution in Fuel Plate

$$T_1 = -\frac{q''' y^2}{2k_{fuel}} + C_1 y + C_2$$

At $y = 0$, $\frac{dT_1}{dy} = 0$. Therefore $C_1 = 0$

$$\frac{\partial^2 T_2}{\partial y^2} = 0 \quad \text{for} \quad \frac{t}{2} \leq y \leq \frac{t}{2} + d$$

$$\frac{dT_2}{dy} = C_3$$

$$T_2 = C_3 y + C_4$$

At $y = \frac{t}{2} + d$, $T_2 = T_s$

At $y = \frac{t}{2}$, $T_1 = T_2$

$$C_2 - \frac{q'''(\frac{t}{2})^2}{2k_{fuel}} = C_3 \frac{t}{2} + C_4$$

$$C_2 = \frac{tC_3}{2} + C_4 + \frac{q'''t^2}{8k_{fuel}}$$

$$T_s = C_3(\frac{t}{2} + d) + \left[T_s - C_3(\frac{t}{2} + d)\right] + \frac{q'''t^2}{8k_{fuel}}$$

$$C_2 = -C_3 d + T_s + \frac{q'''t^2}{8k_{fuel}}$$

$$-k_{fuel} A\frac{dT_1}{dy} = -k_{A\ell} A\frac{dT_2}{dy} \quad \text{at} \quad y = \frac{t}{2}$$

$$-k_{fuel}\left[\frac{-q'''\frac{t}{2}}{k_{fuel}}\right] = -k_{A\ell} C_3$$

$$C_3 = -\frac{q'''t}{2k_{A\ell}}$$

$$C_2 = q'''t\left[\frac{t}{8k_{fuel}} + \frac{d}{2k_{A\ell}}\right] + T_s$$

$$C_4 = T_s + \frac{q'''t}{2k_{A\ell}}\left(\frac{t}{2} + d\right)$$

$$T_1(y) = T_s + q'''t\left[\frac{t}{8k_{fuel}} + \frac{d}{2k_{A\ell}}\right] - \frac{4q'''y^2}{8k_{fuel}}$$

$$\boxed{T_1(y) = T_s + q'''\left[\frac{t^2 - 4y^2}{8k_{fuel}} + \frac{td}{2k_{A\ell}}\right]}$$

$$T_2(y) = \frac{-q'''ty}{2\,k_{A\ell}} + T_s + \frac{q'''t}{2k_{A\ell}} \left(\frac{t}{2} + d\right)$$

$$\boxed{T_2(y) = T_s + \frac{q'''t}{2k_{A\ell}} \left[\frac{t}{2} + d - y\right]}$$

<u>Summary</u>

$$\frac{V_m}{V_{D_2O}} = \frac{TW + 2c(S+T)}{SW + b(S+T)}$$

$$\frac{A_{clad}}{V_{fuel}} = \frac{2\,W\,L}{t\,w\,\ell} \longrightarrow \text{maximize for heat transfer}$$

$$\frac{m_{fuel}}{V_{fuel}} = \frac{\rho_{235}\ x}{100} \longrightarrow \text{maximize}$$

$$q_P = 2\omega\,\Sigma_f^{fuel}\ wt\ A^*\ \frac{L}{\pi} \quad , \quad \text{BTU/hr-cell}$$

where it was assumed that

$$\Phi_T(z) = A^* \sin\frac{\pi}{L}\,z = A^* \sin\beta z$$

$$A^* \equiv \text{power level constant}$$

$$\beta \equiv \pi/L$$

$$T_s(z) - T_f(z) = \frac{Q_o}{2\,W\,U} \sin\frac{\pi}{L}\,z$$

where $Q_o \equiv \omega\,\Sigma_f^{fuel}\ A^*\ wt$

$$T_s(z) - T_f(o) = \frac{Q_o}{\psi}\left[1 - \cos\beta z\right]$$

where $\psi \equiv \beta\ \rho_{D_2O}\ v\ C_p\ A_{D_2O}$

$$T_s(z) - T_f(o) = Q_o\left[\frac{\sin\beta z}{2\,W\,U} + \frac{1 - \cos\beta z}{\psi}\right]$$

$$z \text{ for } T_{max} \equiv z_{max} = \frac{1}{\beta}\tan^{-1}\left(-\frac{\psi}{2\,W\,U}\right)$$

$$T_s(z_{max}) - T_f(o) = \frac{Q_o}{\psi}\,(1 - \sec \alpha_{max})$$

where $\alpha_{max} \equiv \tan^{-1}\left(-\frac{\psi}{2WU}\right)$

$$T_{fuel}\,(y,z) = T_s(z) + q'''\left[\frac{t^2 - 4y^2}{8k_{fuel}} + \frac{td}{2k_{A\ell}}\right]$$

$$T_{fuel(max)} = T_{fuel}\,(y=0) = T_s(z_{max}) + q'''\left[\frac{t^2}{8k_{fuel}} + \frac{td}{2k_{A\ell}}\right]$$

$$T_{clad}\,(y,z) = T_s(z) + \frac{q'''t}{2k_{A\ell}}\left[\frac{t}{2} + d - y\right]$$

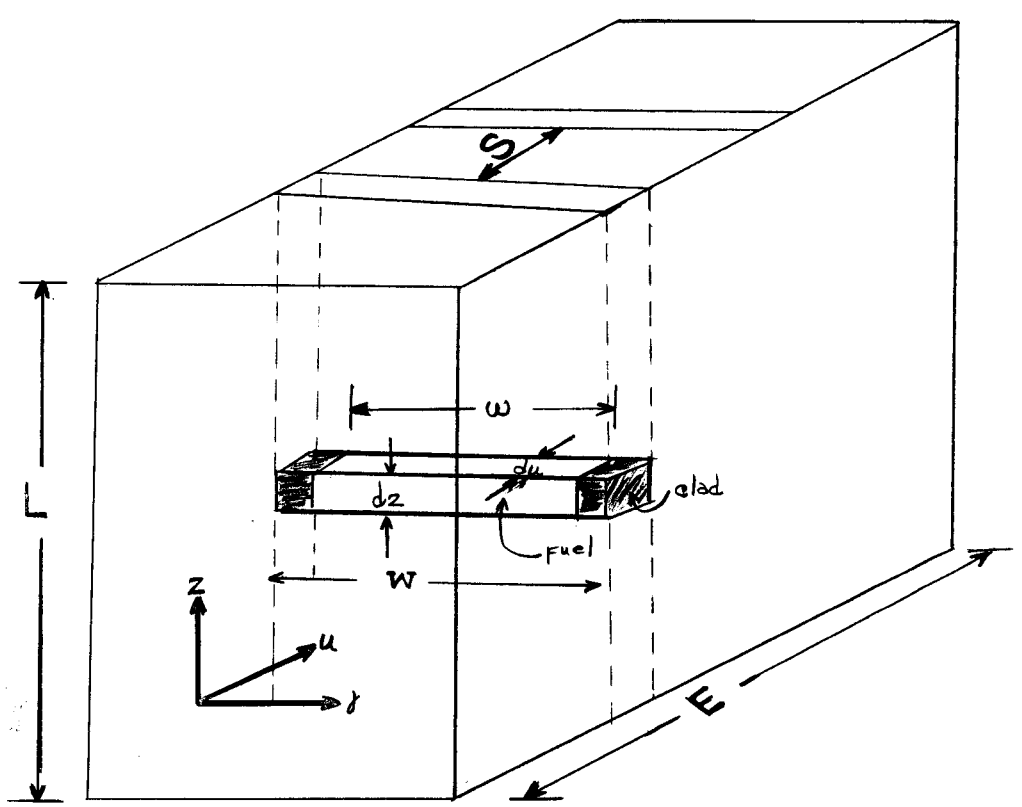

Figure 62

Dimensional Notation

Assume $A_{clad} = 2W\,dz\,[f(u)]$

$f(u)$ = no. of plates between $u = 0$ and $u = u$

$$f(u) = \frac{\text{total no. of plates}}{E}(u) = \frac{n}{E}u$$

$$dA_{clad} = 2Wdz\frac{n}{E}du$$

$$A_{D_2O} = \frac{nWS}{E}u$$

$$dA_{D_2O} = \frac{nWS}{E}du$$

$$dq_R = Uda\Delta T = U(2W\frac{n}{E}du\,dz)\left[T_s(u,z) - T_f(u,z)\right]$$

$$\int_{u=0}^{E}\int_{z=0}^{L} dq_R = 2WU\frac{n}{E}\int_{u=0}^{E}\int_{z=0}^{L}\left[T_s(u,z) - T_f(u,z)\right]dzdu$$

$$dq_P = \omega\Sigma_f^{fuel}\,\Phi_T(u,z)\,dV = \omega\Sigma_f^{fuel}\,\Phi_T(u,z)\,wdzdu$$

Assume: $\Phi_T(u,z) = A^* \sin\beta z \sin\gamma u$

where $\beta = \frac{\pi}{L}$ and $\gamma = \frac{\pi}{E}$

$$dq_P = \omega\Sigma_f^{fuel}\,w\,A^* \sin\beta z \sin\gamma u\,dzdu$$

$$q_P = \omega\Sigma_f^{fuel}\,w\,A^*\int_{z=0}^{z}\sin\beta z dz\int_{u=0}^{u}\sin\gamma u du$$

$$dq_f = \rho_{D_2O}\,C_p\,v\,dA_{D_2O}\,(\Delta T) = \rho_{D_2O}\,C_p\,v\,\frac{nWS}{E}du\left[T_f(z,u) - T_f(o)\right]$$

where $T_f(u,r,o) = T_f(o,r,o) = T_f(u,o,o) \equiv T_f(o)$ = inlet temp.

$$q_P(u,r,z) = q_f(u,r,z)$$

$$\omega\Sigma_f^{fuel}\,wA^*\int_{z=0}^{z}\sin\beta z dz\int_{u=0}^{u}\sin\gamma u du = \int_{u=0}^{u}\frac{nWS}{E}\rho_{D_2O}\,v\,C_p\left[T_f(z,u) - T_f(o)\right]du$$

Define $Q^* \equiv \omega\Sigma_f^{fuel}\,w\,A^*$

$$\psi^* \equiv \frac{nWS}{E}\rho_{D_2O}\,v\,C_p$$

$$Q^* \int_{z=0}^{z} \sin \beta z dz \int_{u=0}^{u} \sin \gamma u du = \psi^* \int_{u=0}^{u} \left[T_f(z,u) - T_f(o) \right] du$$

$$Q^* \int_{z=0}^{z} \sin \beta z dz \sin \gamma u = \psi^* \left[T_f(z,u) - T_f(o) \right]$$

$$\boxed{T_f(z,u) - T_f(o) = \frac{Q^*}{\beta \psi^*} \sin \gamma u \left[1 - \cos \beta z \right]}$$

Likewise $q_R = q_P$

$$2 W U \frac{n}{E} \int_{u=0}^{u} \int_{z=0}^{z} \left[T_s(u,z) - T_f(u,z) \right] dudz = Q^* \int_{z=0}^{z} \sin \beta z dz \int_{u=0}^{u} \sin \gamma u du$$

$$\frac{2 W U n}{E} \left[T_s(u,z) - T_f(u,z) \right] = Q^* \sin \beta z \sin \gamma u$$

$$\boxed{T_s(u,z) - T_f(u,z) = \frac{Q^* E}{2 W U n} \sin \beta z \sin \gamma u}$$

$$T_s(u,z) - \left[T_f(u,z) - T_f(o) \right] - T_f(o) = \frac{Q^* E}{2 W U n} \sin \beta z \sin \gamma u$$

$$T_s(u,z) - \frac{Q^*}{\beta \psi^*} \sin \gamma u \left[1 - \cos \beta z \right] - T_f(o) = \frac{Q^* E}{2 W U n} \sin \beta z \sin \gamma u$$

$$T_s(u,z) - T_f(o) = Q^* \left[\frac{E}{2WUn} \sin \beta z \sin \gamma u + \frac{1}{\beta \psi^*} \sin \gamma u \left\{ 1 - \cos \beta z \right\} \right]$$

$$\boxed{T_s(u,z) - T_f(o) = Q^* \sin \gamma u \left[\frac{E \sin \beta z}{2 W U n} + \frac{1 - \cos \beta z}{\beta \psi^*} \right]}$$

$$\frac{\partial T_s}{\partial z} = Q^* \sin \gamma u \left[\frac{\beta E \cos \beta z}{2 W U n} + \frac{\sin \beta z}{\psi^*} \right] = 0$$

$$\frac{\beta E \cos \beta z_{max}}{2 W U n} + \frac{\sin \beta z_{max}}{\psi^*} = 0$$

$$\frac{\psi^* \beta E}{2 W U n} = - \tan \beta z_{max}$$

$$\tan \beta z_{max} = - \frac{\psi^* \beta E}{2WUn}$$

Define $\alpha_{max} \equiv \beta z_{max}$

$$\boxed{\alpha_{max} = \tan^{-1} \left[- \frac{\psi^* \beta E}{2WUn} \right]}$$

$$\frac{\partial T_s}{\partial u} = Q^* \left[\frac{\beta E \cos \beta z}{2WUn} + \frac{\sin \beta z}{\psi^*} \right] \gamma \cos \gamma u_{max} = 0$$

$$\cos \gamma u_{max} = 0$$

$$\gamma u_{max} = \frac{\pi}{2}$$

$$\frac{\pi}{E} u_{max} = \frac{\pi}{2}$$

$$\boxed{u_{max} = \frac{E}{2}}$$

$$\boxed{T_{s_{max}} (z_{max}, u_{max}) - T_f(o) = Q^* \left[\frac{E \sin \alpha_{max}}{2WUn} + \frac{1 - \cos \alpha_{max}}{\psi^* \beta} \right]}$$

Application of Equations to Double Slab Reactor

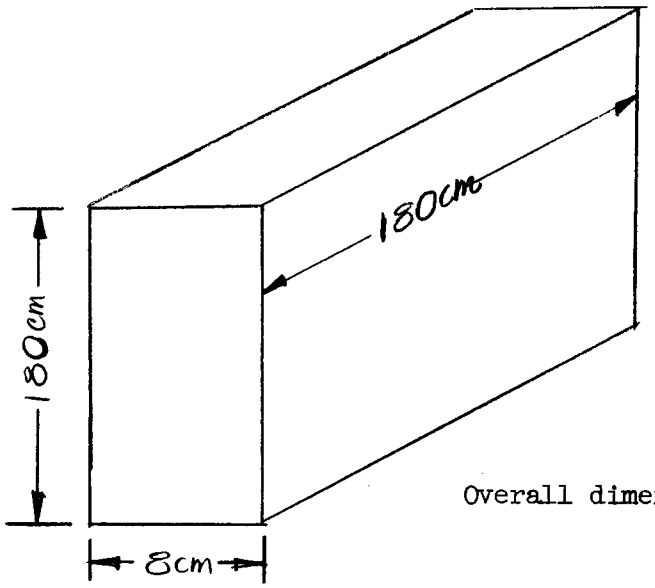

Overall dimensions of one slab

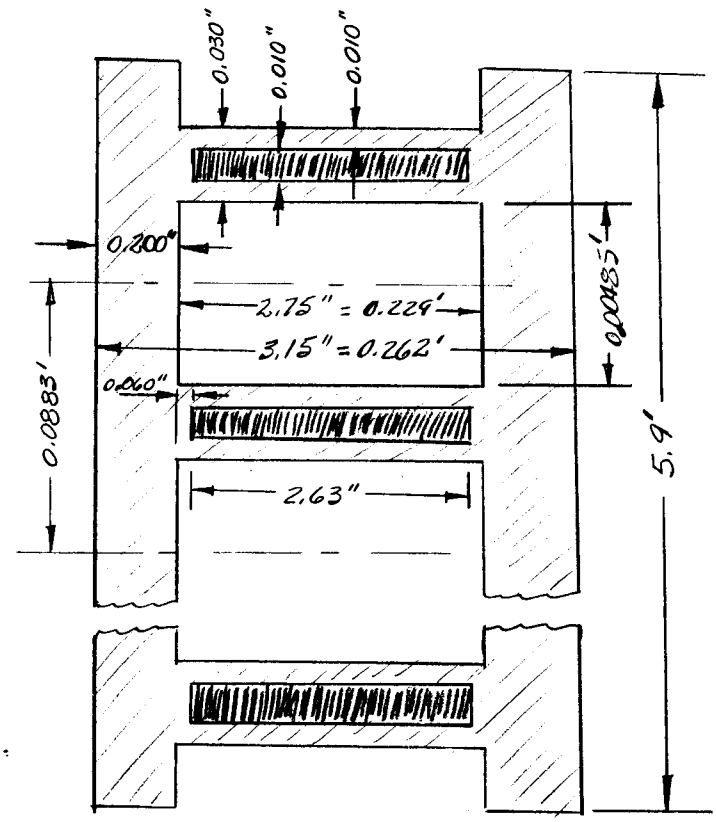

Figure 63

Fuel Element and Fuel Slab Dimensions

Pertinent dimensions:

$$\ell = L = 5.9'$$
$$T = 0.030'' = 0.0025'$$
$$t = 0.010'' = 0.000833'$$
$$d = 0.010'' = 0.000833'$$
$$c = 0.200'' = 0.0167'$$
$$e = 0.060'' = 0.005'$$
$$w = 2.63'' = 0.219'$$
$$P = 250 \text{ Megawatts}$$
$$\frac{V_m}{V_{D_2O}} = 0.73$$
$$m_{235} = 9.273 \text{ kg} = 20.4 \text{ lbs.}$$
$$\text{Atomic conc.} = 9.2 \times 10^{19} \text{ atoms } U^{235}/cm^3$$

$$V_{reactor} = 5.9 \times 5.9 \times 0.262 = 9.12 \text{ ft}^3$$
$$V_{D_2O} + 0.73\, V_{D_2O} = 9.12 \text{ ft}^3$$
$$V_{D_2O} = \frac{9.12}{1.73} = 5.27 \text{ ft}^3$$
$$V_m = 9.12 - 5.27 = 3.85 \text{ ft}^3$$
$$A_{D_2O} = \frac{V_{D_2O}}{L} = \frac{5.27}{5.9} = 0.894 \text{ ft}^2$$
$$A_{clad} = 2WL = 2(0.229)(5.9) = 2.7 \text{ ft}^2$$
$$V_{fuel/cell} = wtL = (0.219)(0.000833)(5.9) = 0.00108 \text{ ft}^3$$
$$W = 2.75'' = 0.229'$$
$$b = 0$$
$$S = 0.0591'' = 0.00492'$$
$$S + T = 0.0891'' = 0.00742'$$
$$n = \frac{5.9}{0.00742} = 795 \text{ cells/slab}$$
$$x = 2.04\%$$
$$f_{D_2O} = \frac{x}{100} = 0.0204$$

$$E = 5.9'$$
$$q_P = 250 \text{ Mwatts} = 8.53 \times 10^8 \text{ BTU/hr}$$
$$h_{H_2O} = 7800 \text{ BTU/hr-ft}^2\text{-}^\circ\text{F}$$

$$h_{D_2O} = 8470 \text{ BTU/hr-ft}^2\text{-}^\circ\text{F}$$

$$U = 7880 \text{ BTU/hr-ft}^2\text{-}^\circ\text{F}$$

$$\rho_{235} = 62.5 \times 18.7 = 1170 \text{ lb/ft}^3$$

$$\rho_{A\ell} = 62.5 \times 2.7 = 169 \text{ lb/ft}^3$$

$$\omega = \frac{\text{BTU/hr}}{\text{fissions/sec}} \left(\frac{\text{cm}^3}{\text{ft}^3}\right) = 1.025 \times 10^{-7}$$

$$\rho_{D_2O} = 68 \text{ lb/ft}^3$$

$$C_p \cong 1.0 \text{ BTU/lb-}^\circ\text{F}$$

$$v = 30 \text{ ft/sec}$$

$$G = \rho v = (68)(30)(3600) = 7.35 \times 10^6 \text{ lb/ft}^2\text{-hr}$$

$$f_{A\ell} = 1 - 0.0204 = 0.9796$$

$$m_{A\ell} = \rho_{A\ell} V_{fuel} f_{A\ell} = 169(0.00108)(0.9796) = 0.1823 \text{ lb/cell}$$

$$\frac{m_{235}}{m_{A\ell}} = \frac{0.0257}{0.1823} = 0.141$$

$$N_{235} = \frac{\text{Avog. No. } \rho_{235}}{235} = \frac{6.023 \times 10^{23} \times 0.0358}{235} = 9.2 \times 10^{19} \text{ atoms/cm}^3$$

$$\psi^* = \frac{n\,W\,S\,\rho_{D_2O}\,v\,CP}{E} = \frac{(795)(0.229)(0.00492)(68)(30)(1)}{5.9} = 310 \text{ BTU/sec-ft-}^\circ\text{F}$$

$$q_P = \omega \Sigma_f^{fuel}\, w\, A^* \left[\frac{1}{\beta\gamma}(1 - \cos\beta z)(1 - \cos\gamma u)\right] \quad \text{at } z = L \text{ and } u = E$$

$$A^* = \frac{q_P\,\beta\gamma}{4\,\omega\,\Sigma_f^{fuel}\,w}$$

$$Q^* = \omega \Sigma_f^{fuel}\, w\, A^* = \frac{\omega \Sigma_f^{fuel}\, w\, q_P\,\beta\gamma}{4\,\omega\,\Sigma_f^{fuel}\,w} = \frac{q_P\,\beta\gamma}{4} = \frac{(8.35 \times 10^8)\left(\frac{\pi}{5.9}\right)\left(\frac{\pi}{5.9}\right)}{4}$$

$$= 6.03 \times 10^7 \text{ BTU/ft}^2\text{-hr}$$

$$\tan\alpha_{max} = \frac{-\psi^*\beta E}{2WUn} = \frac{-(310 \times 3600)\left(\frac{\pi}{5.9}\right)(5.9)}{2(0.229)(7880)(795)} = -1.22$$

$$\frac{\pi}{L} z_{max} = \tan^{-1}(-1.22) = 129.3^\circ$$

$$z_{max} = \frac{L}{\pi}\left(\frac{129.3}{360}\right)(2\pi) = \frac{(5.9)(2)(129.3)}{360} = 4.25 \text{ ft}$$

$$\sin \frac{\pi}{L} z_{max} = 0.773$$

$$\cos \frac{\pi}{L} z_{max} = -0.634$$

$$\sec \alpha_{max} = -1.578$$

$$T_{s_{max}} - T_f(o) = Q^* \left[\frac{E \sin \alpha_{max}}{2 W U n} + \frac{1 - \cos \alpha_{max}}{\phi^* \beta} \right]$$

$$= 6.03 \times 10^7 \left[\frac{5.9 \times 0.750}{2 \times 0.229 \times 7880 \times 795} + \frac{1 + 0.669}{310 \times 3600 \times \pi/5.9} \right]$$

$$= 261°F$$

$$q''' = \omega \Sigma_f \Phi_T(z,u) = \omega \Sigma_f A^* \sin \beta z_{max} \sin \gamma u_{max}$$

$$= \frac{\cancel{\omega \Sigma_f} q_p \beta \gamma}{4 \cancel{\omega \Sigma_f} w} \sin \alpha_{max} = \frac{(8.53 \times 10^8)\left(\frac{\pi}{5.9}\right)\left(\frac{\pi}{5.9}\right)(0.773)}{4(0.219)} = 2.13 \times 10^8 \text{ BTU/ft}^3\text{-hr}$$

$$T_{l_{max}} = T_{s_{max}} + q''' \left[\frac{t^2}{8 k_{A\ell}} + \frac{td}{2 k_{A\ell}} \right] = T_s + q''' \left[\frac{5 t^2}{8 k_{A\ell}} \right]$$

$$= 261°F + 2.13 \times 10^8 \left[\frac{(5)(0.000833)^2}{(8)(117)} \right]$$

$$= 261°F + 0.79°F$$

$$\cong 262°F.$$